N74-18674

NASA CR-132371 - Volume I

ANALYTICAL STUDY TO DEFINE A HELICOPTER STABILITY DERIVATIVE EXTRACTION METHOD

VOLUME I - FINAL REPORT

By John A. Molusis

Prepared under Contract No. NAS1-11613
SIKORSKY AIRCRAFT DIVISION
UNITED AIRCRAFT CORPORATION
Stratford, Conn.

for

USAAMRDL LANGLEY DIRECTORATE

and

NATIONAL AERONAUTICS AND SPACE ADMINISTRATION

FOREWORD

This report was prepared for the U. S. Army Air Mobility R&D Laboratory and NASA, Langley Research Center, Hampton, Virginia by Sikorsky Aircraft Division of the United Aircraft Corporation in partial fulfillment of NASA-Army Contract NAS1-11613.

This report describes work started in July 1972 and completed in May 1973 and the results are presented in two volumes. Volume I contains the text and applications of the derivative extraction method found to be most accurate and Volume II contains the figures leading to the selection of the most accurate method.

The technical monitor for the U. S. Army Air Mobility R&D Laboratory was Mr. Robert Tomaine.

The author wishes to acknowledge the assistance given by the following individuals: E. S. Carter and D. E. Cooper for their review comments; Stan Briczinski who supplied the data used in correlating analytic derivatives versus flight identified derivatives; R. S. Hansen for his consultation and help in analyzing the data for this report; and John Pandoli for consultation regarding the computer program development.

TABLE OF CONTENTS

ANALYTICAL STUDY TO DEFINE A HELICOPTER STABILITY DERIVATIVE EXTRACTION METHOD*

By John A. Molusis
Sikorsky Aircraft Division
United Aircraft Corporation

SUMMARY

A method is developed for extracting six degree-of-freedom stability and control derivatives from helicopter flight data. Different combinations of filtering and a priori derivative estimate are investigated and used with a Bayesian approach for derivative identification. The combination of filtering and a priori estimate found to yield the most accurate time response match to flight test data is determined and applied to CH-53A and CH-54B flight data. The method found to be most accurate consists of (1) filtering flight test data with a digital filter followed by an extended Kalman filter (2) identifying an a priori derivative estimate with a least square estimator and (3) obtaining derivatives with the Bayesian derivative extraction method.

The results demonstrate (1) the importance of the a priori estimate, (2) the least square estimator used with the optimal data filter provides a time history match nearly as well as the Bayesian estimator, (3) identified derivatives only approximate conventional quasi-static derivatives and, (4) the identified derivatives yield the correct characteristic roots.

INTRODUCTION

The ability to identify aerodynamic stability and control derivatives from aircraft flight data has long been recognized as a desirable goal. Improvement in AFCS design, quantification of stability and control characteristics, and improvement of analytic prediction methods are some of the potential benefits to be realized. Identification of potential stability problems in prototype aircraft and flying qualities assessment can also benefit from derivative identification. Because of the complexity and coupled behavior of the helicopter, there is strong motivation for identifying the aerodynamic derivatives that describe flight behavior. For example, present analytic prediction methods show discrepancies in predicting the high speed unstable dutch roll roots associated with the CH-53A helicopter. Additionally, high gains of rate feedback used in the AFCS cause rotor tip path plane oscillations that are not predicted accurately by present analytic methods. Stability derivative identification can provide the potential tool for isolating the causes of these observed discrepancies.

* The contract research effort which has led to the results in this report was financially supported by USAAMRDL (Langley Directorate).

Many applications of derivative identification from fixed wing and VTOL aircraft have appeared in the literature.[1,2,3] These studies have generally been characterized by three degree-of-freedom models, negligible input driving noise (process noise), and sufficiently long data records with properly excited modes. The helicopter and many VTOL aircraft do not fall into this relatively simple characterization. In particular, the typical helicopter requires a minimum of six degrees of freedom and contains significant process noise. Finally, long data records often are unavailable for proper identification.

Many applications of derivative identification have concentrated on curve fitting an assumed mathematical model to test data by minimizing a quadratic function of the fit error. Gradient techniques, least squares methods, and Newton Raphson methods have been used to accomplish the required minimization. The resulting solution generally provides a good fit to the data; however, the identified value of the derivative may depart considerably from the real value of the derivative. This problem can be attributed to improper modelling of the problem, insufficient data, and multiple solutions due to the algorithm used.

Current statistical methods of identification provide the means to treat all the problems normally associated with derivative extraction from test data. The Bayesian approach to estimation treats the derivative identification problem as a stochastic problem. The criterion to be satisfied is to determine the most probable estimates of the stability derivatives and state variables, given noisy measurements. This formulation has advantages in the identification problem. First, we are attempting to determine the most probable derivatives and not simply solve a curve fit problem. Secondly, the approximations made in obtaining a computationally practical algorithm can be justified, or errors resulting from these approximations minimized. Finally, derivative identification from flight test data is indeed a statistical problem, and problems of insufficient data and proper mode excitation can be interpreted conveniently.

An excellent review of methods for system identification can be found in Reference 4. In particular, the Bayesian method is developed and a recursive algorithm provided for the solution. This method is seen to be identical with the extended Kalman filter when the measurement equations are linear. This method is also called a maximum *a posteriori* estimator and is related to the classical maximum likelihood estimator by Bayes' rule. Reference 4 discusses this relationship in more detail. Reference 5 provides applications of a modified Kalman filter algorithm for VTOL aircraft derivative identification. The results demonstrate the superiority of the extended Kalman filter method over standard curve fit methods of Newton Raphson and conjugate gradient. The helicopter derivative identification problem using Kalman filtering methods is described in detail in Reference 6. This paper explored the particular aspects of helicopter derivative extraction that require special consideration and proposed methods for their solution. The paper demonstrates (1) the need for more than one maneuver when using short data records, (2) the existence of significant levels of process noise, and (3) the non-unique character of the six degree-of-freedom derivative model. In addition, the Bayesian maximum likelihood method is extended to process any number of simultaneous maneuvers, and a method for obtaining an *a priori* derivative guess is presented.

This report presents applications of the methods of Reference 6 to actual helicopter flight test data. An overall procedure, including filtering and a priori derivative guess, is developed to yield a helicopter derivative extraction method. The method is applied to CH-53A and CH-54B flight test data and demonstrates the requirements necessary for successful identification.

SYMBOLS

A_{11}	Matrix of partial derivatives obtained by partially differentiating $f(\underline{X}, \underline{X}_p)$ with respect to $\underline{X}$.
A_{1_p}	Matrix of partial derivatives obtained by partially differentiating $f(\underline{X}, \underline{X}_p)$ with respect to $\underline{X}_p$.
A^o	Matrix of stability derivatives used to initialize the Bayesian max. likelihood estimator.
A^*	Matrix of stability derivatives obtained from the Bayesian max. likelihood estimator.
B^o	Matrix of control derivatives used to initialize the Bayesian max. likelihood estimator.
B^*	Matrix of control derivatives obtained from the Bayesian max. likelihood estimator.
A_{1s}, B_{1s}	Lateral and longitudinal cyclic control input, respectively, degrees at the head.
$f(\underline{X}, \underline{X}_p)$	Functional relationship among the state variables and derivatives in the stability derivative model.
f_1, F_1	Lower cutoff frequency used for determining noise statistics from the data, Hz.
f_2, F_2	Upper cutoff frequency used for determining noise statistics from the data, Hz.
f_c	Actual cutoff frequency used on the data, Hz.
G	Process noise gain matrix.
l_1, l_2, l_3	Distance to the center of gravity of the airflow measurement probe, Ft.
L	Normalized rolling moment defined in equation (1).
Lp	Stability derivative $\partial L/\partial P$ defined in equation (2).

M	Normalized pitching moment defined in equation (1).
$M_{B_{1s}}$	Stability derivative $\partial M/\partial B_{1s}$ defined in equation (2).
Mp	Stability derivative $\partial M/\partial p$ defined in equation (2).
Mq	Stability derivative $\partial M/\partial q$ defined in equation (2).
n	Zero mean, white gaussian measurement noise.
N	Normalized yawing moment defined in equation (1).
Nq	Stability derivative $\partial N/\partial q$ defined in equation (2).
P	Covariance matrix for the Kalman filter.
P_{11}	State variable covariance matrix for the MLE.
P_{1p}	Cross covariance matrix for the state and parameter vector of the MLE.
P_{pp}	Parameter covariance matrix for the MLE.
P^o, P^*	Initial and final parameter covariance matricies for the MLE.
p	Aircraft roll rate, radians/sec.
q	Aircraft pitch rate, radians/sec.
Q	Process noise intensity matrix.
r	Aircraft yaw rate, radians/sec.
R	Measurement noise intensity matrix.
t	Time, Secs.
t_o, t_f	Initial and final time respectively, secs.
u, V_x	Aircraft longitudinal velocity, Ft./Sec.
v, V_y	Aircraft lateral velocity, Ft./Sec.
V	True Airspeed, Ft./Sec.
$w(t)$	Zero mean, white gaussian process noise
w, V_z	Aircraft vertical velocity, Ft./Sec. (positive up)
X	Longitudinal normalized force defined in equation (1).

$\underline{X}$ System state vector for the Kalman Filter and MLE.

$\underline{X}_p$ Vector made up of stability derivatives.

Y Lateral normalized force defined in equation (1).

Z Vertical normalized force defined in equation (1).

$\underline{Z}$ Measurement variable.

Zw Stability derivative $\partial Z/\partial W$ defined in equation (2).

α, β Aircraft angle of attack and sideslip respectively, degrees.

δ Perturbation from trim condition.

ϕ, Θ, Ψ Aircraft roll, pitch and yaw attitudes respectively, radians. Positive direction is right roll, up pitch and right yaw.

Θ coll. Collective control input, degrees at the head.

Θ tail Tail rotor collective pitch, degrees.

Subscripts:

$( )_i$ Refers to the ith maneuver number.

$( )^T$ Denotes matrix transpose.

$( )^{-1}$ Denotes matrix inversion.

$(\dot{})$ Denotes time derivative, $\frac{d( )}{dt}$

Miscellaneous:

All stability and control derivatives are presented in either normalized or dimensional form. The units are defined in Table 8 and Table 9. Dimensional derivatives are obtained by multiplying normalized derivatives by the appropriate mass or inertias.

Roll Rate I, Pitch Rate I and Yaw Rate I used in the time history figures refer to the inertial aircraft rates $\dot{\phi}$, $\dot{\Theta}$, $\dot{\psi}$, respectively.

The data supplied by USAAMRDL (Langley Directorate) was chosen at a 45 knot condition and consisted of 4 maneuvers. Subsequently a one maneuver case was selected which is trimmed at 32 knots. All titles for this data, however, indicate a 45 knot trim.

TABLES

LIST OF ILLUSTRATIONS

PROBLEM FORMULATION AND METHOD FOR SOLUTION

The primary difficulty in obtaining accurate stability derivatives from flight test data is due to the noise contaminations present. Additionally, helicopter six-degree-of-freedom derivative models are not uniquely defined due to the lumped effects of the rotor. This section will discuss these particular problems of helicopter derivative identification, present the derivative model which is used throughout this report and discuss in detail the Bayesian approach and procedure used.

Review of System Identification Requirements

Helicopter stability derivative extraction requirements differ from fixed wing or VTOL aircraft primarily in the following ways:

1. The six degree-of-freedom helicopter derivative model consists of the lumped effects of body and rotor.

2. The plant driving noise and measurement noise are larger for helicopters.

3. The number of degrees of freedom to describe helicopter rigid body response is generally greater.

4. The helicopter has unstable phugoid roots and on occasion unstable dutch roll roots.

Reference 6 and Reference 7 describe some of the above differences in detail. A summary of the conclusions and methods for treating these problems will be discussed.

Derivative definition. - The helicopter when interpreted as a six degree-of-freedom derivative model does not possess a unique set of derivatives during actual flight conditions. This is because the rotor effects are assumed to be lumped with the body derivative and since the rotor is always in motion the lumped derivative reflects a combined body and 'average' rotor contribution. The conventional method for obtaining helicopter 6 degree-of-freedom derivatives is based on the assumption that a perturbation in a body attitude, rate or velocity causes the rotor tip path plane to reach a steady state trim. The lumped effect of rotor and body causes a force or moment which divided by the perturbation yields the quasi-static derivative.

It should be clear that under normal flight conditions (pilot excitation and wind gust always taking place) the helicopter does not actually fly like the quasi-static model. This is because the rotor is never in a steady state condition. The six degree-of-freedom model which "best" represents the flight behavior is what is identified from flight test. The identified derivatives can be thought of as an "average" or "nominal" derivative. The quasi-static and derivative identified from flight data are further compared below.

Quasi-Static Derivative	=	Body Contribution	+	Rotor Contribution after tip path plane reaches steady state

System Identified Derivative	=	Body Contribution	+	Average Rotor Contribution

Reference 6 demonstrates that the two derivative models yield nearly the same characteristic roots and both models yield good time history reproduction of the non-linear helicopter simulation from which they were obtained.

Correlation of quasi-static derivatives obtained from a non linear computer simulation against six degree-of-freedom derivatives identified from flight data can not be expected to yield identical results. However, meaningful characteristic root comparisons can be made as well as time response comparisons. Additionally, correlation of derivatives identified from flight test and computer models can be made as long as the same derivative identification method is used.

The fact that six degree-of-freedom derivative models are not uniquely defined is primarily due to the choice of a six degree-of-freedom model rather than a larger more accurate representation. It is possible to approximate quasi-static derivatives from flight data but requires the identification of a nine degree-of-freedom model which includes body and tip path plane degree of freedom. The identified nine degree-of-freedom model can then be perturbed just as a non-linear computer simulation and quasi-static derivatives obtained.

The studies conducted in this report are concerned only with six degree-of-freedom identification. The resulting derivative model can be used to obtain characteristic roots and time history generation.

Noise contamination. - There are several types of noise present in helicopter test data which are of particular concern to the derivative identification problem. These are as follows:

1. Measurement noise resulting from the inaccuracy of the physical transducer used,

2. Measurement Bias resulting from steady drift or calibration errors,

3. Process noise resulting from all effects which physically drive the equations of motion (included are higher degrees of freedom which are not modeled, non linearities which are not modeled, wind gust disturbances and servo actuator errors),

4. Trim errors resulting from the inability of the pilot to perfectly trim the vehicle in flight.

Measurement noise can be accounted for in the problem formulation, however the larger the uncertainty in the measurement the longer the data record required

in the identification. This is why filtering the data first improves the derivative estimates for a fixed data length.

Measurement bias can be formulated as part of the identification problem however this increases the size of the state vector and increases computation time. Alternately the bias can be identified first by using an extended Kalman filter. This approach has the advantage of providing good estimates of the bias as well as excellent estimates of the system state variables. This latter approach is the one used in this study.

Process noise can also be formulated as part of the identification formulation Process noise has two effects on the identification. First, the larger the process noise the more data and input excitation required. Second, process noise tends to make the linearizations used in the derivative identification algorithm less accurate. Additionally process noise is represented in the formulation by white noise with gaussian statistics. This requirement may not always be met, however by using long data records or many short data segments this requirement should be generally satisfied.

Trim errors can be included in the formulation however at the expense of increased computations. For this reason it is important for the vehicle to trim accurately or to fly about a trim condition sufficiently long so that the trim can be easily identified by visually inspecting the data. This is particularly important when using several independent segments of data (multi-maneuver case) in the identification.

Number of degrees of freedom. - As indicated earlier the helicopter requires a minimum of six degrees of freedom. Present algorithms for derivative identification are capable of treating this size problem without excessive computation time. The nine degree-of-freedom problem is dimensionally too large for most methods including the Bayesian technique used in this report. However a slight modification to the Bayesian approach can provide a practical algorithm for treating almost any number of degrees of freedom. This can be done by identifying one row of derivatives at a time while accounting for the errors due to the remaining derivatives by a bias correction term. This approach will not be discussed any further here. This method however can be used to identify very large derivative arrays.

Unstable characteristic roots. - The helicopter possesses unstable phugoid roots and on occassion has unstable dutch roll roots at high speeds. This does not cause problems in the identification, however when correlating the identified derivative model against test data, the error between the time history match is governed by an unstable error equation. The roots of this error equation are the same as the roots of the identified derivative model. Thus, the smallest amount of process noise or initial condition error will cause the linear model response to diverge from the test data even if the correct derivatives are identified. For this reason application of identification techniques will generally provide a much better time response match for fixed wing vehicles which generally have stable characteristic roots.

The Derivative Model

The six degree-of-freedom derivative model used throughout this study is given below:

$$
\begin{aligned}
\dot{\phi} &= p + (r \cos \phi + q \sin \phi) \tan \theta \\
\dot{\theta} &= q \cos \phi - r \sin \phi \\
\dot{\psi} &= (r \cos \phi + q \sin \phi)/\cos \theta \\
\dot{V}_x &= \dot{V}_{x_o} - g \sin \theta + X \\
\dot{V}_y &= \dot{V}_{y_o} + g \sin \phi \cos \theta + Y \\
\dot{V}_z &= \dot{V}_{z_o} + g \cos \phi \cos \theta + Z \\
\dot{p} &= L \\
\dot{q} &= M \\
\dot{r} &= N
\end{aligned}
\tag{1}
$$

where:

$$
\begin{aligned}
X = \frac{\partial X}{\partial V_x} \delta V_x + \frac{\partial X}{\partial V_y} \delta V_y + \frac{\partial X}{\partial V_z} \delta V_z + \frac{\partial X}{\partial p} \delta p + \frac{\partial X}{\partial q} \delta q + \frac{\partial X}{\partial r} \delta r \\
+ \frac{\partial X}{\partial B_{ls}} \delta B_{ls} + \frac{\partial X}{\partial A_{ls}} \delta A_{ls} + \frac{\partial X}{\partial \theta_{TR}} \delta \theta_{TR} + \frac{\partial X}{\partial \theta_c} \delta \theta_c
\end{aligned}
\tag{2}
$$

$Y =$
$Z =$
$L =$ analogous to equation (2)
$M =$
$N =$

It should be noted that the inertial terms which are usually found on the left of the equal sign in equation (1) have been lumped into the derivative terms. The derivatives are thus total force derivatives which are the sum of the aerodynamic and inertial derivatives.

The derivative model is conveniently represented in state variable form by defining the state vector and parameter vector below:

$$\underline{X} = \begin{bmatrix} \phi \\ \theta \\ \psi \\ V_x \\ V_y \\ V_z \\ p \\ q \\ r \end{bmatrix} \qquad \text{and} \qquad \underline{X}_p = \begin{bmatrix} \frac{\partial X}{\partial V_x} \\ \frac{\partial Y}{\partial V_x} \\ \cdot \\ \cdot \\ \cdot \\ \frac{\partial X}{\partial V_y} \\ \frac{\partial Y}{\partial V_y} \\ \cdot \\ \cdot \\ \cdot \\ \cdot \\ \cdot \\ \cdot \\ \frac{\partial X}{\partial \theta_c} \\ \frac{\partial Y}{\partial \theta_c} \end{bmatrix} \tag{3}$$

The derivative model of equation (1) then reduces to the state vector equation

$$\dot{\underline{X}} = f(\underline{X}, \underline{X}_p) \tag{4}$$

Equation (4) is the derivative model used in all the Bayesian maximum likelihood identification studies.

Method For Derivative Identification (The Bayesian Max. Likelihood Estimator)

The derivation of the Bayesian maximum likelihood estimator for simultaneous maneuvers is given in Reference 6. The initials MLE are used throughout this report to represent the Bayesian maximum likelihood estimator and not the

classical maximum likelihood estimator. The actual formulation and equations used will be presented here.

The Bayesian Max. Likelihood Estimator determines the most probable estimates of the state variables and stability derivatives given the measured data. The equations relating the noise contaminations, stability derivative model and measurements are presented below.

System equations.

$$\begin{aligned} \dot{\underline{X}}_i(t) &= f(\underline{X}_i, \underline{X}_p) + G_i \underline{W}_i(t), & \underline{X}_i(t_o) \\ \dot{\underline{X}}_p &= 0 & \underline{X}_p(t_o) \end{aligned} \tag{5}$$

where, i - represents the maneuver number.

Measurement equations.

$$Z_i = \underline{X}_i + \underline{n}_i \tag{6}$$

The best estimate of the state variables and stability derivatives is obtained from the equations below.

The Bayesian Max. Likelihood Estimator.

Filter Equations:

$$\begin{aligned} \dot{\underline{X}} &= f(\underline{X}, \underline{X}_p) + P_{ll} R^{-1} (\underline{Z} - \underline{X}) \\ \dot{\underline{X}}_p &= P_{pl} R^{-1} (\underline{Z} - \underline{X}) \end{aligned} \tag{7}$$

Covariance Equations:

$$\begin{aligned} \dot{P}_{ll} &= A_{ll} P_{ll} + (A_{ll} P_{ll})^T + A_{lp} P_{pl} + (A_{lp} P_{pl})^T - P_{ll} R^{-1} P_{ll} + Q \\ \dot{P}_{pl} &= P_{pl} A_{ll}^T + P_{pp} A_{lp}^T - P_{pl} R^{-1} P_{ll} \\ \dot{P}_{pp} &= -P_{pl} R^{-1} P^T_{pl} \end{aligned} \tag{8}$$

The individual terms in equations (7) & (8) are defined in Appendix A.

Initialization of The MLE and Noise Statistics.

Equations (7) and (8) require the following quantities before a solution can be obtained;

(1) Measurement Noise Covariance - R

(2) Process Noise Covariance - Q

(3) Initial State Estimate - $\underline{X}(t_o)$

(4) Initial State Covariance - $P_{11}(t_o)$

(5) Initial Derivative Estimate - $\underline{X}_p(t_o)$

(6) Initial Derivative Covariance - $P_{pp}(t_o)$

Physically the measurement noise covariance represents the amplitude of the power spectrum of the assumed white noise contamination on the state variables. Figure 1 shows a spectrum of white noise and the rigid body signals which the derivative model is to reproduce.

The calculation of the measurement noise covariance R can be automated by filtering the raw data at frequencies f_1 and f_2 and computing the corresponding mean square value of the filtered data. The measurement noise covariance is then

$$R = \frac{(\sigma_2^2 - \sigma_1^2)}{\pi (f_2 - f_1)} \tag{9}$$

where;

σ_2^2 = the mean square value of the raw data filtered at f_2

σ_1^2 = the mean square value of the raw data filtered at f_1

The process noise covariance can be computed in an analogous manner by operating on the accelerations. Since the accelerations contain both process noise and sensor noise, the sensor noise should be subtracted out. A reasonable estimate is obtained without subtracting the sensor noise and this is the approach used in this study to obtain process noise covariance.

The initial conditions on the system equations were obtained from the first data point of the measured data. The initial state covariance is then

$$P_{11}(t_o) = R\pi f_c \tag{10}$$

where; f_c = the filtering cutoff used on the data.

R = computed from equation (9) for each state.

The initial derivative guess and variance in the guess was obtained using two methods. First, a least square estimator was employed which operates on data filtered by an extended Kalman filter. The least square estimator provides an estimate of the derivatives and variance. The variance required modification in each case. The least square estimator is discussed in Appendix B. The second method employes engineering judgement to select the derivative guess and variance.

The Data Filters

Three filtering methods are investigated in this study as follows:

1. First order low pass with cutoff freq. of 10 cps (8 cps for the CH-54B data).

2. Graham Digital Filter with cutoff frequency (FC) of 3 cps and termination frequency (FT) of 4 cps.

3. A Kalman filter (state variable estimator) which minimizes the overall uncertainty in the data and removes bias error.

The first order low pass filter with cutoff frequency at 10 cps was chosen to represent the case in which little or no filtering is done to the data. Since all instrumentation contains inherent filtering and an aliasing filter is needed before discretizing the data, the 10 cps filtered data represents essentially no filtering with respect to rigid body modes (typically less than 4 cps).

The Graham digital filter represents a high quality zero phase shift filter which has extremely high roll off rate. The cutoff frequency of 3 cps and termination frequency of 4 cps essentially retains only rigid body frequencies and low frequency contaminations.

The Kalman filter is the highest quality filter of the three in that it accounts for random discrepancies of related measurements and also can remove bias error. The Kalman filter is really a state variable estimator. The predicted state estimates do not in general filter out high frequency data. Many of the high frequency effects are a part of the true motion of the vehicle due to higher modes of motion and it is only the engineering modelling requirement to obtain rigid body data that the high frequency data is labeled as undesirable. Since rigid body motion is what is desired, all data used by the Kalman filter is first filtered with the Graham zero phase shift digital filter. Thus only low frequency data is predicted by the Kalman estimator.

The equations describing the three filters are presented in Appendix C.

Determination of the Noise Statistics for the Kalman Filter. - The Kalman filter requires (1) measurement noise statistics, (2) process noise statistics and (3) an initial state estimate and variance. Table 1 summarizes the method used to obtain the measurement noise statistics while Table 2 summarizes the method used to obtain process noise statistics. Statistics computed from the data without engineer interaction and statistics inputed by the engineer are presented. Table 3 presents the equations used to compute the initial state and variance from the data.

Procedure To Determine A Helicopter Derivative Extraction Method

The procedure to determine the most accurate helicopter derivative extraction method is shown in the flow diagram of Figure 2. Three different filtering techniques are employed; a first order low pass, a Graham digital and a Kalman filter. Additionally two different methods for obtaining the a priori derivative guess and variance are used; a least square method and by using engineering judgement. Combinations of the above filtering methods and a priori guess are used in conjunction with the Bayesian Max. Likelihood Estimator. A discussion of the criteria used to determine the most accurate method is presented in a subsequent section.

TEST DATA USED AND HELICOPTER DESCRIPTION

Flight test data from two different helicopters are used in this study; a CH-53A at both 100 knots and 150 knots trim condition and flight data from a CH-54B at 45 knots trim which was supplied by AAMRDL, Langley Research Center. The most accurate method is determined from CH-53A data at 100 knot trim.

The data used in this study is summarized below.

Flight Test Data	No. of Independent Maneuvers used	Comments
CH-53A (100 kts, 352"C.G.)	6 (6 secs. length each) (4 maneuvers in Identification, 2 maneuvers used to determine the most accurate method)	This case was used to determine the most accurate method.
CH-53A (150 kts, 352"C.G.)	4 (5 seconds length each)	using most accurate method
CH-54B (45 kts, 346" C.G.)	4 (6 seconds length each)	using most accurate method
CH-54B (45 kts, 346" C.G.)	1 (16 seconds length)	using most accurate method

CH-53A Helicopter

The flight test data from the CH-53A was obtained from a handling qualities flight test program conducted for the Navy by Sikorsky Aircraft. Extensive dynamic stability data are recorded on magnetic tape and selected maneuvers from the data are used for derivative identification.

Description of Test Vehicle. - The test aircraft is a CH-53A helicopter modified into a CH-53D configuration by the installation of YT64-GE-12 engines and an up-rated transmission. Figure 3 shows a photo of a CH-53A in flight. Table 4 gives the physical characteristics of the test CH-53A helicopter.

Test Data at 100 Knots Using the Three Filters. - Six maneuvers are selected with at least one of the primary control inputs excited for each maneuver. All four control inputs are excited in the four maneuvers used in the identification. The inputs used are typically 1 degree - ½ second duration pulse inputs and thus a data record length of 6 seconds' duration is used to prevent large deviations from linearity.

Figure 4 through Figure 9 show the six maneuvers of CH-53A data at 100 knot trim condition filtered at 10 HZ. with the first order low pass filter. These data are not corrected for c.g. location and represent the outputs of the physical transducer. These same data filtered with the Graham digital filter at 3.0 HZ can be found in Volume II (Figure 1 through Figure 6).

Figure 10 through Figure 15 show the same six maneuvers of CH-53A data (100 kts) converted to body axis. The Kalman and digital filtered data are shown superimposed. Examination of these figures reveal the ability of the Kalman filter to remove bias error and make use of the coupled information in several channels to predict a more accurate estimate.

Test Data at 150 Knots Using The Three Filters. - Figure 16 through Figure 19 show the four maneuvers of CH-53A flight data at a 150 knot trim condition filtered at 10 Hz with the first order low pass filter. These data are not corrected for c.g. location and represent the outputs of the physical transducer. These same data filtered with the Graham digital filter at 3.0 Hz can be found in Volume II (Figure 7 through Figure 10).

Figure 20 through Figure 23 show the same four maneuvers of CH-53A data (150 knots) converted to the body axis. The Kalman and digital filtered data are shown superimposed. The Kalman filter is shown with bias error removed and the uncertainty due to random errors minimized.

CH-54B Helicopter

The flight test data from the CH-54B was supplied by Langley Directorate, USAAMRDL, and stored on magnetic tape. Selected maneuvers from this tape are used to identify derivatives. Two cases are under investigation; identification of derivatives from four 6-second simultaneous maneuvers and identification from one 16-second maneuver.

Description of test vehicle. - The test aircraft is a CH-54B Army crane. Figure 24 shows a photo of a CH-54B in flight. Table 5 gives the physical characteristics of the test CH-54B helicopter.

Test data at 45 knots using the three filters (4 maneuver case). - Four maneuvers are selected which contain excitation from all four input controls. The four maneuvers chosen contained in some cases dramatic differences in trim condition. These maneuvers were selected primarily because all control inputs were excited and good excitation was not available in other segments of data that was supplied by Langley Directorate, USAAMRDL. The large differences in the trim condition led to a poor identification as was later accessed by resimulation of the identified model and comparing against the test data. Since this case contained improper trim all test data and results are presented in Volume II of this report.

Volume II (Figure 11 through Figure 14) show the CH-54B flight test data (four maneuver case) filtered at 8 HZ. with the first order low pass filter. These data are not corrected for c.g. location and represent the outputs of the physical transducer. These same data filtered with the Graham digital filter at 3.0 HZ. is shown in Volume II (Figure 15 through Figure 18).

Volume II (Figure 19 through Figure 22) shows the same four maneuvers of CH-54B data (45 kts.) converted to the body axis. The Kalman and digital filtered data are shown superimposed.

Test data at 45 knots using the three filters (one 16-second maneuver case). - A single 16-second data record from the CH-54B flight data was selected. All control inputs are excited and a well defined trim was apparent from the data. Figure 25 shows these data filtered at 8 HZ. with the first order low pass filter, uncorrected for c.g. location and represent the outputs of the physical transducer. These same data filtered with the Graham digital filter at 3.0 HZ. is shown in Volume II (Figure 23).

Figure 26 shows the 16-second maneuver of the CH-54B data (45 kts.) converted to the body axis. The Kalman and digital filtered data are shown superimposed. The Kalman filtered data is shown with bias error removed and the large random error appearing in the linear velocities is also shown removed.

DETERMINATION OF THE MOST ACCURATE HELICOPTER DERIVATIVE EXTRACTION METHOD

Ten methods consisting of different data filtering and a priori derivative guess were investigated in this study. The purpose of this investigation is to examine the three data filters previously discussed, access the least square method and determine the best method for obtaining an a priori derivative estimate for initializing the maximum likelihood method. Table 6 lists the ten methods used in determining the best overall approach. The arbitrary derivative guess noted in Table 6 was obtained as follows. The control derivatives were obtained by examination of the test data, measuring the accelerations where the pulse inputs reached their peak and dividing the accelerations by the magnitude of the control input pulse. The stability derivatives Z_q and Y_r are known approximately and have a magnitude of 169 ft/sec.(approximately the trim condition.) All other stability derivatives were set to zero. The variance on the derivatives were guessed using engineering judgment. Table 7 summarizes the derivative value and variance for the "arbitrary" guess.

Criteria for Selection of the Most Accurate Method

The most accurate derivative identification method is determined by using four maneuvers of CH-53A flight test data at 100 knot trim condition in the identification process. The identified derivative model is then simulated and compared against two independent maneuvers not used in the identification. The root mean square (RMS) error between the time histories of the identified derivative model and test data are then computed. RMS error for both test data used in the identification and not used in the identification is computed. The RMS error for all state variables and acceleration time responses are summed and the method yielding the lowest resultant RMS error for the two maneuvers not used in the identification is selected as the optimum method. The resultant RMS error for the four maneuvers used in the identification is used as a secondary check for selecting the optimum method.

Results Using the Ten Methods

The ten methods of Table 6 were used to obtain stability derivatives from the four maneuvers of CH-53A flight test data previously presented. Table 8 presents the values of the identified stability derivatives while Table 9 presents the identified control derivatives. The time history comparisons of the ten methods investigated are presented in Volume II with the exception of the method found to be most accurate. The ten methods are presented in the following figures:

Method	Volume	Figure
1 & 7	II	24-29
2 & 8	II	30-35
3 & 9	II	36-41
4	II	42-47
5	II	48-53
6	II	54-59
3 & 10	I	27-32

The Most Accurate Method

The most accurate method was chosen by computing the RMS error between the test data (Kalman filtered) and the output of the identified derivative model. This was done for data used in the identification and data not used in the identification. The results are shown in Table 10. Table 10 shows that Method 10 yields the smallest RMS error for both data used in the identification and data not used in the identifications.

Table 10 clearly indicates the improvement made with the Kalman Filter when using the least square estimator (Method 1, 2 and 3). Also the Kalman Filtered data gives superior results when using the MLE with the arbitrary

initial derivative guess (Method 4, 5 and 6). Contrary to the above, the Kalman Filter did not yield the best result when using the MLE with the least square initial derivative guess. The best result according to the RMS criteria used was obtained with the digital filtered data into the MLE. This conflicting fact is attributed to two factors. First, the RMS error criterion used does not include the effects of wind gust disturbances and thus can not be expected to yield consistant results when these disturbances are present. Second, the small RMS error difference between Method 9 and Method 10 requires more data to provide statistically consistent results.

It is felt at this stage of the study that the method outlined above (Method 10) is the best approach using the 100 knot data and detailed results of this method are presented below. However, application of both Method 9 and Method 10 to the 150 knot data shows the opposite conclusion; that is Method 9 provides the best result. This will be discussed under the section Application to CH-53A at 150 knots.

The RMS error criteria can not be expected to yield consistant results in the presence of wind gust and for unstable models. This method of evaluation is particularly unsatisfactory for comparing small differences in RMS error. Since both Method 9 and Method 10 yield very close RMS error values the most accurate method could not be clearly identified. At this stage of the study both Method 9 and Method 10 are acceptable even though Method 10 shows a slightly improved RMS error. Method 10 is selected for the 100 knot CH-53A data.

The results obtained thus lead to the following procedure for the most accurate helicopter derivative identification method.

1. Process the raw data with the Graham digital filter to provide data with zero phase shift and frequency content only pertinent to rigid body response.

2. Process the digital filtered data with the Kalman filter to remove bias error and provide consistent estimate of the state variables.

3. Use these data to obtain the initial derivative guess by the least square estimator (LSE). Modify the derivatives' variance from the LSE by multiplying the variance by a constant factor (multiplication by 100 yields good results).

4. Use the LSE derivatives and modified variance in conjunction with the Digital or Kalman filtered data to obtain optimal derivatives from the Bayesian Maximum Likelihood Estimator (MLE).

One conclusion which is apparent from this study is that the least square estimator (LSE) when used with the Kalman data yields an RMS error nearly as good as Method 9 or Method 10. In fact, the LSE with Kalman data is superior to the MLE with the first order filter. In view of the fact that the LSE requires considerably less computation for solution than the MLE, the LSE may prove to be valuable in studies where computer time is important and particularly when large derivative arrays are required.

IDENTIFICATION OF DERIVATIVES FROM TEST DATA USING THE MOST ACCURATE METHOD

This section discusses in detail the results obtained using the method found most accurate as determined in the last section. Applications to CH-53A data at both 100 knots and 150 knots trim and to the CH-54B data which was supplied by the Army (AAMRDL) are presented.

Application To CH-53A at 100 Knots

The preceeding section discussed the selection of the optimum method and it was found that Method 10 gave the best results. This method is used to obtain the results of this section.

Interpretation of helicopter 6 degree-of-freedom derivatives. - Before proceeding with the evaluation of the identified derivatives it is important to understand precisely how to interpret helicopter derivatives identified from flight test data.

The helicopter 6 degree-of-freedom derivative represents the lumped sum of the rotor contribution and body contribution. The helicopter in actual flight conditions consists of low frequency modes of motion (body D.O.F.) and high frequency modes of motion (rotor D.O.F.). If we choose to represent the helicopter by a 6 D.O.F. model obtained by identification from input/output data, then the identified coefficients represent the lumped contribution of body plus average rotor. This is a different interpretation than the conventional quasi-static derivative which represents the lumped contribution of body plus the rotor in a steady state trim condition. This difference arises because the helicopter/rotor has characteristic motion consisting of more than six degrees of freedom, and the 6 D.O.F. model is a low order approximation to actual flight behavior. The identified 6 D.O.F. model is a better representation than the quasi-static model. The helicopter rotor in flight, being continually excited, is not characterized correctly by static data and thus the body motion is more accurately approximated by the derivative made up of lumped body and average rotor contribution.

The helicopter 6 D.O.F. derivatives can best be interpreted by referring to Figure 33. This figure was obtained from a nonlinear computer helicopter simulation. Figure 33 shows one typical stability derivative obtained from the nonlinear helicopter computer simulation. This derivative, M_p, is obtained by peturbing roll rate (Δp) holding all body variable constant and allowing the rotor to reach a new steady state trim. The resulting pitch acceleration divided by Δp is the conventional quasi-static derivative (i.e. $Mp = \Delta\dot{q}/\Delta p$). A 6 DOF model obtained by using a system identification method is also shown superimposed on Figure 33. It is seen that the 6 DOF identified value represents the body plus average rotor contribution. This behavior occured with nearly all derivatives investigated and thus we conclude that the 6 DOF identified value is a very meaningful quantity although it must be compared to the quasi-static value in the manner outlined above.

Also superimposed on Figure 33 is an identified 9 DOF model derivative value. Perturbing this model results in the dashed line and reduces to a 6 DOF quasi-static derivative value. This figure shows that while the identified 6 D.O.F. derivative lends itself to physical interpretation, it requires at least a 9 DOF model to identify the complete derivative behavior of a helicopter.

The suggested procedure for comparing derivatives identified from flight data with quasi-static derivatives is to multiply the flight identified derivative by a correction factor. The correction factor can be determined from a nonlinear computer simulation set up to duplicate the flight conditions of the vehicle under study. This correction is an approximate method to account for the absence of the rotor degrees of freedom. The correction is as shown below;

$$\text{Quasi-static Derivative} = \text{Flight Identified Derivative} \times \frac{\text{Computer Model Quasi-static Derivative}}{\text{Computer Model Identified Derivative}} \quad *$$

*The computer model Identified Derivative can be approximated by computing the average value over one rotor revolution of time from each derivative time plot (a sample plot is illustrated in Figure 33).

The identified derivatives. - Table 11 shows the values of the identified derivatives from CH-53A flight data (100 knots) using Method 10. These derivatives were presented earlier in Table 8 and Table 9 and are repeated here in a more convenient form. Inspection of the derivative array of Table 11 shows that Mq was identified with a positive sign. This fact is attributed to the a priori derivative value used. Derivative identification from noisy data in general yields nonunique solutions. A reasonably close a priori value must be provided to guarantee convergence to the correct solution.

The derivative values identified in Table 11 represent the body contribution plus average rotor contribution as discussed previously. This is further exemplified in Figure 34 which shows two of the identified derivatives (Lp and Zw) compared against theoretically predicted values. Again the complete derivative variation with time due to a perturbation is shown. The theoretical quasi-static value and 6 DOF identified value is compared. This figure demonstrates quite good correlation. Figure 35 shows Mp compared in an analogous manner and is shown identified with the opposite sign.

Derivative convergence. - One way to access if sufficient data has been used in the identification is to inspect the convergence plots of all stability and control derivatives. Figure 36 shows the derivative Lp obtained using the Bayesian estimator as data is processed from one data point to the next. Four maneuvers of 6 seconds' duration each were processed simultaneously in the identification. Derivative convergence for Lp, $M_{B_{1s}}$ and Mq are shown in Figure 36, Figure 37 and Figure 38 respectively. Two different a priori

derivative values and variance were used in each case; a least square guess and arbitrarily selected values. These curves demonstrate that the amount of data used was sufficient to allow convergence and that the better the initial guess and smaller variance, the faster the convergence. Reference 7 discusses further the implications of derivative convergence.

Characteristic roots. - Although the derivatives obtained from a 6 D.O.F. identification must be interpreted differently than the quasi-static derivatives, the characteristic roots should be nearly the same for both identified and quasi-static derivatives. This assumes the effect of nonlinearities does not cause the time history responses to differ significantly from linearity. Figure 39 shows the characteristic roots obtained from the least square and Bayesian estimated derivatives. This figure demonstrates that the least square method when used with Kalman filtered data yields reasonably good derivative estimates. Figure 40 shows the characteristic roots obtained from the Bayesian identified derivatives compared against those obtained from Sikorsky Aircraft's nonlinear helicopter computer simulation. Correlation is excellent except for the spiral mode and the lateral-to-longitudinal coupling roots. The presence of the high frequency rotor D.O.F. always effect the lateral-to-longitudinal roots, thus we conclude the spiral mode is the only mode which does not show good correlation.

Time response comparison. - The most accurate method for identifying derivatives from the CH-53A at the 100 knot trim condition was discussed in detail previously. This consisted of a least square guess (Method 3) and the Bayesian estimator using digital filtered data (Method 10). The time history comparisons were presented in Figure 27 through Figure 33. Inspection of these figures reveals that generally the time response comparisons of the identified derivative model shows excellent fit to the primary channels associated with each input (i.e. B_{1_s} input shows good fit to longitudinal D.O.F.). The cross response (i.e. B_{1_s} input producing lateral response) generally shows a fair to poor match.) This behavior is due to the fact that only a 6 D.O.F. model is being compared. Generally it requires a higher D.O.F. linear model to yield good correlation to the cross response.

Application To CH-53A At 150 Knots

The method found most accurate (Method 10) was applied to the CH-53A data at 150 knot trim condition. The initial derivative guess was obtained from Method 3 (Least square estimator using Kalman data). The computed RMS error showed considerably lower RMS error for the LSE than for the MLE (Method 10) The LSE (Method 3) and the MLE (Method 10) was found to have RMSvalues of 25.6 and 31.7 respectively. These results are in conflict with the study to determine the most accurate method in the last section. It was previously found that the RMS error for Method 10 was lower than the LSE (Method 3) which was used as the a priori estimate. This was true for both data used in the identification and for data not used in the identification.

Method 9 was then applied to the 150 knot data and the RMS error was found to be 22.7 which is considerably less than both Method 3 (LSE) and Method 10. It was concluded that Method 9 provides the most accurate derivative model for

the 150 knot data. Figure 46 through Figure 49 shows the time response comparison for Method 9. Volume II (Figures 60 through 63) shows the time response comparison of the identified derivative model (Method 2 and Method 10) against the flight test data. Table 12 compares the RMS error in the test data for the three identified derivative models (Method 3, Method 10, and Method 9).

The identified derivatives. - Method 9 was applied to the four 5-second maneuvers (discussed in the section on test data used) of CH-53A data at 150 knots trim condition. Table 13 shows the identified derivative values for the LSE while Table 14 shows the derivative values using the MLE. The derivatives X_u, M_q, and Y_v were identified with positive values and are expected to all have negative signs. This problem was discussed in the section on identification from the CH-53A at 100 knots from flight data and the positive sign is a result of not using a close enough a priori derivative guess.

Derivative convergence. - Figure 41 shows the identified derivative L_p obtained from the MLE (Method 9). The least square guess is shown and the convergence indicates more data could have been used in the identification. The lateral cyclic inputs (roll inputs) are shown applied in the middle and also at the end of the data record. It is clear that the application of the input causes rapid reduction of the uncertainty. It is emphasized that derivative convergence plots for all derivatives should be inspected to ensure enough data has been used in the identification.

Characteristic roots. - Figure 42 shows the characteristic roots obtained from the identified derivatives for both the LSE (Method 3) and the MLE (Method 9). Again the characteristic roots from the LSE are quite close to the MLE roots. Figure 43 shows the characteristic roots identified using the MLE from flight data compared against roots obtained from Sikorsky Aircrafts nonlinear helicopter computer simulation of the CH-53A at 150 knots. The correlation is poor and further examination is necessary. Figure 43 also shows the frequency of the dutch roll roots obtained by visual inspection of the flight data. This can only be done with the pitch AFCS on since the vehicle's motion diverges too rapidly to access the dutch roll because the phugoid roots are unstable. It was found that the presence of the pitch AFCS increases the dutch roll frequency slightly. Excellent agreement of the dutch roll roots from the identified derivatives compared with roots obtained by visual inspection of the test data (AFCS on) is obtained.

An investigation was made to determine which derivatives are the cause of the unstable dutch roll roots. Figure 44 shows the characteristic roots of the identified derivatives when the longitudinal and lateral degrees of freedom are completely decoupled. It can be observed from Figure 44 that the dutch roll roots are now stable indicating coupling as the cause of the instability. Also notice that the phugoid roots are now aperiodic. Thus it is concluded that coupling is the cause of the unstable dutch roll roots and oscillatory phugoid roots which is not predicted using Sikorsky Aircraft's helicopter computer simulation.

Figure 45 shows the characteristic roots of the complete coupled derivative array and the characteristic roots obtained when the derivative N_q is set to zero. The dutch roll roots migrate toward the left half plane. Many other derivatives and derivative pairs were set to zero and the derivative N_q was found to have the most influence on the dutch roll instability.

Time response comparison. - The four maneuvers used in the identification were discussed in a previous section. Figure 46 through Figure 49 show the time history comparison of the identified derivative models using Method 3 and Method 9 against the CH-53A, 150 knot flight data. The time history match is considered a good fit. Discrepancies are apparent, however they are due mainly to (1) the larger number of degrees of freedom not modeled and (2) the highly unstable roots which cause the resimulated derivative model to diverge from the data even with perfectly identified derivatives. This second fact is discussed in detail in Appendix D.

Application To CH-54B At 45 Knots

Using four maneuvers of 6 seconds' duration each. - Method 9 is considered the most accurate method for obtaining helicopter derivatives. Method 9 is selected for identifying derivatives from the CH-54B data because the RMS error obtained for the 150 knot CH-53A data was approximately 40% lower than that of Method 10, whereas for the 100 knot case Method 10 was only slightly better than Method 9. This method was applied to four maneuvers of CH-54B data supplied by AAMRDL Langley Research Center. The data was found to yield considerably different trim conditions and the identified derivative model obtained was considered a poor estimate of the characteristic motion due to the inconsistant trims selected. These maneuvers were selected primarily because all control inputs were excited and good excitation could not be found in any other segments of data. Volume II (Figure 64 through Figure 67) shows the time response comparison for the four maneuver case. Table 15 and Table 16 shows the identified derivatives using the LSE (Method 3) and the MLE (Method 9). Since the four maneuver case represents an unacceptable run due to the poor trims, a second case consisting of one long data record was made.

Using one maneuver of 16 seconds duration (Arbitrary selection of derivative variance). - Method 9 was applied to one long data record of CH-54B data which was discussed previously. Method 9 consists of (1) Kalman filtering the data, (2) obtaining an initial derivative estimate with the LSE, (3) modifying the derivative variance obtained from the LSE and (4) inputing this into the MLE to obtain final derivative estimates. Step (3) above was accomplished by arbitrarily multiplying all derivative variances by a constant factor (a value of 100 was found to yield the best results). Since in general the best variance to use is dependent on the particular problem under study, a different approach was used for selecting this variance. This was obtained by observing the derivatives and variance from the LSE and using engineering judgement to appropriately modify the derivative variance. (This method is called Method 11). Table 17 shows the identified derivatives using the LSE. Table 18 shows the 1 sigma uncertainty obtained from the least square estimator after multiplication by 10 and the value selected using engineering judgement.

Method 11 was used with the derivative variance selected by engineering judgement (Table 18) to obtain MLE derivatives. These derivatives are presented in Table 19 and the time history response comparison is presented in Volume II (Figure 68). This figure requires further elaboration. Because the characteristic roots of the identified model are unstable the identified derivative model when compared to the test data diverges in proportion to the unstable roots. Figure 68 (Volume II) thus is reinitialized after each 4 seconds because of this divergence. This divergence is discussed in detail in Appendix D. The time history comparison shows that the MLE derivative model yields a larger fit error than the LSE derivative model. This is a direct result of using too large an initial derivative variance. This problem is corrected by reducing the magnitude of the derivative variance. Selecting too large a derivative variance causes the MLE to effectively ignor the a priori derivative estimate and weight heavily the data being processed. Thus a longer data record is needed to cause proper derivative convergence.

Using one maneuver of 16 seconds duration (Optimum selection of derivative variance). - Examination of the initial derivative variance led to the conclusion that too large a value was used. A second run was made with derivative variances divided by four (This is called Method 12). The resulting MLE derivatives are shown in Table 20. The time history comparison of the LSE model, MLE model and test data is shown in Figure 50. It is clear from this figure that the MLE model is now superior to the LSE model.

Derivative convergence plots were obtained for all 60 stability and control derivatives using Method 12. Figure 51 presents the complete set of derivative convergence plots. It can be seen from Figure 51 that most of the derivatives have converged to within an acceptable engineering variance.

Examination of the derivatives yields the conclusion that the collective and tail rotor control derivatives are different than what analytic prediction would show. This difference is a direct result of linearly dependent control inputs. Since the tail rotor input is coupled to collective stick through the mixing box, collective inputs cause proportional tail rotor inputs which are linearly dependent. The tail rotor was not excited independently with sufficient magnitude to remove this linear dependence. Linear dependent inputs do not in general cause errors in the other derivatives or effect the time rssponse.

The characteristic roots from the identified derivative model (Method 12) were obtained. The roots are presented in Figure 52 and demonstrate a highly unstable phugoid pair and an unstable spiral mode.

RECOMMENDED PROCEDURE FOR OBTAINING STABILITY DERIVATIVES FROM FLIGHT DATA

The results obtained to date in helicopter derivative identification indicate that flight test data should meet specified requirements for accurate identification. This conclusion is based upon the experience gained from applications to computer simulations, CH-53A flight data at 100 and 150 knot trim conditions and CH-54B flight data. A set of guidelines and recommended procedures is given below which should be followed in order to obtain data which is suitable for 6 degree-of-freedom derivative identification.

Preflight Considerations

Instrumentation.- The instrumentation which should be included in the flight test vehicle is listed below.

Attitude Gyros; Roll, Pitch, Yaw.

Rate Gyros; Roll, Pitch, Yaw

Angular Accelerometers; Roll, Pitch, Yaw

Airflow Measurements; Airspeed, Angle of Attack, Sideslip

Linear Accelerometers; Longitudinal, Lateral, Vertical

Control Inputs; Longitudinal Cyclic, Lateral Cyclic, Main Rotor Collective, Tail Rotor Collective.

The control input measurements should be made as close to the actual aerodynamic surface as is possible. Primary control servo or secondary servos are most desirable with stick inputs considered acceptable but less desirable. Compound or unconventional vehicles will require different and additional control input measurements.

The identification of derivatives from the hover regime would benefit with the inclusion of instrumentation designed to measure rotor downwash vector or other suitable airspeed information and is recommended where possible.

Redundant instrumentation will always improve the identification accuracy and is recommended whenever the added weight and expense is justified. Redundant linear accelerometers and/or airflow instrumentation would be the most beneficial in terms of improved accuracy.

Sampling rate.- Sufficient sampling rate should be employed to avoid sampling errors (aliasing) and to allow for identification of rigid body short period dynamics. Fifty to one hundred samples per second is recommended. This sample rate is required to keep the numerical computation in the algorithm accurate.

Filtering of data before sampling.- Standard hardware filters (Butterworth, 3rd order low pass, etc.) are generally used on the data before sampling.

A high cutoff frequency is desirable since it eliminates excessive phase shift near rigid body modes. Typically 10 cps to 25 cps filters are recommended. Additionally, a high cutoff frequency allows automatic determination of noise statistics from the data as discussed in this report.

Data storage.- Magnetic tape is the most convenient format for data storage. This is particularly true for processing large amounts of flight data.

Wind gusts.- The presence of wind gusts degrades the accuracy in the identified derivatives. Generally the larger the magnitude of wind gust present, the longer the data records required to average out their effects to achieve the accuracy attainable without gusts. For this reason it is recommended that the flights take place during days of negligible gust or when this is not possible sufficiently long data records should be used to properly identify the derivatives.

Flight Testing Procedure

There are four key requirements that the pilot of the test aircraft must meet in order to obtain proper data for identification; (1) obtain good initial trims, (2) exercise the input controls to excite all modes; (3) obtain data records long enough to yield sufficient information for accurate identification and (4) keep the vehicles motion resonably close to the initial trim to stay within a linear, small perturbation region. Each of the above four requirements is necessary to obtain accurate derivatives. These requirements will be discussed in detail with the aid of Figure 53 which gives instructions as to typical pilot inputs which will yield data suitable for identification.

Aircraft trims.- Since the stability derivative model represents the characteristic motion of the test aircraft about a trim condition, it is important to properly trim the aircraft before the start of a maneuver. At least 5 seconds duration of stick input excitation should be made to clearly identify a trim condition (the longer the better). Figure 53 shows this trimming time segment at the start of the data record for a single maneuver identification. When using discrete segments of data (i.e. the multimaneuver identification) the same initial trims for each maneuver must be obtained by the pilot. This includes stick positions as well as V, β, α ,ϕ and θ.

Pilot inputs.- After the initial trim period the first pilot input can be conducted. Figure 53 shows typical good inputs for identification corresponding to time t = 0 for the longitudinal cyclic. While this input is exercised all other controls should be held at their trim. The longitudinal cyclic is a doublet which is positive for ½ second then switched to negative for ½ second and then returned to trim for 1 second. The next several seconds (2 to 5 seconds) are used to bring the aircraft back to the original trim. All inputs are exercised in accomplishing this. This trim should be approximately the same as the starting trim (i.e. all stick positions and V, α, β, ϕ ,θ). The doublet input allows (1) good excitation of the modes while the "return to trim" portion ensures the small perturbation assumption is not violated, (2) provides additional excitation of the modes of the system and (3) retrims the aircraft for the next input (Lateral Cyclic). The above procedure (i.e. doublet

then retrim) is then repeated for lateral cyclic, rudder and collective inputs respectively as shown in Figure 53. Thus all controls have been exercised both individually and collectively for approximately 20 seconds. The aircraft is now at its original trim and the pilot should now fly the aircraft about this trim, exercising all control inputs as shown in Figure 53. Switching inputs (i.e. sharp edge pulse type inputs) generally provide the best information for identification and these should be used where possible when retrimming and flying about a trim.

Figure 53 is intended to be only a guide for generating flight test data. The time scale shown may not be realistic for all vehicles and thus only represents an example. The switching type inputs also represent an ideal input which is only an approximation.

Length of Maneuver. - The maneuver of Figure 53 is considered, heuristically, the most desirable and the pilot should use this figure as a guide to generating data for derivative identification. Figure 53 shows about 30 seconds of data used. This should yield sufficient data for identification as shown by the studies in this report. Alternately discrete segments could be used in the identification but this requires excellent initial trims for each individual maneuver.

Factors Effecting Accuracy

Three important influences which adversely effect the accuracy of the identified derivatives are 1) nonlinearities, 2) poor quality data and, 3) improper a priori derivative estimate. The nature of these influences are as follows:

1. Nonlinearities are not modeled as part of the identification and thus they tend to bias some of the identified derivatives from their expected value. It is thus important to keep the aircraft near the trim condition to minimize the nonlinear effect.

2. Poor quality data caused by either poor instrumentation or significant wind gust can effect the accuracy of the identified derivatives. Every effort should be made to use as good instrumentation as is considered practical and flights should be conducted during days of calm air. When these conditions are not met, the use of long data records can offset to some degree these effects.

3. An a priori derivative estimate and variance is required to initialize the Bayesian maximum likelihood derivative estimation method used in this report. The a priori derivative variance must be chosen large enough so that false convergence does not occur but not so large that long data records are required for convergence to an accurate identification. A good a priori derivative estimate is considered important when only short data records are available or when other influences such as nonlinearities and poor quality data as discussed above deteriorate the identification. A good a priori derivative guess will tend to offset the bias introduced in the identified derivatives due to nonlinearities and poor quality data.

An accurate a priori guess is very important for obtaining accurate derivatives. Since derivative identification from noisy data in general has a nonunique solution, a close guess must be provided to guarantee convergence to the correct solution. This is often true with the pitch derivatives Mq and Mw. Often Mq would take on a positive value and M_w a negative valve which is just the opposite from what analytical prediction would show. This uniqueness problem is eliminated by providing a accurate initial derivative guess and uncertainty in the guess.

Interpretation of Identified Derivatives

Helicopter 6 degree-of-freedom (DOF) derivatives identified from flight data are found to differ from conventional quasi-static derivatives. This difference is because the helicopter has additional rotor degrees of freedom which cause the rotor/vehicle to fly differently than a 6 DOF quasi-static model would predict. The conclusions obtained regarding interpretation of derivatives identified from flight data are summarized as follows:

1. Helicopter 6 DOF derivatives as defined in this report represent the lumped contribution of the body plus rotor. The quasi-static derivatives assume that the rotor instantaneously follows the rigid body motion and, thus, the rotor contribution neglects rotor dynamic effects. System identified derivatives are found to consist of the time averaged rotor contribution over one rotor revolution and thus includes an average rotor contribution.

2. Correlation of derivatives identified from flight data vs. analytic computer generated derivatives must take into account the considerations discussed in 1) above. If a nonlinear computer model is used, correlation with flight identified derivatives can be made directly from the nonlinear computer model, since derivatives which consist of the body contribution and the time averaged rotor contribution can be obtained from the computer model.

3. Six DOF identified derivatives yield characteristic roots which can be directly compared against roots from quasi-static derivatives (i.e. the phugoid, dutch roll, spiral and longitudinal drag characteristic roots). The coupled longitudinal-to-lateral roots are generally affected by rotor dynamics and thus cannot be directly compared.

Procedure To Identify Derivatives

The derivative identification procedure found to be most accurate in this study consists of a) filtering the data with a Kalman filter formulated to remove bias error and minimize random error while not identifying derivatives, b) using least square identified derivatives for the a priori estimate and c) obtaining final derivative estimates using the Bayesian maximum likelihood estimator (MLE). This procedure is shown in block diagram form in Figure 54.

The overall procedure which should be followed when attempting 6 DOF derivative identification from helicopters is outlined below.

1. When flight testing helicopters for derivative identification, the preflight considerations and flight testing procedure discussed in the preceeding sections should be followed. Clearly defined initial trims, continuously switched inputs (primarily pulse type), long data records and small deviations from the selected trim condition are considered important to successful identification.

2. The data should be filtered with the Kalman filter to remove bias error and reproduce all state variables with minimum uncertainty.

3. An a priori derivative guess should be obtained using the least square estimator. This guess should be modified as required. (Modification will be required if nonlinearity is present in the data or if poor quality data is obtained due to poor instrumentation or due to the presence of significant wind gusts.) The variance as computed by the LSE is always computed too small and should either be multiplied by a constant factor or selected using engineering judgement.

4. Derivatives can be obtained from the Bayesian MLE using the Kalman filtered data and the a priori derivative estimate and variance determined in step 3. Derivative convergence from the MLE should be plotted and inspected to ensure sufficient data lengths have been used to yield the required accuracy in the derivatives. If the required accuracy has not been achieved the final derivative estimates and variance may be used to reinitialize the MLE and a second pass over the same data (or new data) can be made.

5. After derivative convergence has occurred the identified derivative model should be resimulated against both the data used in the identification and data that was not used in the identification (if available) to test the validity of the identified model. This time history comparison is usually valid for only 4 to 6 seconds length due to the unstable characteristic roots associated with most helicopters. The time history match for the six degree-of-freedom model compared against the test data may show error in some cases. This error is often attributed to the rotor degrees of freedom and unstable characteristic roots and is generally not attributed to the identified derivatives.

CONCLUSIONS

Analysis and applications of the Bayesian approach to identification of stability derivatives from helicopter flight data have led to the following conclusions:

1. Six, degree-of-freedom stability and control derivative identification from flight test data is a feasible method for obtaining and evaluating the stability characteristics of helicopters.

2. Six degree-of-freedom derivatives identified from flight data were found to represent the combined body plus time averaged rotor contribution over one rotor revolution. This is an approximate representation and differs from the conventional quasi-static derivative interpretation, which assumes that the rotor instantaneously follows the rigid body. The system identified and quasi-static derivatives both yield nearly the same low frequency characteristic roots. Differences appear only in the high frequency coupled longitudinal to lateral roots.

3. The procedure that yields the most accurate derivatives is as follows: a) filter the data with a zero phase shift digital filter to remove high frequency content followed by a Kalman filter to remove bias error and obtain consistency of data, b) obtain an a priori derivative estimate and variance with a least squares estimator, c) modify this derivative estimate and variance to reflect a priori knowledge more accurately, and d) obtain final derivative estimates using the Bayesian maximum likelihood method.

4. The least square estimator, when used with the Kalman filtered data, was shown to yield a time history match nearly as accurate as the Bayesian method described in 3) above. Since the least square estimator is computationally much more efficient than the Bayesium method, this approach deserves consideration for those problems where computer time is important.

5. Factors that adversely influence the accuracy of the identified derivatives are: nonlinearities, poor initial trims, poor quality data, incorrect a priori derivative estimate and variance in the estimate, wind gust disturbances, insufficient data lengths, and improper pilot control input excitation. Each of these factors can be overcome or minimized to achieve accurate derivative identification.

6. An accurate a priori derivative estimate must be used to ensure convergence to the correct derivative value. Failure to provide an accurate a priori estimate will result in identified derivatives which do not represent the correct physical derivative value, however, the characteristic roots in general should provide the correct modes of the system.

7. Characteristic roots and time history response provide a useful test of the accuracy of the identified derivatives. Errors in the time response match are caused by higher degrees of freedom, wind gust disturbance, initial condition errors, control input trim errors, and errors in the identified derivatives. An identified derivative model with unstable characteristic roots will diverge in the time response match even with perfectly identified derivatives.

8. Results obtained to date in helicopter derivative identification from flight data indicate that this approach will play an increasing role in understanding the coupling effects and stability characteristics of present helicopters.

The list of specific conclusions presented below are a result of stability derivative identification from the CH-53A and CH-54B helicopters (AFCS off).

CH-53A 100 kts

1. The CH-53A at 100 knots trim and aft C.G. shows stable dutch roll, unstable phugoid and a slightly unstable spiral divergent mode as determined from the identified derivatives. Inspection of independent test data reveals the above characteristic roots to be correctly identified.

2. Correlation of characteristic roots identified from flight data vs. roots obtained from Sikorsky Aircraft's General Helicopter simulation program shows excellent agreement except for the spiral mode.

3. The identification of derivatives from CH-53A data confirms the lumped interpretation (body plus average rotor), shows generally good agreement against theoretically predicted values for those derivatives compared and yields what are believed to correct characteristic roots.

CH-53A 150 kts

1. The CH-53A at 150 knots trim and aft C.G. shows unstable dutch roll, unstable phugoid and stable spiral mode as determined from the identified derivatives. Visual inspection of independent test data confirms the unstable dutch roll roots.

2. Discrepancies are found to exist between characteristic roots identified from flight data vs. roots obtained from analytic prediction. Analytic prediction shows aperiodic phugoid and stable dutch roll roots while identification from flight data reveals oscillatory phugoid and unstable dutch roll.

CH-54B 45 kts

1. Identification of one long data record was found to yield better results than four short segments. This was primarily due to the different initial trims for the four segments.

2. The identified derivatives were found to yield unstable phugoid and unstable spiral mode.

3. Time history comparison of the derivative model against test data shows good results and clearly shows the unstable error divergence due to the unstable phugoid roots.

RECOMMENDATIONS

The procedure developed in this report for six degree-of-freedom stability derivative identification has had only limited actual application. The potential achievable from helicopter derivative identification remains to be realized. The following areas of application can provide for cost reductions, better aircraft designs, and further understanding of the stability characteristics of present day helicopters.

1. Use identified derivatives to reduce flight test AFCS development time and to achieve superior handling qualities characteristics through improved design.

2. Use derivative identification during initial flight tests of prototype aircraft to assess and locate any flight dynamic problems.

3. Use derivative identification to expand the flight envelope of present and new aircraft.

4. Use derivative identification as support in upgrading analytic prediction methods so that future aircraft can be designed more accurately.

To progress toward the above goals, it is essential to pursue applications and continue developments and refinements of derivative identification. New developments in low speed airspeed instrumentation, automatic instrumentation trimming, and redundant instrumentation are some refinements that could be made. The need to separate rotor degrees-of-freedom effects from body degrees of freedom requires 9 or 12 DOF identification. The same analytic methods developed in this report apply to this problem with minor modifications. Continued research in this area can provide for total flight dynamic derivative correlation.

The following specific areas are recommended for further research:

1. Development and application of a computationally efficient algorithm for identification of 9 and 12 DOF models. For the articulated rotor helicopter, this allows body, tip-path-plane, and lag DOF. The methods developed in this report are applicable to this problem with slight modifications.

2. Incorporation of the fixed interval smoothing solution to yield gust and initial condition identification. Improved derivative estimates can then be obtained on the second pass, using the estimated gusts as additional inputs and using the estimated initial conditions.

APPENDIX A

THE BAYESIAN MAXIMUM LIKELIHOOD ESTIMATOR

The equations used for the MLE are presented in equation (7) and equation (8) of the text. The symbols and terms used in these equations will be presented here.

The system equations for a single maneuver are defined in equation (1) and equation (2), the state and parameter vector defined in equation (3) and the state veriable form is given by equation (4). For the multi-maneuver case the vector function $f(\underline{X}, \underline{X}_p)$ is defined in equation (1a) for 4 maneuvers.

$$f(\underline{X}, \underline{X}_p) = \begin{bmatrix} f_1(\underline{X}_1, \underline{X}_p) & 0 & 0 & 0 \\ 0 & f_2(\underline{X}_2, \underline{X}_p) & 0 & 0 \\ 0 & 0 & f_3(\underline{X}_3, \underline{X}_p) & 0 \\ 0 & 0 & 0 & f_4(\underline{X}_4, \underline{X}_p) \end{bmatrix} \tag{1a}$$

For the 4 maneuver case the definitions given below are made, where the subscript pertains to the particular maneuver number.

$$\underline{X} = \begin{bmatrix} \underline{X}_1 \\ \underline{X}_2 \\ \underline{X}_3 \\ \underline{X}_4 \end{bmatrix} \qquad \underline{Z} = \begin{bmatrix} \underline{Z}_1 \\ \underline{Z}_2 \\ \underline{Z}_3 \\ \underline{Z}_4 \end{bmatrix} \tag{2a}$$

$$R = \begin{bmatrix} R_1 & 0 & 0 & 0 \\ 0 & R_2 & 0 & 0 \\ 0 & 0 & R_3 & 0 \\ 0 & 0 & 0 & R_4 \end{bmatrix} \qquad Q = \begin{bmatrix} Q_1 & 0 & 0 & 0 \\ 0 & Q_2 & 0 & 0 \\ 0 & 0 & Q_3 & 0 \\ 0 & 0 & 0 & Q_4 \end{bmatrix} \tag{3a}$$

$$A_{11} = \begin{bmatrix} \frac{\partial f_1}{\partial X_1} & 0 & 0 & 0 \\ 0 & \frac{\partial f_2}{\partial X_2} & 0 & 0 \\ 0 & 0 & \frac{\partial f_3}{\partial X_3} & 0 \\ 0 & 0 & 0 & \frac{\partial f_4}{\partial X_4} \end{bmatrix} \qquad A_{1p} = \begin{bmatrix} \frac{\partial f_1}{\partial X_p} \\ \frac{\partial f_2}{\partial X_p} \\ \frac{\partial f_3}{\partial X_p} \\ \frac{\partial f_4}{\partial X_p} \end{bmatrix} \tag{4a}$$

Expansion of the partial derivatives in equation (4a) results in the matricies in the following pages.

MATRIX $A = \frac{\partial \underline{f}_i}{\partial \underline{X}_i}$, (i represents maneuver number)

$$A = \begin{bmatrix}
a_{11} & a_{12} & 0 & 0 & 0 & 0 & 1 & a_{18} & a_{19} \\
a_{21} & 0 & 0 & 0 & 0 & 0 & 0 & a_{28} & a_{29} \\
a_{31} & a_{32} & 0 & 0 & 0 & 0 & 0 & a_{38} & a_{39} \\
a_{41} & 0 & 0 & X_{p1} & X_{p7} & X_{p13} & X_{p19} & X_{p25} & X_{p31} \\
a_{51} & a_{52} & 0 & X_{p2} & X_{p8} & X_{p14} & X_{p20} & X_{p26} & X_{p32} \\
a_{61} & a_{62} & 0 & X_{p3} & X_{p9} & X_{p15} & X_{p21} & X_{p27} & X_{p33} \\
0 & 0 & 0 & X_{p4} & X_{p10} & X_{p16} & X_{p22} & X_{p28} & X_{p34} \\
0 & 0 & 0 & X_{p5} & X_{p11} & X_{p17} & X_{p23} & X_{p29} & X_{p35} \\
0 & 0 & 0 & X_{p6} & X_{p12} & X_{p18} & X_{p24} & X_{p30} & X_{p36}
\end{bmatrix}$$

$$a_{11} = (-r\sin\phi + q\cos\phi) \cdot \tan\theta$$

$$a_{12} = (r\cos\phi + q\sin\phi) \cdot \sec^2\theta$$

$$a_{18} = \tan\theta \sin\phi$$

$$a_{19} = \cos\phi \tan\theta$$

$$a_{21} = -q\sin\phi - r\cos\phi$$

$$a_{28} = \cos\phi$$

$$a_{29} = -\sin\phi$$

$$a_{31} = (-r\sin\phi + q\cos\phi) / \cos\theta$$

$$a_{32} = (r\cos\phi + q\sin\phi) \cdot \tan\theta \cdot \sec\theta$$

$$a_{38} = \sin\phi/\cos\theta$$

$$a_{39} = \cos\phi/\cos\theta$$

$$a_{41} = -g\cos\theta$$

$$a_{51} = +g\cos\theta\cos\phi$$

$$a_{52} = -g\sin\phi \cdot \sin\theta$$

$$a_{61} = -g\cos\theta \cdot \sin\phi$$

$$a_{62} = -g\cos\phi \cdot \sin\theta$$

MATRIX $F = \frac{\partial f_i}{\partial \underline{X}_p}$, (i represents maneuver number)

All elements of F are zero except as defined below.

$F_{41} = \delta V_x$ $F_{47} = \delta V_y$ $F_{4,13} = \delta V_z$ $F_{4,19} = \delta p$

$F_{52} = \delta V_x$ $F_{58} = \delta V_y$ $F_{5,14} = \delta V_z$ $F_{5,20} = \delta p$

$F_{63} = \delta V_x$ $F_{69} = \delta V_y$ $F_{6,15} = \delta V_z$ $F_{6,21} = \delta p$

$F_{74} = \delta V_x$ $F_{7,10} = \delta V_y$ $F_{7,16} = \delta V_z$ $F_{7,22} = \delta p$

$F_{85} = \delta V_x$ $F_{8,11} = \delta V_y$ $F_{8,17} = \delta V_z$ $F_{8,23} = \delta p$

$F_{96} = \delta V_x$ $F_{9,12} = \delta V_y$ $F_{9,18} = \delta V_z$ $F_{9,24} = \delta p$

$F_{4,25} = \delta q$ $F_{4,31} = \delta r$ $F_{4,37} = \delta B_{ls}$ $F_{4,43} = \delta A_{ls}$

$F_{5,26} = \delta q$ $F_{5,32} = \delta r$ $F_{5,38} = \delta B_{ls}$ $F_{5,44} = \delta A_{ls}$

$F_{6,27} = \delta q$ $F_{6,33} = \delta r$ $F_{6,39} = \delta B_{ls}$ $F_{6,45} = \delta A_{ls}$

$F_{7,28} = \delta q$ $F_{7,34} = \delta r$ $F_{7,40} = \delta B_{ls}$ $F_{7,46} = \delta A_{ls}$

$F_{8,29} = \delta q$ $F_{8,35} = \delta r$ $F_{8,41} = \delta B_{ls}$ $F_{8,47} = \delta A_{ls}$

$F_{9,30} = \delta q$ $F_{9,36} = \delta r$ $F_{9,42} = \delta B_{ls}$ $F_{9,48} = \delta A_{ls}$

$F_{4,49} = \delta\theta_T$ $F_{4,55} = \delta\theta_c$

$F_{5,50} = \delta\theta_T$ $F_{5,56} = \delta\theta_c$

$F_{6,51} = \delta\theta_T$ $F_{6,57} = \delta\theta_c$

$F_{7,52} = \delta\theta_T$ $F_{7,58} = \delta\theta_c$

$F_{8,53} = \delta\theta_T$ $F_{8,59} = \delta\theta_c$

$F_{9,54} = \delta\theta_T$ $F_{9,60} = \delta\theta_c$

The preceding equations along with equation (1), (2), (3), (7) and (8) of the text comprise the Maximum Likelihood Estimator.

APPENDIX B

THE INITIAL DERIVATIVE GUESS USING LEAST SQUARE ESTIMATION

The MLE as presented in the report requires an initial derivative guess and variance in the guess. An accurate guess helps keep the linearizations required in the algorithm valid and permits the use of less data to obtain the desired accuracy. This latter point is important due to the dimensionally large problem for 6 degree-of-freedom identification and reduces computer time for a solution. It is for these reasons that considerable effort is expended in obtaining a close initial derivative guess.

It is well known that the LSE provides estimates for the derivatives which are biased whenever measurement noise is present. Also the variance in the estimate tends to be smaller then is actually the case. In addition the presence of process noise causes further error in the variance.

The use of a digital filter followed by a Kalman filter before using the least square estimator minimizes the error due to measurement noise and provides a good derivative initial estimate. The variance is still too small and must be increased to approximate more accurately the uncertainty in the derivative estimate.

This section presents the development of the LSE which is used to initialize the MLE. The development allows processing of more than one maneuver and permits the use of a priori derivative information.

The differential equations of motion including the derivatives to be identified are given in equations (1) of this report. When using these equations with the LSE only the unknown derivatives are required thus all known quantities are placed on the left of the equal sign and the derivative terms on the right. The equation containing longitudinal acceleration is repeated below in this form.

$$\dot{V}_x - V_{xo} + g\sin\theta = \frac{\partial X}{\partial V_x}\delta V_x + \frac{\partial X}{\partial V_y}\delta V_y + \ldots\ldots \qquad (1b)$$

Let all terms on the left of the equal sign be equal to Z', the perturbation state variables and control inputs equal the vector $\underline{Z}$ and all derivatives in equation (1b) equal the vector $\underline{p}$.

Thus equation (1b) can be written as

$$Z'_j = \underline{p}^T \cdot \underline{Z}_j \qquad (2b)$$

where; $j = 1, 2 \ldots$. n-maneuvers

Equation (2b) is in the form required for the LSE. The subscript j implies this equation holds for each maneuver j.

The problem is to determine the parameter vector $\underline{p}$ which minimizes the least square performance index of equation (3b).

$$J = \sum_{j=1}^{n} \int_{o}^{t_f} (Z'_{m_j} - Z'_j)^2 W_j^{-1} \, dt + (p_o - p)^T W_o^{-1} (p_o - p) \qquad (3b)$$

where;

Z'_{m_j} represents the terms to the left of the equal sign in equation (1b) with the measured data substituted for θ and V_x.

Z'_j is defined in equation (2b)

j denotes the maneuver number

W_j is the noise intensity of $\underline{Z}'_{m_j}$

$\underline{p}$ represents the true parameters to be identified

W_o represents the covariance of the initial parameter estimate $\underline{p}_o$

Equation (3b) takes on a minimum value by setting to zero the gradient of J with respect to $\underline{p}$ and solving the resulting simultaneous equations for $\underline{p}$.

The resulting solution for p is given in equation (4b) and is repeated for each row of derivatives.

$$\hat{\underline{p}} = \left(W_o^{-1} + \sum_{j=1}^{n} \int_{o}^{t_f} \underline{Z}_j \, W_j^{-1} \, \underline{Z}_j^T \, dt\right)^{-1}. \qquad (4b)$$

$$\left(W_o^{-1} \, p_o + \sum_{j=1}^{n} \int_{o}^{t_f} \underline{Z}_j \, W_j^{-1} \, Z'_{m_j} \, dt\right)$$

If no a priori information is available W_o approaches ∞ and $W_o^{-1} = 0$. Also replacing integrals by summations results in the discrete equation (5b).

$$\hat{\underline{p}} = \left(\sum_{j=1}^{n} \sum_{k=1}^{K} \underline{Z}_j(k)\, \underline{Z}^T(k) \right)^{-1} \cdot \left(\sum_{j=1}^{n} \sum_{k=1}^{K} \underline{Z}_j(k)\, Z'_{m_j}(k) \right) \quad (5b)$$

where; k represents the data sample number.

Equation (5b) was used throughout this study to obtain the least square derivative estimate.

The covariance of the derivative estimate is just the inverted matrix of equation (4b). Since the noise intensity W_j^{-1} is not usually known before hand, this quantity can be determined approximately by the fit error between the measured data $\underline{Z}'_{m_j}$ and $\underline{p}^T \underline{Z}_m$ as in equation (6b) for the discrete case.

$$W'_j = \frac{1}{n} \sum_{j=1}^{n} \cdot \frac{1}{K} \sum_{k=1}^{K} \left(Z'_{m_j}(k) - \hat{\underline{p}}^T \underline{Z}_m(k) \right)^2 \quad (6b)$$

The covariance of the parameter estimate is then given by equation (7b).

$$\mathrm{COV}\left(\hat{\underline{p}} - \underline{p} \right) = W'_j \cdot \left(\sum_{j=1}^{n} \sum_{k=1}^{K} \underline{Z}_j(k)\, \underline{Z}_j^T(k) \right)^{-1} \quad (7b)$$

Equation (7b) was used throughout this study to determine the initial derivative variance.

APPENDIX C

THE DATA FILTERS

(Low Pass, Digital and Kalman)

Low Pass

The Low Pass filter used in this report is simply a first order transfer function converted to discrete form for use on a digital computer. Equation (1c) represents the equation used.

$$w_c = 2\pi f_c$$

$$y^k = (1 - \Delta t \cdot w_c)\, y^{k-1} + (\Delta t \cdot w_c) \cdot Z^k \qquad (1c)$$

where;

y^k represents the output of the filter

Z^k represents the input data to the filter

f_c is the cutoff frequency

Δt is the time between samples

k represents the data point number

Digital (Graham)

This zero phase shift digital filter used is discussed in Reference 8 in complete detail. The basic weight equation used is given in equation (2c).

$$h(k.\Delta t) = \frac{\pi}{2k.\Delta t} \cdot \frac{(\sin(w_t k\Delta t) + \sin(w_c k\Delta t))}{\pi^2 - (w_t - w_c)^2 (k\Delta t)^2} \qquad (2c)$$

This equation is evaluated for every data point over an interval $-K<k>K$ and then normalized by the sum of all the values. The smoothed output Z'_i for each data point, i, then is obtained by equation (3c).

$$Z'_i = \sum_{k=-k}^{+k} h_k \cdot Z_{(K+k)+i} \qquad i = 1, \ldots, 2K + 1 \qquad (3c)$$

$w_c = 2\pi f_c$, f_c is the cutoff frequency

$w_t = 2\pi f_c$, f_t is the termination frequency

The Kalman Filter

State variable definitions

$X_1 = \phi$

$X_2 = \theta$

$X_3 = \psi$

$X_4 = V_x$

$X_5 = V_y$

$X_6 = V_z$

$X_7 = p$

$X_8 = q$

$X_9 = r$

$X_{10} = \text{bias}_{w_1}$

$X_{11} = \text{bias}_{w_2}$

$X_{12} = \text{bias}_{w_3}$

$X_{13} = \text{bias}_{w_4}$

$X_{14} = \text{bias}_{w_5}$

$X_{15} = \text{bias}_{w_6}$

$X_{16} = \text{bias}_1$

$X_{17} = \text{bias}_2$

$X_{18} = \text{bias}_3$

$X_{19} = \text{bias}_4$

$X_{20} = \text{bias}_5$

$X_{21} = \text{bias}_6$

$X_{22} = \text{bias}_7$

$X_{23} = \text{bias}_8$

$X_{24} = \text{bias}_9$

Measurement definitions

$Z_1 = \phi_m$

$Z_2 = \theta_m$

$Z_3 = \psi_m$

$Z_4 = V_m$

$Z_5 = \beta_m$

$Z_6 = \alpha_m$

$Z_7 = p_m$

$Z_8 = q_m$

$Z_9 = r_m$

Distance to c.g.

l_x - V,β,α	x - distance to c.g.
l_y - V,β,α	y - distance to c.g.
l_z - V,β,α	z - distance to c.g.
l_{x1} - X - Accel	x - distance to c.g.
l_{y1} - X - Accel	y - distance to c.g.
l_{z1} - X - Accel	z - distance to c.g.
l_{x2} - Y - Accel	x - distance to c.g.
l_{y2} - Y - Accel	y - distance to c.g.
l_{z2} - Y - Accel	z - distance to c.g.
l_{x3} - Z - Accel	x - distance to c.g.
l_{y3} - Z - Accel	y - distance to c.g.
l_{z3} - Z - Accel	z - distance to c.g.

Subscripts

cg - center of gravity

I - Instrument

m - measured

The equations used in the Kalman filter are based on the general equations of motion for a rigid body in flight and the equations relating the state variables to the measurements. The equations used to obtain the Kalman filtered data will be presented in this section.

The general equations of motion for a rigid body in flight are

$$
\begin{aligned}
\dot{\phi} &= p + (r\cos\phi + q\sin\phi)\tan\theta \\
\dot{\theta} &= q\cos\phi - r\sin\phi \\
\dot{\psi} &= (r\cos\phi + q\sin\phi)/\cos\theta \\
\dot{V}_x &= V_y\, r - V_z\, q - g\sin\theta + X_{cg} \\
\dot{V}_y &= V_z\, p - V_x\, r + g\sin\phi\,\cos\theta + Y_{cg} \\
\dot{V}_z &= V_x\, q - V_y\, p + g\cos\phi\,\cos\theta + Z_{cg} \\
\dot{p} &= L_{cg} \\
\dot{q} &= M_{cg} \\
\dot{r} &= N_{cg}
\end{aligned}
\tag{4c}
$$

The linear accelerations at the center of gravity can be expressed in terms of the accelerometer instrumentation by equation (5c).

$$
\bar{a}_{cg} = \bar{a}_I - \left[\dot{\bar{\omega}} \times \bar{r} + \bar{\omega} \times (\bar{\omega} \times \bar{r})\right] \tag{5c}
$$

Equation (5c) thus becomes

$$
\begin{aligned}
X_{cg} &= X_I - \left[\dot{q}\, l_{zl} - \dot{r}\, l_{yl} - (q^2 + r^2)\, l_{xl} + q\, p\, l_{yl} + r\, p\, l_{zl}\right] \\
Y_{cg} &= Y_I - \left[\dot{r}\, l_{x2} - \dot{p}\, l_{z2} + p\, q\, l_{x2} - (p^2 + r^2)\, l_{y2} + r\, q\, l_{z2}\right] \\
Z_{cg} &= Z_I - \left[\dot{p}\, l_{y3} - \dot{q}\, l_{x3} + p\, r\, l_{x3} + q\, r\, l_{y3} - (p^2 + q^2)\, l_{z3}\right]
\end{aligned}
\tag{6c}
$$

The angular accelerations at the center of gravity are directly expressed in terms of the angular accelerometers and are given by equation (7c).

$$
\begin{aligned}
L_{cg} &= L_I \\
M_{cg} &= M_I \\
N_{cg} &= N_I
\end{aligned}
\tag{7c}
$$

The accelerometers will in general contain both random errors and bias errors. A good estimate of the actual acceleration can be obtained by filtering the accelerometer measurement with a digital filter and subtracting a constant bias term. Thus the accelerations as read by the accelerometers can be written as

$$
\begin{aligned}
X_I &= w_1 - \text{bias}_{w_1} \\
Y_I &= w_2 - \text{bias}_{w_2} \\
Z_I &= w_3 - \text{bias}_{w_3} \\
L_I &= w_4 - \text{bias}_{w_4} \\
M_I &= w_5 - \text{bias}_{w_5} \\
N_I &= w_6 - \text{bias}_{w_6}
\end{aligned}
\tag{8c}
$$

where; w_i, $i = 1, 2 \ldots 6$ represents process noise and has mean value $\bar{w}_i$; the mean value is obtained by filtering the accelerometers with a digital filter.

Substituting equation (8c) into equation (7c) and equation (6c) and then substituting the result into equation (4c), yields the general system equations for the Kalman filter. Using the state variable notation as defined in the list of symbols, the system equations become

$$
\begin{aligned}
\dot{X}_1 &= X_7 + (X_9 \cos X_1 + X_8 \sin X_1) \tan X_2 \\
\dot{X}_2 &= X_8 \cos X_1 - X_9 \sin X_1 \\
\dot{X}_3 &= (X_9 \cos X_1 + X_8 \sin X_1)/\cos X_2 \\
\dot{X}_4 &= X_5 X_9 - X_6 X_8 - g \sin X_2 - X_{10} + X_{14} l_{z1} - X_{15} l_{y1} \\
&\quad + (X_8^2 + X_9^2) l_{x1} - X_8 X_7 l_{y1} - X_9 X_7 l_{z1} + w_1 - l_{z1} w_5 + l_{y1} w_6 \\
\dot{X}_5 &= X_6 X_7 - X_4 X_9 + g \sin X_1 \cos X_2 - X_{11} + X_{15} l_{x2} - X_{13} l_{z2} \\
&\quad - X_7 X_8 l_{x2} + (X_7^2 + X_9^2) l_{y2} - X_9 X_8 l_{z2} + w_2 + l_{z2} w_4 - l_{x2} w_6
\end{aligned}
\tag{9c}
$$

$$\dot{X}_6 = X_4 X_8 - X_5 X_7 + g\cos X_1 \cos X_2 - X_{12} + X_{13}\, l_{y3} - X_{14}\, l_{x3}$$
$$- X_7 X_9\, l_{x3} - X_8 X_9\, l_{y3} + (X_7^2 + X_8^2)\, l_{z3} + w_3 - l_{y3}\, w_4 + l_{x3}\, w_5$$

$$\dot{X}_7 = -X_{13} + w_4$$

$$\dot{X}_8 = X_{14} + w_5$$

$$\dot{X}_9 = X_{15} + w_6$$

$$\dot{X}_{10} = 0$$
$$"$$
$$"$$
$$"$$
$$"$$
$$"$$

$$\dot{X}_{24} = 0$$

The measurement equations are

$$\phi_m = \phi + \text{bias}_1 + n_1$$

$$\theta_m = \theta + \text{bias}_2 + n_2$$

$$\psi_m = \psi + \text{bias}_3 + n_3$$

$$V_m = (V_{xI}^2 + V_{yI}^2 + V_{zI}^2)^{1/2} + \text{bias}_4 + n_4 \qquad (10c)$$

$$\beta_m = \tan^{-1}(V_{yI}/V_{xI}) + \text{bias}_5 + n_5$$

$$\alpha_m = \tan^{-1}(V_{zI}/V_{xI}) + \text{bias}_6 + n_6$$

$$p_m = p + \text{bias}_7 + n_7$$

$$q_m = q + \text{bias}_8 + n_8$$

$$r_m = r + \text{bias}_9 + n_9$$

where $\begin{bmatrix} V_{xI} \\ V_{yI} \\ V_{zI} \end{bmatrix} = \begin{bmatrix} V_x \\ V_y \\ V_z \end{bmatrix}_{c.g.} + \bar{\omega} \times \bar{r}$ (11c)

Substituting equation (11c) into equation (10c) and rewriting in the state variable notations as defined in the list of symbols results in the measurement equation (12c).

$$Z_1 = X_1 + X_{16} + n_1$$

$$Z_2 = X_2 + X_{17} + n_2$$

$$Z_3 = X_3 + X_{18} + n_3$$

$$Z_4 = (X_4 + X_8 l_z - X_9 l_y)^2 + (X_5 + X_9 l_x - X_7 l_z)^2 + (X_6 + X_7 l_y - X_8 l_x)^{2\ 1/2} + X_{19} + n_4 \quad (12c)$$

$$Z_5 = \tan^{-1} (X_5 + X_9 l_x - X_7 l_z)/(X_4 + X_8 l_z - X_9 l_y) + X_{20} + n_5$$

$$Z_6 = \tan^{-1} (X_6 + X_7 l_y - X_8 l_x)/(X_4 + X_8 l_z - X_9 l_y) + X_{21} + n_6$$

$$Z_7 = X_7 + X_{22} + n_7$$

$$Z_8 = X_8 + X_{23} + n_8$$

$$Z_9 = X_9 + X_{24} + n_9$$

Equation (9c) and equation (12c) are the system and measurement equations respectively and are rewritten below in vector notation.

$$\dot{\underline{X}} = f(\underline{X}, t) + Gw(t) \quad (13c)$$

$$\underline{Z} = h(\underline{X}, t) + \underline{n} \quad (14c)$$

Equation (13c) and (14c) are precisely in the form for use with the extended Kalman filter.

The extended Kalman filter has the solution presented below.

$$\dot{\underline{X}} = f(\underline{X}, t) + G\,\underline{\bar{w}} + P \left.\frac{\partial h}{\partial \underline{X}}\right|^{T}_{\underline{X}} \cdot R^{-1} (\underline{Z} - H(\underline{X})) \tag{15c}$$

$$\dot{P} = \left.\frac{\partial f}{\partial \underline{X}}\right|_{\underline{X}} \cdot P + P \left.\frac{\partial f}{\partial \underline{X}}\right|^{T}_{\underline{X}} + G\,Q\,G^{T} - P \left.\frac{\partial h}{\partial \underline{X}}\right|_{\underline{X}} \cdot R^{-1} \cdot \left.\frac{\partial h}{\partial \underline{X}}\right|^{T}_{\underline{X}} P \tag{16c}$$

The initial conditions are given by

$$\underline{X}(t_o) = \underline{X}_o \tag{17c}$$

$$P(t_o) = P_o \tag{18c}$$

This equation set is solved by forward processing of the data. At the end of the data record an estimate of the bias is available. This bias is then used as initial estimate and equations (15c) and (16c) processed a second time. The state estimates are considerably improved on the second pass.

APPENDIX D

The Unstable Error Variance Equation

After stability derivatives are identified the linear model can be simulated and compared against the flight data. The error between the outputs of the derivative model and the test data is governed by an error equation and error variance equation which has eigenvalues equal to the eigenvalues of the identified derivative. The error variance equation is similar to equation (8) of the text with R^{-1} set to zero. The equation is rewritten below.

$$\dot{P}_{ll} = \overbrace{A_{ll} P_{ll} + (A_{ll} P_{ll})^T}^{\text{Term 1}} + \overbrace{GQG^T}^{\text{Term 2}} + \overbrace{(P_{pl}^T A_{lp}^T)^T + P_{pl}^T A_{lp}^T}^{\text{Term 3}} \qquad (1d)$$

$$\dot{P}_{pl}^T = \underbrace{AP_{pl}^T}_{\text{Term 4}} + \underbrace{A_{lp} P_{pp}}_{\text{Term 5}} \qquad (2d)$$

P_{ll} (to) = Initial State Covariance

Each term in equation (1d) and equation (2d) has the effect indicated below.

Term 1 - The matrix A_{ll} represents the identified stability derivatives. The stability of equation (1d) and equation (2d) depends on the eigenvalues of this matrix.

Term 2 - This term represents the amount of process noise present and acts like a step input to equation (1d).

Term 3 - This term is due to errors in the identified derivatives and acts like an input driving equation (1d).

Term 4 - This term determines the stability of equation (2d).

Term 5 - This term acts like an input driving term to equation (2d). P_{pp} represents the covariance of the identified derivatives.

Interpretation of the error variance equation

The error between the outputs of the identified linear model and the test data is governed by an error equation. The actual error can be established by observing the simulated response. The degree to which we can believe this error (ie the variance in the error) is governed by equation (1d) and (2d). The usefulness of the equation can best be understood by example.

Suppose the derivatives were identified without error . The terms in equation (1d) and (2d) would all go to zero except Term 1 and Term 2. If the matrix A_{11} had stable eigenvalues then errors due to initial conditions should diminish with time and should show perfect correlation of linear model output and test data. If process noise is present there can be an error after transients die out within an error band governed by equation (1d).

If the matrix A_{11} is unstable then the error will diverge and it is expected to be within an error band governed by equation (1d).

The importance of this equation is that it tells us on the average how accurate we should expect the output of the linear model to match the test data. For the case with perfectly identified derivatives and unstable eigenvalues the expected error grows with time; due to initial condition errors and process noise. If there are errors in the identified derivative then this error will be even greater as governed by equation (1d) and (2d).

REFERENCES

1. Taylor, L.W.; Iliff, K.W. and Powers, B.G.: A Comparison of Newton-Raphson and Other Methods for Determining Stability Derivatives from Flight Data. AIAA Third Flight Test Simulation and Support Conference, 1969.

2. Gilyard, G.W.: Flight Determined Derivatives and Dynamic Characteristics of the CV-990 Airplane. NASA TND-6777, May 1972.

3. Chen, R.T.N.; Weingarten, N.; Mesiah, G. and Close, V.: Application of Conjugate Gradient Method to the Estimation of VTOL Aircraft Parameter and State. JACC Preprint, 1970.

4. Sage, A.P. and Melsa, J.L.: System Identification. Academic Press, New York and London, 1971.

5. Chen, R.T.N.; Eulrich, B.J. and Labacqz, J.V.: Development of Advanced Techniques for the Identification of V/STOL Aircraft Stability and Control Parameters. Cornell Aeronautical Laboratory, Inc. CAL Report No. BM-2820-F-1, August 1971.

6. Molusis, J.A.: Helicopter Stability Derivative Extraction and Data Processing Using Kalman Filtering Techniques. Presented at the 28th Annual National Forum of the American Helicopter Society, Washington, D.C., Preprint No. 641, May 1972.

7. Molusis, J. and Briczinski S.: Helicopter Derivative Identification from Analytic Models and Flight Test Data. Presented at NASA Sponsored Symposium; Parameter Estimation Techniques and Applications in Aircraft Flight Testing, Edwards AFB, April 24, 1973.

8. Graham, R.J.: Determination and Analysis of Numerical Smoothing Weights. NASA TR R-179, December 1963.

Table 1. - Calculation of Measurement Noise Statistics for the Kalman Filter

Measurement Number	Measurement Name	Statistics Computed From the Data		Statistics Inputed By the Engineer	
		Measurement Noise Intensity R_i*	Measurement Noise Variance σ^2	Measurement Noise Variance σ^{2}**	Measurement Noise Intensity R_i
1	ϕ	.	.		
2	θ	.	.		
3	ψ	.	.		
4	V	.	.		
5	β	$R_i = \left[\frac{\sigma_2^2 - \sigma_1^2}{\pi(f_2 - f_1)}\right]_i$	$\left[\sigma^2\right]_i = R_i \pi f_c$	$\left[\sigma^2\right]_i$	$R_i = \left[\frac{\sigma^2}{\pi f_c}\right]_i$
6	α		.		
7	p	.	.		
8	q	.	.		
9	r	.	.		

* This quantity is computed from the Data (See Text)

** This quantity is Inputed by the Engineer when not computed from the Data.

Table 2. - Calculation of Process Noise Statistics for the Kalman Filter

NO.	EQUATION EFFECTED BY PROCESS NOISE	STATISTICS COMPUTER FROM THE DATA		STATISTICS INPUTED BY THE ENGINEER	
		PROCESS NOISE INTENSITY Q_i*	PROCESS NOISE VARIANCE σ^2	PROCESS NOISE VARIANCE σ^2**	PROCESS NOISE INTENSITY Q_i
1	Long. Accel.				
2	Lat. Accel.				
3	Vert. Accel.	$Q_i = \left[\frac{\sigma_2^2 - \sigma_1^2}{\pi(f_2 - f_1)}\right]_i$	$\left[\sigma^2\right]_i = Q_i \pi f_c$	$\left[\sigma^2\right]_i$	$Q_i = \left[\sigma^2/\pi f_c\right]_i$
4	Roll Accel.				
5	Pitch Accel.				
6	Yaw Accel.				

* This Quantity Computed from Acceleration Data (see Text)

** This Quantity Inputed by the Engineer when not Computed from the Data.

Table 3. - Calculation of Initial State and Variance For the Kalman Filter

State Variable No.	State Variable Name	Statistics Computed From The Data: Initial State Estimate $\underline{X}$	Statistics Computed From The Data: Variance In Initial State Estimate $P(to)$	Statistics Computed When Measurement Not Available: Initial State Estimate $\underline{X}$	Statistics Computed When Measurement Not Available: Variance In Initial State Estimate $P(to)$
1	ϕ	First Data Point	$P_1 = R_{1\pi}f_c + P_{16}$	Guess the value	Guess the value
2	Θ	First Data Point	$P_2 = R_{2\pi}f_c + P_{17}$	Guess the value	Guess the value
3	ψ	First Data Point	$P_3 = R_{3\pi}f_c + P_{18}$	Guess the value	Guess the value
4	V_x	Equation (1)	P_4 = Equation (4)	Guess the value	Guess the value
5	V_y	Equation (2)	P_5 = Equation (5)	Guess the value	Guess the value
6	V_z	Equation (3)	P_6 = Equation (6)	Guess the value	Guess the value
7	p	First Data Point	$P_7 = R_{7\pi}f_c + P_{22}$	Guess the value	Guess the value
8	q	First Data Point	$P_8 = R_{8\pi}f_c + P_{23}$	Guess the value	Guess the value
9	r	First Data Point	$P_9 = R_{9\pi}f_c + P_{24}$	Guess the value	Guess the value
10	Bias in Long.Accel.	Guess the Value	P_{10} = Guess	0	0
11	Bias in Lat. Accel.	Guess the Value	P_{11} = Guess	0	0
12	Bias in Vert. Accel.	Guess the Value	P_{12} = Guess	0	0
13	Bias in Roll Accel.	Guess the Value	P_{13} = Guess	0	0
14	Bias in Pitch Accel.	Guess the Value	P_{14} = Guess	0	0
15	Bias in Yaw Accel.	Guess the Value	P_{15} = Guess	0	0
16	Bias in ϕ	Guess the Value	P_{16} = Guess	0	0
17	Bias in Θ	Guess the Value	P_{17} = Guess	0	0
18	Bias in ψ	Guess the Value	P_{18} = Guess	0	0
19	Bias in V	Guess the Value	P_{19} = Guess	0	0
20	Bias in β	Guess the Value	P_{20} = Guess	0	0
21	Bias in α	Guess the Value	P_{21} = Guess	0	0
22	Bias in p	Guess the Value	P_{22} = Guess	0	0
23	Bias in q	Guess the Value	P_{23} = Guess	0	0
24	Bias in r	Guess the Value	P_{24} = Guess	0	0

Table 3. - Concluded.

$$V_o = (V - X_{19})/(1 + \tan^2(\beta - X_{20}) + \tan^2(\alpha - X_{21}))^{\frac{1}{2}}$$

(1) $V_x = V_o - ql_3 + rl_2$

(2) $V_y = V_o \tan(\beta - X_{20}) - rl_1 + pl_3$

(3) $V_z = V_o \tan(\alpha - X_{21}) - pl_2 + ql_1$

(4) $P_4 = R_4 \pi f_c + P_{19} + (P_8 l_3^2 + P_9 l_2^2)$

(5) $P_5 = P_4 + (P_9 l_1^2 + P_7 l_3^2)$

(6) $P_6 = P_4 + (P_7 l_2^2 + P_8 l_1^2)$

Table 4. - Description of CH-53A Test Vehicle

Description of Test Vehicle

Helicopter Model:	Sikorsky Aircraft	S-65
	U. S. Navy	CH-53A
Aircraft BuNo.		153728
Number of Engines		2
Engine Manufacturer		General Electric
Engine Type		YT64-GE-12 T64-GE-413
Longitudinal C. G. range		328" to 352"
Aircraft Datum		84" Forward of nose
Main Rotor:	Number of Blades	6
	Diameter	72.225 ft.
	Airfoil	NACA 0011 (mod)
	Chord	26.0 in.
	Total Blade Area	374.95 sq. ft.
	Disc Area	4098.13 sq. ft.
	Solidity Ratio - effective	0.1158
	Blade Twist	-6°
	Shaft Tilt - longitudinal	5°
Tail Rotor:	Number of Blades	4
	Diameter	16 ft.
	Airfoil	NACA 0012
	Chord	15.4 in.
	Total Blade Area	33.12 sq. ft.
	Disc Area	201.1 sq. ft.
	Solidity Ratio - effective	0.1980
	Blade Twist	-8°
	Pitch Range standard	-2° to $+24^{\circ}$
	Pitch Range extended range	-2° to $+28^{\circ}$
Horizontal Stabilizer:	Area	40.0 sq. ft.
	Airfoil Section - tip	NACA 0012
	Airfoil Section - root	NACA 0016
	Aspect Ratio	2.5
	Taper Ratio	0.6
	Incidence Angle	$+ 3.5^{\circ}$
	Dihedral Angle	$+ 5.0^{\circ}$
Weight And Inertias:	W	35000 Lbs.
	Ixx	34250 Ft-Lbs-Sec^2
	Iyy	166100 Ft-Lb-Sec^2
	Izz	153600 Ft-Lb-Sec^2
	Ixz	Assumed zero

Table 5. - Description of CH-54B Test Vehicle

Description of Test Vehicle

Aircraft Bu. No.		6401-10005
Helicopter Model:	Sikorsky Aircraft	S-64A
	U. S. Army	CH-54B
Aircraft Govt. No.		69-18467
Number of Engines		2
Engine Manufacturer		Pratt & Whitney
Engine Type		JFTD12A-3
Longitudinal C.G. range		328" to 346"
Aircraft Datum		34" Forward of nose
Main Rotor:	Number of Blades	6
	Diameter	72.0 ft.
	Airfoil	NACA 0010.91
	Chord	23.65 in.
	Total Blade Area	352.2 sq. ft.
	Disc Area	4072.0 sq. ft.
	Solidity Ratio - effective	0.1021
	Blade Twist	-7.2°
	Shaft Tilt - longitudinal	3°
	- lateral	3°
Tail Rotor:	Number of Blades	4
	Diameter	16 ft.
	Airfoil	NACA 0012
	Chord	15.4 in.
	Total Blade Area	33.12 sq. ft.
	Disc Area	201.1 sq. ft.
	Solidity Ratio - effective	0.1980
	Blade Twist	-8°
	Pitch Range	-2° to $+24^{\circ}$
Horizontal Stabilizer:	Area	25.89 sq. ft.
	Airfoil Section	NACA 0012
	Aspect Ratio	1.74
	Taper Ratio	1.0
	Incidence Angle	0°
	Dihedral Angle	0°
Weight And Inertias:	W	28000 Lbs
	Ixx	29329 Ft-Lbs-Sec^2
	Iyy	150198 Ft-Lbs-Sec^2
	Izz	130999 Ft-Lbs-Sec^2
	Ixz	Assumed zero

Table 6. - Methods Used in Determination of The Most Accurate Approach For Derivative Extraction.

Method No.	Data Filter For LSE	A Priori Derivative Guess For MLE	Data Filter For MLE	Derivative Extraction Method
1	First Order	-	-	Least Square
2	Digital	-	-	Least Square
3	Kalman	-	-	Least Square
4	-	Arbitrary(1)	First Order	Max. Likelihood
5	-	Arbitrary(1)	Digital	Max. Likelihood
6	-	Arbitrary(1)	Kalman	Max. Likelihood
7	First Order	Least Square(2)	First Order	Max. Likelihood
8	Digital	Least Square(2)	Digital	Max. Likelihood
9	Kalman	Least Square(2)	Kalman	Max. Likelihood
10	Kalman	Least Square(2)	Digital	Max. Likelihood
11*	Kalman	Least Square(3)	Kalman	Max. Likelihood
12*	Kalman	Least Square(4)	Kalman	Max. Likelihood

(1) See Table 7. for the Arbitrary Guess.

(2) Variances Multiplied by 100.

(3) Variance obtained by engineering judgement (See Table 18).

(4) Variance of Method 11 divided by 4.

* Method 11 and Method 12 were not used in selecting the most accurate method, but were used on the CH-54B data.

Table 7. - The Arbitrary Derivative Guess and Variance Used to Initialize the Max. Likelihood Method

	u	w	q	v	p	r	β_{ls}	A_{ls}	θ_T	θ_c
X	.0 (±1.)*	.0 (±1.)	.0 (±10.)	.0 (±1.)	.0 (±10.)	.0 (±10.)	.59 (±.29)	.25 (±.25)	.238 (±.12)	-1.56 (±.54)
Z	.0 (±1.)	.0 (±1.)	169. (±10.)	.0 (±1.)	.0 (±10.)	.0 (±10.)	1.47 (±.29)	-2.5 (±.5)	.0 (±.12)	-7.10 (±1.05)
M	.0 (±.1)	.0 (±.1)	.0 (±1.)	.0 (±.1)	.0 (±1.)	.0 (±1.)	-.056 (±.011)	-.017 (±.008)	.0 (±.004)	.063 (±.01)
Y	.0 (±1.)	.0 (±1.)	.0 (±10.)	.0 (±1.)	.0 (±10.)	-169. (±10.)	.0 (±.12)	2.5 (±.5)	2.86 (±.48)	-4.05 (±.76)
L	.0 (±.1)	.0 (±.1)	.0 (±1.)	.0 (±.1)	.0 (±1.)	.0 (±1.)	.0 (±.03)	.244 (±.026)	.054 (±.008)	.101 (±.029)
N	.0 (±.1)	.0 (±.1)	.0 (±1.)	.0 (±.1)	.0 (±1.)	.0 (±1.)	.0 (±.01)	.0 (±.017)	-.095 (±.012)	.019 (±.017)

* Quantity in parenthisis represents 1 sigma uncertainty

Table 8a. - Identified Stability Derivatives from CH-53A Flight Data at 100 Knot Trim Using The Ten Methods (Presented in Normalized Form, British System of Units).

DERIVATIVE NAME	UNITS	VALUE OF IDENTIFIED DERIVATIVES USING METHOD									
		1	2	3	4	5	6	7	8	9	10
X_u	1/sec	-.0534	-.0715	-.1348	-.2884	-.2559	-.2509	-.1894	-.1920	-.2036	-.1880
Y^u	1/sec	-.1042	-.0906	-.0194	.4798	.6457	-.1657	.0476	-.3204	-.1647	-.2389
Z^u	1/sec	.2308	.1534	.2457	.6545	.3225	.0507	.3849	.4168	.0777	.4191
L^u	1/ft-sec	-.0030	-.0071	.0008	-.0217	-.0192	.0005	-.0152	-.0141	.0008	-.0123
M^u	1/ft-sec	-.0013	.0011	.0005	.0016	-.0010	-.0003	.0014	.0010	.0001	.0009
N^u	1/ft-sec	-.0098	.0022	.0045	.0065	-.0019	.0052	.0062	.0055	.0050	.0065
X_v	1/sec	-.0808	-.0904	-.0964	-.2531	-.1982	-.1703	-.1275	-.1147	-.1373	-.1081
Y^v	1/sec	-.0841	-.0665	.0029	.2171	.3214	-.0475	.0666	-.1925	-.0258	-.1062
Z^v	1/sec	.0292	.0071	.0963	.2494	.0523	-.0026	.0682	.1013	.0253	.0990
L^v	1/ft-sec	-.0083	-.0107	-.0052	-.0209	-.0185	-.0051	-.0168	-.0164	-.0049	-.0151
M^v	1/ft-sec	-.0001	.0012	.0005	.0017	.0002	-.0000	.0015	.0012	.0003	.0011
N^v	1/ft-sec	-.0048	.0016	.0040	.0044	-.0006	.0049	.0039	.0040	.0045	.0044
X_w	1/sec	-.1339	-.1317	-.0325	.0501	-.1240	-.0069	.0362	-.0616	-.0388	-.0540
Y^w	1/sec	-.0956	-.0167	.7638	.6594	.8853	.8680	1.027	.5204	1.006	.8018
Z^w	1/sec	-.3421	-.3292	-.1772	-.3779	-.4840	-.4084	-.3188	-.3127	-.3365	-.3915
L^w	1/ft-sec	-.0080	-.0075	-.0038	.0030	-.0050	-.0012	-.0022	-.0046	-.0022	-.0040
M^w	1/ft-sec	-.0016	-.0014	-.0009	.0005	.0002	-.0007	.0005	-.0000	-.0006	.0001
N^w	1/ft-sec	-.0009	.0003	-.0035	-.0017	-.0075	-.0026	-.0033	-.0040	-.0034	-.0058
X_p	ft/sec	-1.454	-1.291	-3.088	-14.00	-9.030	-7.831	-7.166	-5.119	-3.849	-5.858
Y^p	ft/sec	10.52	11.52	20.85	48.30	48.88	20.46	30.54	17.95	21.29	16.79
Z^p	ft/sec	-27.16	-28.84	-4.950	6.200	-.7470	-10.16	-.2788	1.616	-7.102	4.249
L^p	1/sec	-.3812	-.5356	-.3855	-1.258	-1.098	-.4551	-.9793	-.9224	-.3813	-.8872
M^p	1/sec	-.1454	-.0542	-.1261	-.0978	-.2315	-.1676	-.1082	-.1197	-.1396	-.1353
N^p	1/sec	-.8788	-.4121	-.0412	-.2124	-.4101	.0160	-.1474	-.1382	-.0183	-.0223
X_q	ft/sec	-19.05	-20.33	-19.32	-21.79	-1.537	-32.52	-19.49	-8.758	-25.03	-10.18
Y^q	ft/sec	18.76	7.156	-63.02	23.10	-15.67	-85.19	-62.89	-27.79	-103.9	-69.53
Z^q	ft/sec	87.72	82.31	98.13	138.6	148.6	114.2	128.6	134.6	101.6	143.1
L^q	1/sec	2.242	1.859	1.742	.0660	.6481	1.323	1.03	1.269	1.492	1.294
M^q	1/sec	.2236	.3742	.2516	.0554	-.1469	.1187	.0701	.1188	.1608	.0867
N^q	1/sec	-.4838	.2168	.8122	.4907	.8230	.7091	.7463	.8896	.8490	1.188
X_r	ft/sec	13.44	10.21	9.704	16.40	3.738	9.756	7.812	7.815	9.154	7.650
Y^r	ft/sec	-155.6	-159.3	-123.5	-145.5	-143.6	-128.0	-131.5	-141.7	-128.0	-145.4
Z^r	ft/sec	27.00	28.59	18.90	25.61	28.83	15.64	22.72	29.93	7.525	26.20
L^r	1/sec	.5327	.3757	.8622	.4711	-.1711	.6793	.4751	.2912	.8282	.4263
M^r	1/sec	-.0198	.0059	-.0406	.0180	.0648	-.0489	.0176	.0161	-.0529	.0074
N^r	1/sec	-.5206	-.5892	-.7861	-.7255	-.9295	-.7567	-.8223	-.7820	-.7957	-.8762

Table 8b. - Identified Stability Derivatives from CH-53A Flight Data at 100 Knot Trim Using The Ten Methods (Presented in Dimensional Form, British System of Units).

Derivative Name	Units	VALUE OF IDENTIFIED DERIVATIVES x 10^{+3} USING METHOD									
		1	2	3	4	5	6	7	8	9	10
X_u	lb-sec/ft	-.0581	-.0778	-.1467	-.3138	-.2784	-.2730	-.2061	-.2089	-.2216	-.2046
Y^u	lb-sec/ft	-.1134	-.0987	-.0211	.5220	.7024	-.1803	.0518	-.3486	-.1792	-.2599
Z^u	lb-sec/ft	.2511	.1670	.2674	.7120	.3508	.0552	.4188	.4535	.0845	.4559
L^u	lb-sec	-.1053	-.2445	.0285	-.7456	-.6594	.0196	-.5229	-.4851	.0275	-.4220
M^u	lb-sec	-.2201	.1899	.0969	.2685	-.1676	-.0624	.2447	.1691	.0170	.1623
N_u	lb-sec	-1.516	.3392	.6972	1.004	-.2942	.8027	.9668	.8491	.7752	1.003
X_v	lb-sec/ft	-.0879	-.0984	-.1049	-.2754	-.2156	-.1854	-.1387	-.1248	-.1494	-.1176
Y^v	lb-sec/ft	-.0915	-.0724	.0033	.2362	.3497	-.0517	.0725	-.2094	-.0282	-.1156
Z^v	lb-sec/ft	.0319	.0077	.1048	.2714	.0570	-.0029	.0743	.1103	.0276	.1078
L^v	lb-sec	-.2852	-.3691	-.1792	-.7186	-.6366	-.1753	-.5760	-.5644	-.1681	-.5184
M^v	lb-sec	-.0189	.2122	.0945	.2858	.0430	-.0002	.2526	.1997	.0518	.1965
N_v	lb-sec	-.7463	.2485	.6204	.6776	-.0958	.7532	.6002	.6245	.6976	.6883
X_w	lb-sec/ft	-.1458	-.1433	-.0355	.0546	-.1350	-.0076	.0394	-.0670	-.0422	-.0588
Y^w	lb-sec/ft	-.1040	-.0182	.8310	.7174	.9631	.9443	1.117	.5662	1.095	.8722
Z^w	lb-sec/ft	-.3722	-.3581	-.1928	-.4112	-.5266	-.4444	-.3468	-.3403	-.3661	-.4259
L^w	lb-sec	-.2741	-.2589	-.1305	.1040	-.1745	-.0419	-.0759	-.1579	-.0765	-.1397
M^w	lb-sec	-.2794	-.2471	-.1529	.0899	.0476	-.1176	.0968	-.0064	-.1003	.0273
N_w	lb-sec	-.1469	.0537	-.5393	-.2627	-1.153	-.4028	-.5089	-.6213	-.5375	-.8982
X_p	lb-sec	-1.583	-1.405	-3.360	-15.24	-9.824	-8.520	-7.796	-5.569	-4.188	-6.373
Y^p	lb-sec	11.45	12.54	22.68	52.55	53.18	22.26	33.23	19.53	23.16	20.45
Z^p	lb-sec	-29.55	-31.38	-5.385	6.746	-.8127	-11.06	-.3033	1.758	-7.726	4.623
L^p	lb-sec	-13.06	-18.35	-13.21	-43.11	-37.63	-15.59	-33.54	-31.59	-13.06	-30.39
M^p	ft-lb-sec	-24.16	-9.007	-20.95	-16.25	-38.45	-27.85	-17.98	-19.90	-23.19	-22.48
N_p	ft-lb-sec	-135.0	-63.31	-6.329	-32.63	-63.00	2.459	-22.65	-21.24	-2.901	-3.440
X_q	lb-sec	-20.73	-22.12	-21.02	-23.71	-1.672	-35.38	-21.21	-9.528	-27.29	-11.09
Y^q	lb-sec	20.41	7.785	-68.56	25.13	-17.05	-92.68	-68.42	-30.24	-113.1	-75.64
Z^q	lb-sec	95.43	89.54	106.7	150.8	161.7	124.3	140.0	146.5	110.6	155.7
L^q	ft-lb-sec	76.80	63.69	59.70	2.263	22.20	45.34	35.37	43.47	51.12	44.35
M^q	ft-lb-sec	37.16	62.19	41.81	9.217	-24.42	19.72	11.64	19.74	26.72	14.40
N_q	ft-lb-sec	-74.31	33.30	124.8	75.38	126.4	108.9	114.6	136.6	130.4	182.5
X_r	lb-sec	14.63	11.11	10.56	17.85	4.066	10.61	8.499	8.502	9.959	8.323
Y^r	lb-sec	-169.3	-173.3	-134.4	-158.3	-156.3	-139.3	-143.1	-154.2	-139.2	-158.2
Z^r	lb-sec	29.38	31.10	20.57	27.86	31.37	17.02	24.72	32.57	8.186	28.51
L_r	ft-lb-sec	18.25	12.87	29.53	16.14	-5.861	23.27	16.28	9.975	28.36	14.60
M_r	ft-lb-sec	-3.289	.9880	-6.747	2.993	10.76	-8.130	2.936	2.681	-8.797	1.234
N_r	ft-lb-sec	-79.97	-90.51	-120.7	-111.4	-142.8	-116.2	-126.3	-120.1	-122.2	-134.6

Table 9a. - Identified Control Derivatives from CH-53A Flight Data at 100 Knot Trim Using the Ten Methods (Presented in Normalized Form, British System of Units).

DERIVATIVE NAME	UNITS	VALUE OF IDENTIFIED DERIVATIVE USING METHOD									
		1	2	3	4	5	6	7	8	9	10
$X_{B_{ls}}$	ft/sec^2-deg	-.1111	-.4679	-.3429	.2316	1.081	-.4637	.3461	.0735	-.6972	.0186
$Y_{B_{ls}}$	ft/sec^2-deg	-.1321	-.4827	.0879	-.2569	.0985	-.1495	-3.978	.2690	-1.203	-.4017
$Z_{B_{ls}}$	ft/sec^2-deg	.4728	-.3471	.6131	1.984	1.494	.8454	1.841	1.439	.3225	1.809
$L_{B_{ls}}$	1/sec^2-deg	.0290	.0082	.0146	-.0220	.0091	.0300	-.0088	-.0134	.0061	-.0176
$M_{B_{ls}}$	1/sec^2-deg	-.0359	-.0347	-.0296	-.0468	-.0404	-.0360	-.0474	-.0352	-.0338	-.0351
$N_{B_{ls}}$	1/sec^2-deg	.0206	.0109	.0355	.0122	.0104	.0072	.0563	.0295	.0380	.0412
$X_{A_{ls}}$	ft/sec^2-deg	-.4563	-.3428	-.5920	.1830	-.0014	-.4654	-.3926	-.3562	-.9526	-.2961
$Y_{A_{ls}}$	ft/sec^2-deg	2.622	2.494	.6422	-.4473	-.1877	.5596	-3.549	-1.964	.2852	-4.215
$Z_{A_{ls}}$	ft/sec^2-deg	.1938	.1486	-1.146	-1.553	-1.614	-1.010	-.3681	-.5643	-1.900	-.9405
$L_{A_{ls}}$	1/sec^2-deg	.1829	.1870	.1990	.2178	.1999	.2144	.2220	.2229	.2005	.2231
$M_{A_{ls}}$	1/sec^2-deg	-.0134	-.0112	-.0080	-.0154	-.0206	-.0099	-.0120	-.0088	-.0096	-.0078
$N_{A_{ls}}$	1/sec^2-deg	.0397	.0348	-.0126	.0110	.0010	-.0088	.0173	.0163	-.0070	.0035
$X_{\theta_{tr}}$	ft/sec^2-deg	.3734	.3000	.2664	.1746	.1930	.0962	-.2939	-.1112	.0161	-.1402
$Y_{\theta_{tr}}$	ft/sec^2-deg	.8593	.7668	.6394	-1.923	-1.088	.4573	-2.376	-.8946	.4526	-2.722
$Z_{\theta_{tr}}$	ft/sec^2-deg	-.1254	-.1246	-.5216	.0753	.1098	-.3406	.6020	.6335	-1.069	.4998
$L_{\theta_{tr}}$	1/sec^2-deg	.0649	.0628	.0848	.0667	.0619	.0696	.0718	.0717	.0834	.0734
$M_{\theta_{tr}}$	1/sec^2-deg	.0007	.0016	-.0011	-.0027	-.0010	-.0016	-.0020	-.0013	-.0030	-.0022
$N_{\theta_{tr}}$	1/sec^2-deg	-.0667	-.0716	-.0969	-.0836	-.0840	-.0955	-.0800	-.0756	-.0971	-.0809
X_{θ_c}	ft/sec^2-deg	-1.009	-.9953	-1.170	-.3850	-.7176	-1.025	-.3604	-.6485	-.8715	-.6781
Y_{θ_c}	ft/sec^2-deg	-.0010	.0594	1.403	-1.135	-.9657	1.546	-.1329	-1.023	.9245	-1.801
Z_{θ_c}	ft/sec^2-deg	-4.682	-4.682	-5.420	-5.928	-5.935	-5.971	-5.152	-5.049	-5.009	-5.090
L_{θ_c}	1/sec^2-deg	-.0252	-.0289	-.0213	.0300	.0396	.0124	.0059	-.0015	-.0201	.0028
M_{θ_c}	1/sec^2-deg	.0382	.0392	.0407	.0533	.0542	.0507	.0405	.0407	.0399	.0407
N_{θ_c}	1/sec^2-deg	.0149	.0195	-.0036	.0136	.0069	.0057	-.0078	-.0082	-.0058	-.0133

Table 9b. - Identified Control Derivatives from CH-53A Flight Data at 100 Knot Trim Using The Ten Methods (Presented in Dimensional Form, British System of Units)

DERIVATIVE NAME	UNITS	VALUE OF IDENTIFIED DERIVATIVES USING METHOD ($X10^3$)									
		1	2	3	4	5	6	7	8	9	10
$X_{B_{ls}}$	lb/rad	-.1209	-.5090	-.3731	.2520	1.176	-.5045	.3765	.0801	-.7585	.0203
$Y_{B_{ls}}$	lb/rad	-.1438	-.5251	.0957	-.2795	.1072	-.1627	-4.328	.2927	-1.309	-.4371
$Z_{B_{ls}}$	lb/rad	.5144	-.3776	.6670	2.158	1.626	.9202	2.003	1.566	.3509	1.969
$L_{B_{ls}}$	ft-lb/rad	.9937	.2815	.5011	-.7554	.3128	1.028	-.3028	-.4605	.2111	-.6034
$M_{B_{ls}}$	ft-lb/rad	-5.970	-5.769	-4.919	-7.782	-6.716	-5.985	-7.886	-5.853	-5.626	-5.846
$N_{B_{ls}}$	ft-lb/rad	3.173	1.683	5.468	1.874	1.611	1.121	8.656	4.546	5.846	6.335
$X_{A_{ls}}$	lb/rad	-.4965	-.3729	-.6440	.1991	-.0015	-.5063	-.4271	-.3875	-1.036	-.3222
$Y_{A_{ls}}$	lb/rad	2.853	2.713	.6987	-.4866	-.2043	.6088	3.861	-2.137	.3103	-4.585
$Z_{A_{ls}}$	lb/rad	.2109	.1617	-1.247	-1.690	-1.756	-1.099	-.4005	-.6139	-2.067	-1.023
$L_{A_{ls}}$	ft-lb/rad	6.267	6.408	6.818	7.463	6.847	7.345	7.606	7.636	6.870	7.644
$M_{A_{ls}}$	ft-lb/rad	-2.238	-1.861	-1.342	-2.565	-3.424	-1.659	-2.002	-1.472	-1.598	-1.302
$N_{A_{ls}}$	ft-lb/rad	6.104	5.352	-1.949	1.700	.1572	-1.355	2.663	2.505	-1.077	.5420
$X_{\theta_{tr}}$	lb/rad	.4062	.3264	.2899	.1900	.2100	.1047	-.3198	-.1210	.0176	-.1526
$Y_{\theta_{tr}}$	lb/rad	.9349	.8342	.6957	-2.092	-1.184	.4975	-2.585	-.9733	.4924	-2.961
$Z_{\theta_{tr}}$	lb/rad	-.1365	-.1356	-.5674	.0820	.1195	-.3706	.6549	.6892	-1.164	.5437
$L_{\theta_{tr}}$	ft-lb/rad	2.224	2.154	2.905	2.287	2.121	2.385	2.460	2.457	2.859	2.517
$M_{\theta_{tr}}$	ft-lb/rad	.1281	.2736	-.1959	-.4636	-.1709	-.2806	-.3381	-.2240	-.5042	-.3726
$N_{\theta_{tr}}$	ft-lb/rad	-10.26	-11.00	-14.89	-12.85	-12.91	-14.68	-12.29	-11.62	-14.92	-12.44
X_{θ_c}	lb/rad	-1.098	-1.083	-1.273	-.4188	-.7807	-1.116	-.3921	-.7055	-.9481	-.7377
Y_{θ_c}	lb/rad	-.0012	.0647	1.527	-1.235	-1.051	1.682	-.1446	1.114	1.006	-1.960
Z_{θ_c}	lb/rad	-5.094	-5.093	-5.900	-6.450	-6.457	-6.496	-5.605	-5.493	-5.449	-5.537
L_{θ_c}	ft-lb/rad	-.8638	.9917	-.7312	1.030	1.358	.4278	.2032	-.0529	-.6913	.0992
M_{θ_c}	ft-lb/rad	6.356	6.522	6.773	8.857	9.012	8.432	6.732	6.762	6.633	6.776
N_{θ_c}	ft-lb/rad	2.300	3.005	-.5531	2.103	1.069	.8838	-1.202	-1.274	-.9022	-2.056

Table 10. - RMS Error Between Test Data and Identified Derivative Model For the Ten Methods (CH-53A, 100 knots).

Method	RMS* Error in Test Data		
	Maneuvers 1 through 4 Used in I.D.	Maneuvers 5 & 6 Not used in I.D.	Maneuvers 1 through 6
1	47.3	70.6	85.2
2	29.3	34.0	45.0
3	19.2	19.4	27.3
4	19.4	27.8	33.9
5	20.1	19.8	28.3
6	18.9	19.9	27.5
7	20.4	27.0	35.4
8	16.6	17.8	24.6
9	17.8	19.7	26.6
10	16.0	17.8	24.0

* Total RMS Error For All State Variables and Accelerations

Table 11. - Derivatives Identified from CH-53A Data at 100 Knots Using the Method Found Most Accurate (Method 10) (Presented in Normalized Form).

	u	w	q	v	p	r	B_{is}	A_{is}	Θ_T	Θ_C
X	-.188	-.054	-10.2	-.108	-5.85	7.65	.018	-.296	-.140	-.678
Z	.419	-.392	143.1	.099	4.25	26.2	1.81	-.94	.499	-5.09
M	.0009	.0001	.086	.001	-.135	.007	-.035	-.008	-.002	.041
Y	-.238	.802	-69.5	-.106	18.8	-145.4	-.402	-4.22	-2.72	-1.80
L	-.012	-.004	1.29	-.015	-.887	.426	-.017	.223	.073	.003
N	.0065	-.0058	1.18	.004	-.022	-.876	.041	.004	-.081	-.013

Table 12. - RMS Error Between Test Data and Identified Derivative Model For the CH-53A at 150 Knots.

Method	RMS* Error in the Test Data Maneuvers 1 through 4 (Used in the Identification)
3	25.6
9	22.7
10	31.1

* Total RMS error for all State Variables and Accelerations

Table 13. - Derivatives Identified from CH-53A Data at 150 Knots Using the Least Square Method (Method 3) (Presented in Normalized Form)

	u	w	q	v	p	r	B_{1s}	A_{1s}	Θ_T	Θ_c
X	.448	.061	18.3	-.023	4.72	-15.9	.983	-.971	.095	-1.58
Z	-1.71	-.422	141.6	.226	4.44	34.5	1.49	1.59	-.256	-.531
M	-.0056	-.0026	.644	-.0015	-.251	-.072	-.041	.019	-.011	.068
Y	-.838	-.257	-23.6	.061	-21.3	-261.8	-.412	1.92	.644	.715
L	.010	.0021	1.04	-.012	-.574	2.50	.019	.250	.064	.0064
N	-.012	-.0039	.591	.0029	.048	-.623	.046	.011	-.062	-.0086

Table 14a - Derivatives Identified from CH-53A Data at 150 knots using the Max. Likelihood Method (Method 9). (Presented in Normalized Form, British System of Units)

	u	w	q	v	p	r	B_{is}	A_{is}	Θ_T	Θ_c
X	.314	.097	7.35	-.0086	4.46	-10.6	.767	-.867	.117	-1.42
Z	-1.88	-.680	163.4	.054	-11.12	34.6	1.93	1.14	.545	-6.3
M	-.0044	-.002	.521	-.0016	-.302	-.109	-.041	.026	-.011	.066
Y	-.626	-.270	-16.4	.0024	-25.8	-256.4	.058	2.03	.642	-.077
L	.016	.0036	.97	-.012	-.654	2.24	.012	.235	.065	.008
N	-.0098	-.0026	.631	.0035	.114	-.785	.049	.013	-.069	-.005

Table 14b - Derivatives Identified from CH-53A Data at 150 knots using the Max. Likelihood Method (Method 9). (Presented in Dimensional Form, British System of Units).

	u	w	q	v	p	r	B_{is}	A_{is}	Θ_T	Θ_c
X	341.4	106.3	7991.	-9.43	4851.	-11499.	834.4	-943.5	127.2	-1550.
Z	-2050.	-739.8	177781.	58.7	-12102.	37621.	2094.	1235.	592.4	-6863.
M	-736.1	-333.9	86563.	-282.2	-50132.	-18200.	-6783.	4399.	-1813.	11072.
Y	-681.3	-294.2	-17816.	2.65	-28146.	-278941.	63.9	2210.	898.0	-84.5
L	549.2	124.3	33238.	-423.1	-22410.	76619.	400.	8047.	2277.	304.7
N	-1517.	-408.5	96978.	542.9	17460.	-120627.	7659.	2081.	-10678.	-788.6

Table 15. - Derivatives Identified from CH-54B Data at 45 knots using the Least Square Method. (Method 3) (Using Four 6-second Maneuvers, Presented in Normalized Form).

	u	w	q	v	p	r	B_{is}	A_{is}	θ_T	θ_c
X	.141	.203	10.1	.0006	-1.02	4.17	.144	1.05	-.183	-1.55
Z	-.29	.088	60.1	.0011	-.446	2.27	.071	-.705	-.016	-.147
M	-.0034	-.0065	.259	.0019	-.338	-.313	-.041	.0088	.022	-.058
Y	-.112	-.0044	13.7	-.344	-30.7	3.55	.660	.848	-2.49	2.94
L	.0091	.037	-.108	-.0044	-.011	-.408	.011	.570	-.033	-.119
N	-.0007	.0056	.015	.0044	.0728	-.116	.003	.081	.011	-.035

Table 16. - Derivatives Identified from CH-54B Data at 45 knots using the Max. Likelihood Method. (Method 9) (Using Four 6-second Maneuvers, Presented in Normalized Form).

	u	w	q	v	p	r	B_{is}	A_{is}	Θ_T	Θ_c
X	-.025	.190	27.5	.054	-1.54	5.16	-.129	.591	.0012	-1.11
Z	-.393	.027	62.5	.031	-2.61	3.28	.076	-2.01	.197	.646
M	-.0014	-.0058	.179	.0023	-.371	-.360	-.047	.0068	.025	-.056
Y	-.337	.102	39.9	-.275	-36.4	2.21	.872	2.18	-2.49	2.67
L	.0111	.039	-.054	-.0024	-.256	-.514	.0074	.549	-.019	-.106
N	-.0024	.0048	.133	.0046	.0039	-.147	.0043	.073	.0125	-.036

Table 17. - Derivatives Identified from CH-54B Data at 45 knots using the Least Square Method (Method 3) (Using one 16-second Maneuver, Presented in Normalized Form).

	u	w	q	v	p	r	B_{is}	A_{is}	Θ_T	Θ_c
X	-.118	.167	28.5	-.269	-5.5	21.1	-.361	1.63	-.145	.882
Z	-.168	-.535	55.2	.086	4.42	-1.21	.858	-.973	-.069	-4.09
M	-.0126	-.0033	.230	.019	-.233	-.337	-.038	-.018	-.079	.088
Y	.088	-.15	16.6	-.422	-14.4	-64.3	-.245	-1.36	2.98	-4.63
L	-.0360	.0255	-.668	.025	-.054	2.42	.027	.643	-.424	.645
N	-.0207	.0039	-.051	.028	.345	.016	.0021	.091	-.205	.289

Table 18. - Initial Derivative 1 Sigma Uncertainty Obtained from the Least Square Method (Method 3) and Modified using Engineering Judgement. (Used to Initialize the MLE of Method 9, CH-54B Data, One Maneuver Case).

	u	w	q	v	p	r	B_{is}	A_{is}	Θ_T	Θ_c
X	.22*	.11	8.9	.35	6.0	23.7	.32	1.4	1.8	2.4
	(1.)**	(1.)	(10.)	(1.)	(10.)	(10.)	(1.)	(1.)	(1.)	(1.)
Z	.15	.078	6.2	.24	4.2	16.5	.22	.99	1.3	1.7
	(1.)	(1.)	(10.)	(1.)	(10.)	(10.)	(1.)	(1.)	(1.)	(1.)
M	.0055	.0027	.21	.0086	.14	.57	.0078	.034	.044	.060
	(.1)	(.1)	(1.)	(.1)	(1.)	(1.)	(.05)	(.05)	(.05)	(.05)
Y	.12	.062	4.9	.19	3.3	13.1	.17	.79	1.0	1.3
	(1.)	(1.)	(10.)	(1.)	(10.)	(10.)	(1.)	(.2)	(1.)	(1.)
L	.026	.013	1.0	.042	.72	2.8	.038	.16	.21	.29
	(.1)	(.1)	(1.)	(.1)	(1.)	(1.)	(.05)	(.1)	(.2)	(.3)
N	.0064	.0032	.25	.010	.17	.67	.0092	.041	.052	.071
	(.1)	(.1)	(1.)	(.1)	(1.)	(1.)	(.05)	(.05)	(.05)	(.05)

* LSE 1 Sigma Uncertainties Multiplied by 10.

** Quantity in Parenthesis obtained by Engineering Judgement.

Table 19. - Derivatives Identified from CH-54B Data at 45 knots using the Max. Likelihood Method (Method 11). (Initial Derivative Variance obtained using Engineering Judgement, one Maneuver Case, Presented in Normalized Form).

	u	w	q	v	p	r	B_{is}	A_{is}	Θ_T	Θ_c
X	-.335	.0301	37.4	.153	-.609	15.9	-.463	-.649	-.125	.561
Z	-.0311	-.377	46.5	-.375	-.732	22.5	.464	2.22	.173	-3.76
M	-.0193	-.0031	.252	.0357	-.0225	-.918	-.0380	-.0493	-.192	.228
Y	.301	-.121	27.6	-1.59	-7.29	-7.65	-.730	-.502	5.96	-7.08
L	-.0502	.0296	-1.97	.114	-.519	4.46	.0574	.588	-.665	.898
N	-.0181	.0028	.213	.0262	.479	-.691	-.0080	.0543	-.202	.275

Table 20a - Derivatives Identified from CH-54B Data at 45 knots using the Max. Likelihood Method (Method 12). (Optimum Initial Derivative Variance Used, One Maneuver Case, Presented in Normalized Form).

	u	w	q	v	p	r	B_{is}	A_{is}	Θ_T	Θ_c
X	-.135	.187	32.0	-.204	-.736	20.6	-.795	1.16	.263	.669
Z	-.173	-.520	56.2	.0007	.636	.173	.851	-.229	-.0101	-4.17
M	-.0167	-.0043	.382	.0282	-.133	-.759	-.0382	-.0417	-.122	.136
Y	.120	-.135	22.7	-.698	-13.7	-69.1	-.160	-1.21	3.76	-5.13
L	-.0433	.0236	-1.05	.0550	-.308	3.21	.035	.619	-.483	.678
N	-.0223	.0017	.081	.0341	.421	-.471	.0015	.0555	-.221	.293

Table 20b - Derivatives Identified from CH-54B Data at 45 knots using the Max. Likelihood Method (Method 12). (Optimum Initial Derivative Variance Used, One Maneuver Case, Presented in Dimensional Form).

	u	w	q	v	p	r	B_{is}	A_{is}	Θ_T	Θ_c
X	-117.5	163.2	27859.	-178.2	-640.	17999.	-692.	1012.	229.	582.
Z	-150.9	-452.8	48968.	.660	553.9	150.8	740.	-199.7	-8.84	-3633.
M	-2521.	-656.6	57399.	4242.	-20032.	-114008.	-5733.	-6270.	-18414.	20444.
Y	104.6	-117.8	19826.	-607.6	-11969.	-60138.	-139..	-1054.	3280.	-4465.
L	-1271.	693.3	-31041.	1614.	-9040.	94095.	1028.	18161.	-14176.	19910.
N	-2927.	222.3	10609.	4468.	55255.	-61650.	202.	7276.	-28900.	38430.

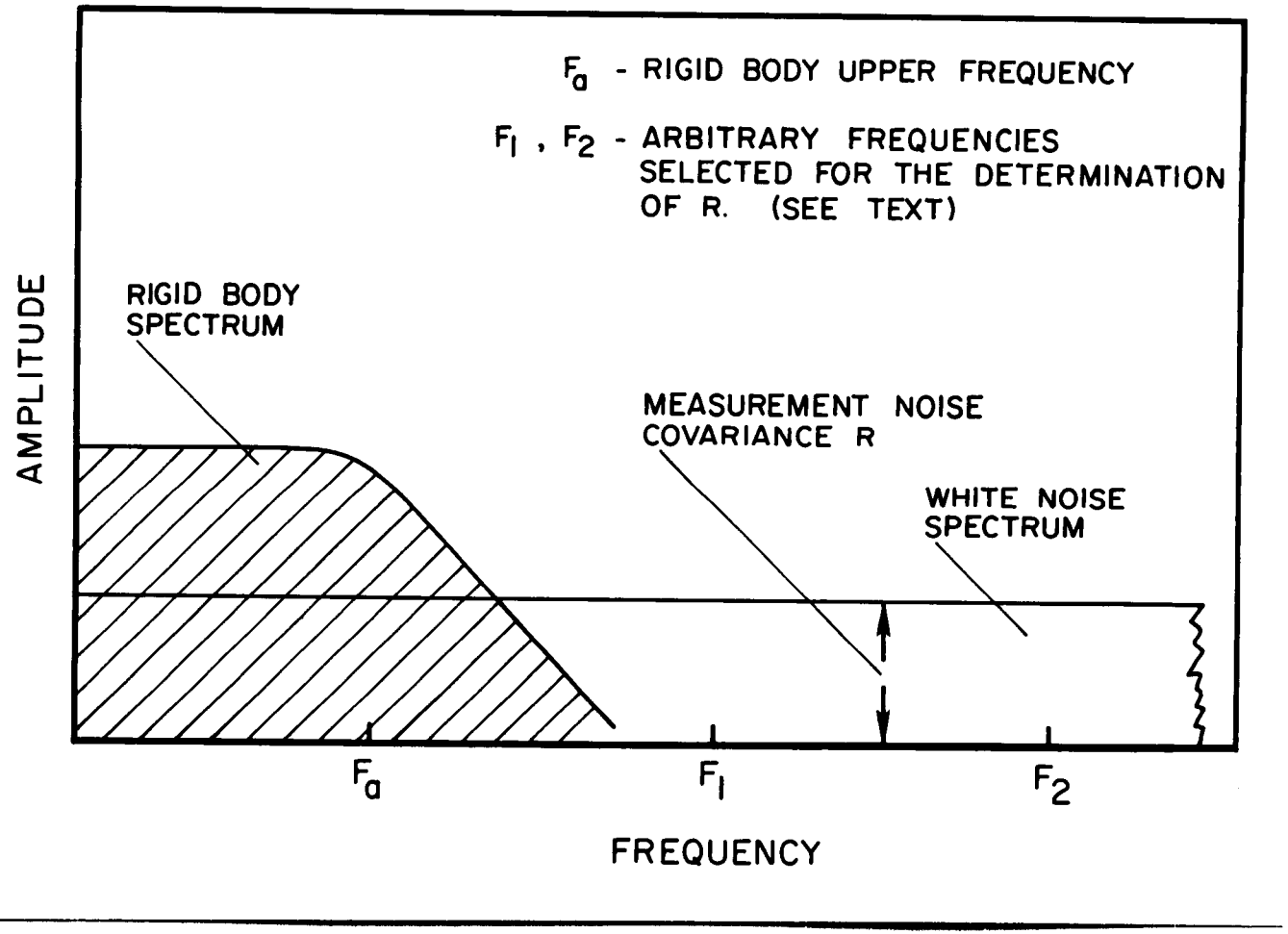

Figure 1. Power Spectrum of Measured Data Showing The Physical Interpretation of Measurement Noise Covariance R.

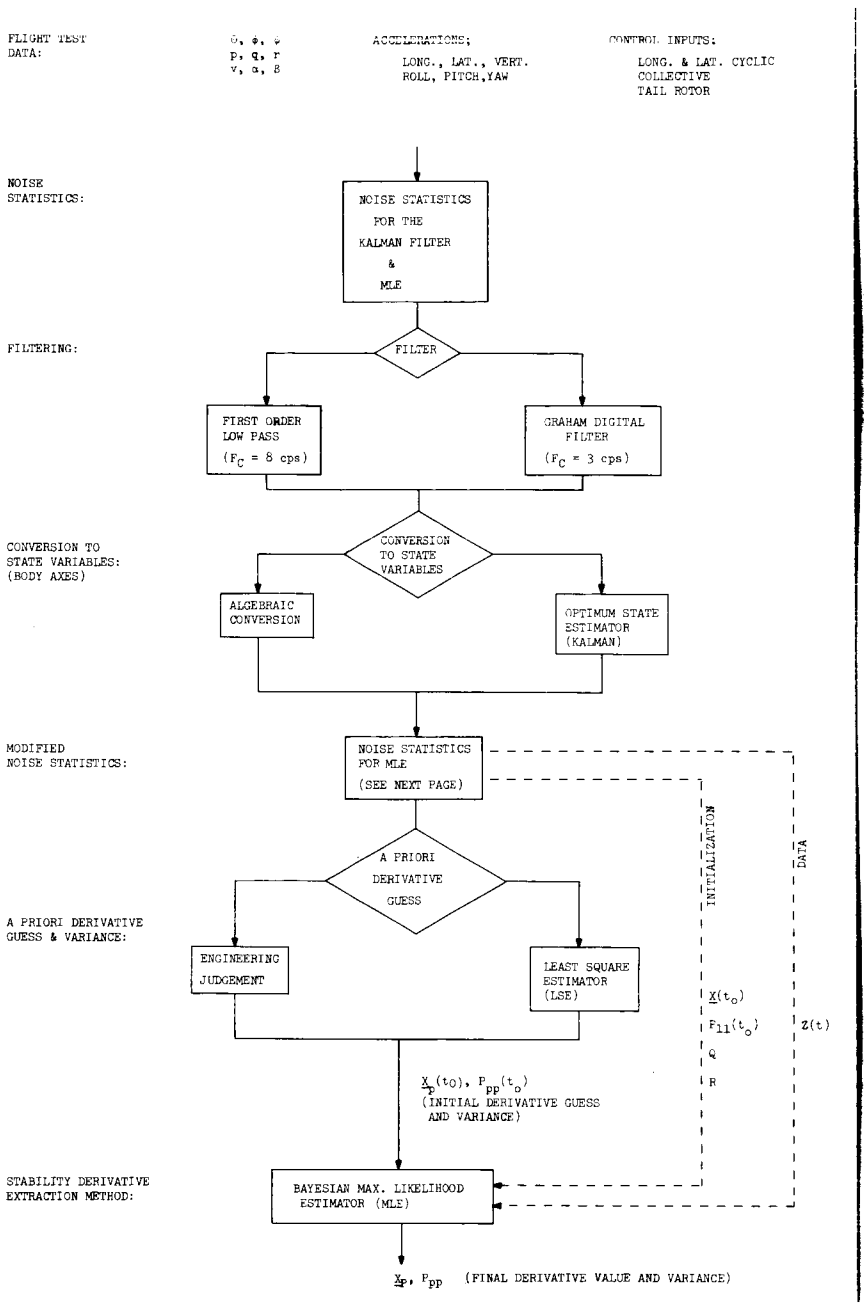

Figure 2. Flow Diagram of the Procedure Used to Determine the Most Accurate Helicopter Derivative Extraction Method.

Initializations for the Max. Likelihood Estimator

Symbol	Description	How Computed
$\underline{X}(t_o)$	Initial State	Same as for the Kalman Filter (See Table 3.)
$P_{11}(t_o)$	Initial State Covariance	Same as for the Kalman Filter (See Table 3.)
Q	Process Noise Intensity	Same as for the Kalman Filter (See Table 2.)
R	Measurement Noise Intensity	(1) $R = (P_{11}(t_f) + P_{11}(t_o)) \cdot \Delta t/2$, When using Kalman Data (2) $R = P_{11}(t_o) \cdot \Delta t$, when using Digital or Low Pass Data
$\underline{X}_p(to)$	A Priori Derivative Estimate	Obtained from the LSE or Using Engineering Judgement
$P_{pp}(to)$	A Priori Derivative Variance	Obtained from the LSE or Using Engineering Judgement

Figure 2. - Concluded.

Figure 3. CH-53A Test Aircraft

Fig 3. 95

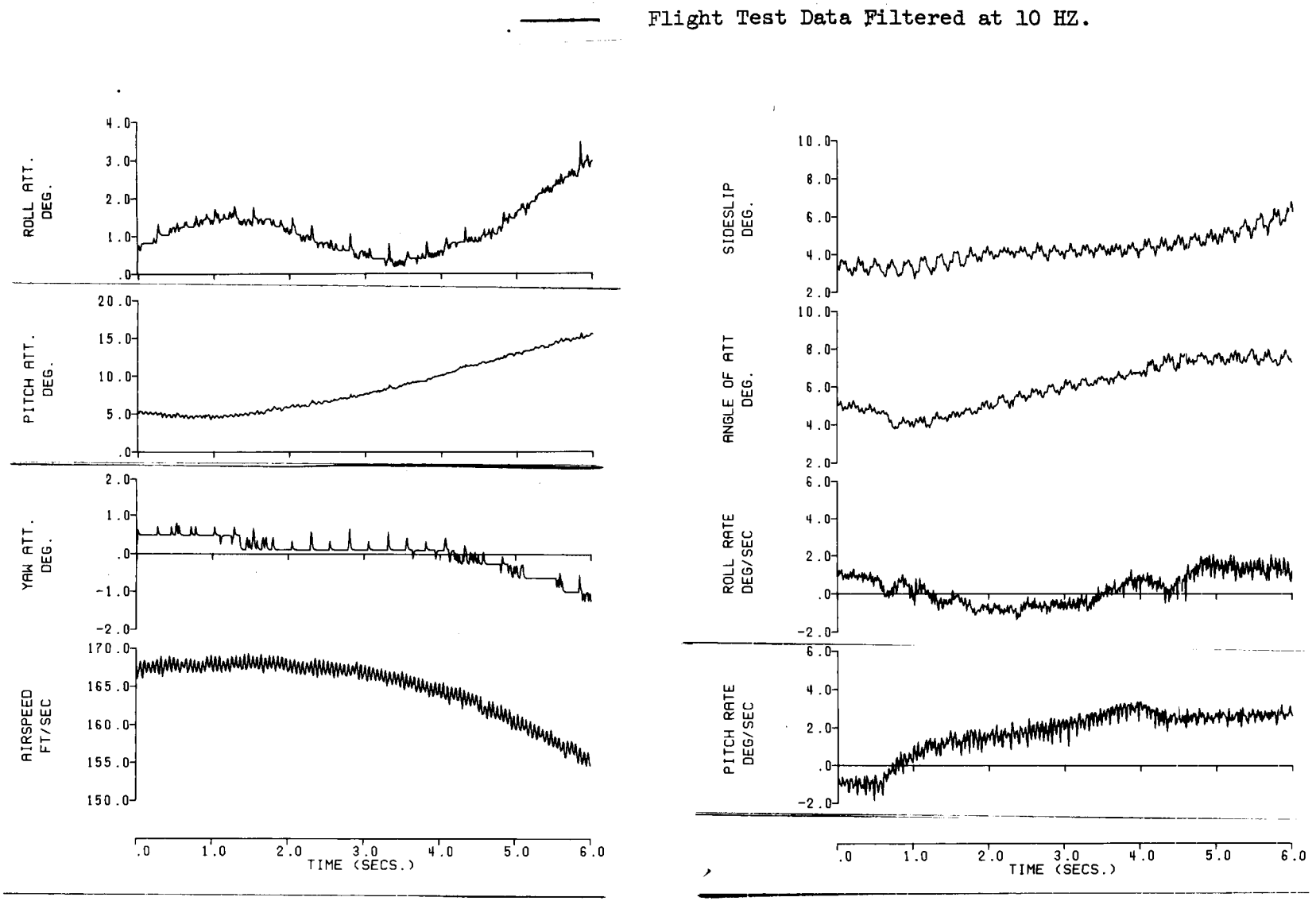

Figure 4 . - Flight Test Data From CH-53A Filtered With A First Order Low Pass Filter at 10 HZ. (100 knots, Maneuver 1.)

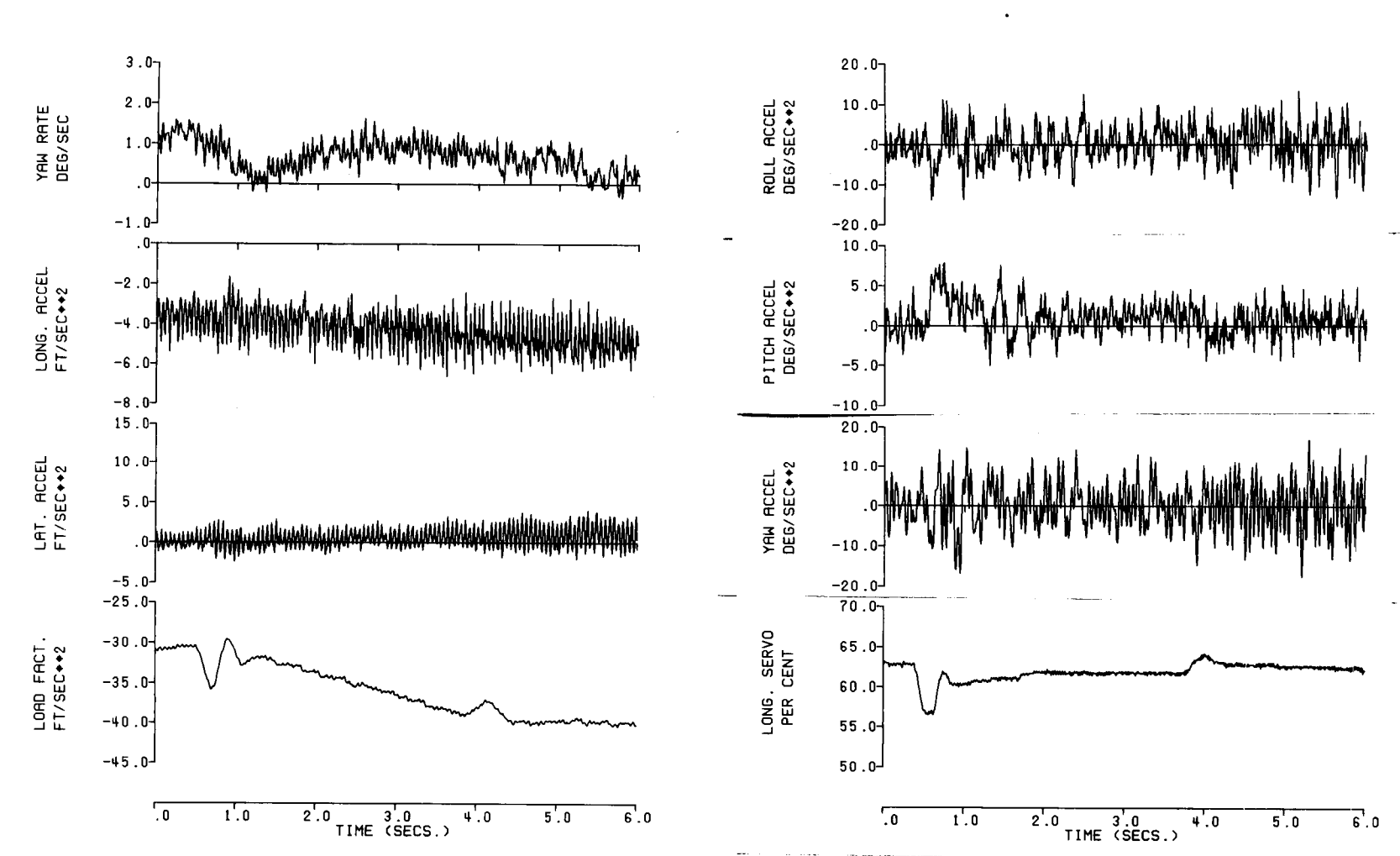

Figure 4 . - Continued.

——— Flight Test Data Filtered At 10 HZ.

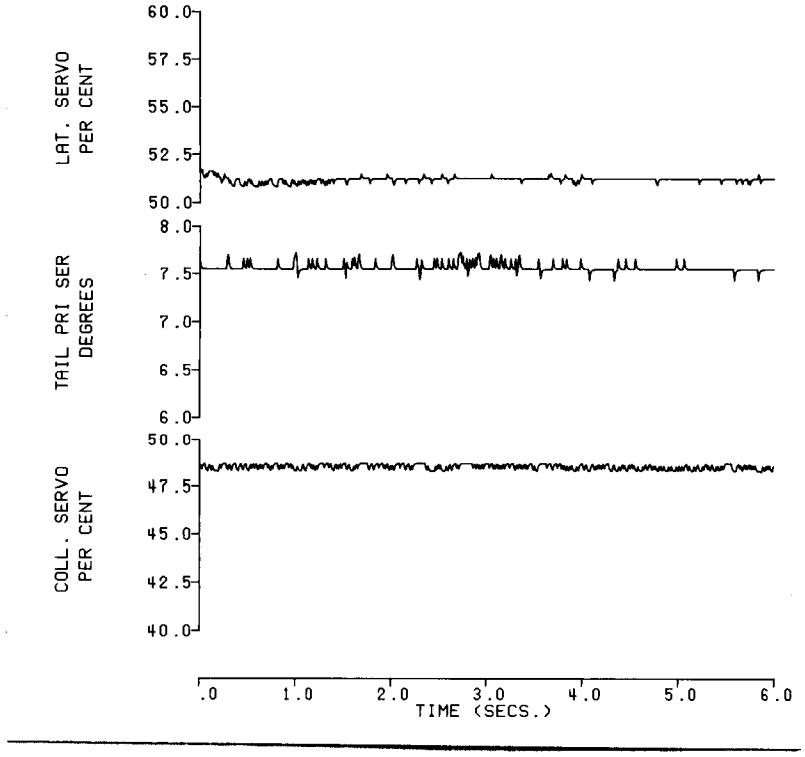

Figure 4 . - Concluded.

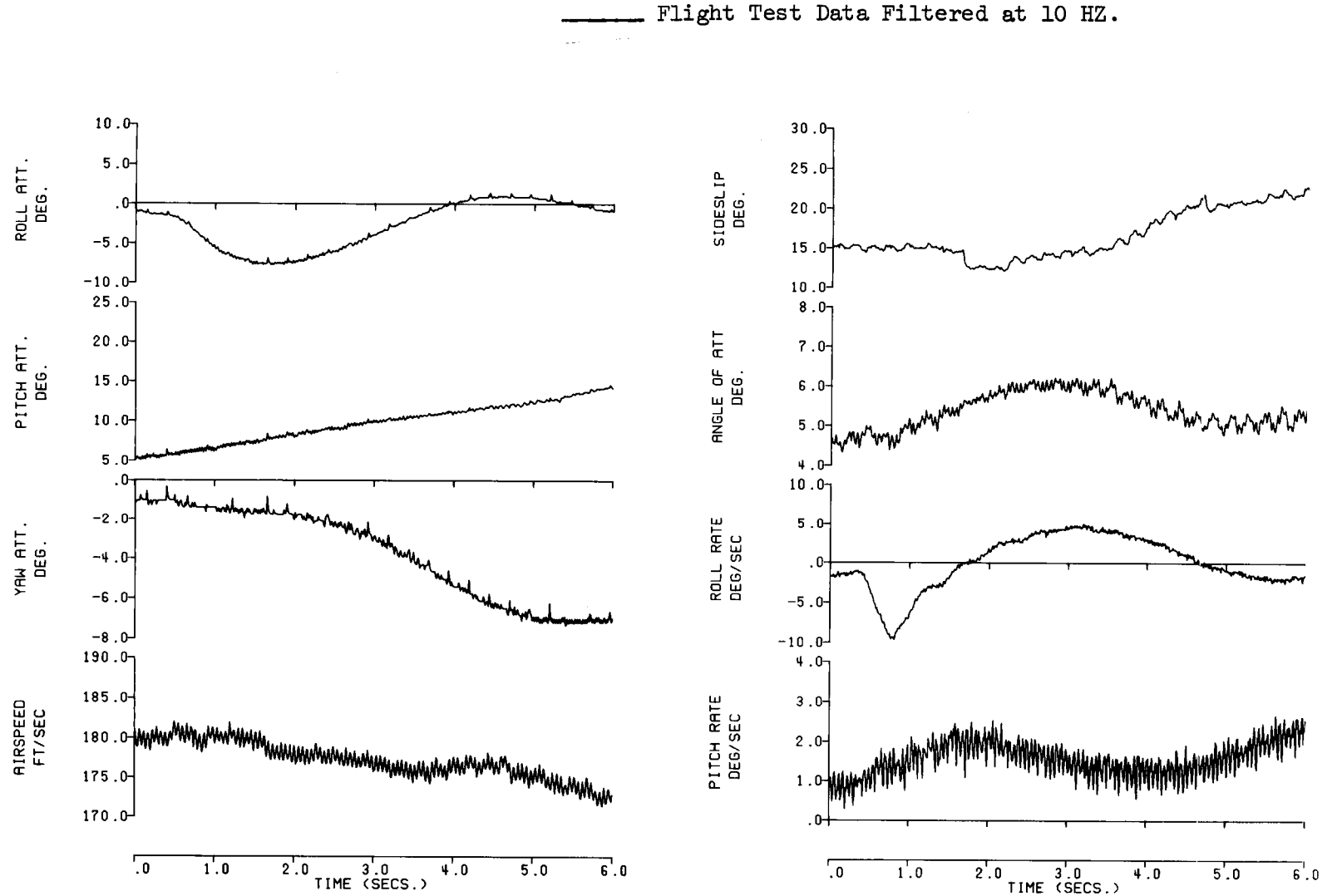

Figure 5 . - Flight Test Data FROM CH-53A Filtered With A First Order Low Pass Filter at 10 HZ. (100 knots, Maneuver 2).

Flight Test Data Filtered At 10 HZ.

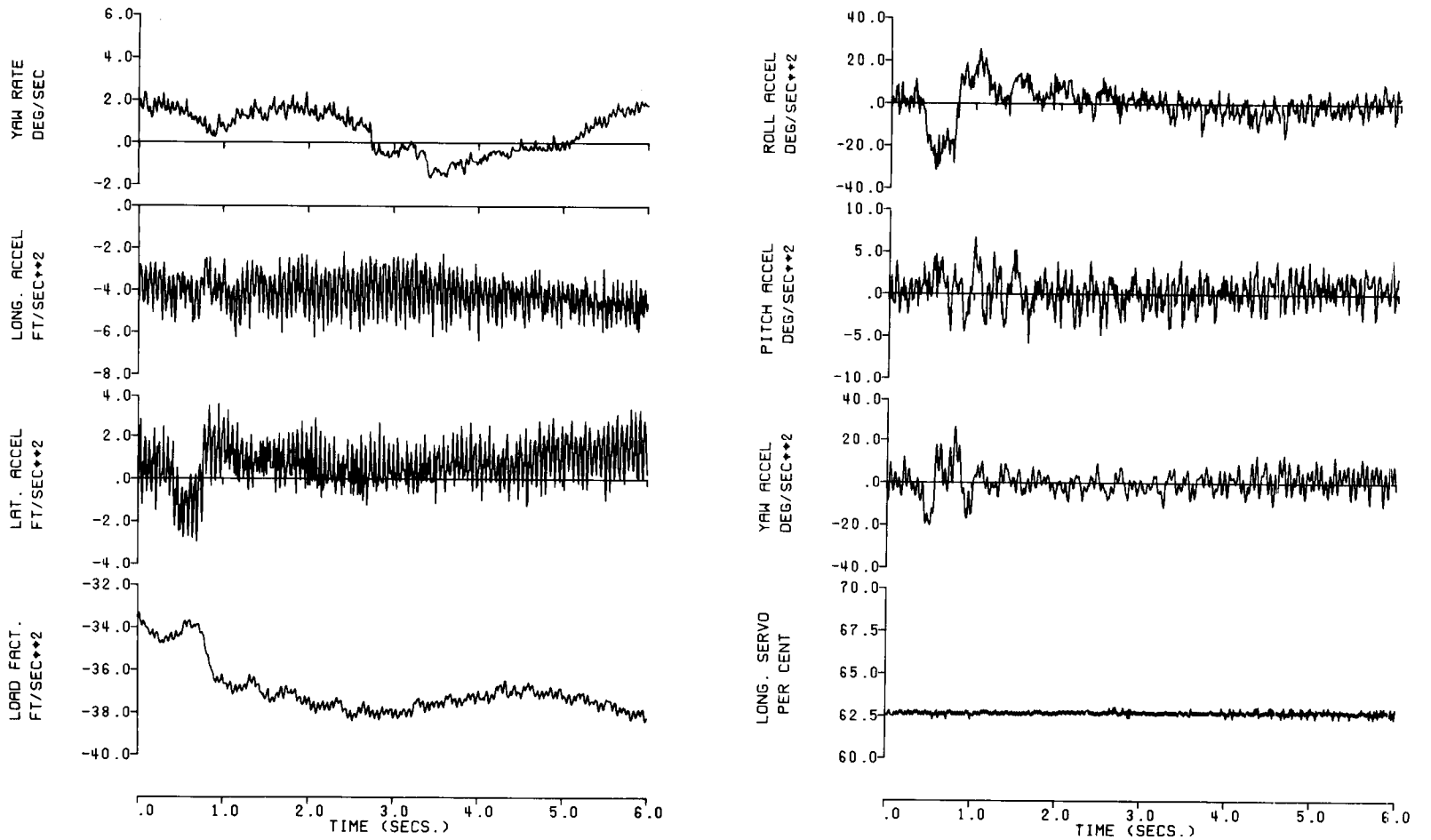

Figure 5 . - Continued.

_____ Flight Test Data Filtered At 10 HZ.

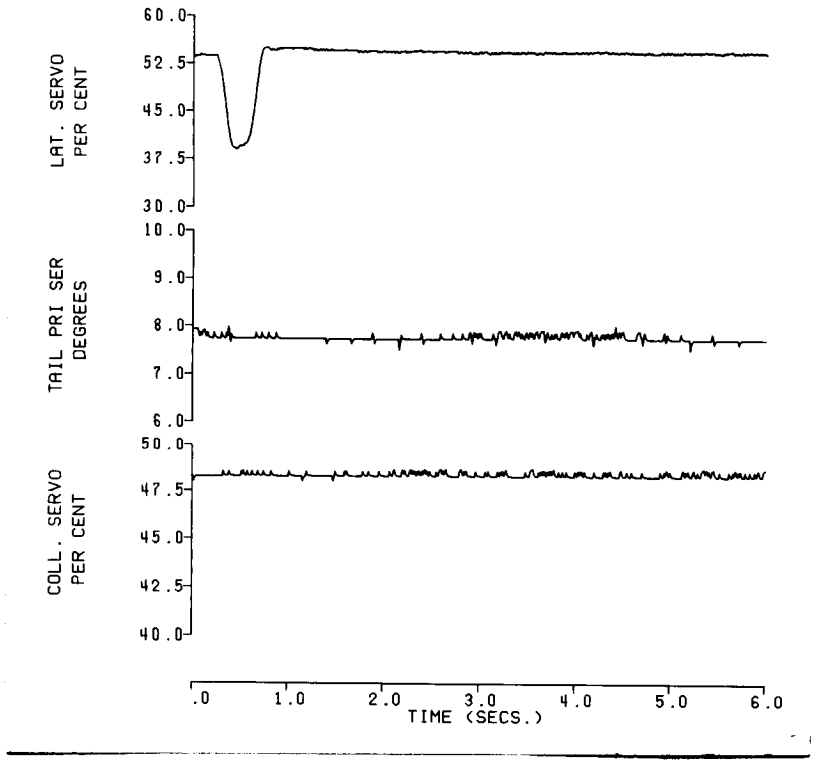

Figure 5 . - Concluded.

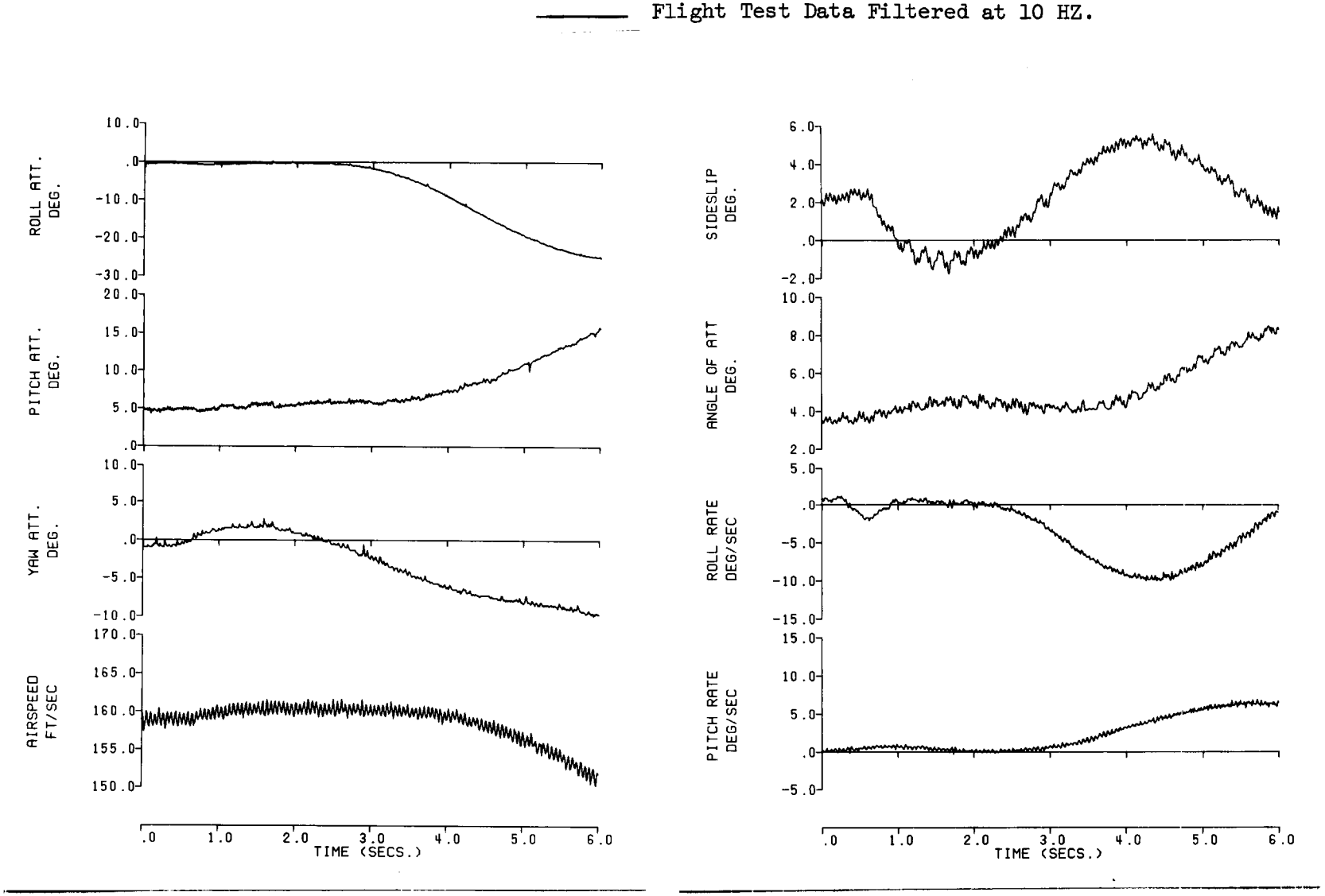

Figure 6 . - Flight Test Data From CH-53A Filtered With A First Order Low Pass Filter At 10 HZ. (100 knots, Maneuver 3).

——— Flight Test Data Filtered At 10 HZ.

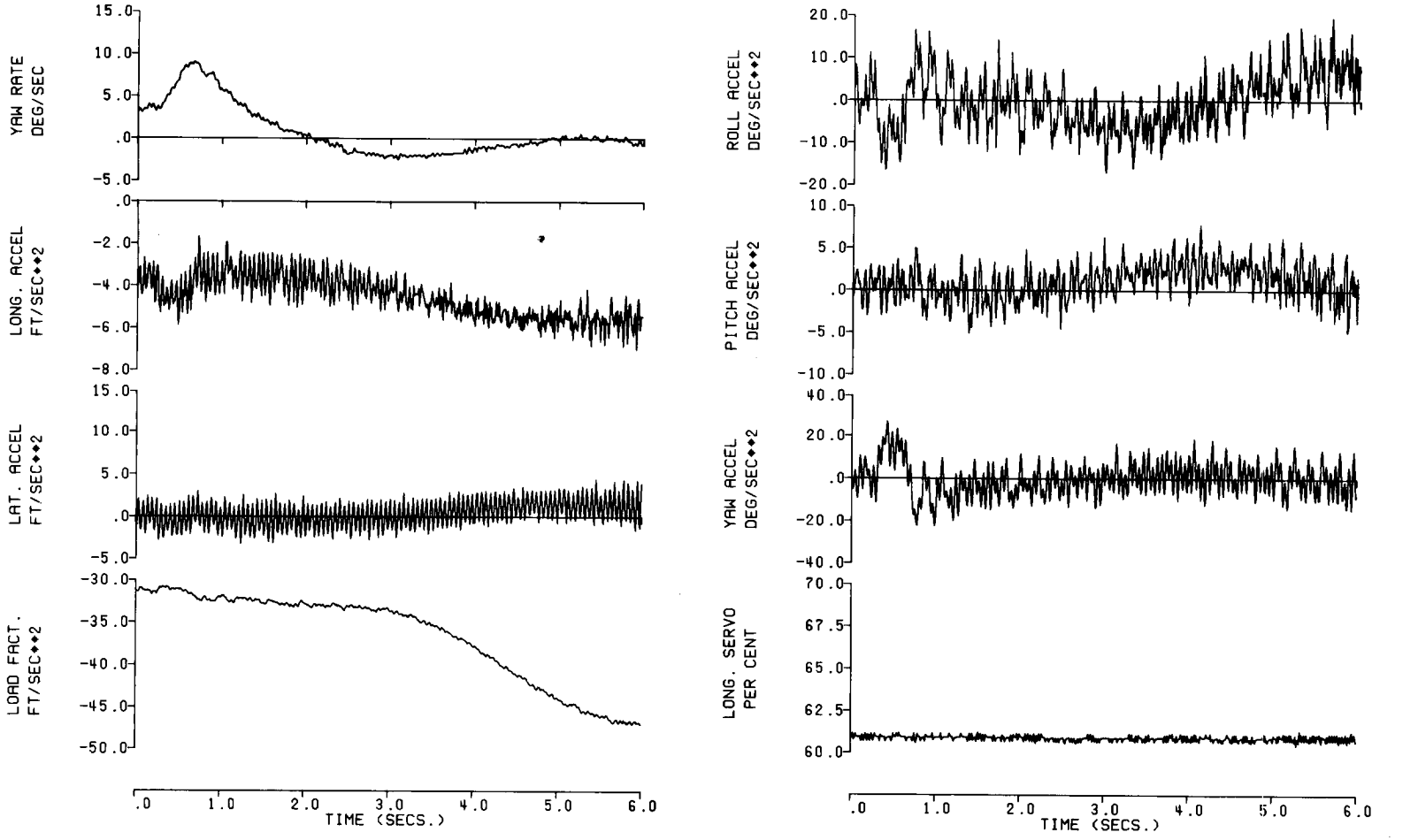

Figure 6 . - Continued.

——— Flight Test Data Filtered At 10 HZ.

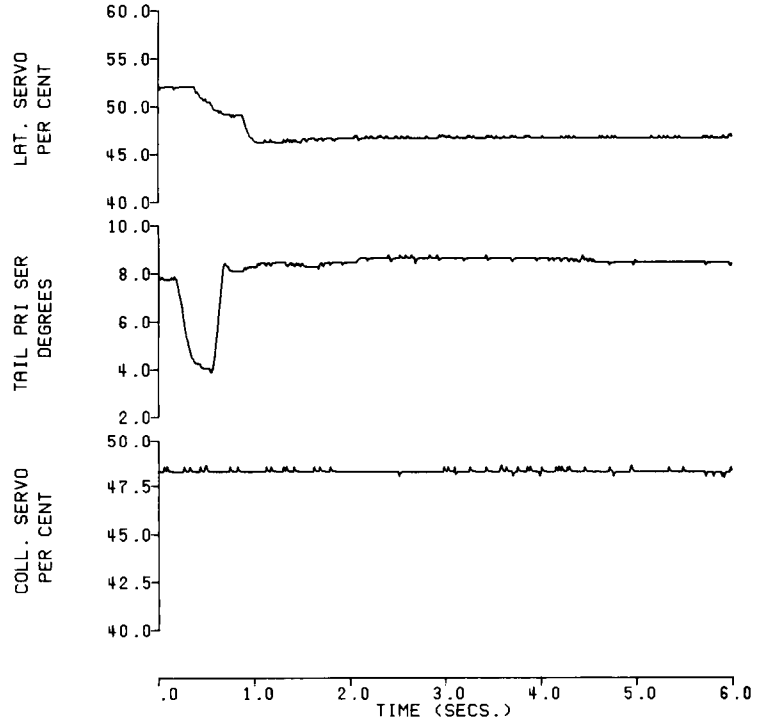

Figure 6 . - Concluded.

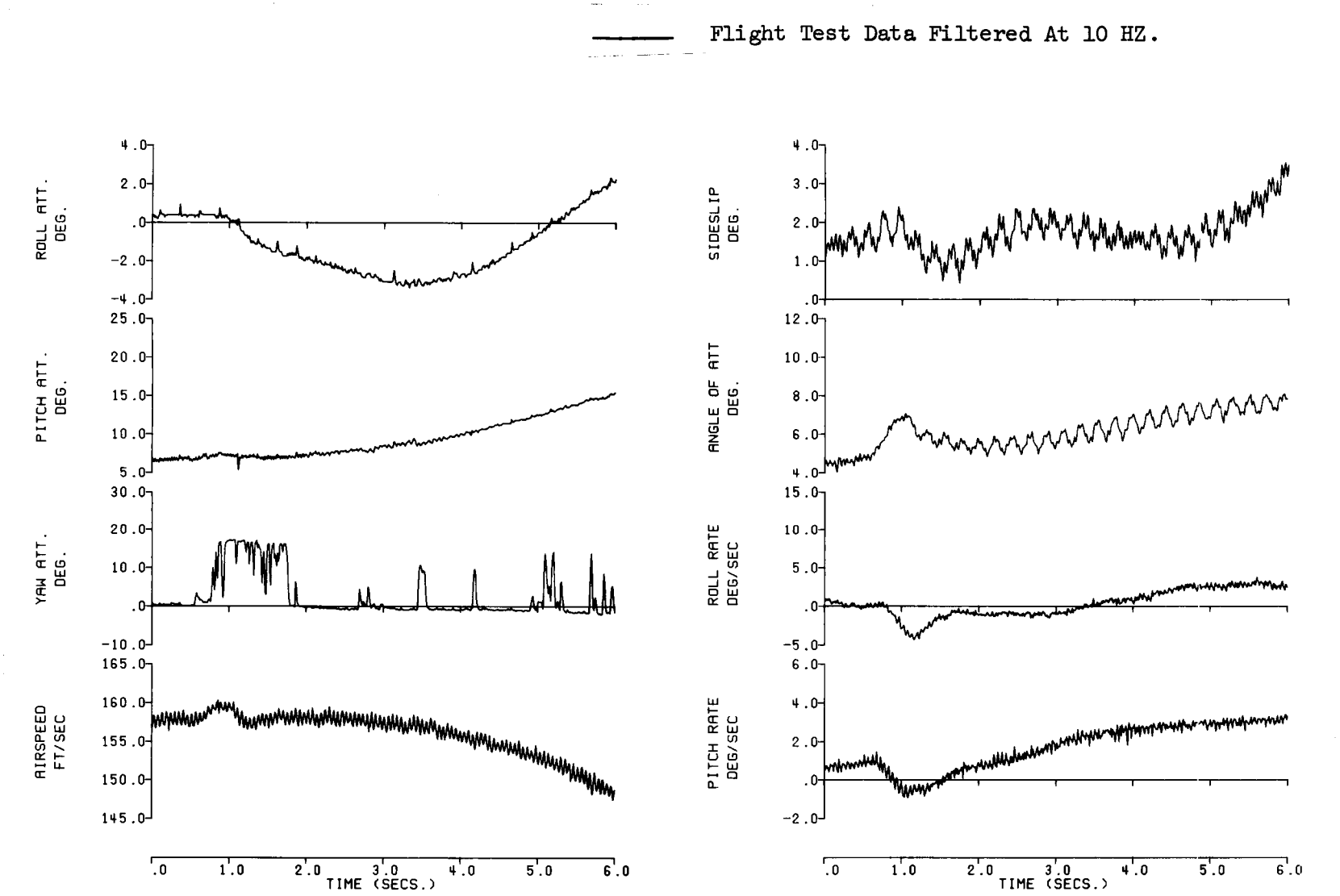

Figure 7 . - Flight Test Data From CH-53A Filtered With a First Order Low Pass Filter At 10 HZ. (100 knots, Maneuver 4).

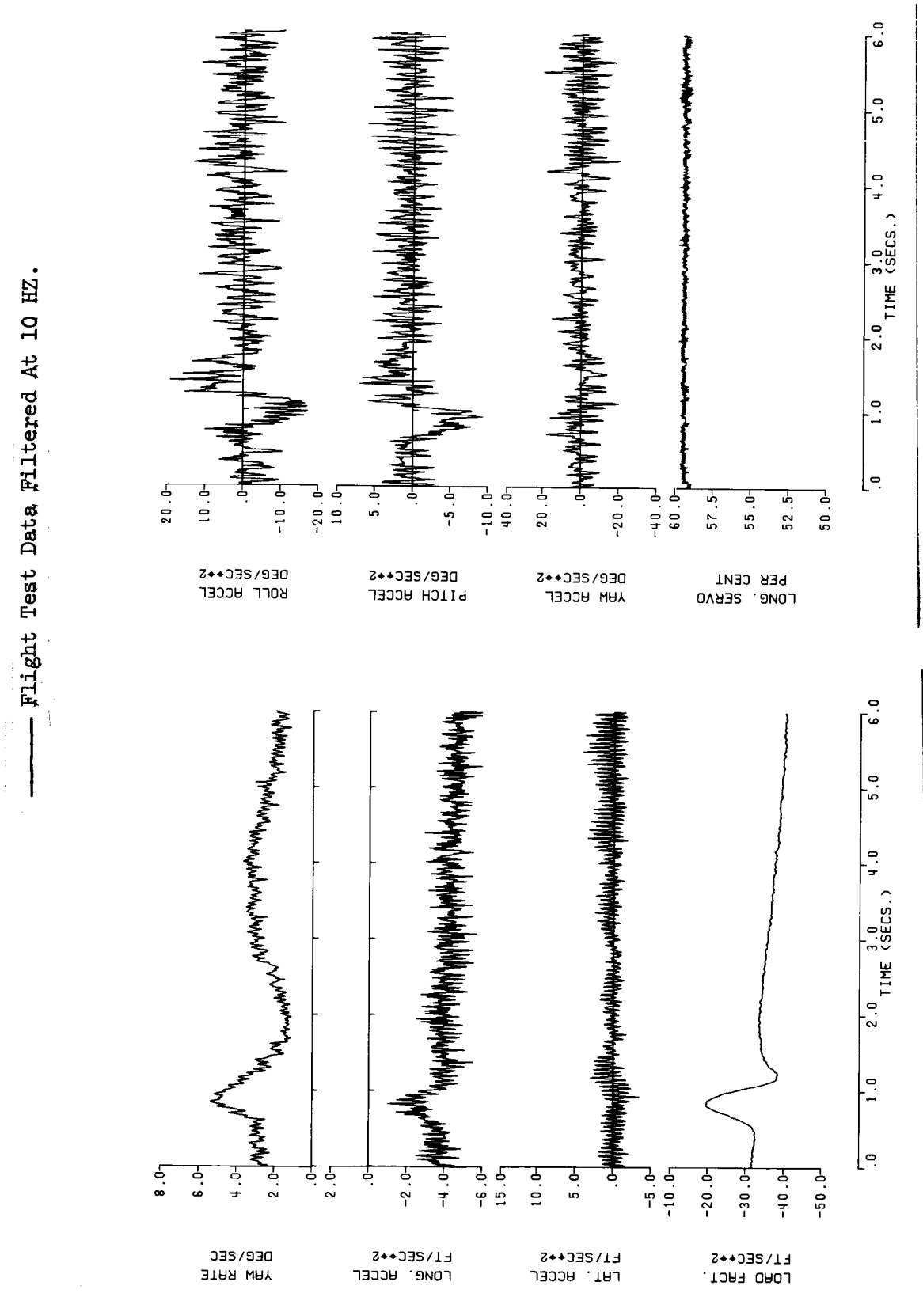

Figure 7 . - Continued.

——— Flight Test Data Filtered At 10 HZ

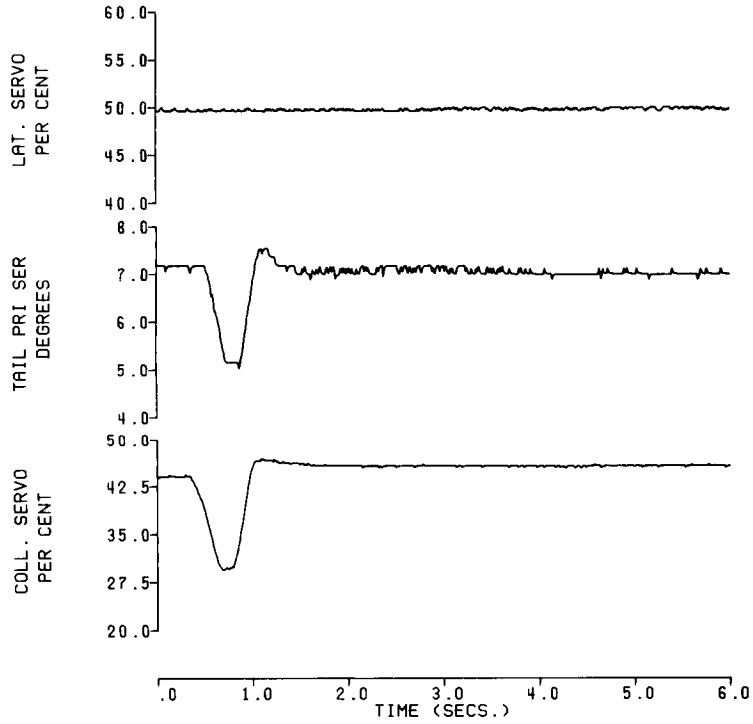

Figure 7 . - Concluded.

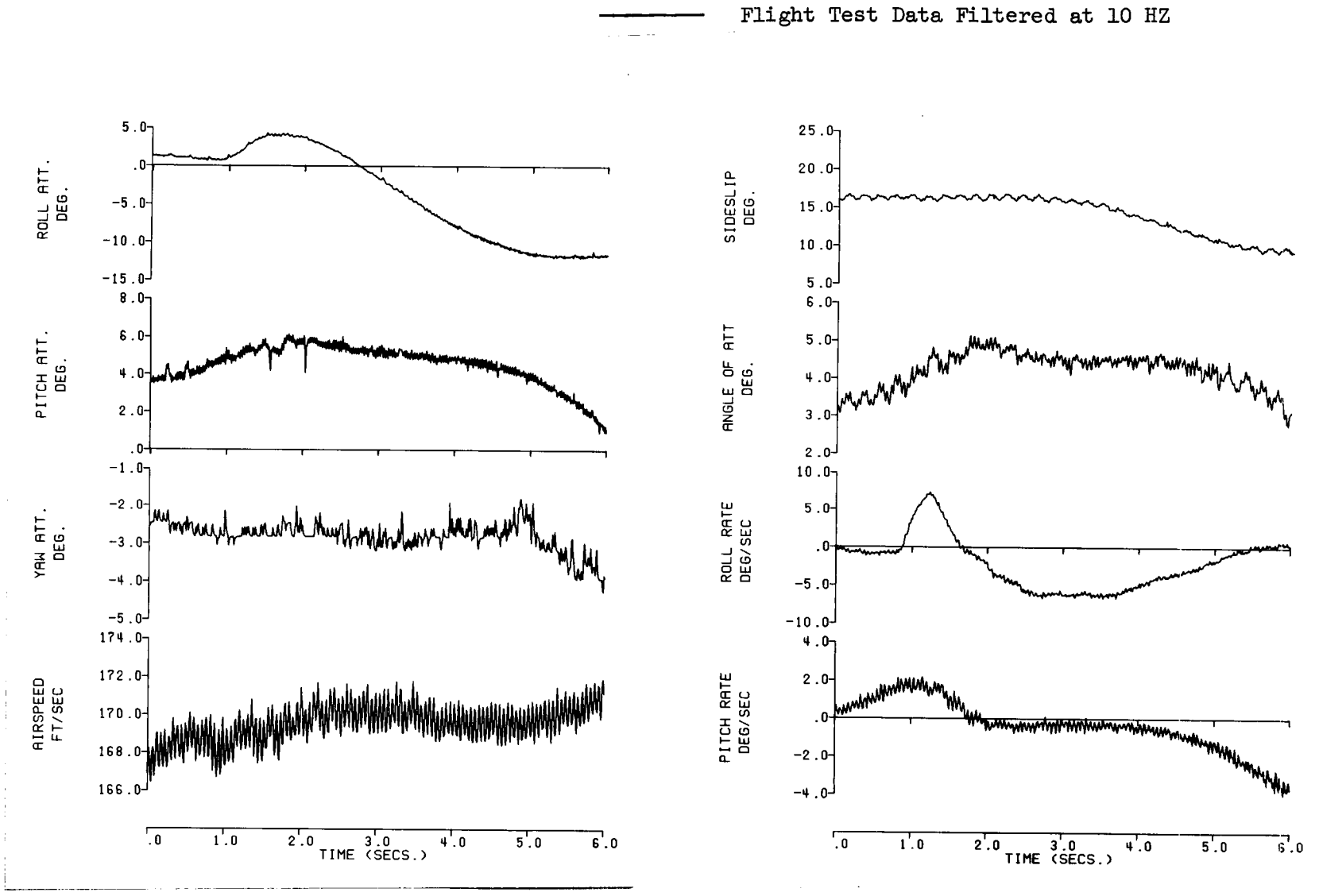

Figure 8. - Flight Test Data From CH-53A Filtered With A First Order Low Pass Filter At 10 HZ. (100 knots, Maneuver 5). (Data not used in the Identification.)

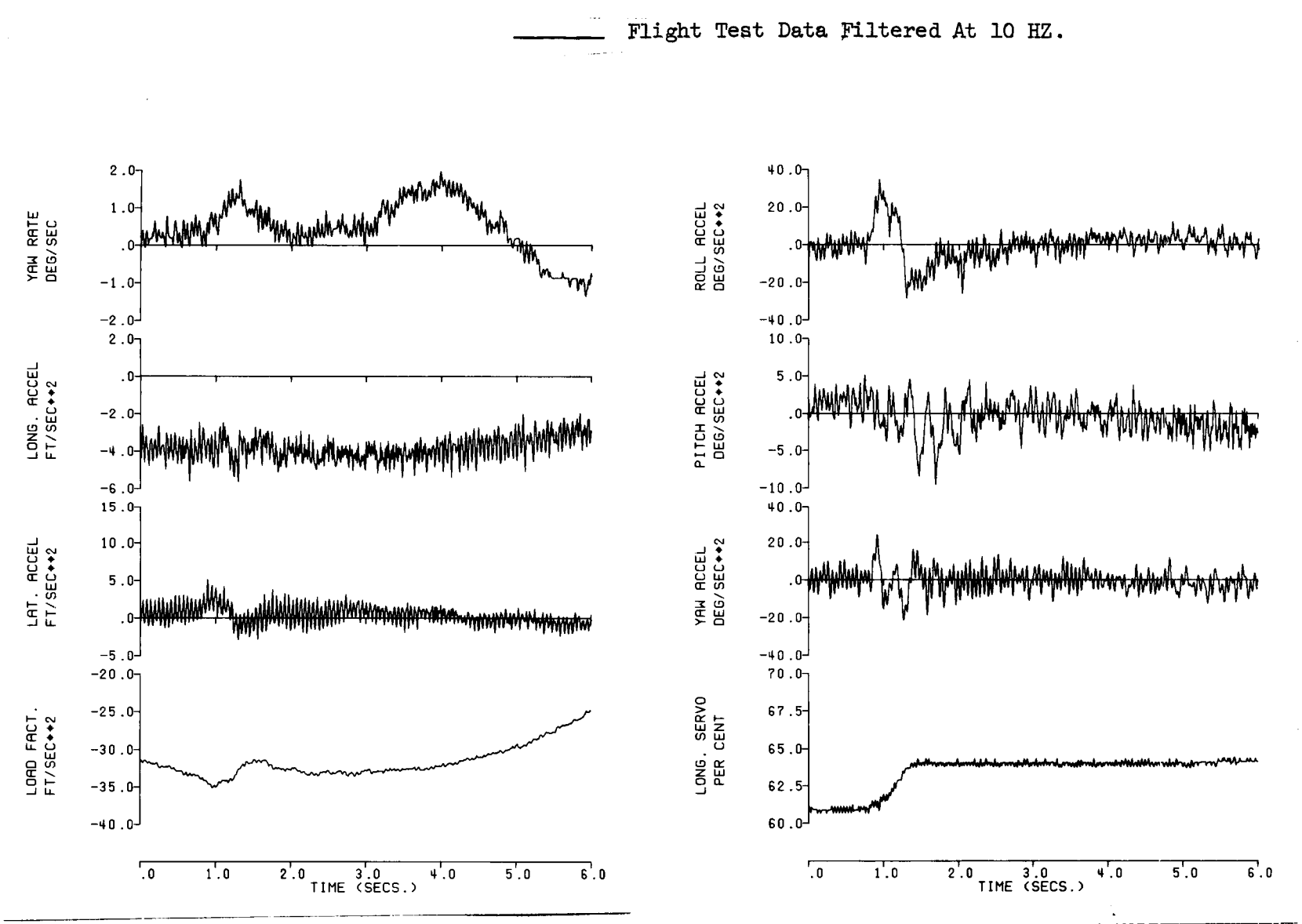

Figure 8. - Continued.

——— Flight Test Data Filtered At 10 HZ.

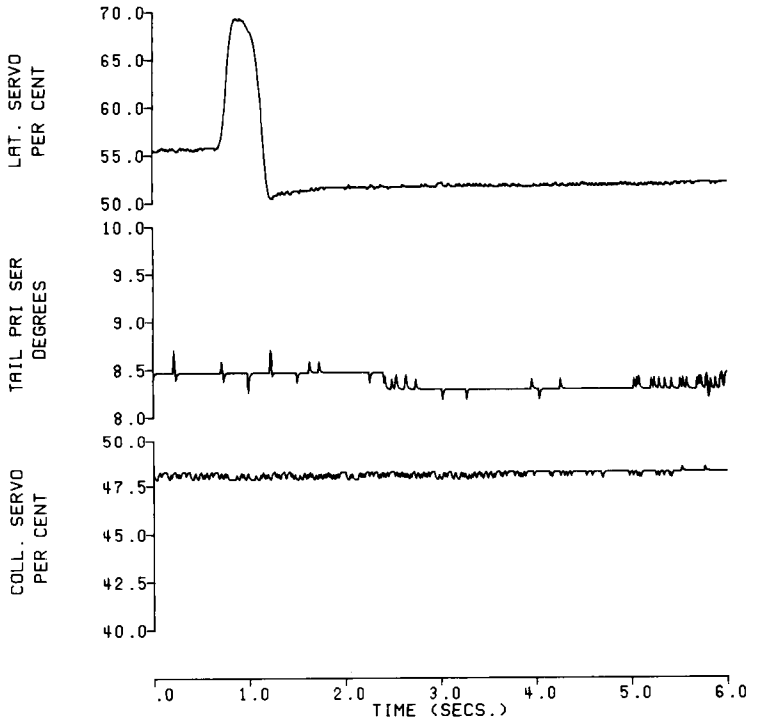

Figure 8 . - Concluded.

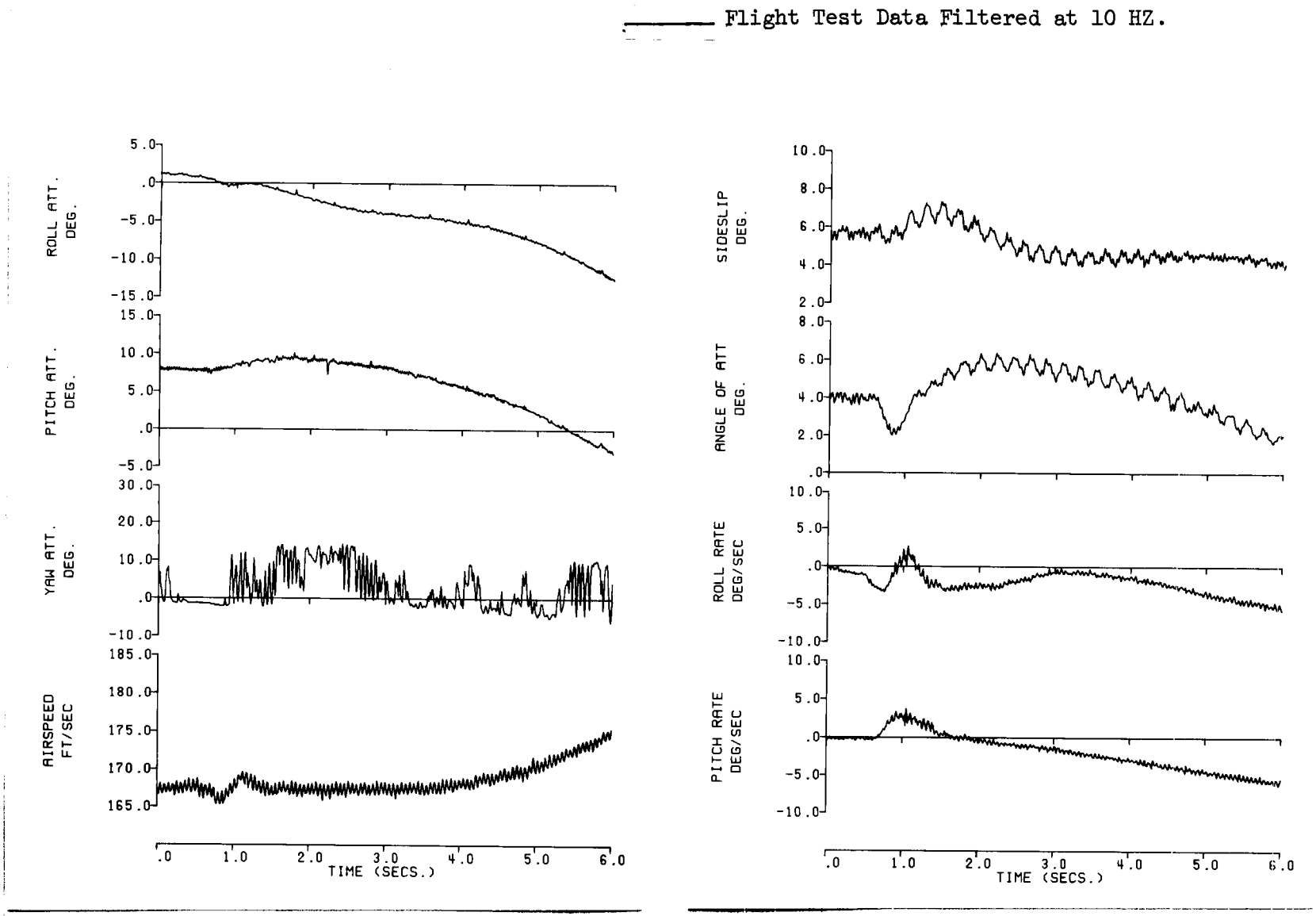

Figure 9 . - Flight Test Data From CH-53A Filtered With A First Order Low Pass Filter At 10 HZ (100 knots, Maneuver 6). (Data not used in the Identification.)

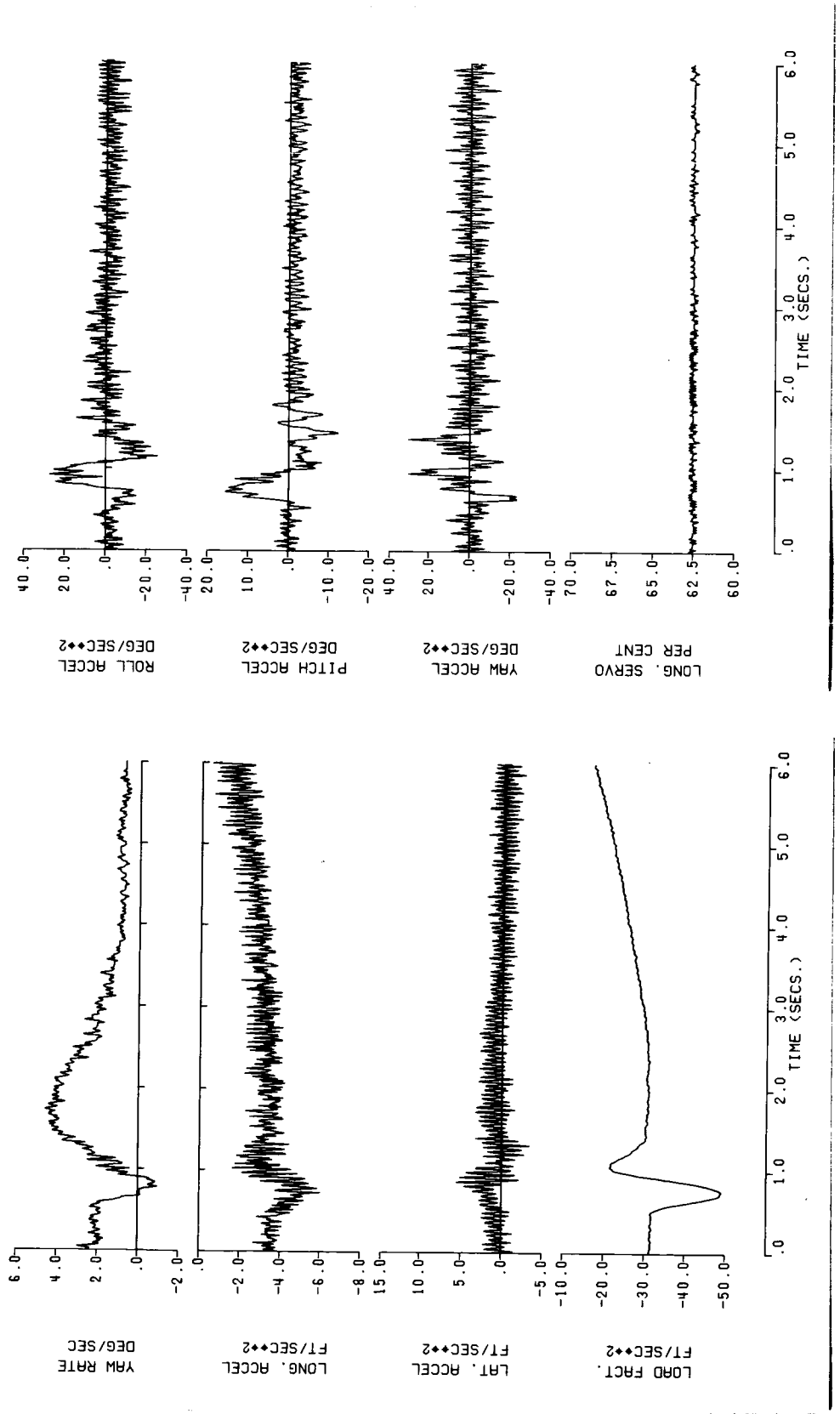

Figure 9 . - Continued.

——— Flight Test Data Filtered At 10 HZ.

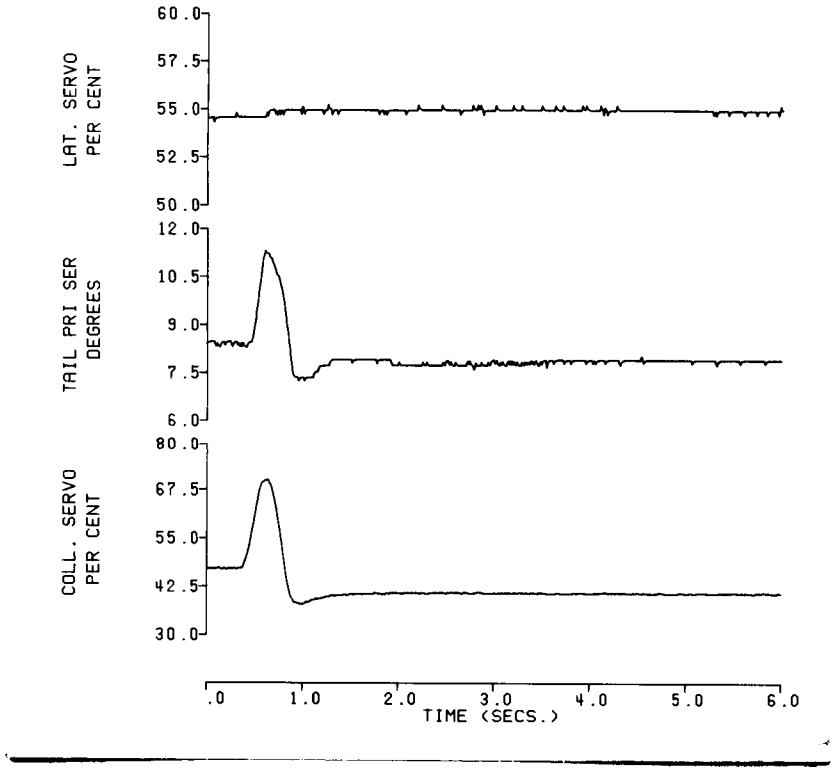

Figure 9. - Concluded.

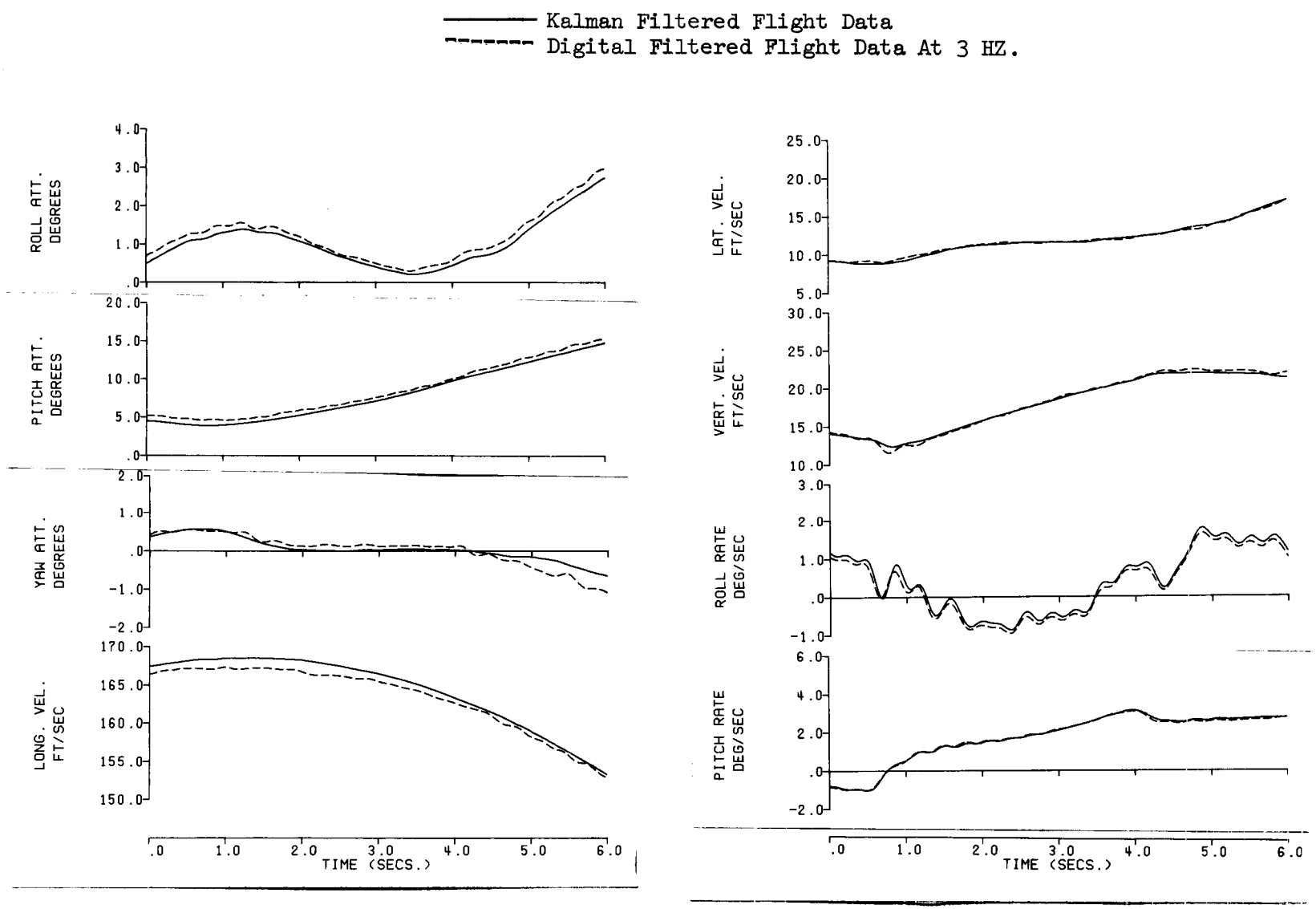

Figure 10 . - Comparison of Flight Test Data From CH-53A using the Kalman and Digital Filtering Methods (100 knots, Maneuver 1).

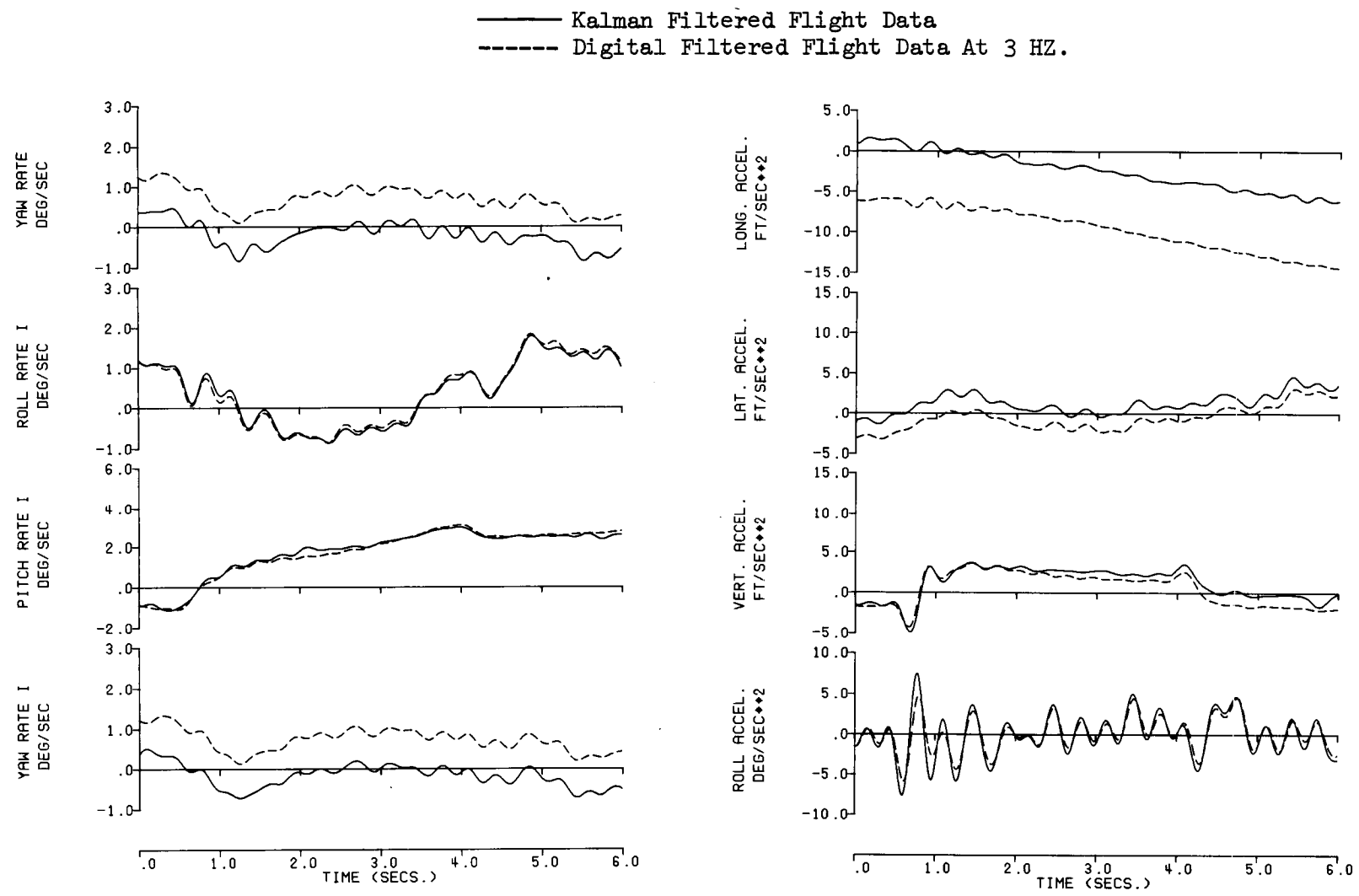

Figure 10. - Continued.

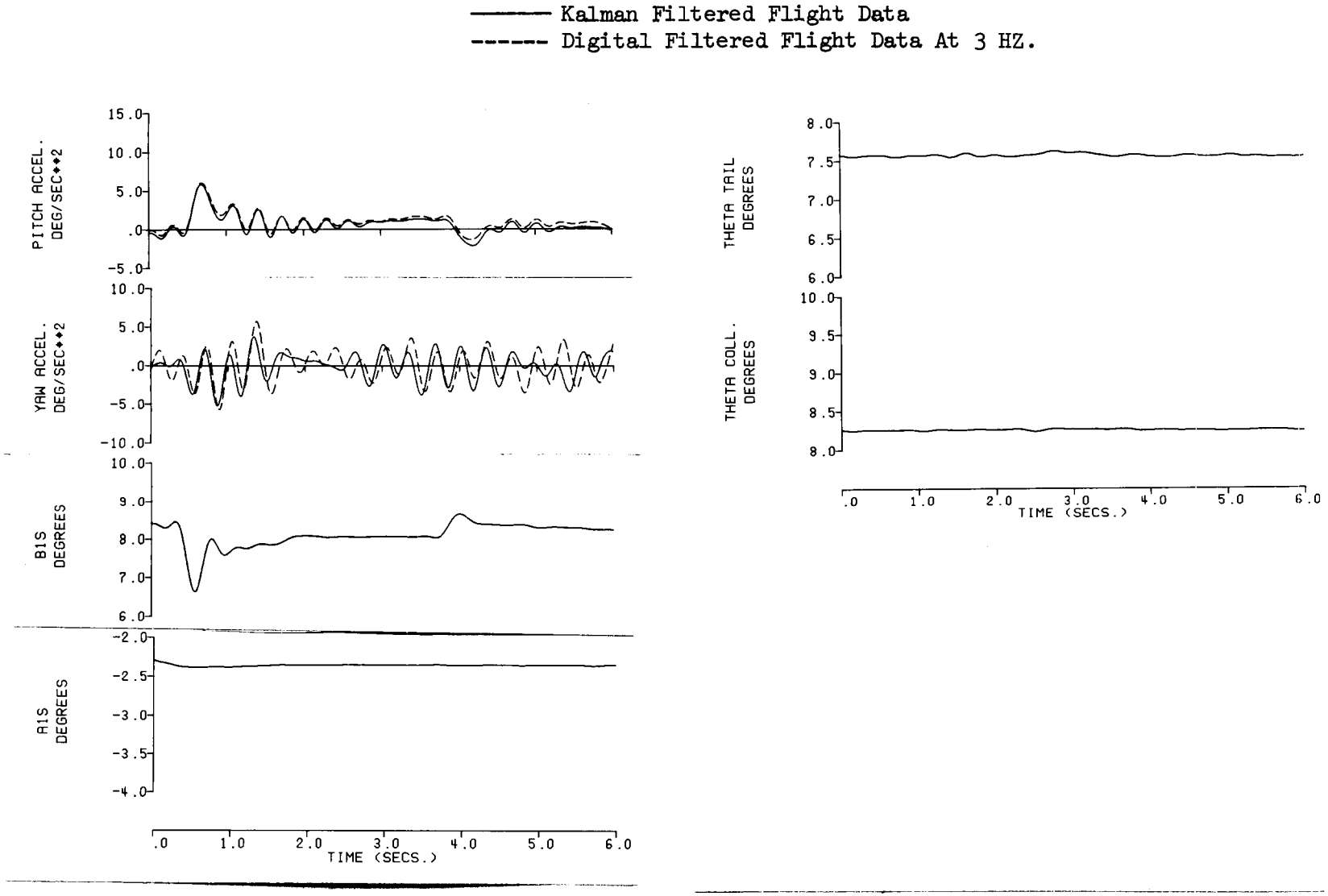

Figure 10 . - Concluded.

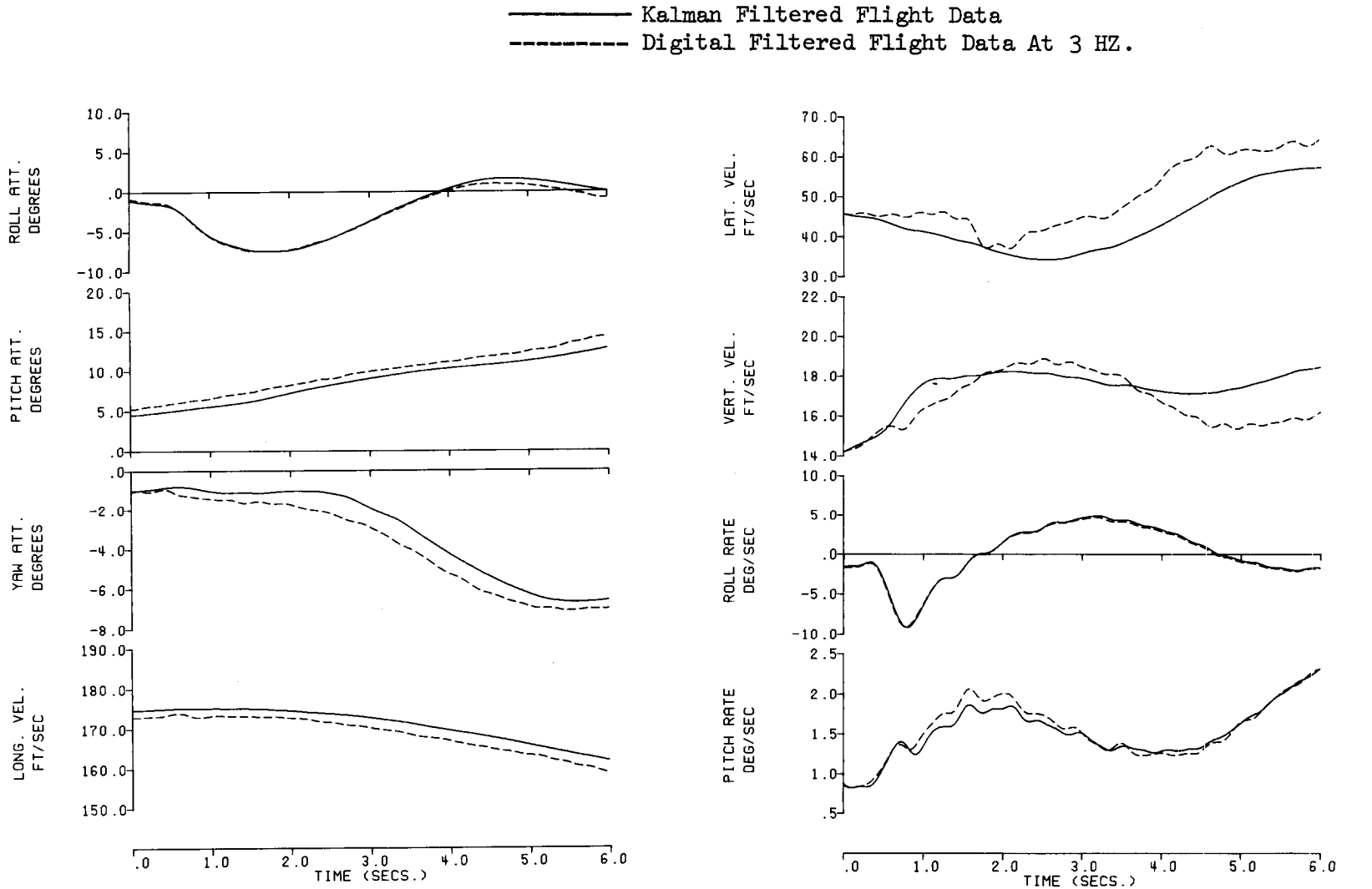

Figure 11 . - Comparison of Flight Test Data From CH-53A using the Kalman and Digital Filtering Methods (100 knots, Maneuver 2).

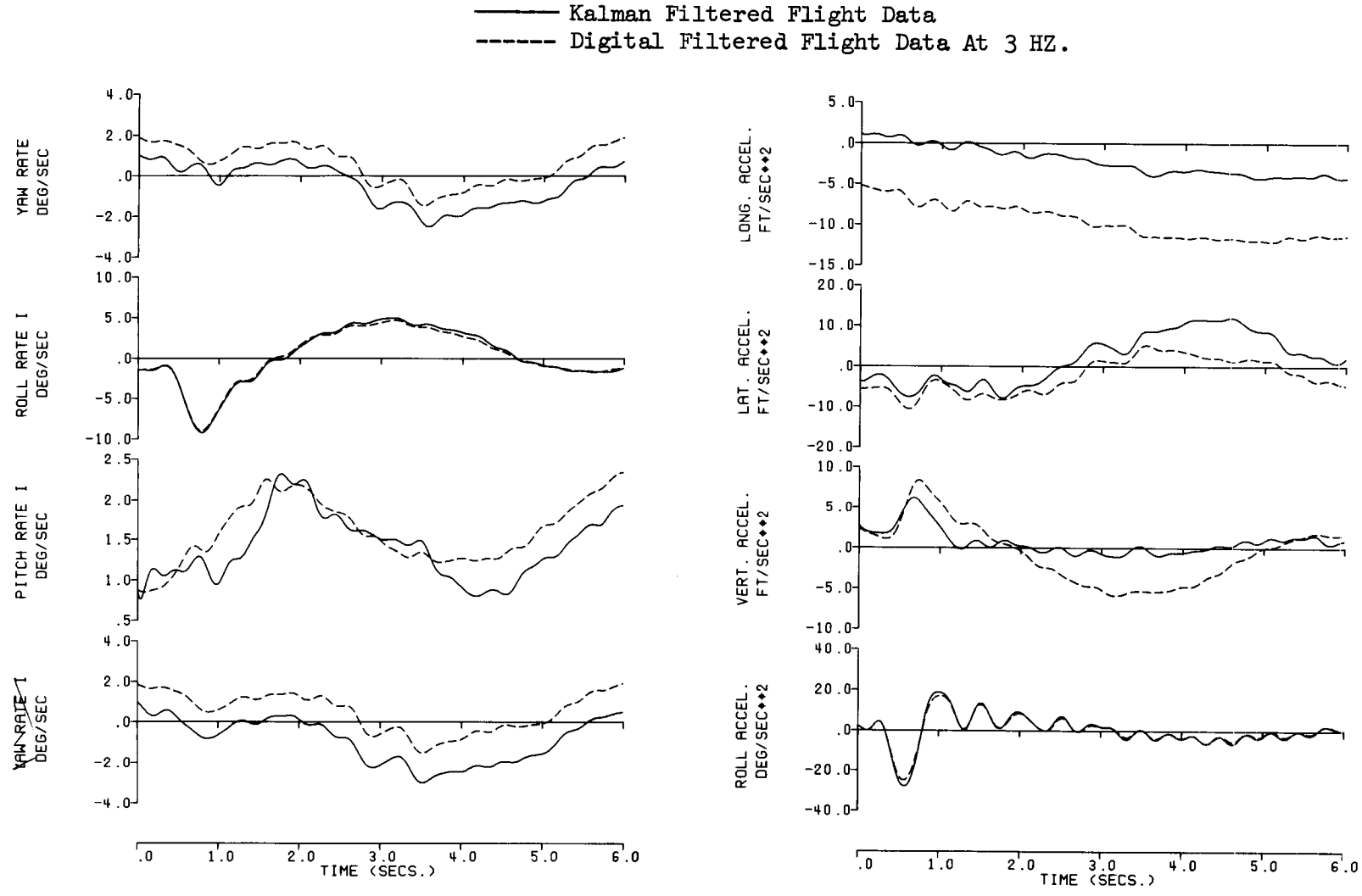

Figure 11 . - Continued.

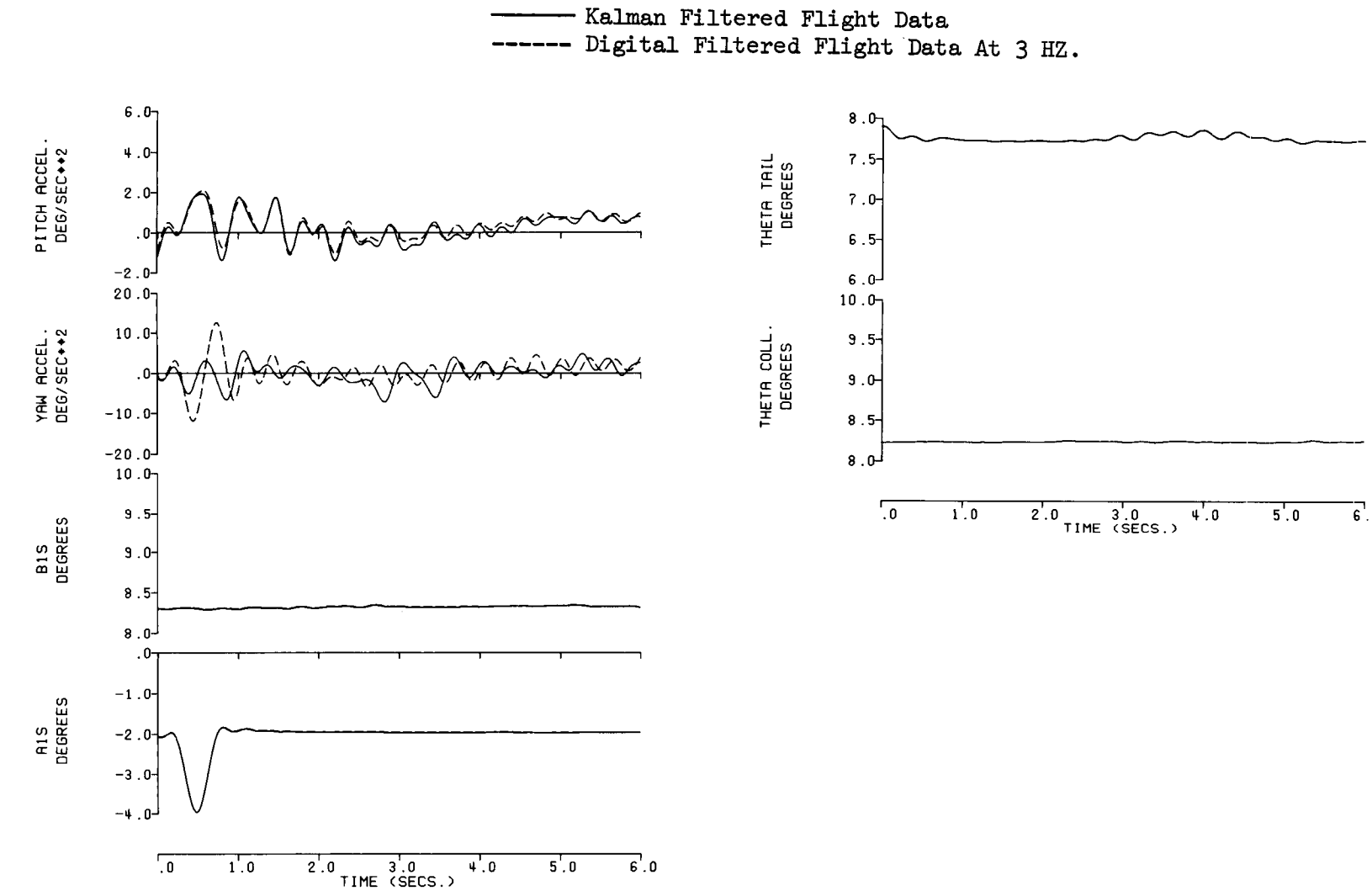

Figure 11 . - Concluded.

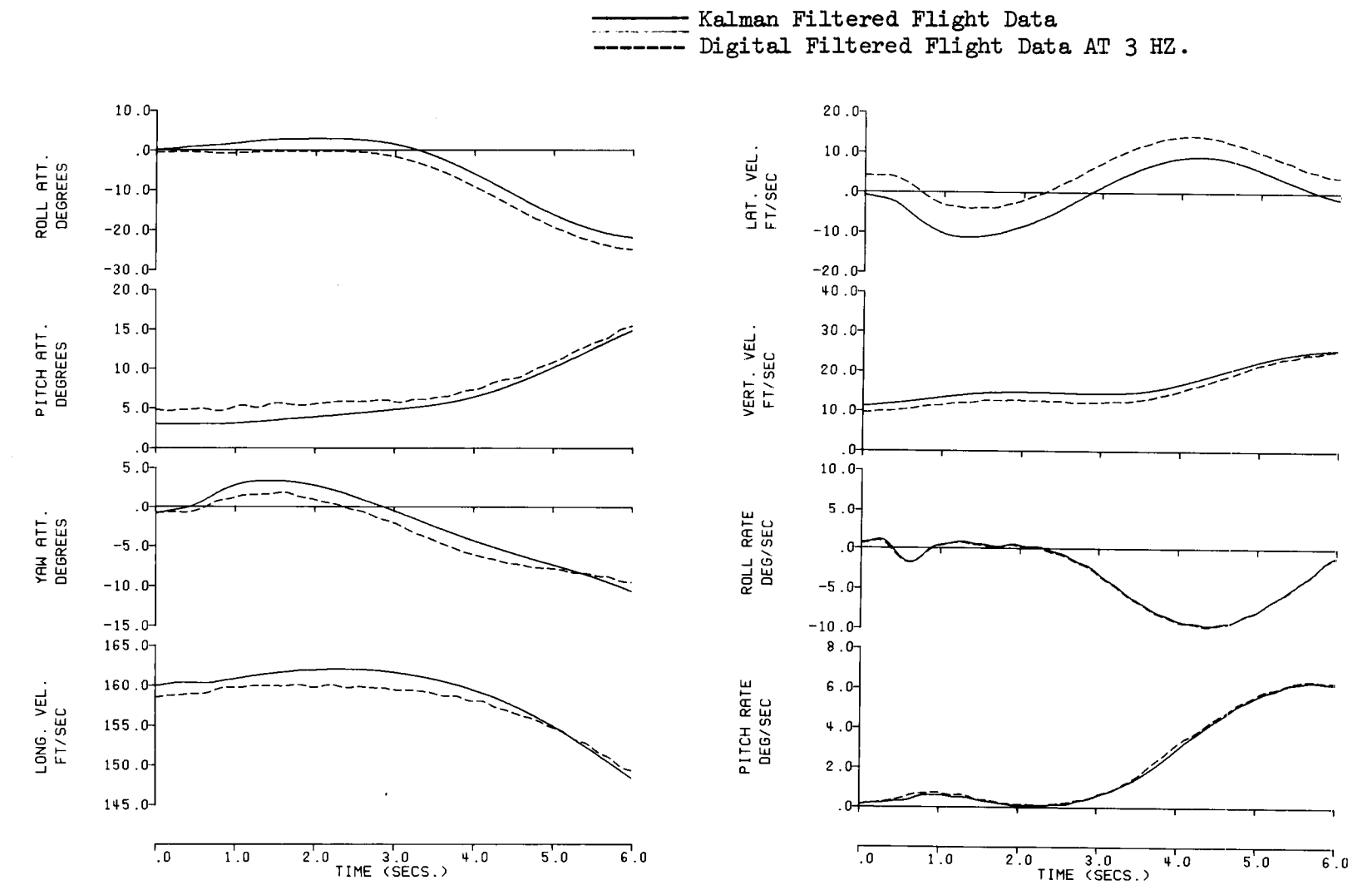

Figure 12. - Comparison of Flight Test Data From CH-53A using the Kalman and Digital Filtering Methods (100 knots, Maneuver 3).

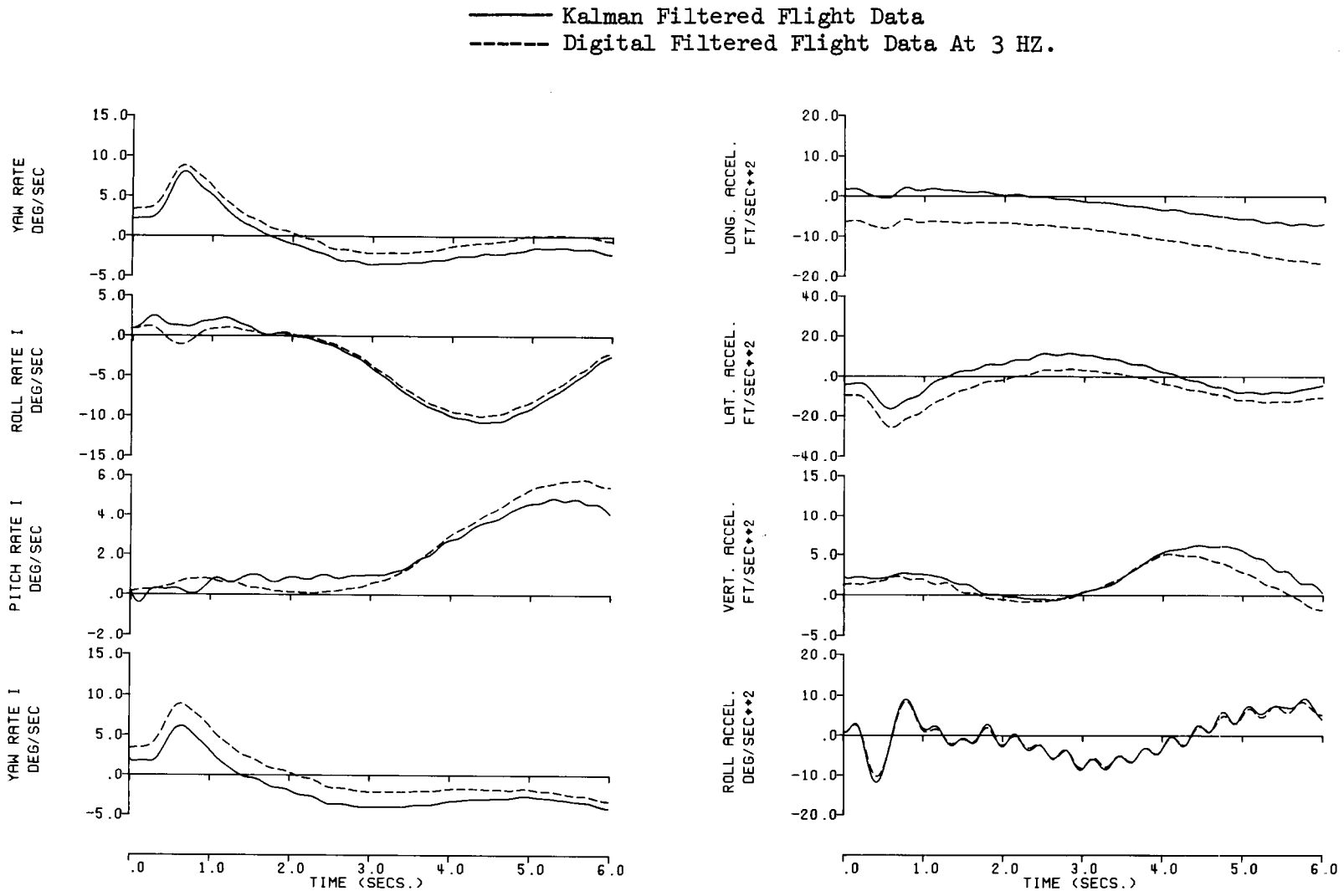

Figure 12 - Continued.

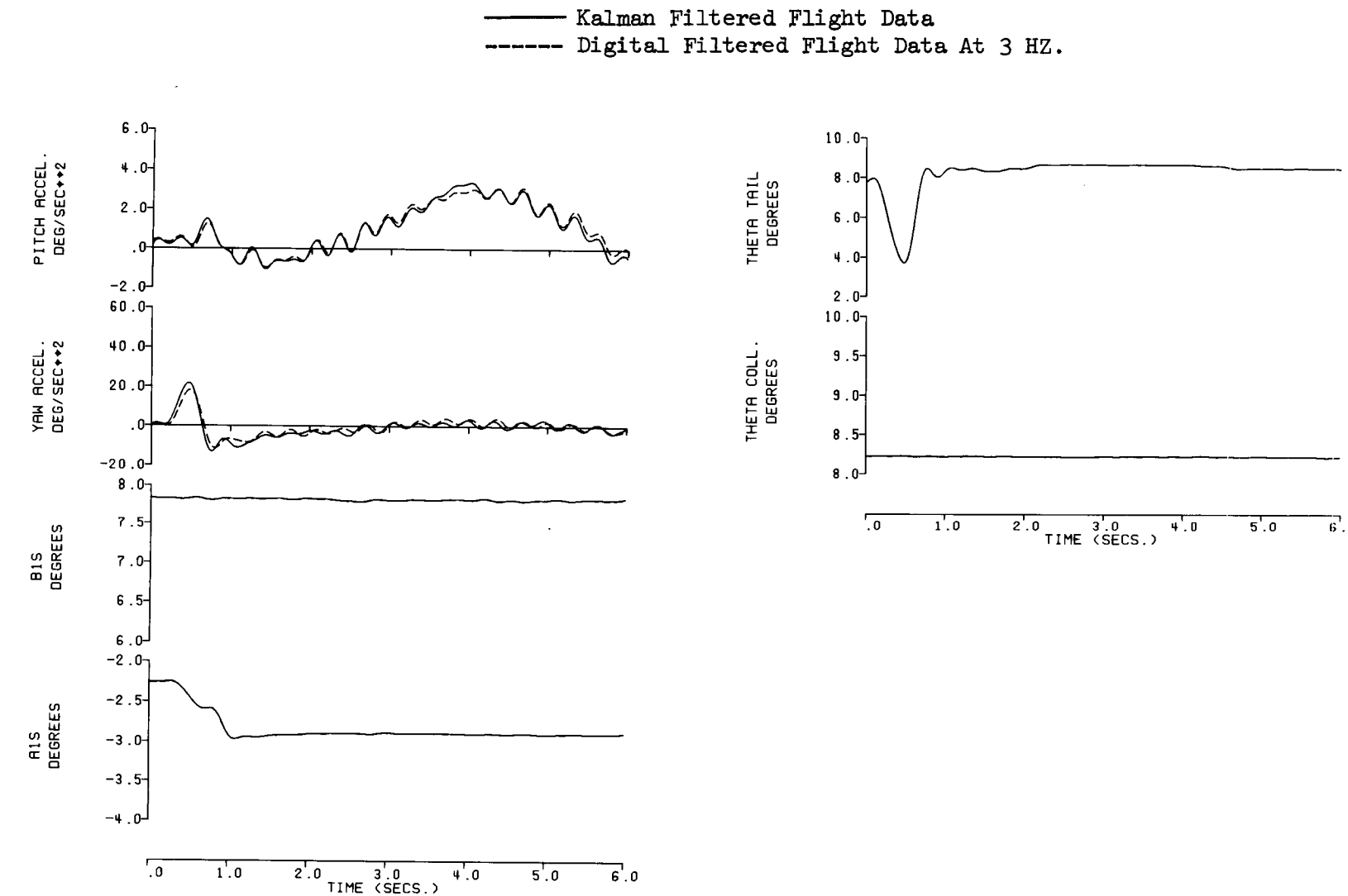

Figure 12 . - Concluded.

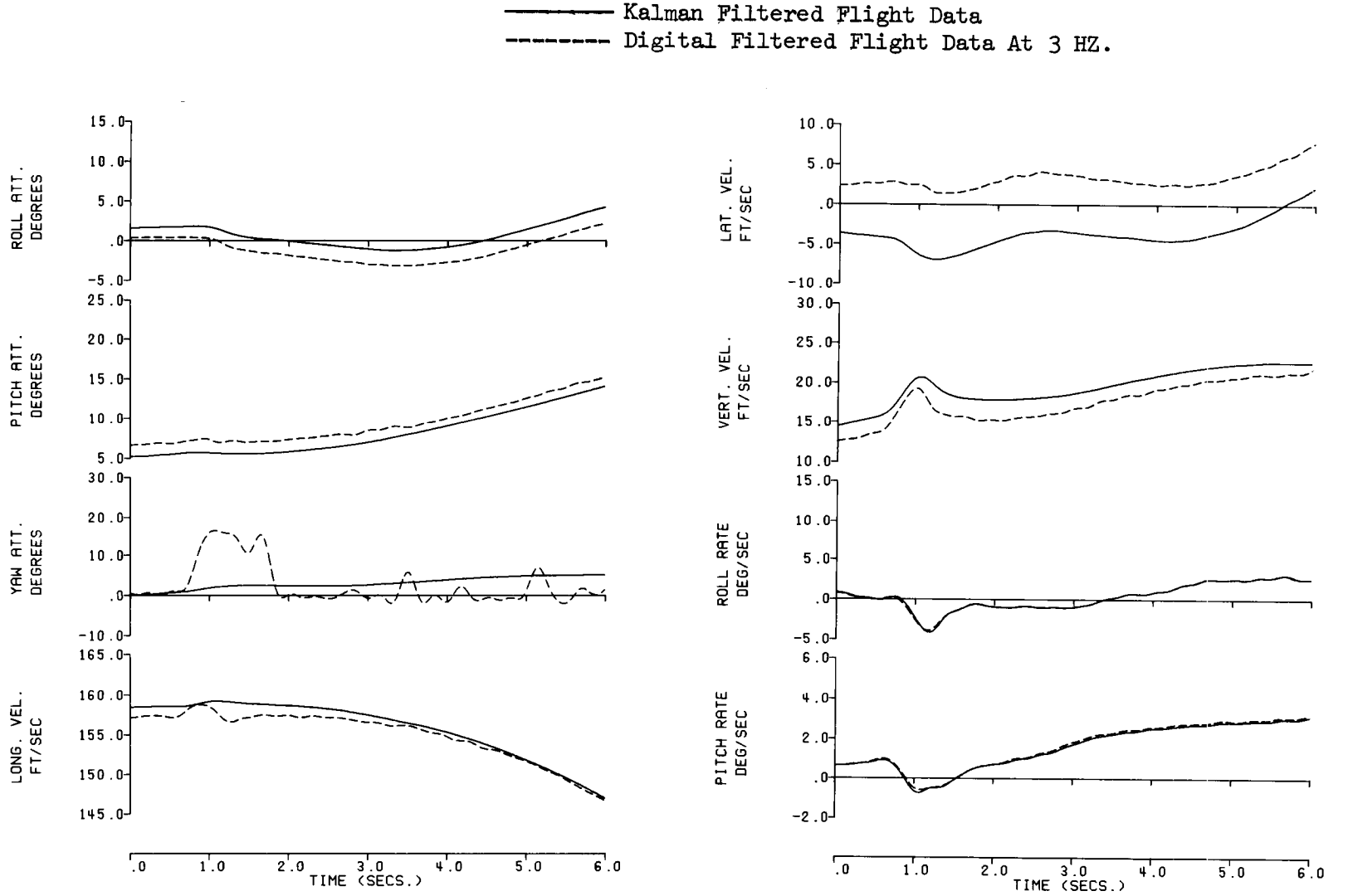

Figure 13. - Comparison of Flight Test Data From CH-53A using the Kalman and Digital Filtering Methods (100 knots, Maneuver 4).

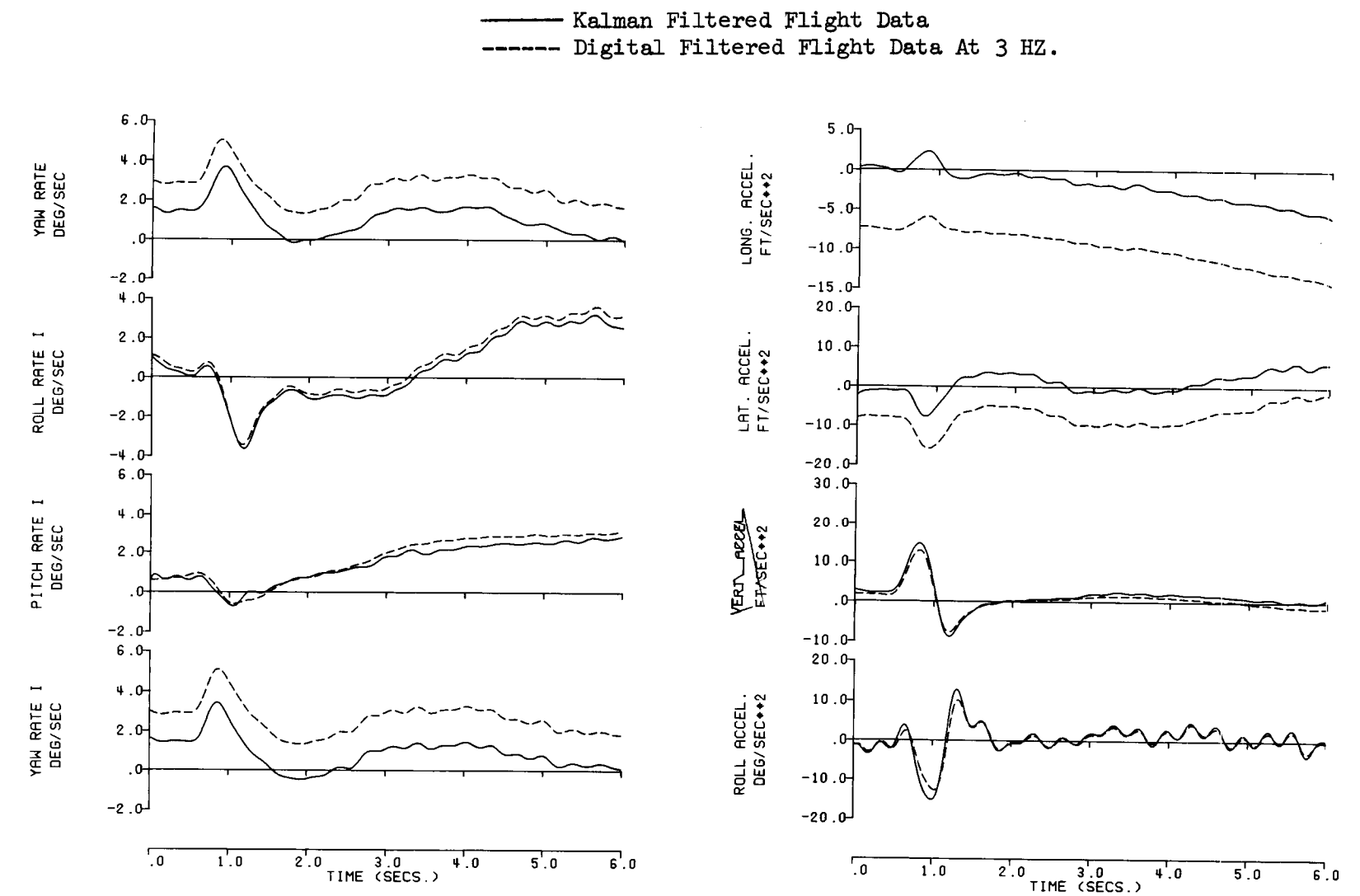

Figure 13 - Continued.

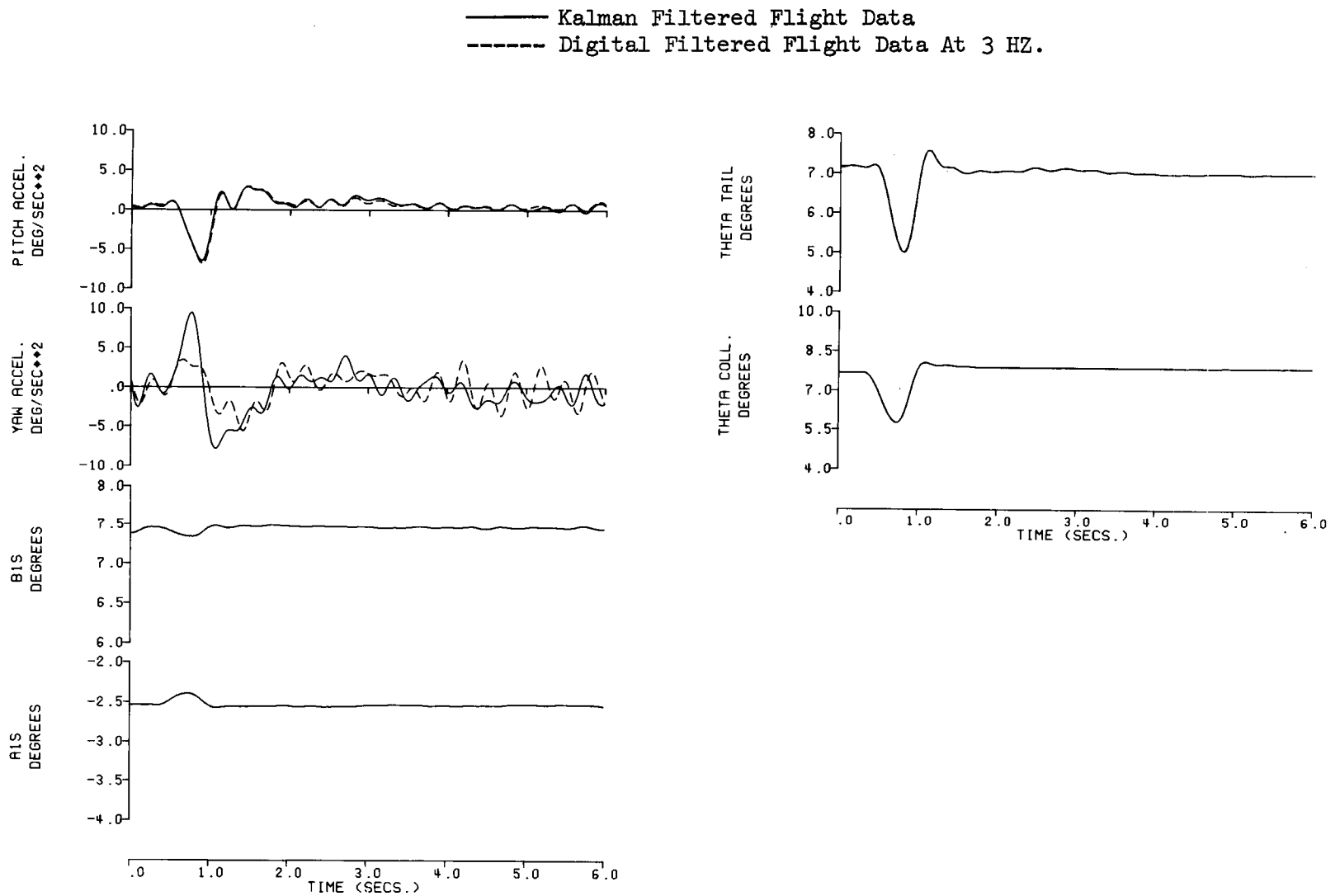

Figure 13. - Concluded.

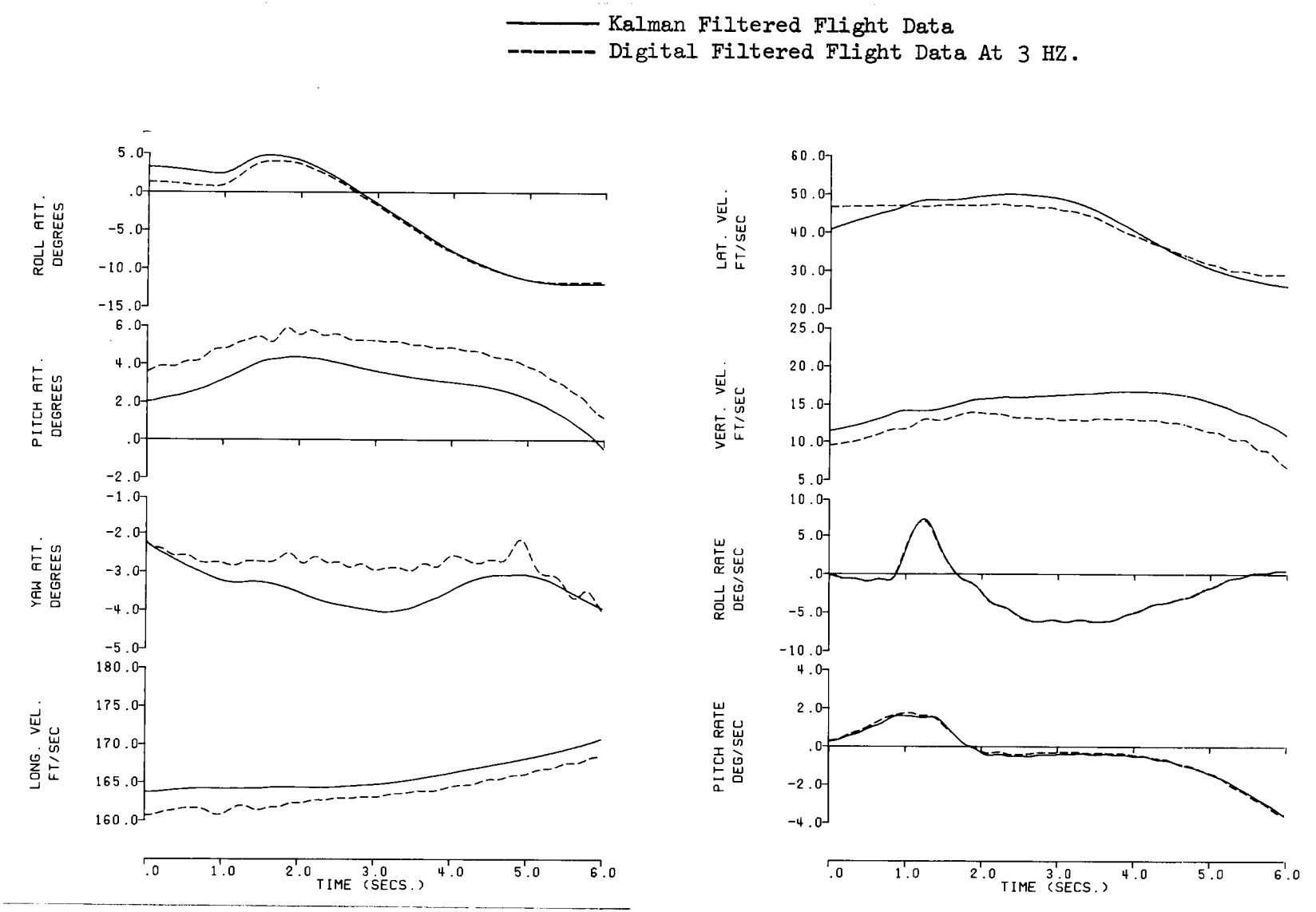

Figure 14 . - Comparison of Flight Test Data From CH-53A using the Kalman and Digital Filtering Methods (100 knots, Maneuver 5).(Data not used in the Identification.)

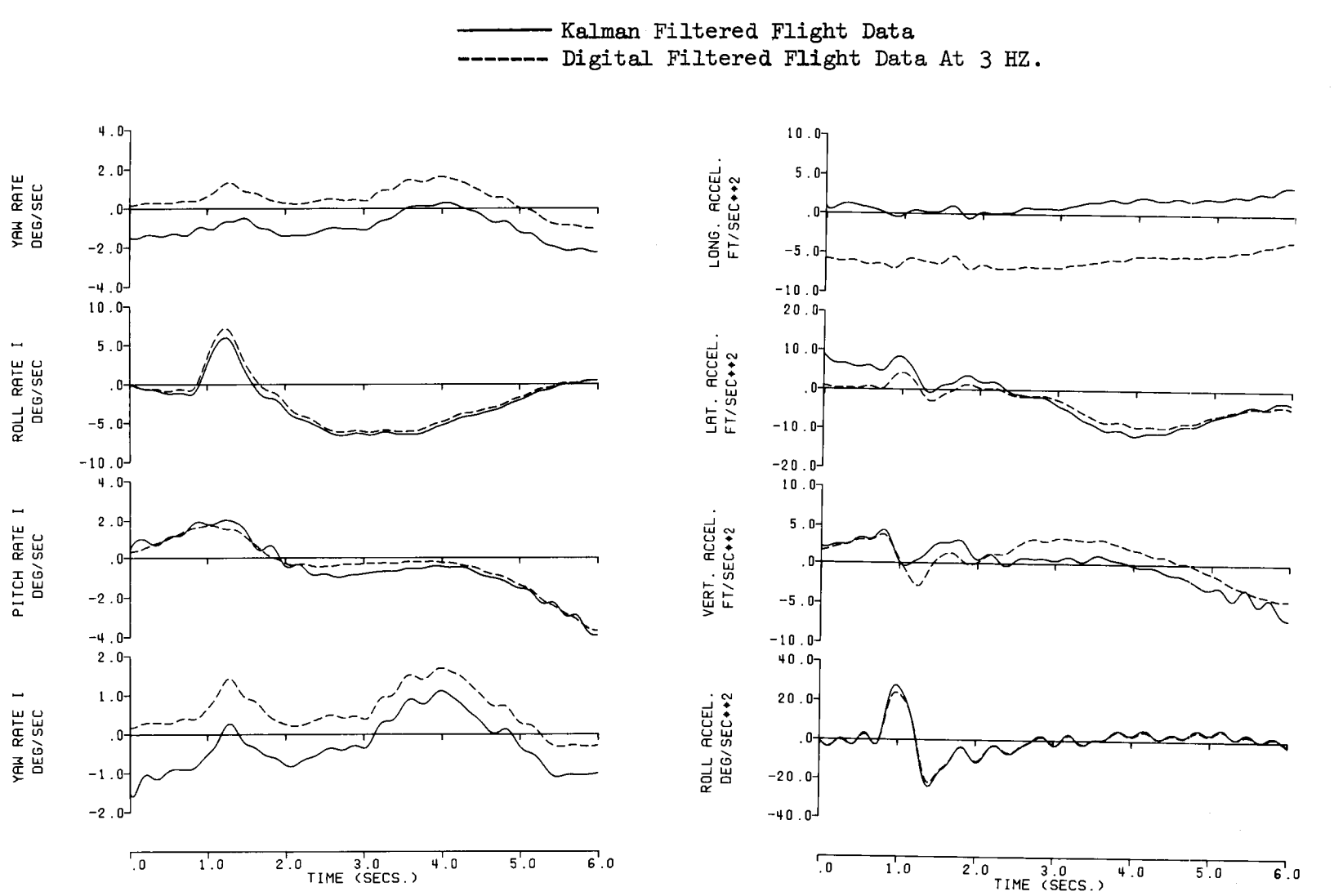

Figure 14 - Continued.

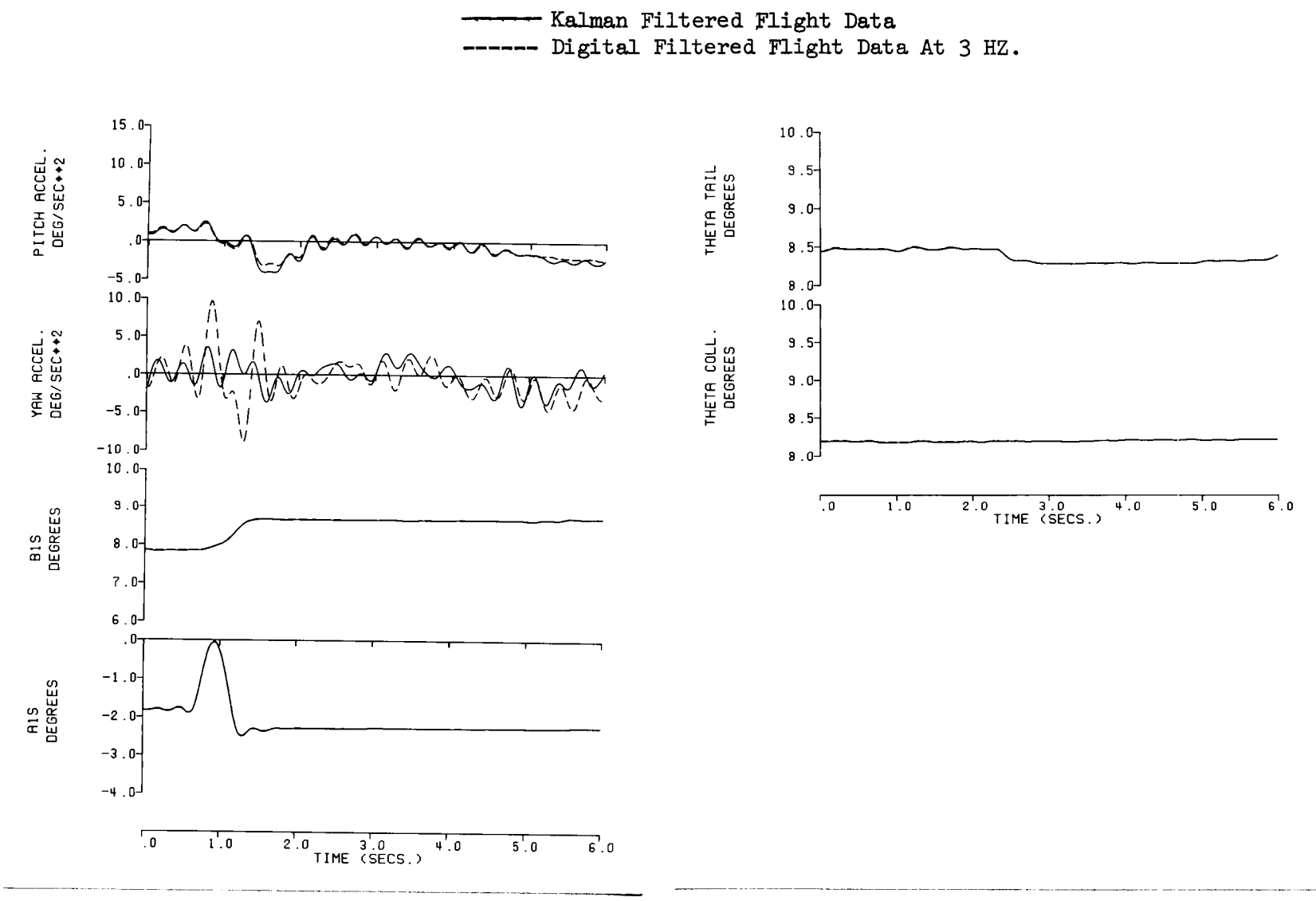

Figure 14. - Concluded.

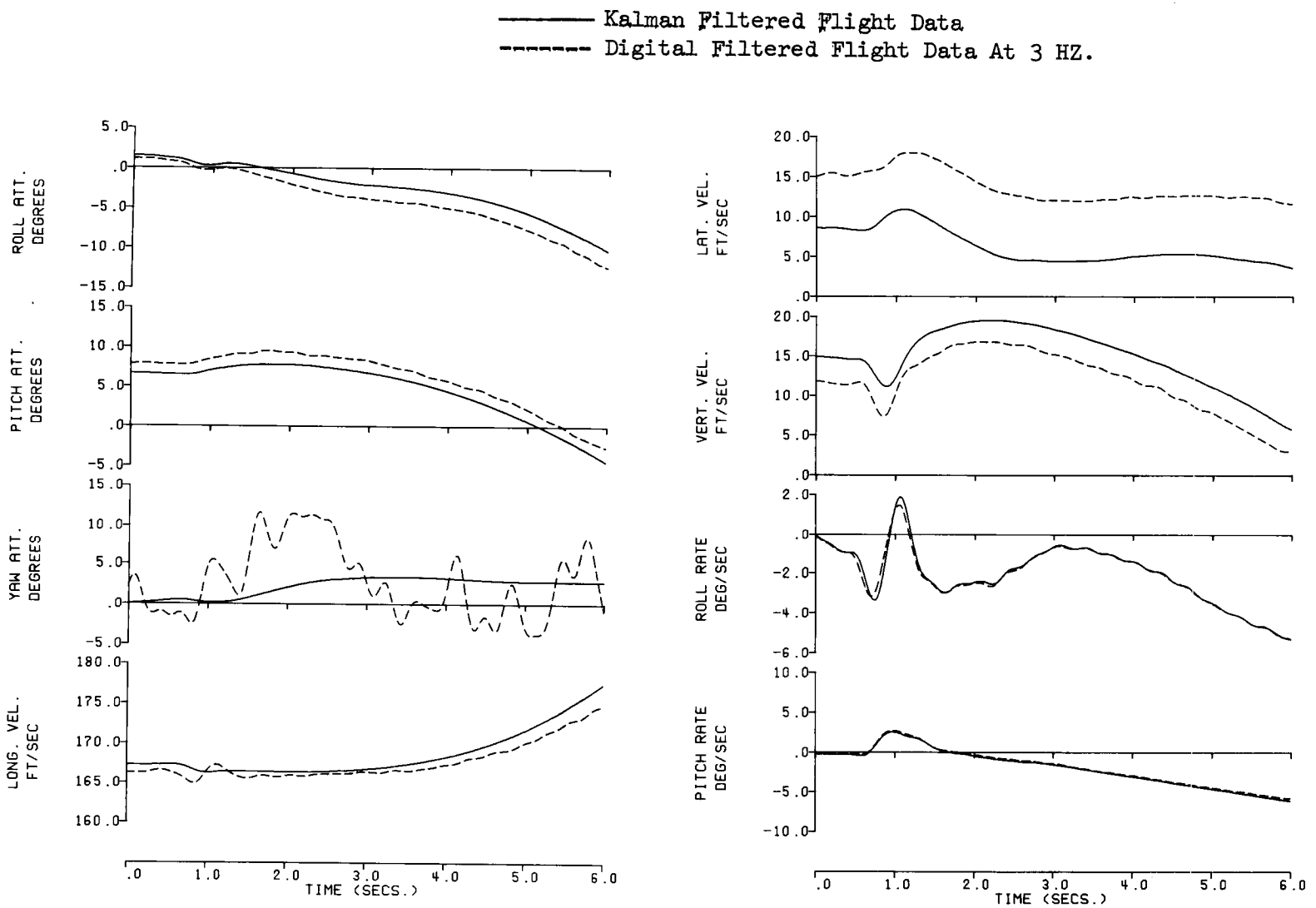

Figure 15. - Comparison of Flight Test Data From CH-53A using the Kalman and Digital Filtering Methods (100 knots, Maneuver 6). (Data not Used in the Identification.)

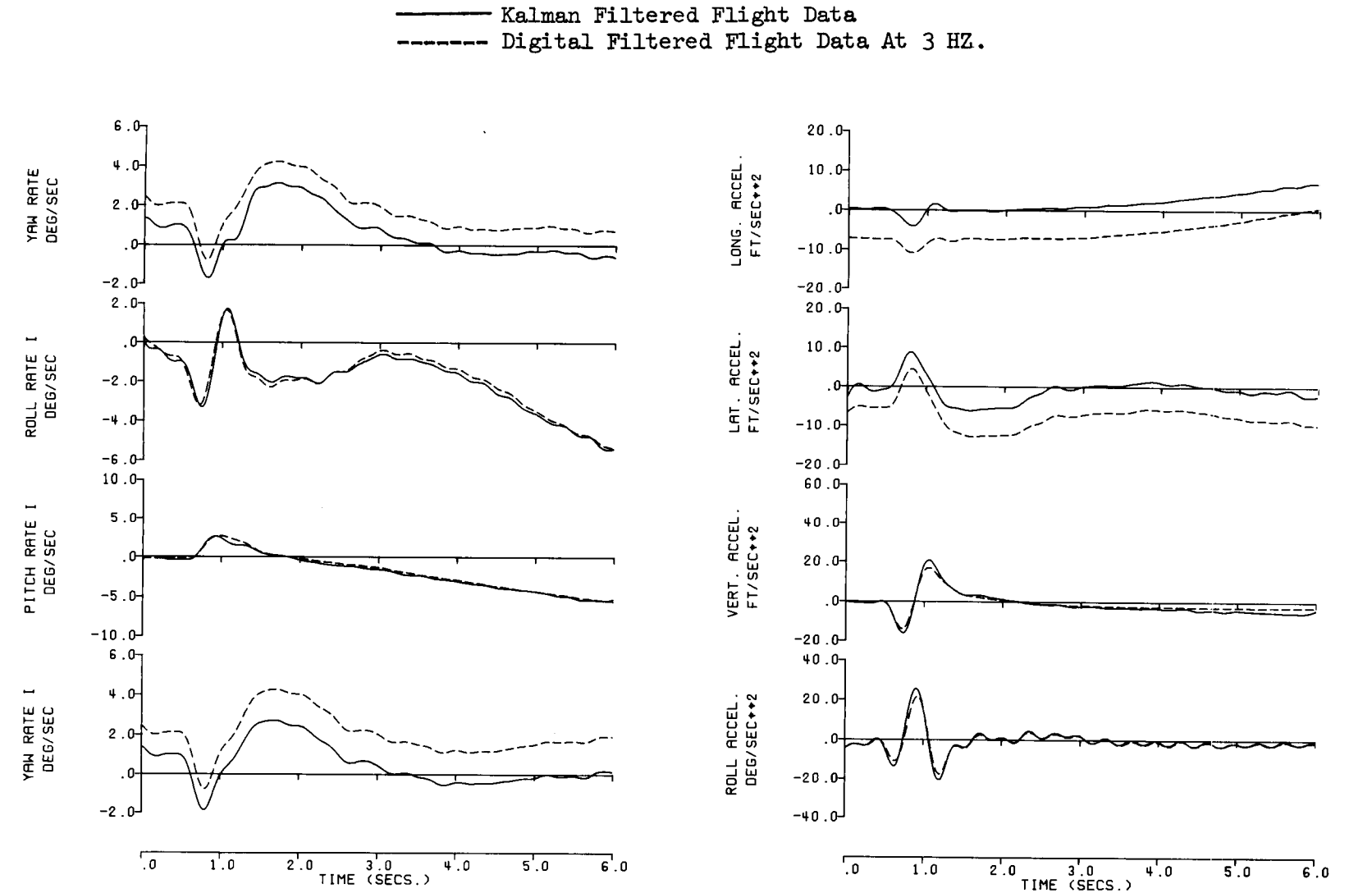

Figure 15 - Continued.

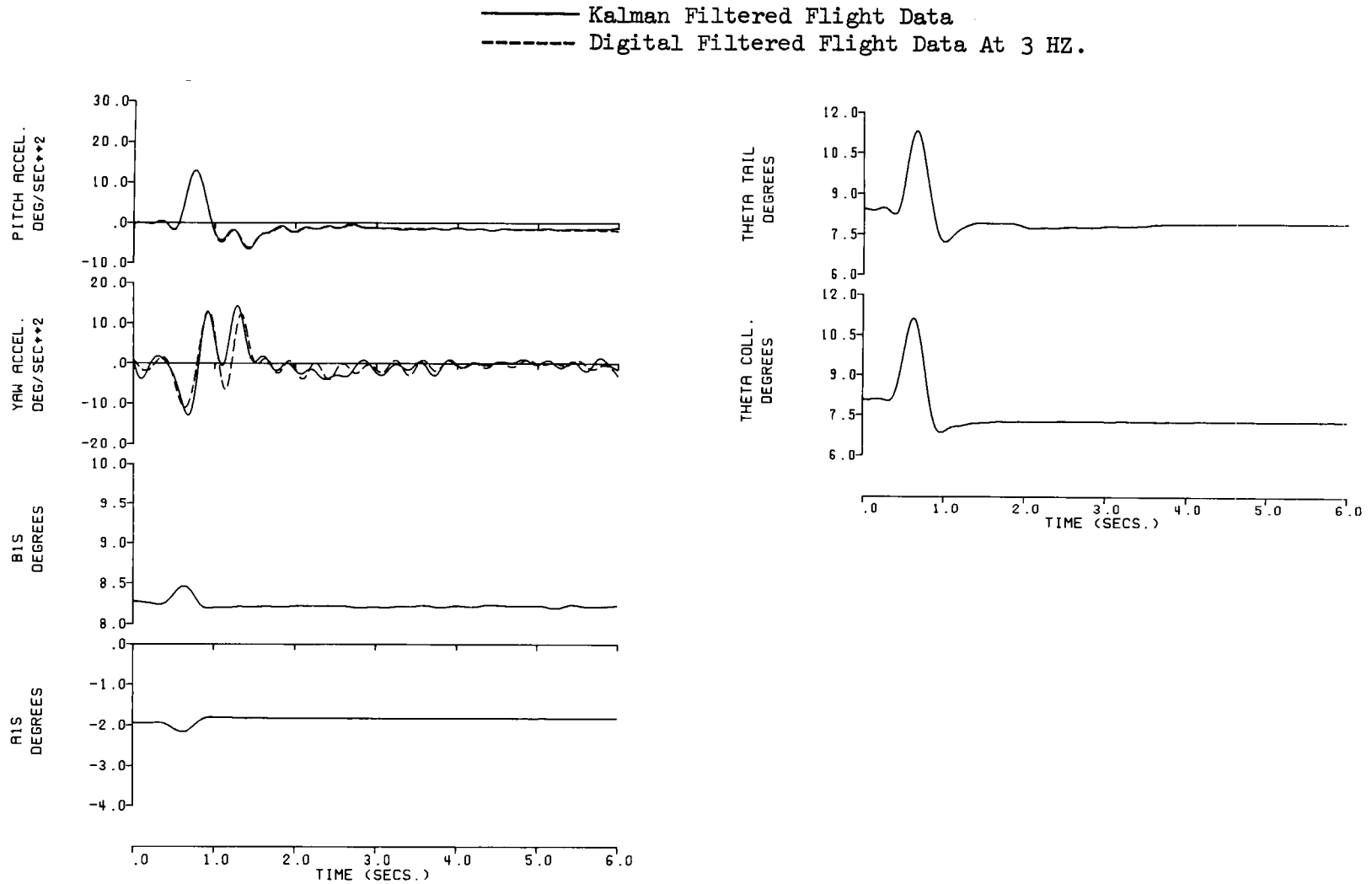

Figure 15. - Concluded.

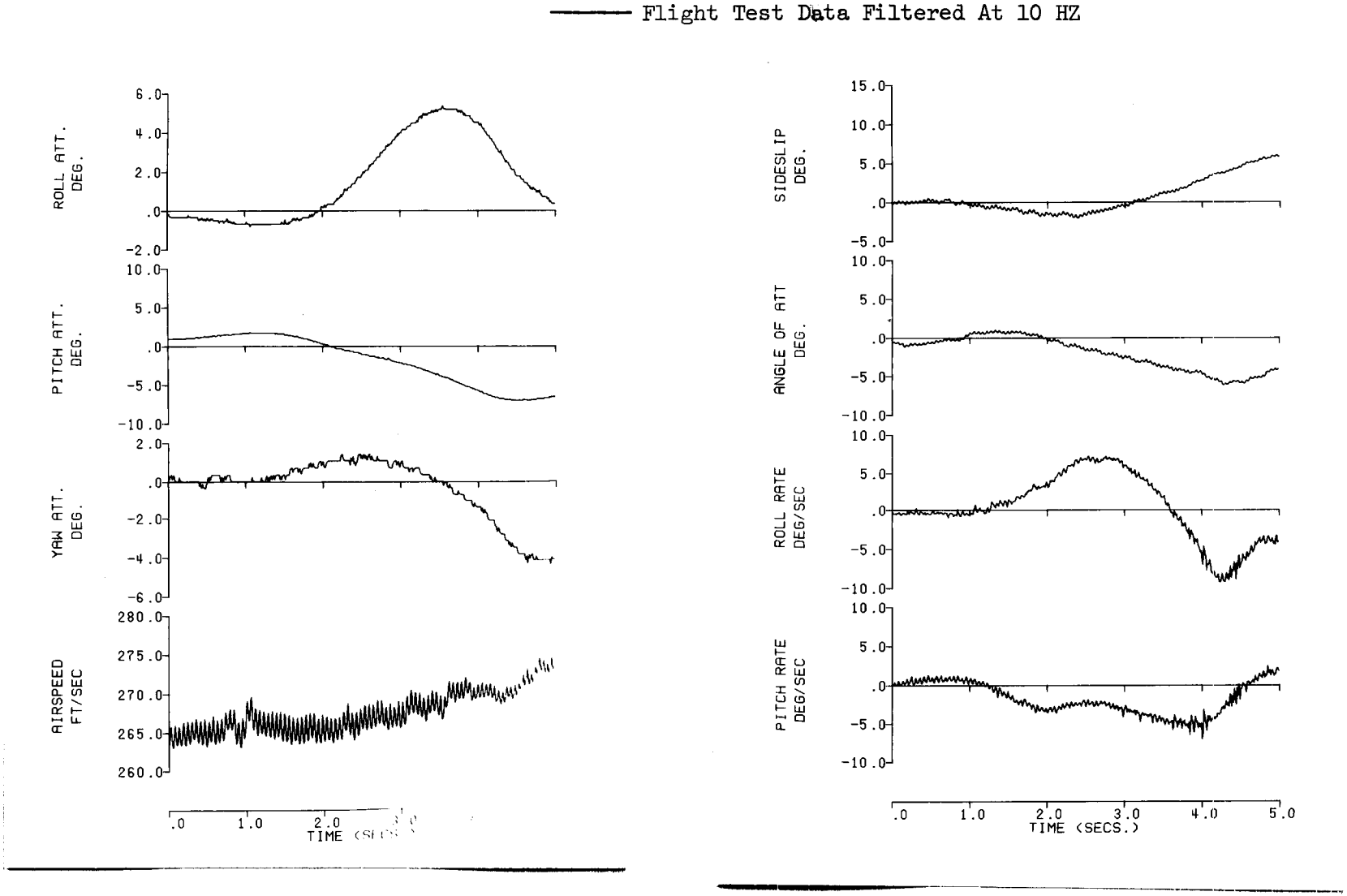

Figure 16. - Flight Test Data From CH-53A Filtered With A First Order Low Pass Filter At 10 HZ. (150 knots, Maneuver 1).

——— Flight Test Data Filtered At 10 HZ.

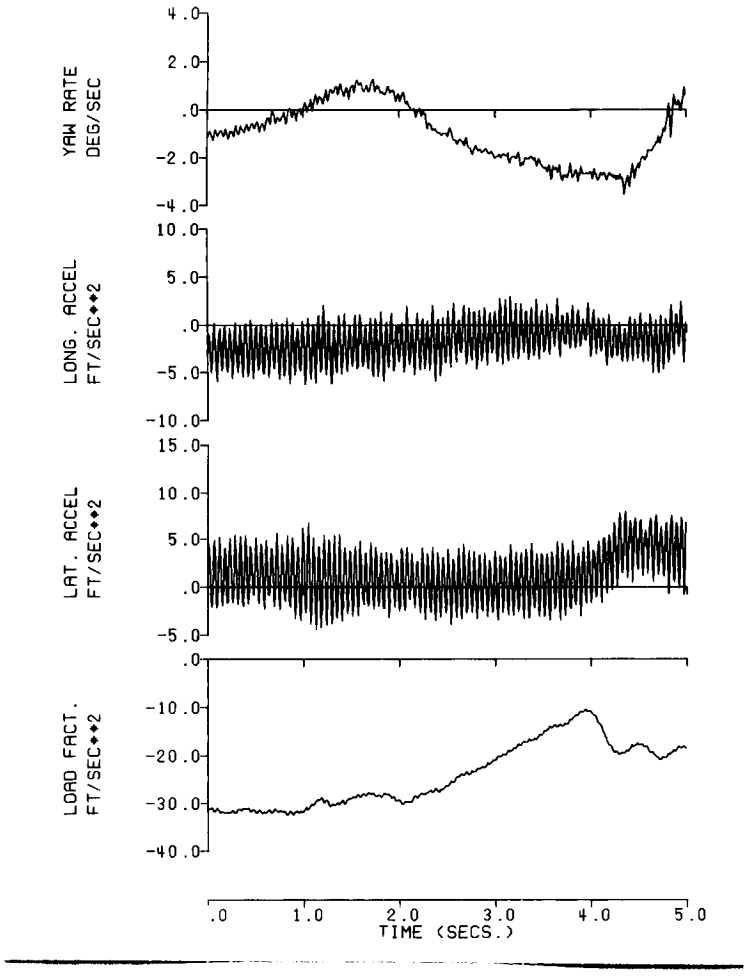

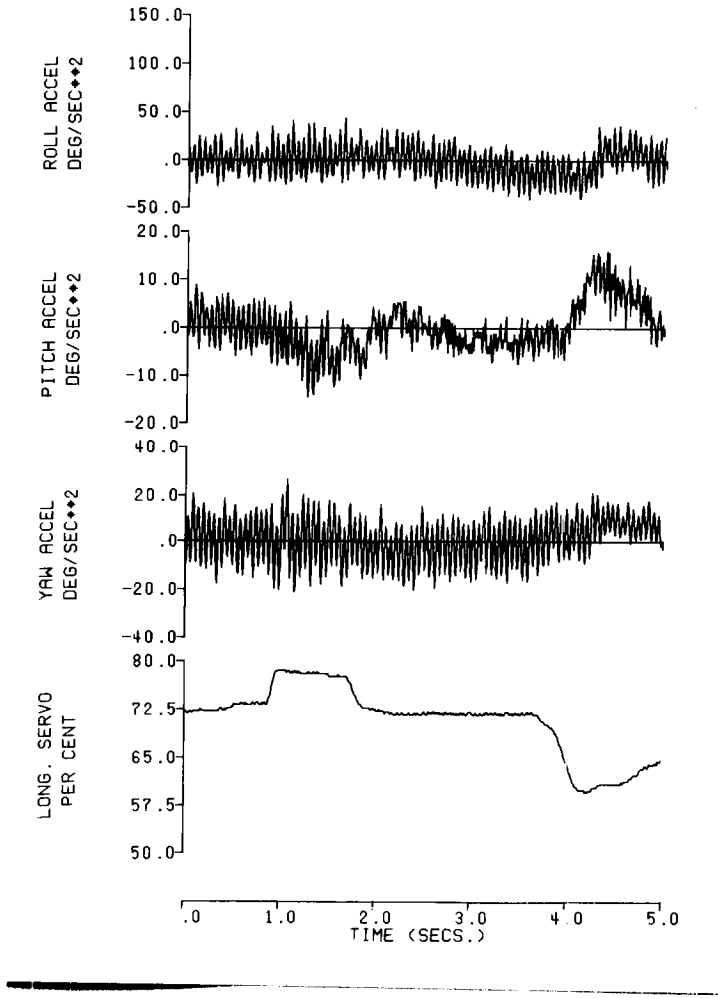

Figure 16. - Continued.

——— Flight Test Data Filtered At 10 HZ.

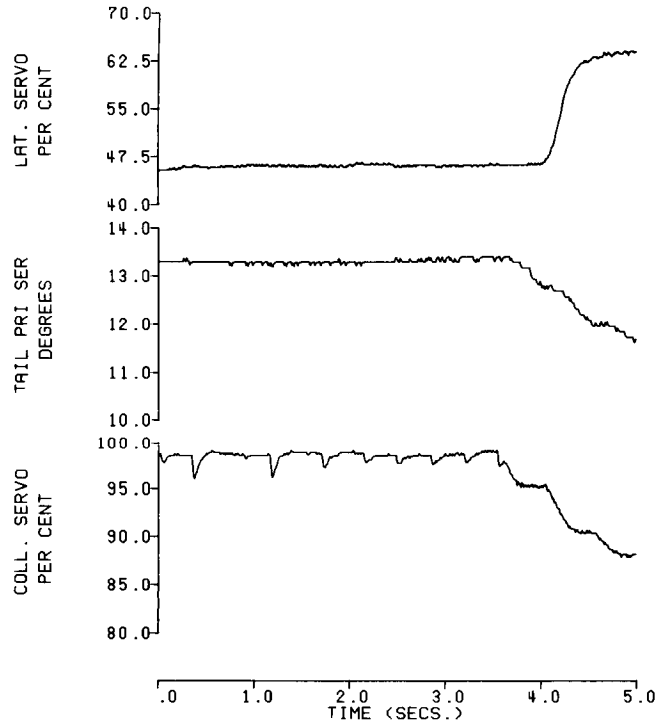

Figure 16. - Concluded.

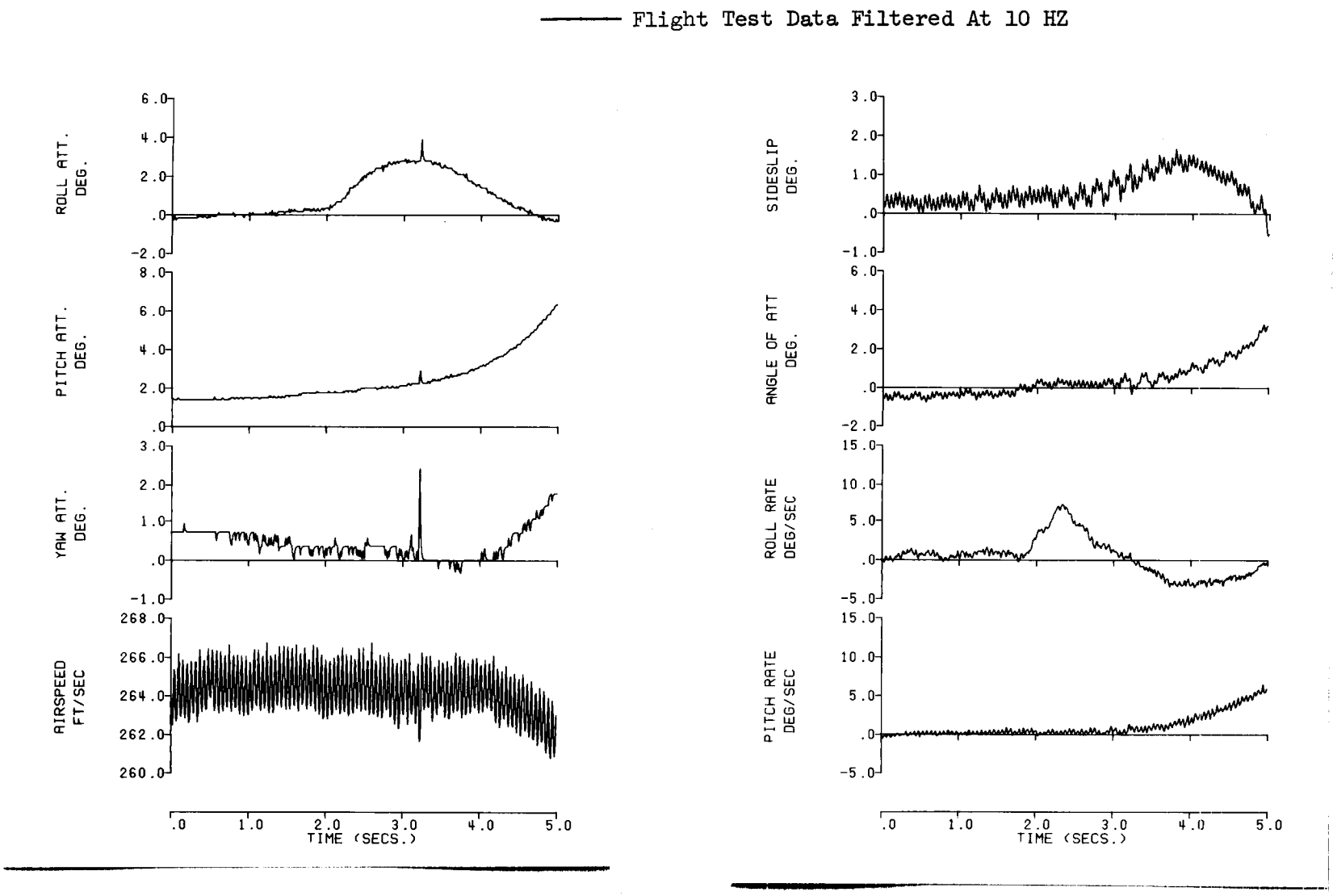

Figure 17 . - Flight Test Data From CH-53A Filtered With A First Order Low Pass Filter AT 10 HZ. (150 knots, Maneuver 2).

——— Flight Test Data Filtered At 10 HZ.

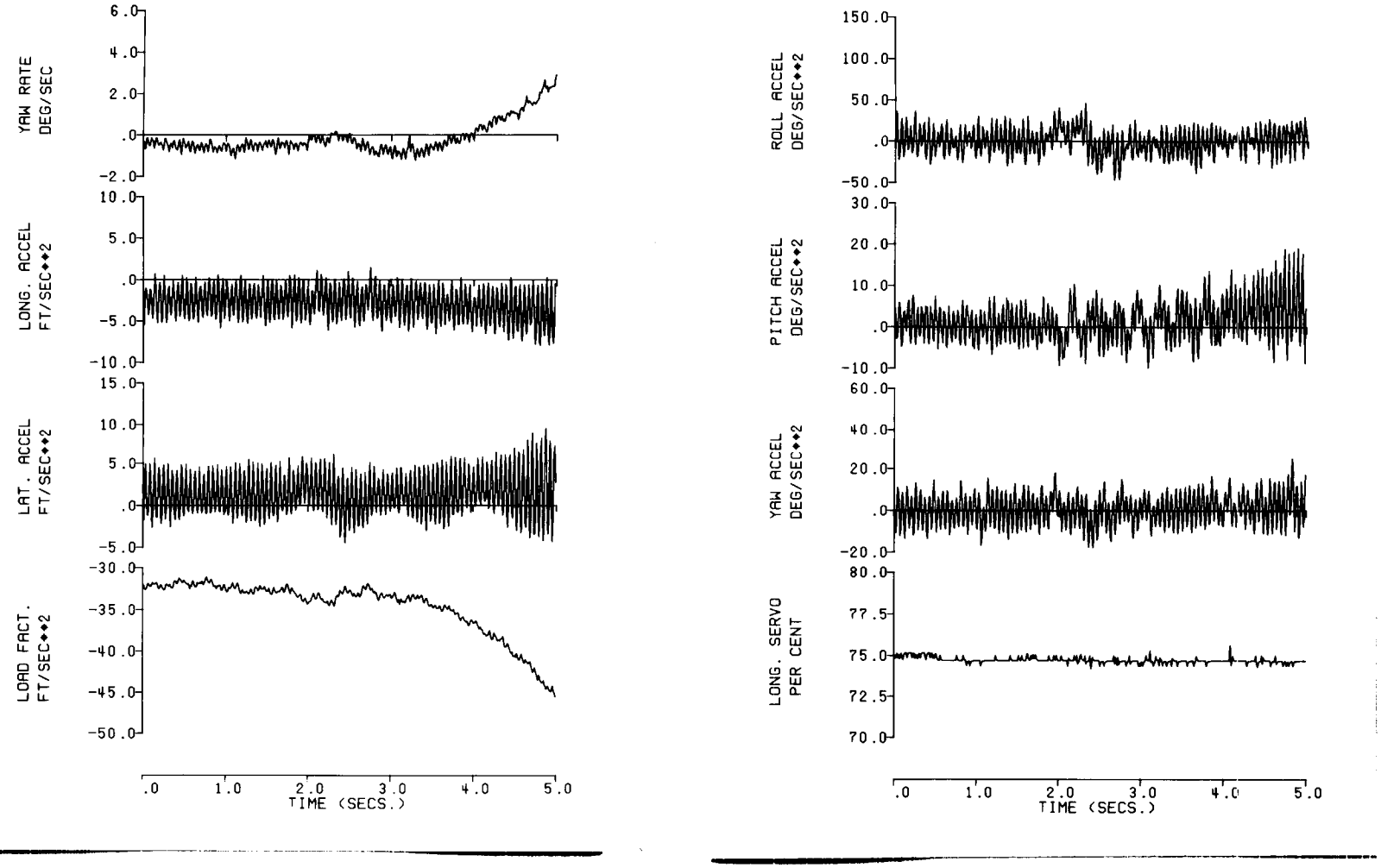

Figure 17 . - Continued.

——— Flight Test Data Filtered At 10 HZ.

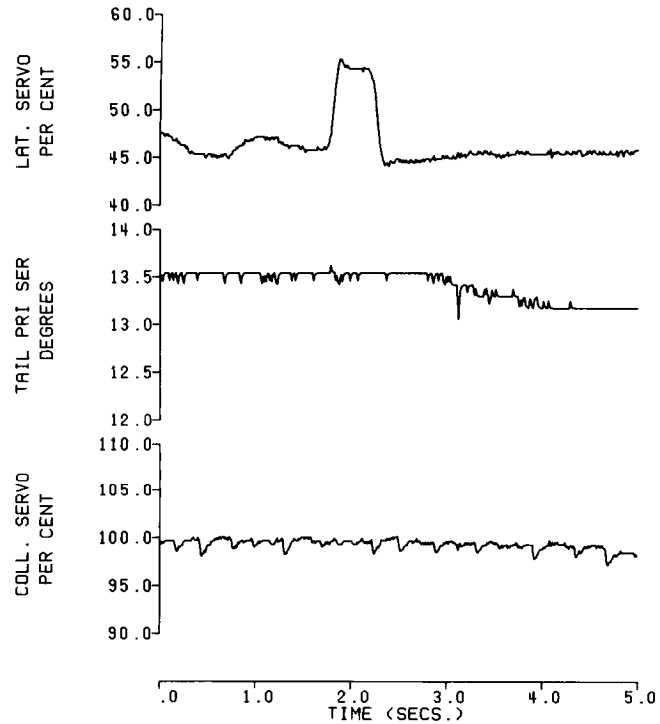

Figure 17. - Concluded.

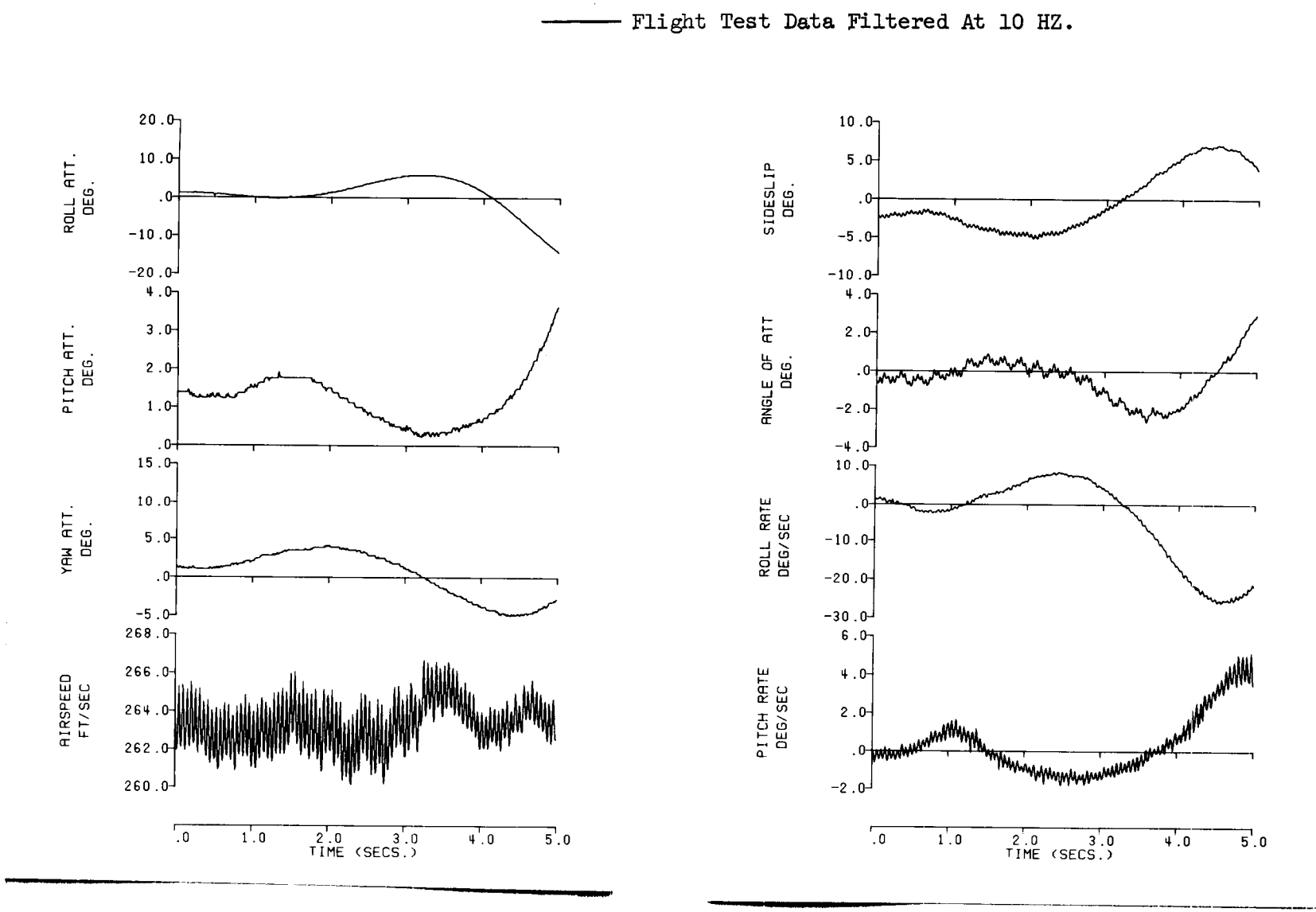

Figure 18 . - Flight Test Data From CH-53A Filtered With A First Order Low Pass Filter At 10 HZ. (150 knots, Maneuver 3).

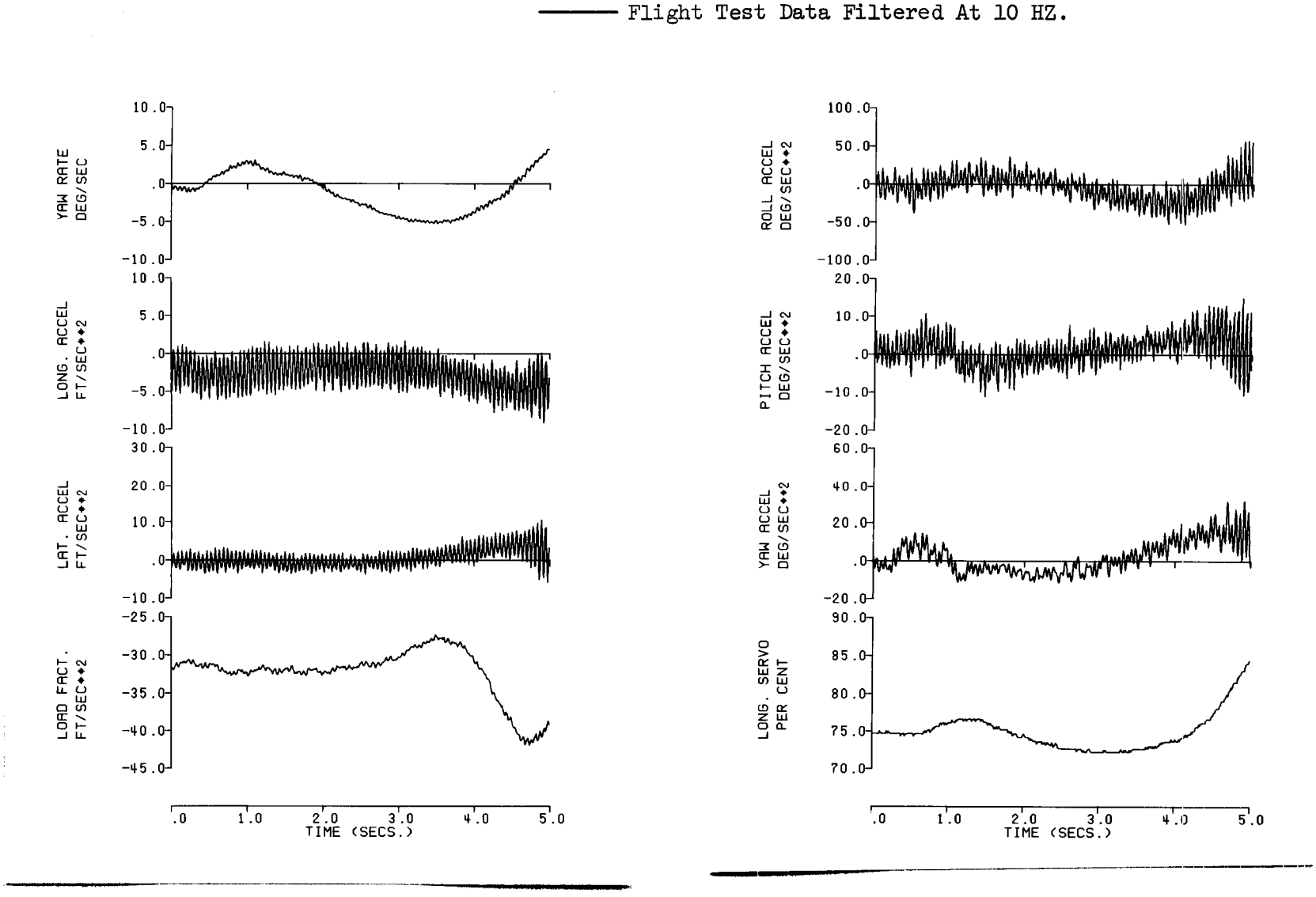

Figure 18. - Continued.

——— Flight Test Data Filtered AT 10 HZ.

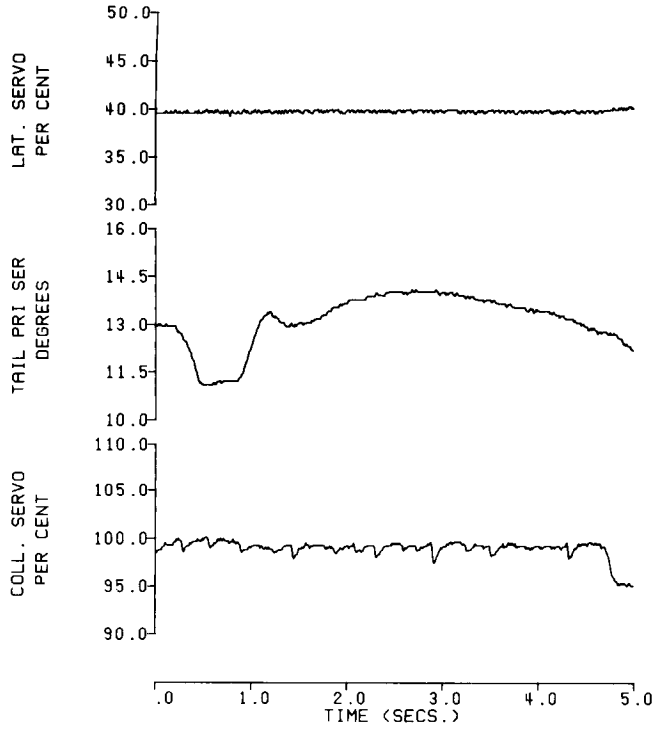

Figure 18 . - Concluded.

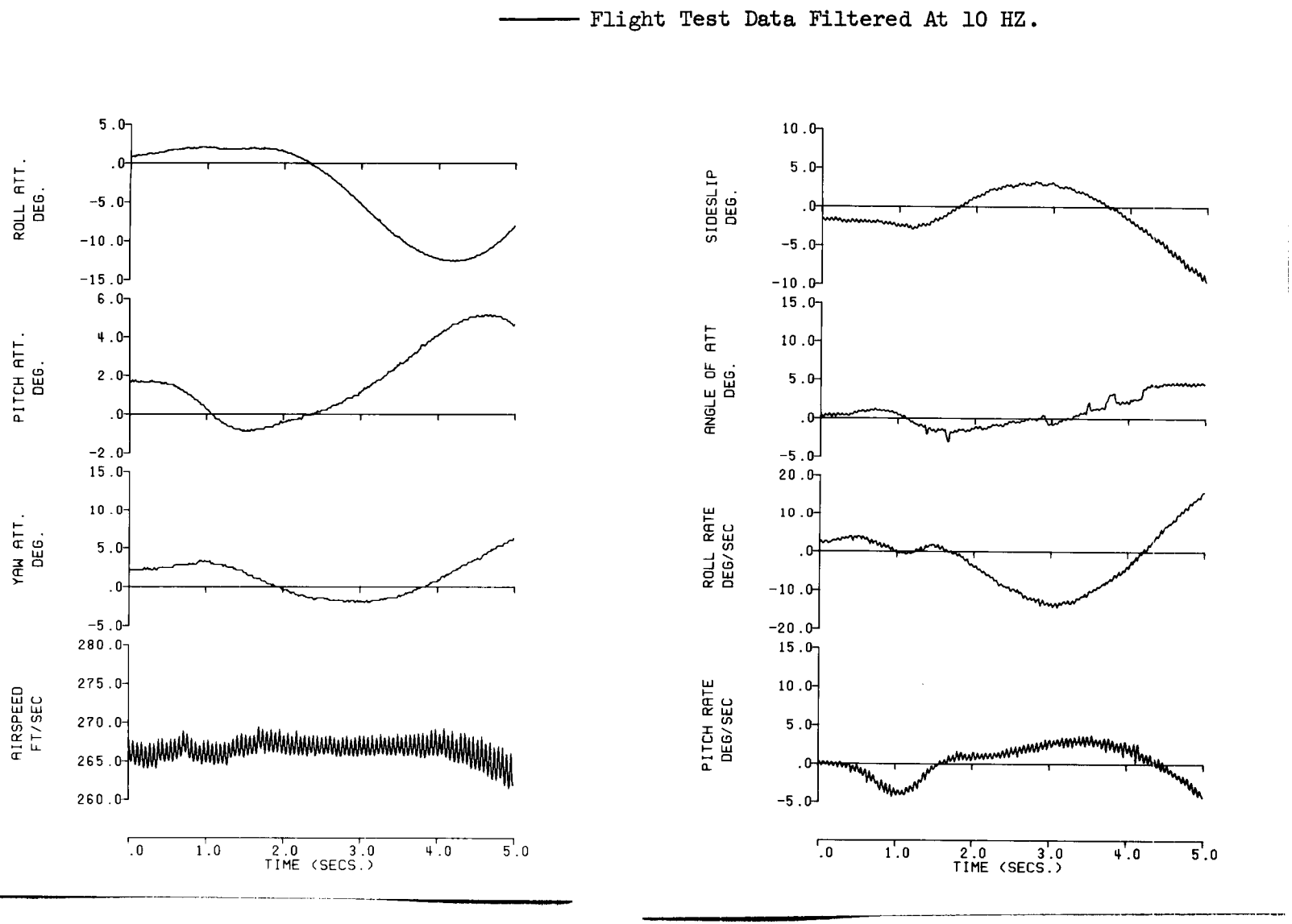

Figure 19. - Flight Test Data From CH-53A Filtered With A First Order Low Pass Filter At 10 HZ. (150 knots, Maneuver 4).

——— Flight Test Data Filtered At 10 HZ.

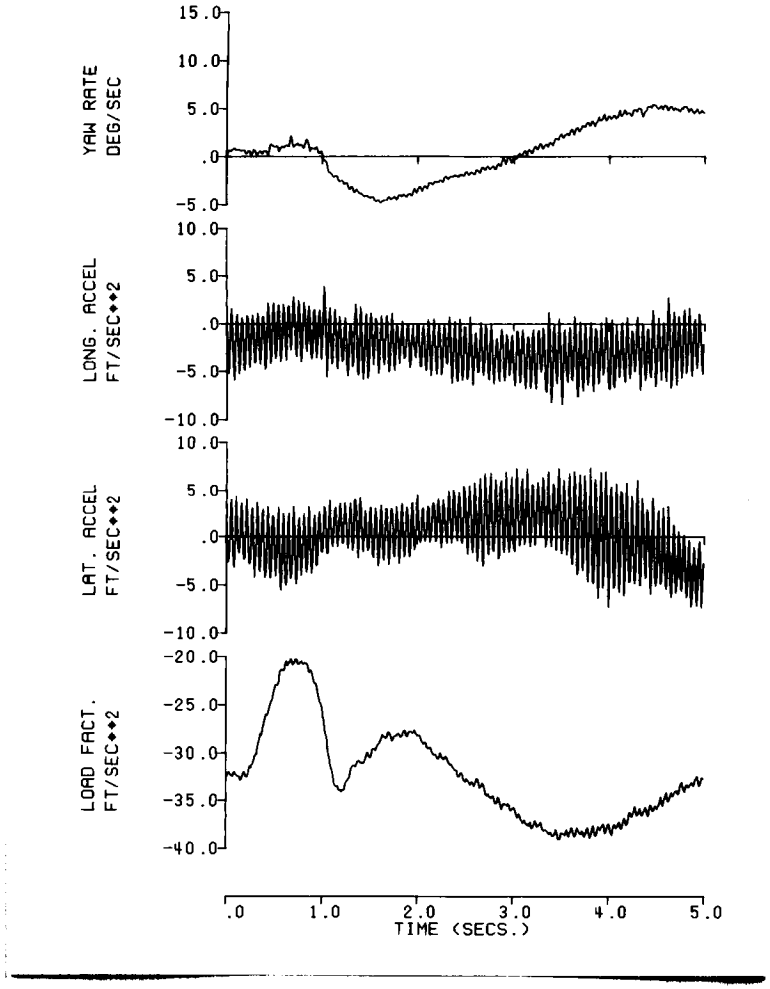

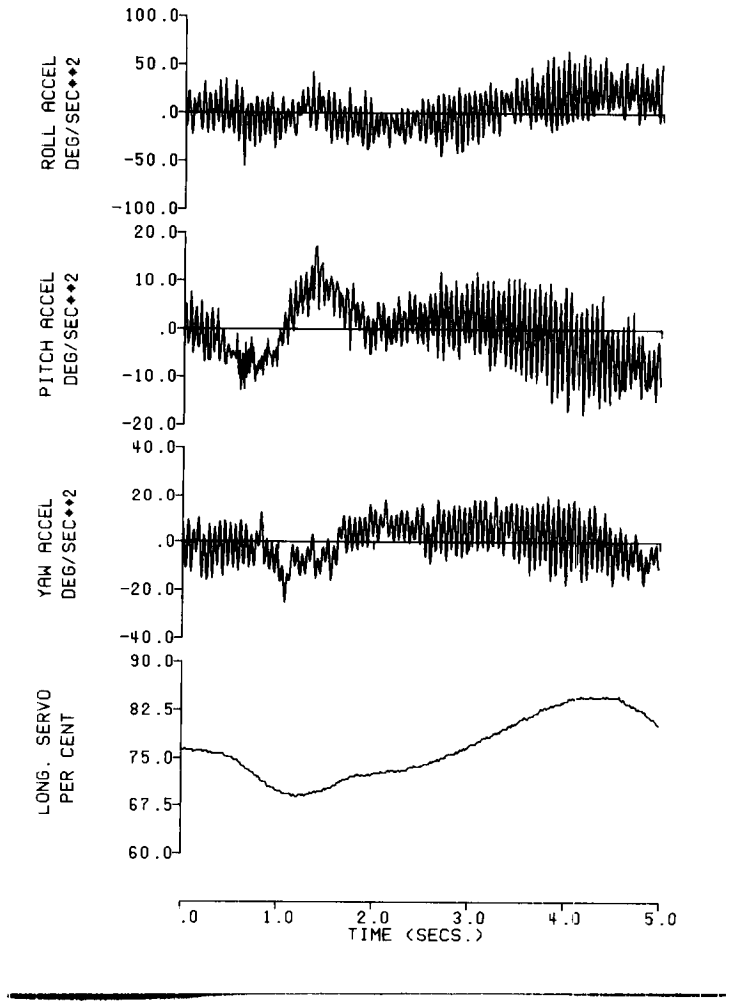

Figure 19. - Continued.

——— Flight Test Data Filtered At 10 HZ.

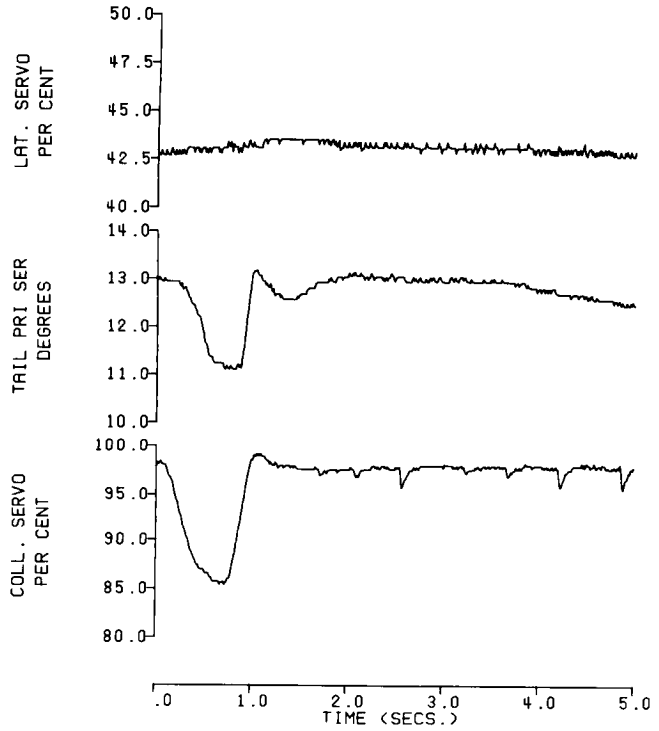

Figure 19. Concluded.

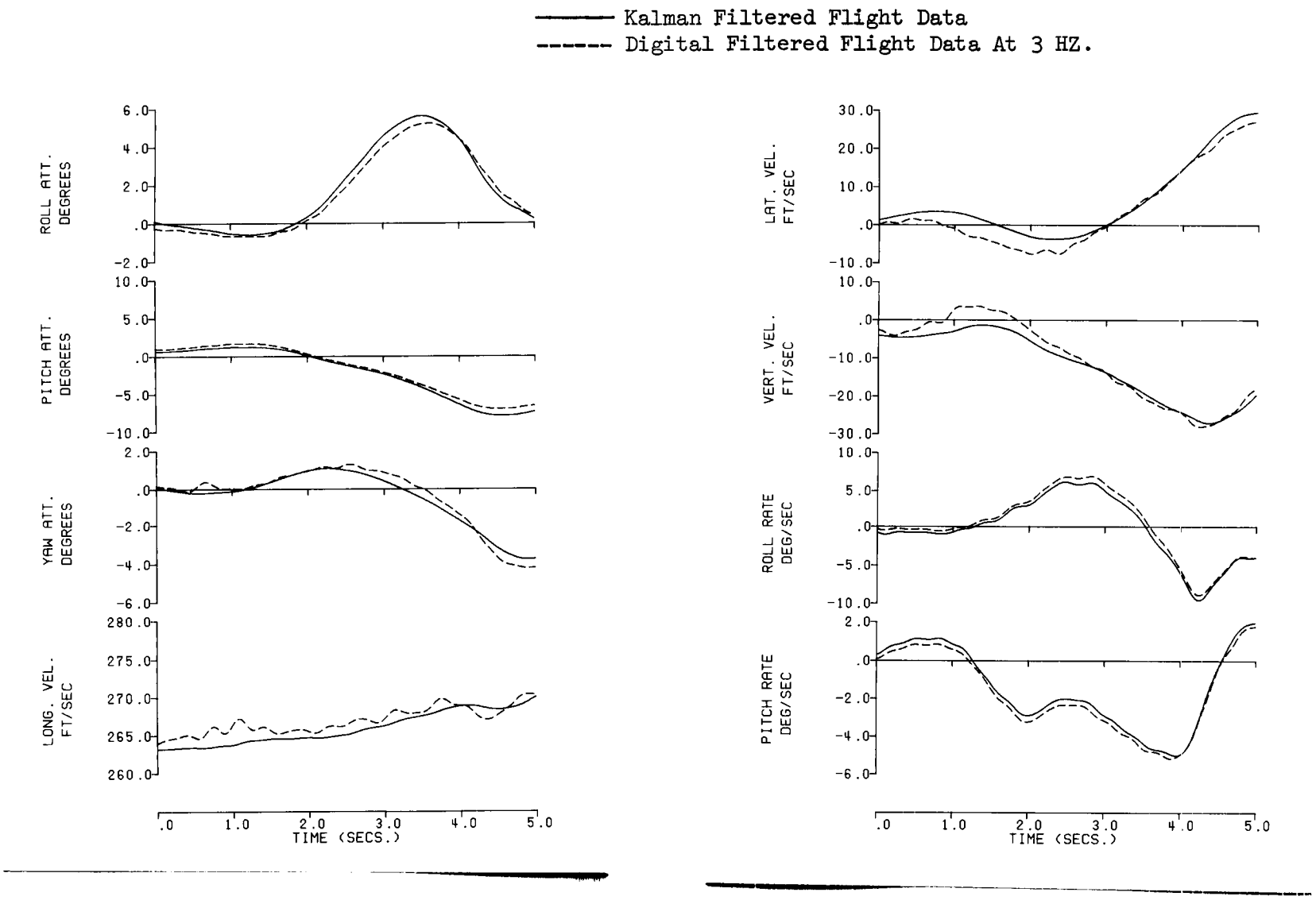

Figure 20. - Comparison of Flight Test Data From CH-53A Using The Kalman And Digital Filtering Methods (150 knots, Maneuver 1).

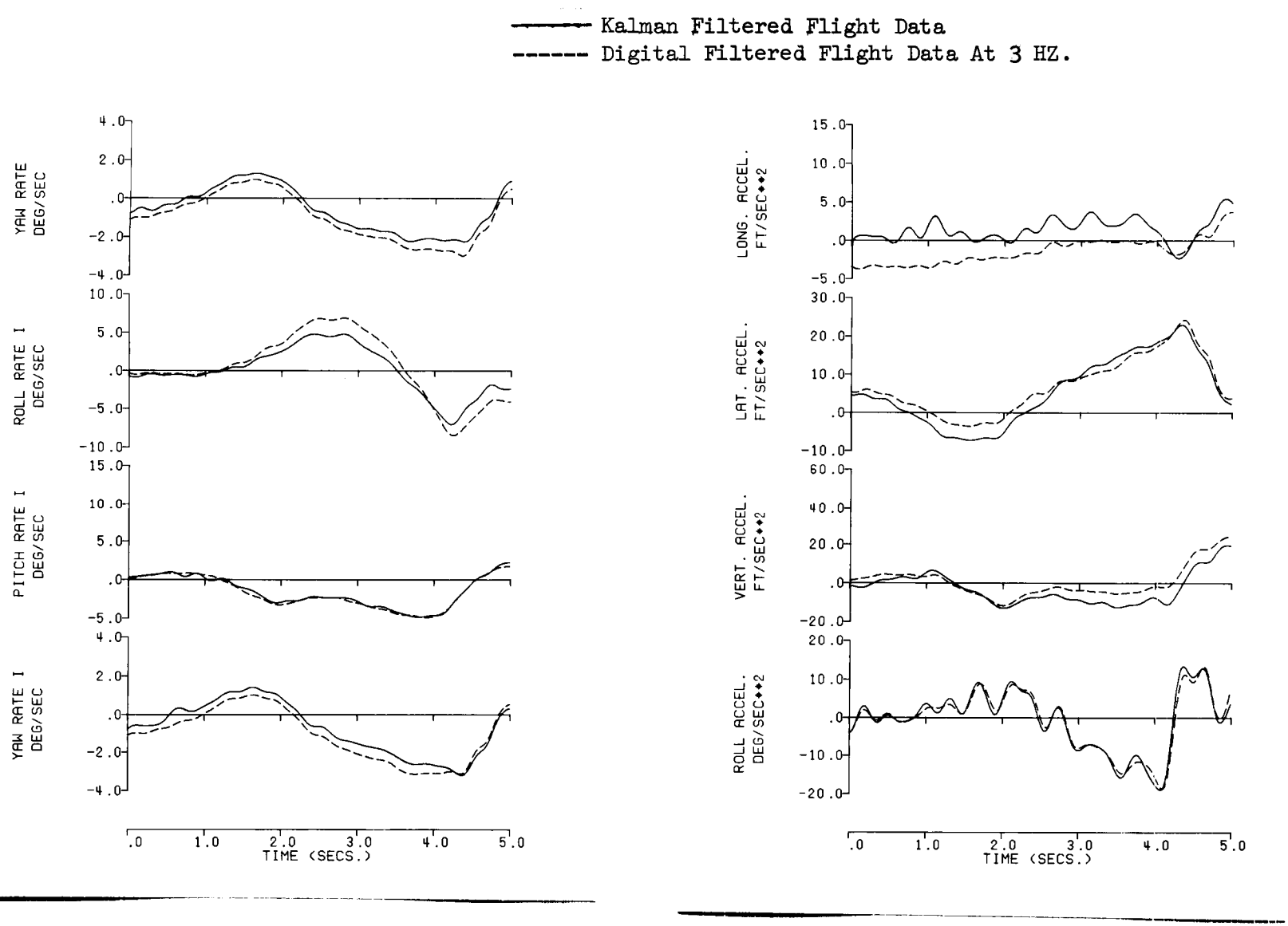

Figure 20. - Continued.

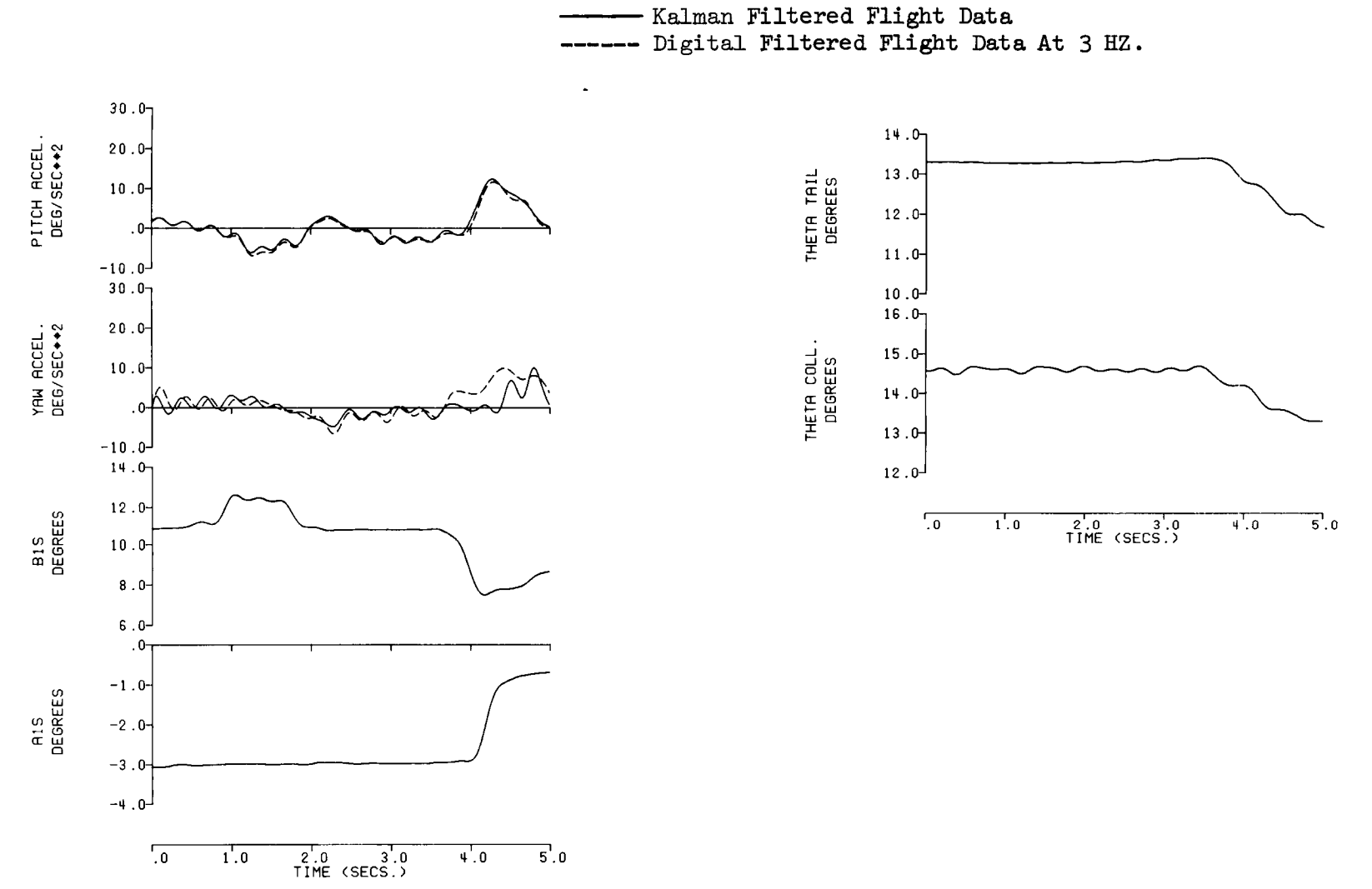

Figure 20. - Concluded.

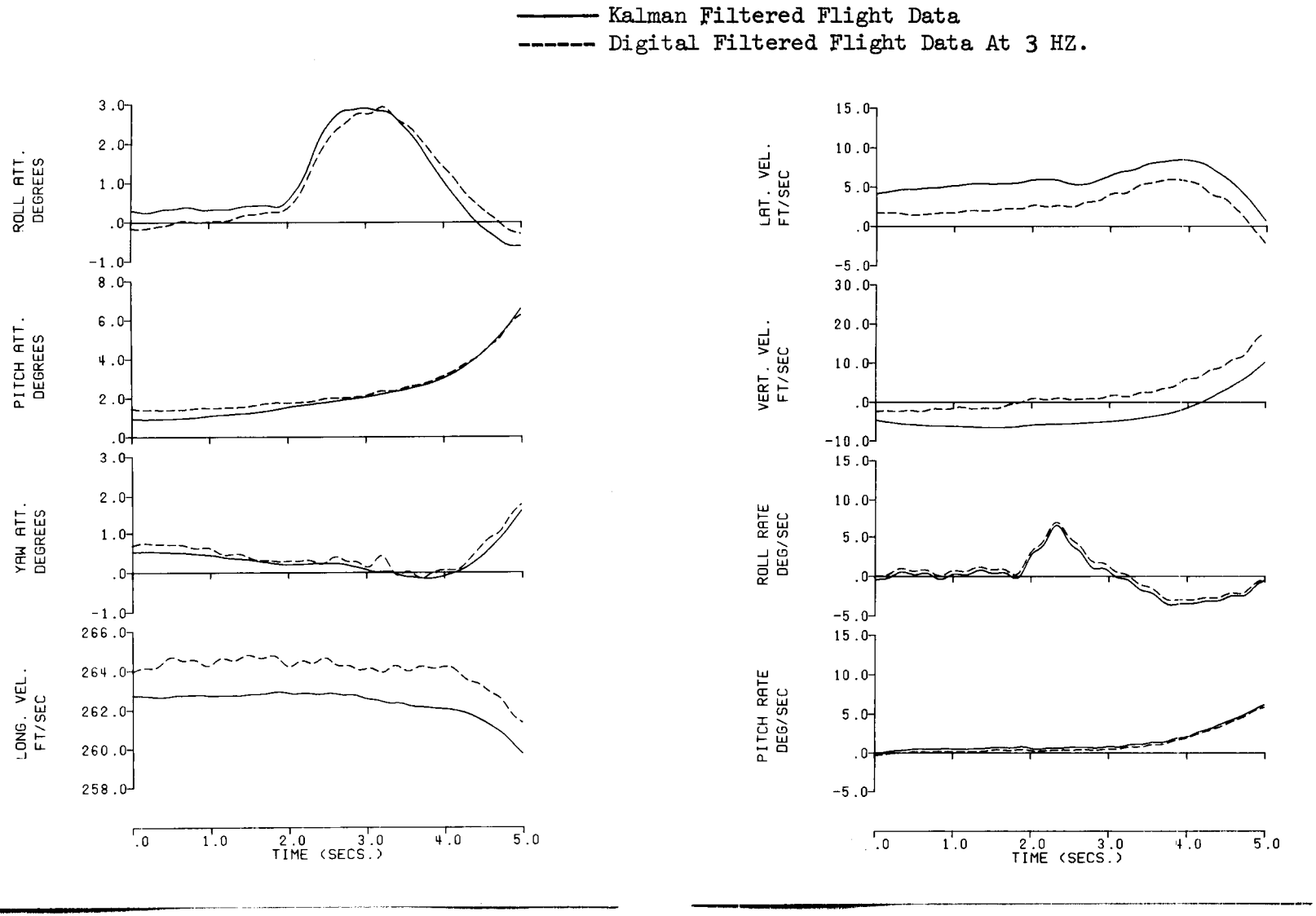

Figure 21. - Comparison of Flight Test Data From CH-53A Using The Kalman And Digital Filtering Methods (150 knots, Maneuver 2).

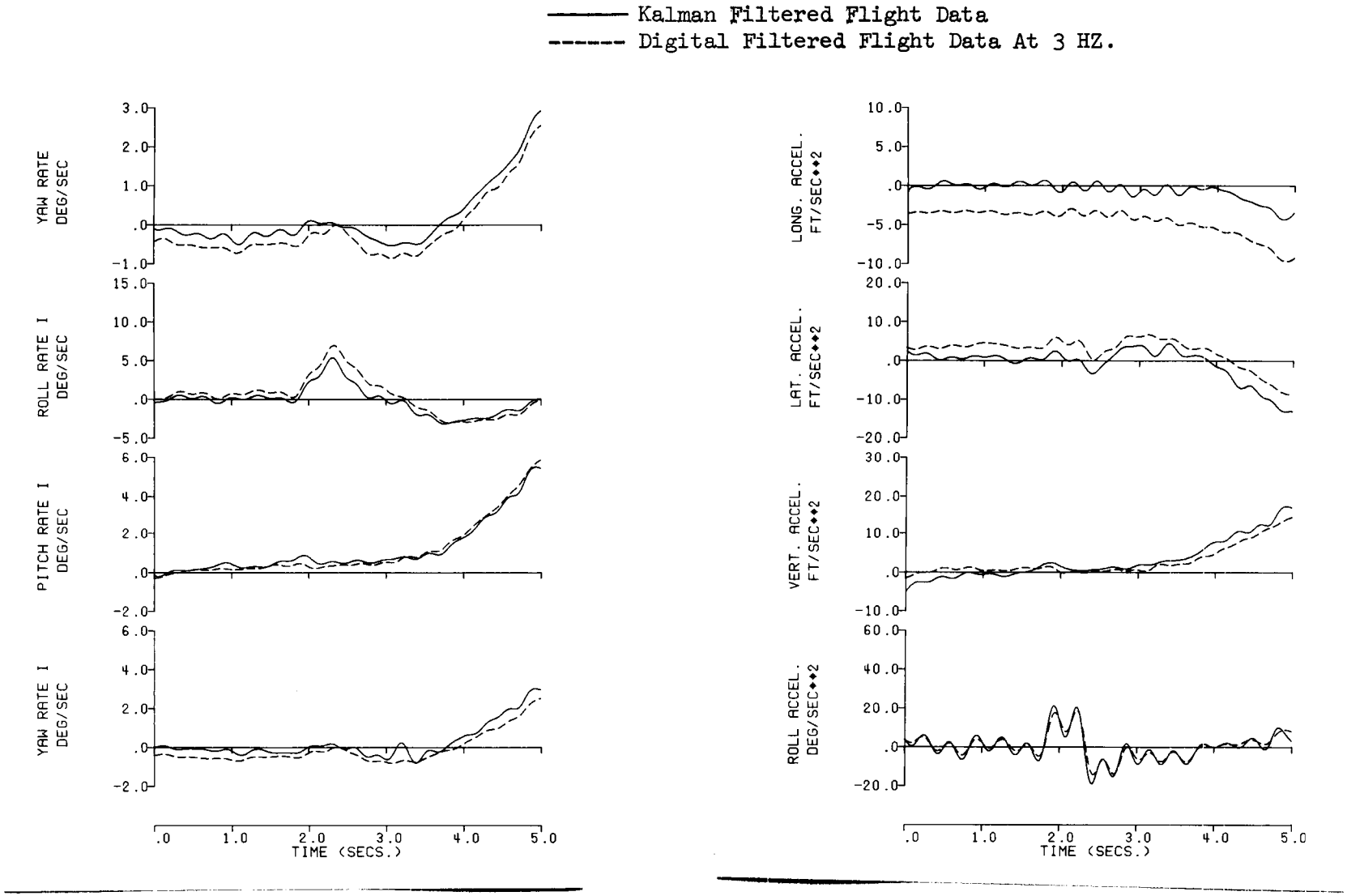

Figure 21. - Continued.

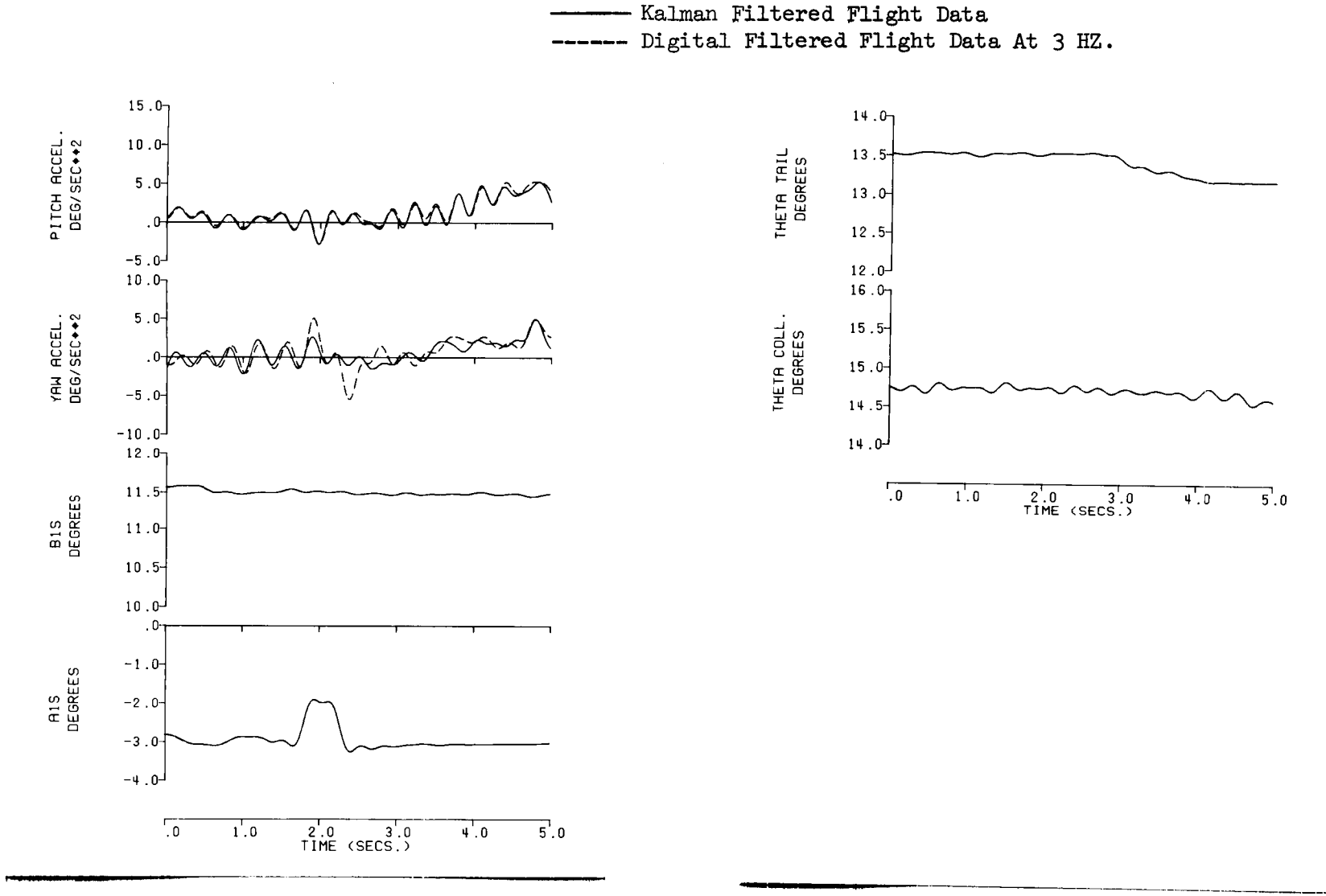

Figure 21. - Concluded.

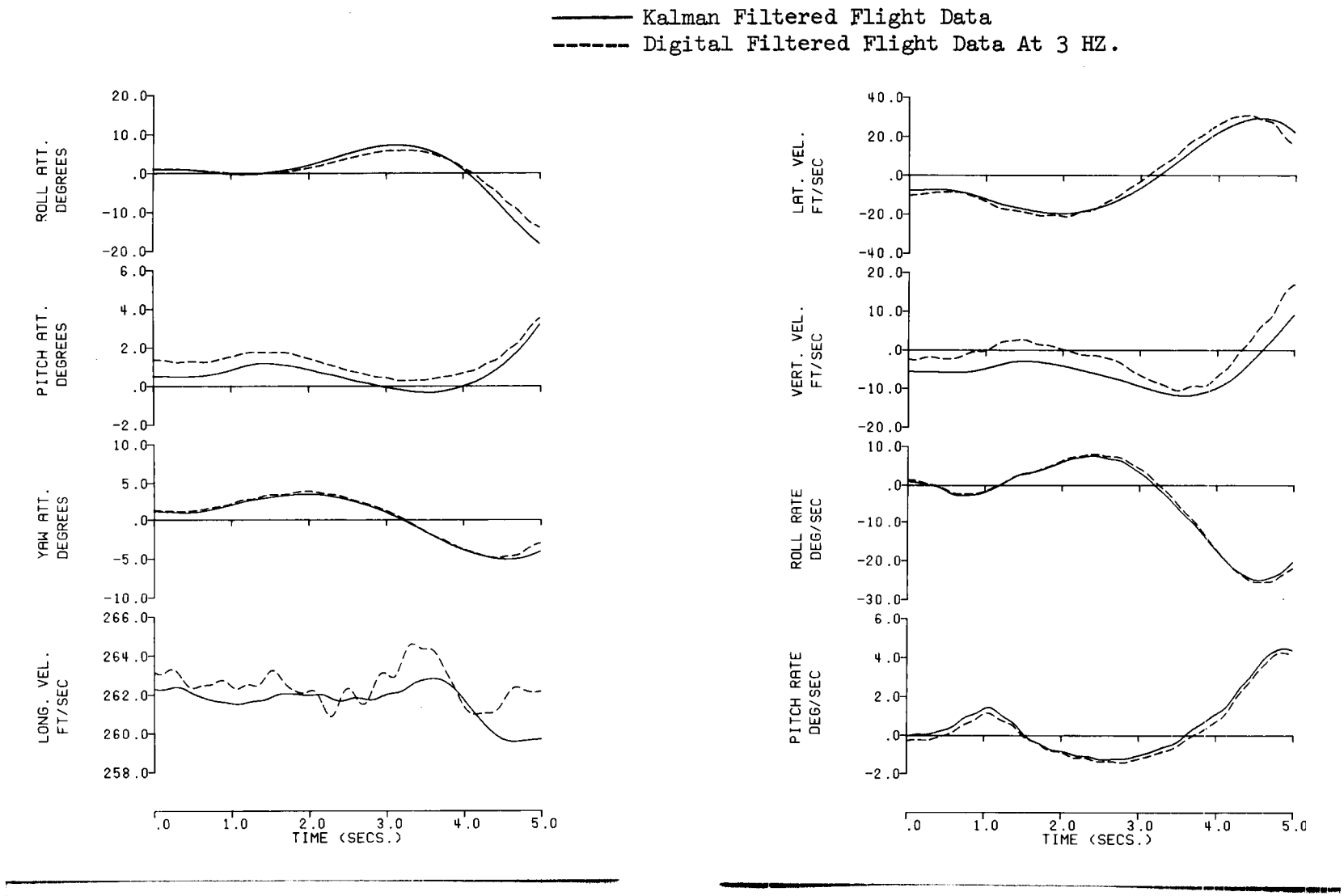

Figure 22. - Comparison of Flight Test Data From CH-53A Using The Kalman And Digital Filtering Methods (150 knots, Maneuver 3).

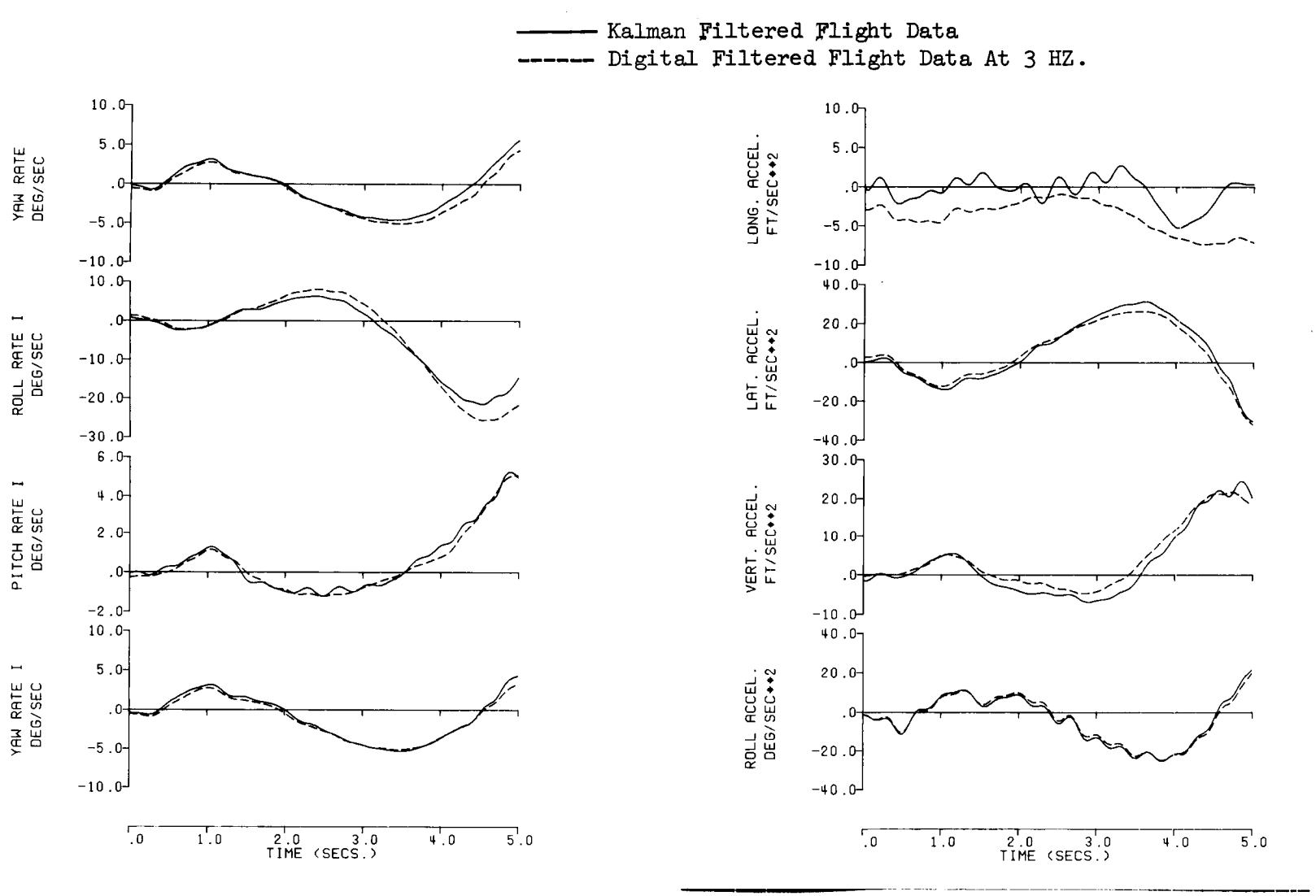

Figure 22. - Continued.

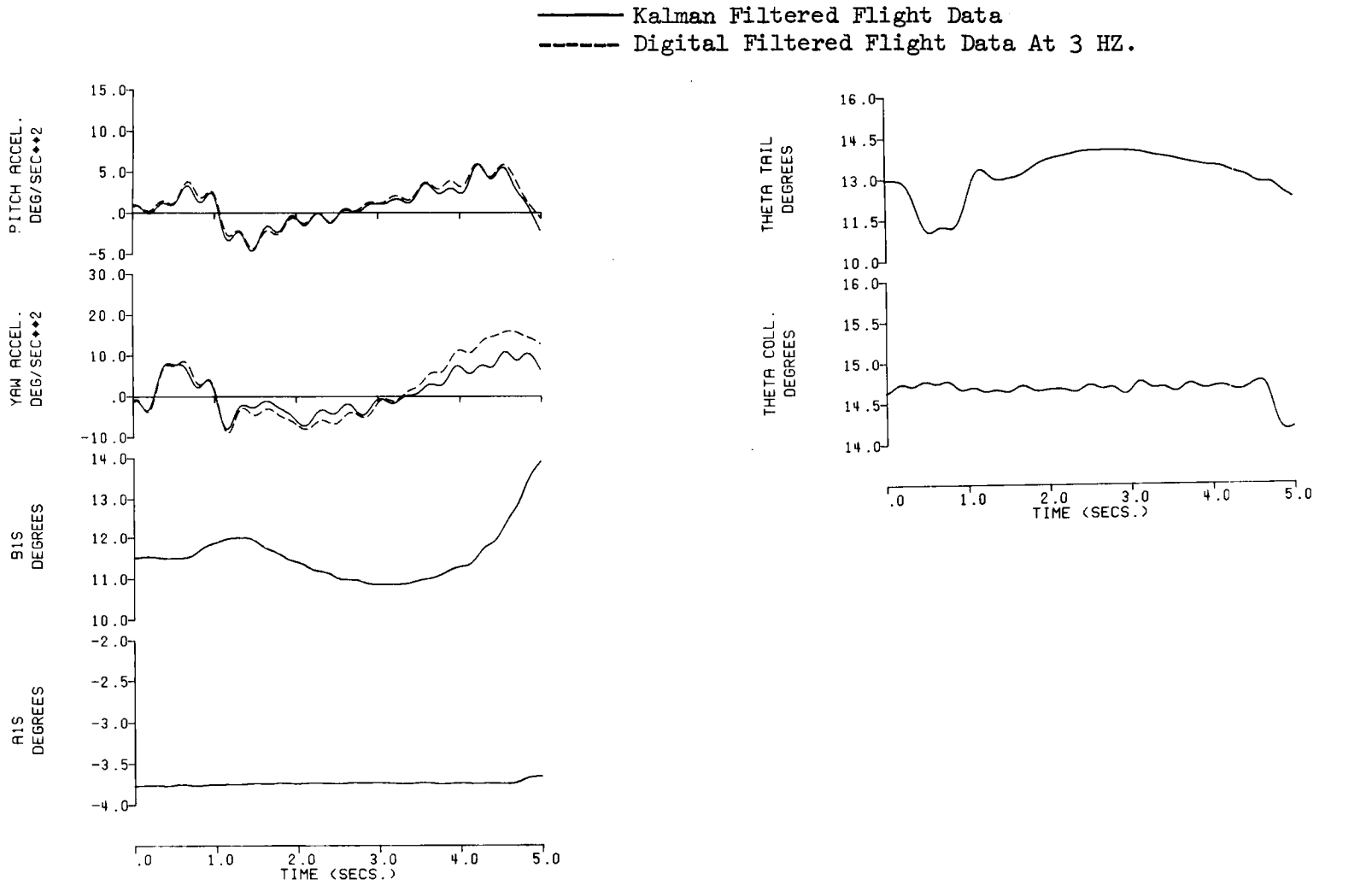

Figure 22. - Concluded.

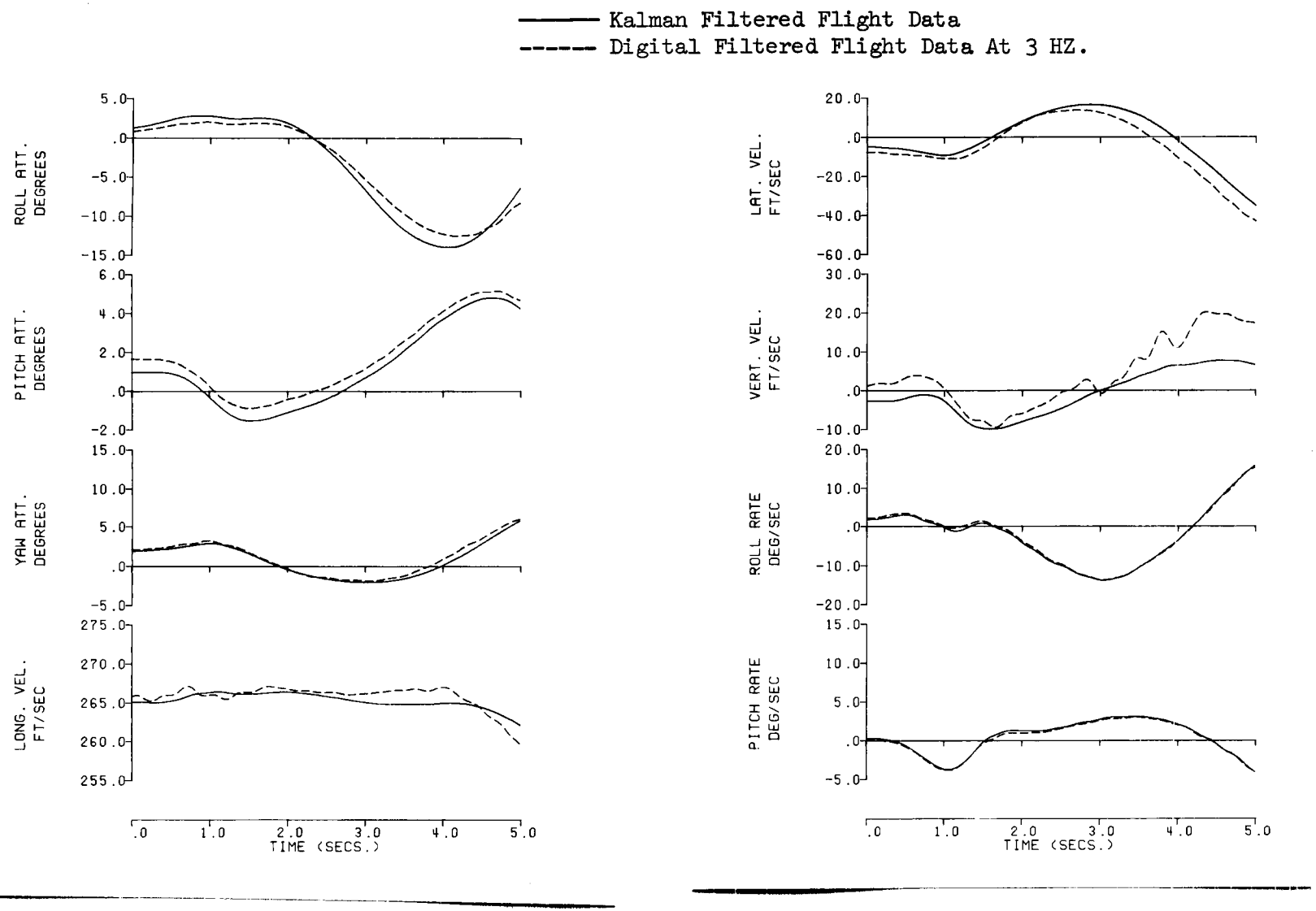

Figure 23. - Comparison of Flight Test Data From CH-53A Using The Kalman And Digital Filtering Methods (150 knots, Maneuver 4).

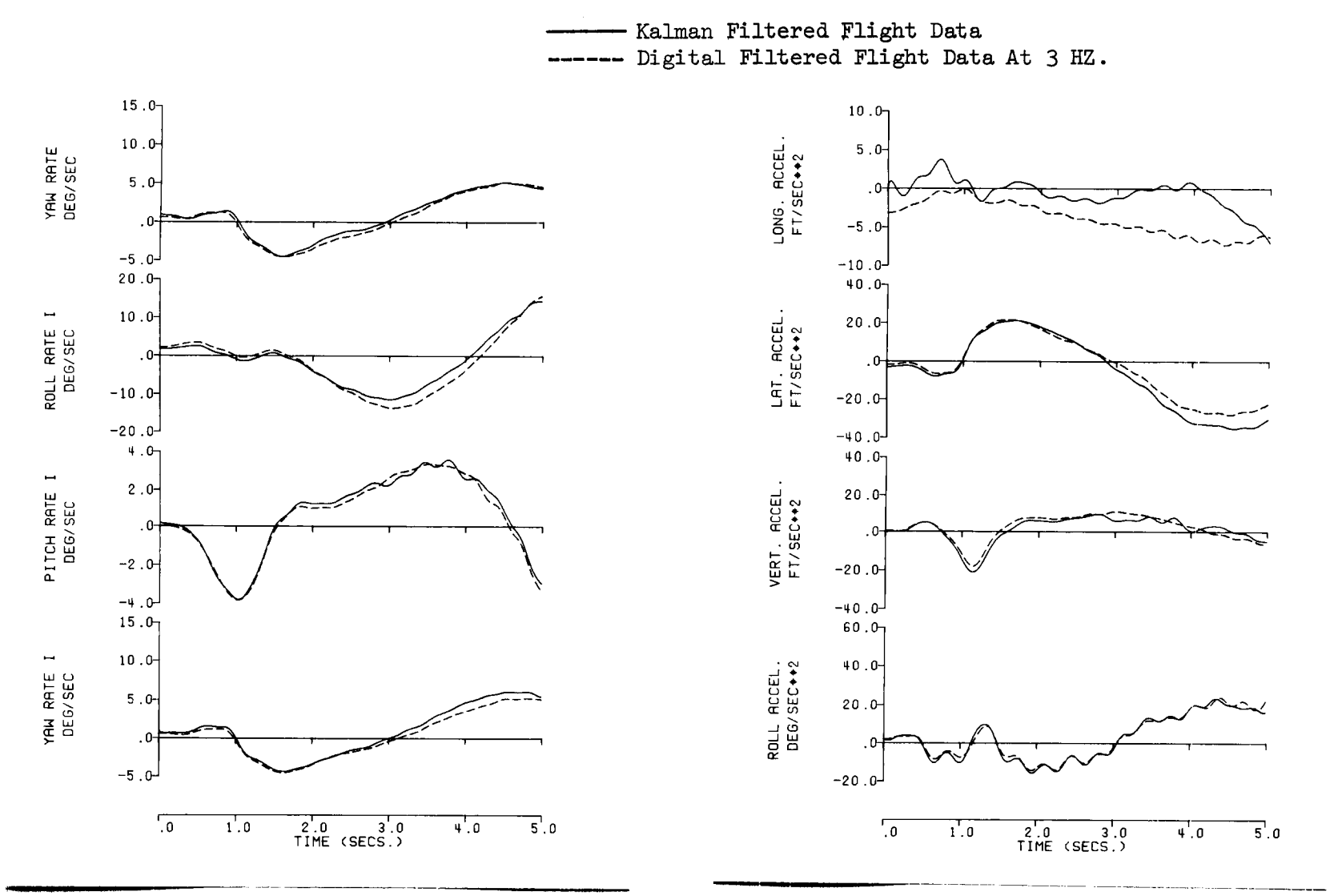

Figure 23. - Continued.

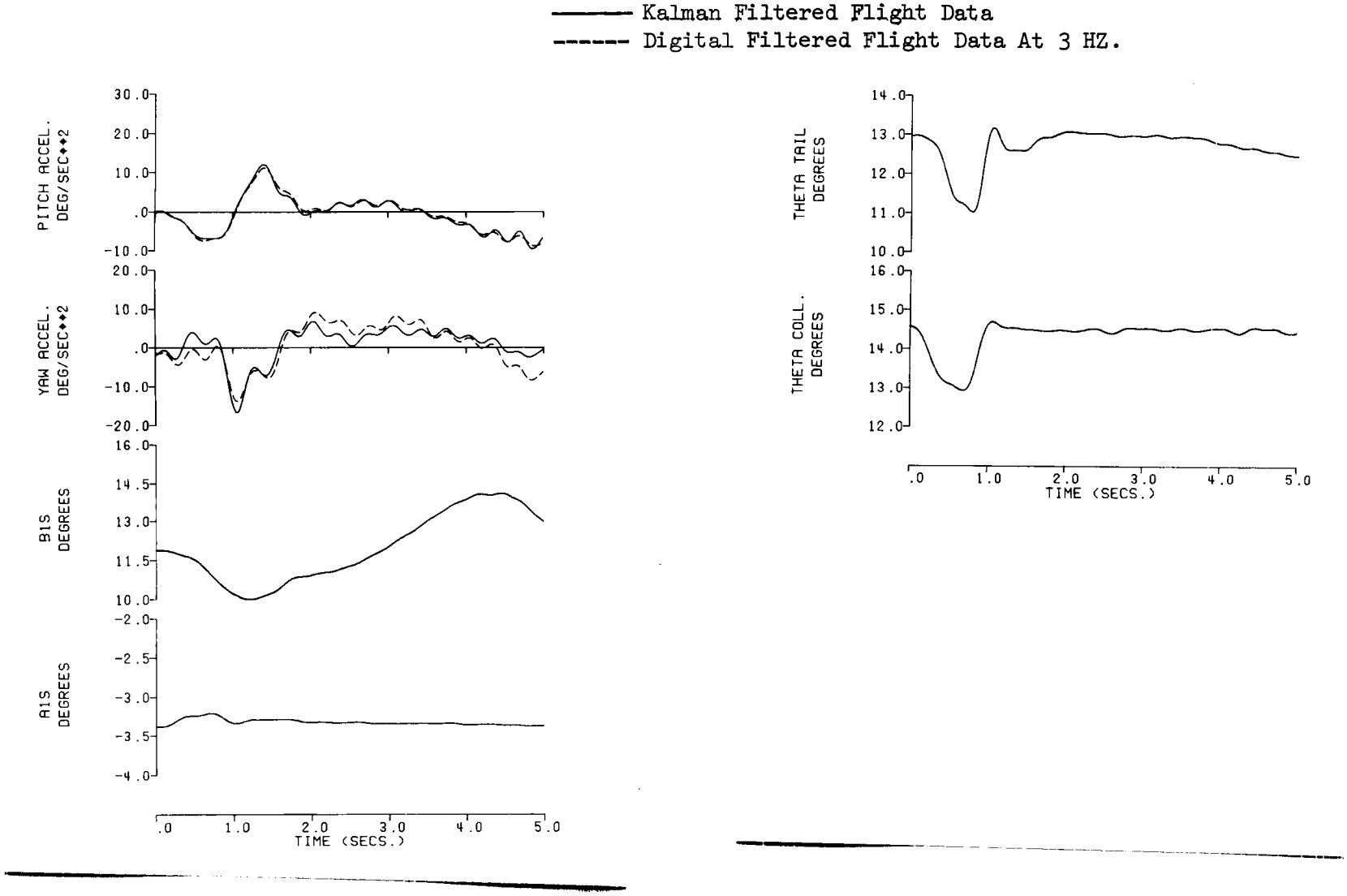

Figure 23. - Concluded.

Figure 24. CH-54B Test Aircraft

Fig. 24 146

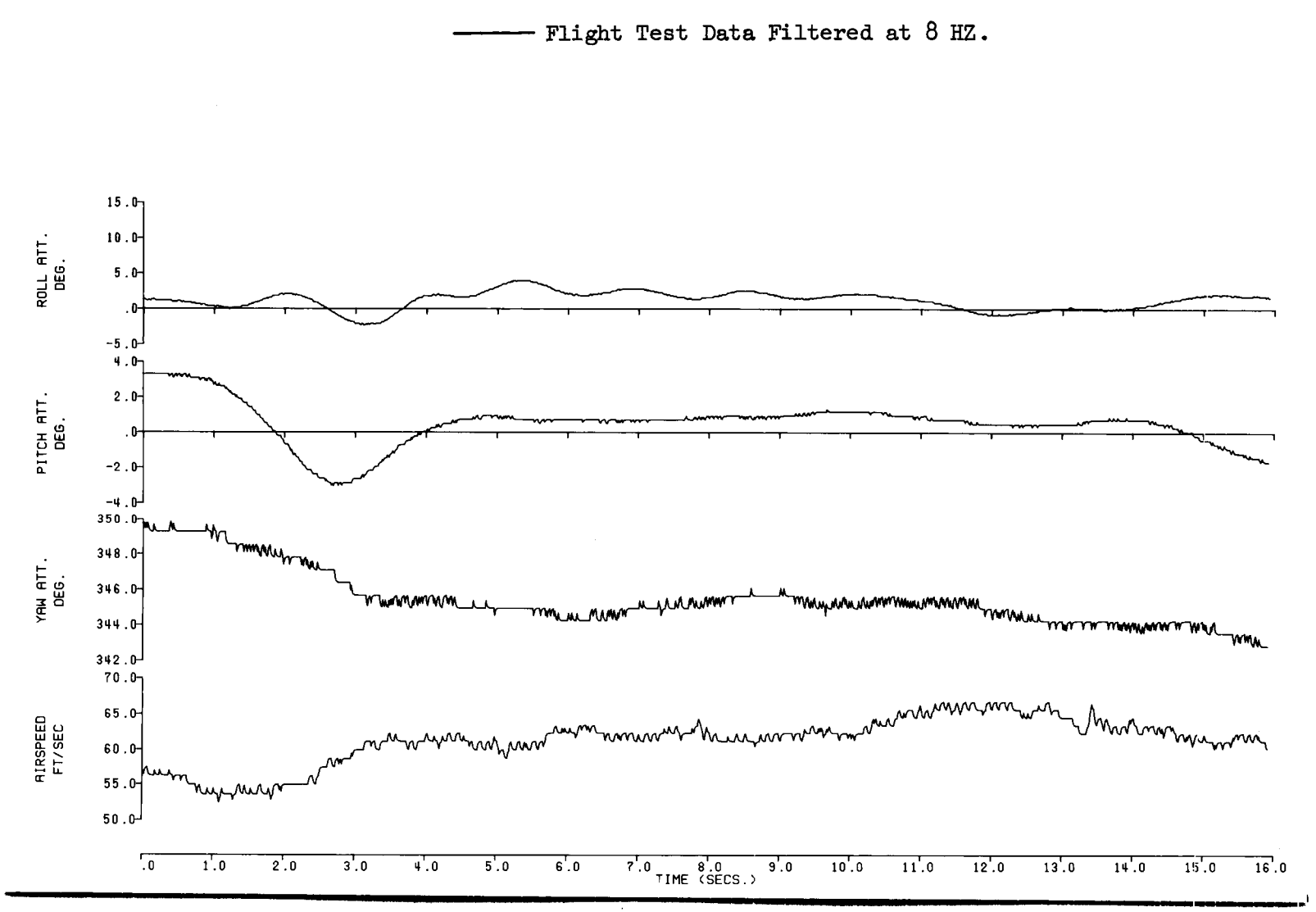

Figure 25. - Flight Test Data From CH-54B Filtered With a First Order Low Pass Filter at 8 HZ. (45 knots, 16 sec. Maneuver).

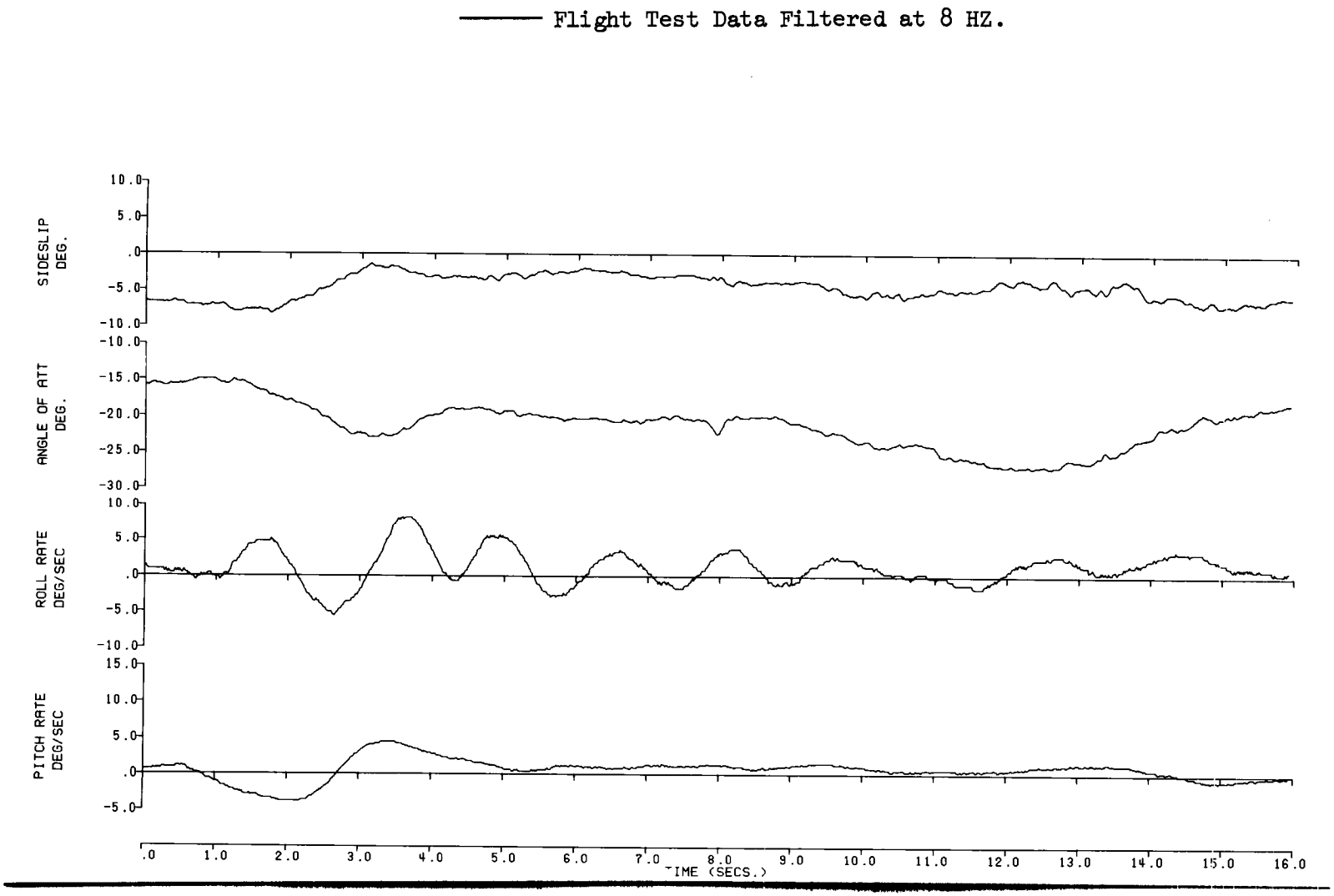

Figure 25. - Continued.

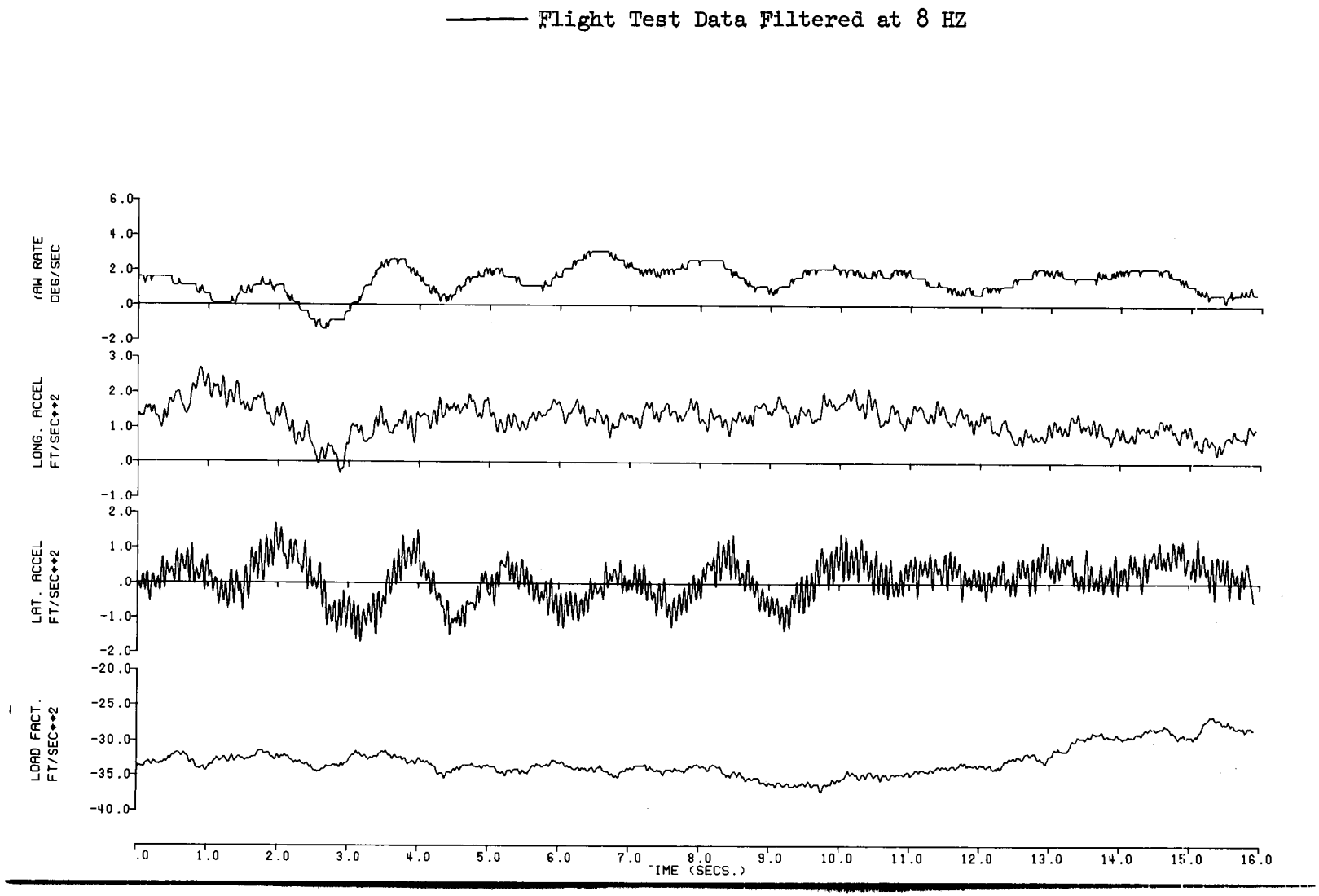

Figure 25 - Continued.

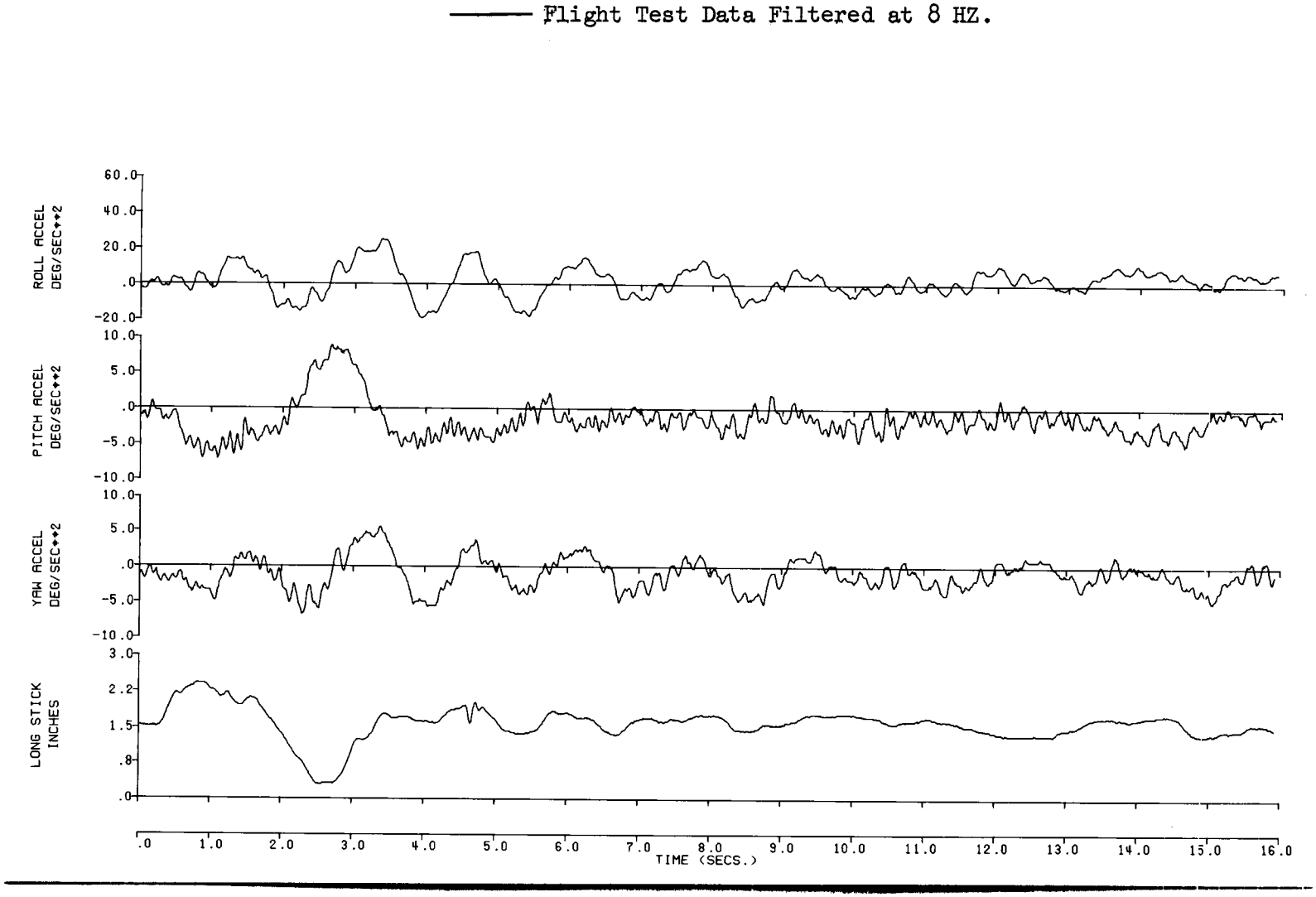

Figure 25. - Continued.

——— Flight Test Data Filtered at 8 HZ.

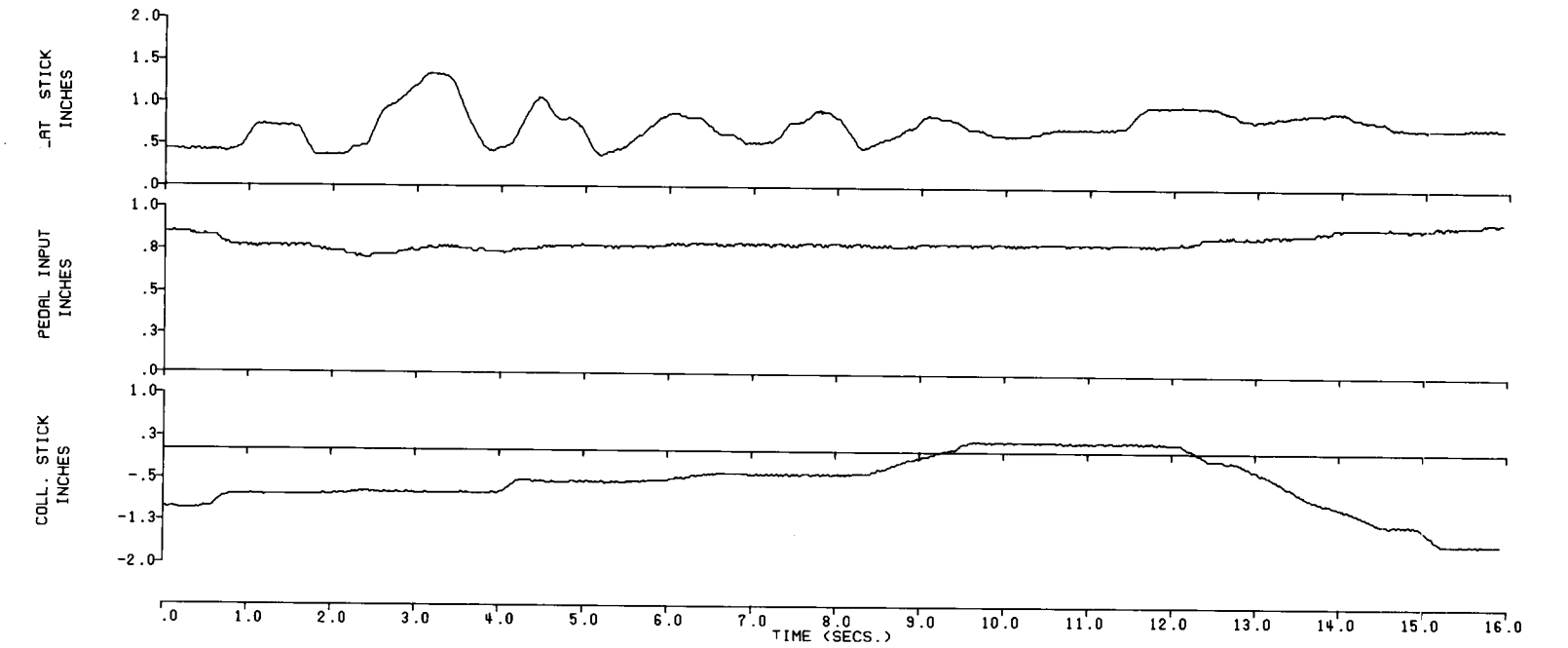

Figure 25. - Concluded.

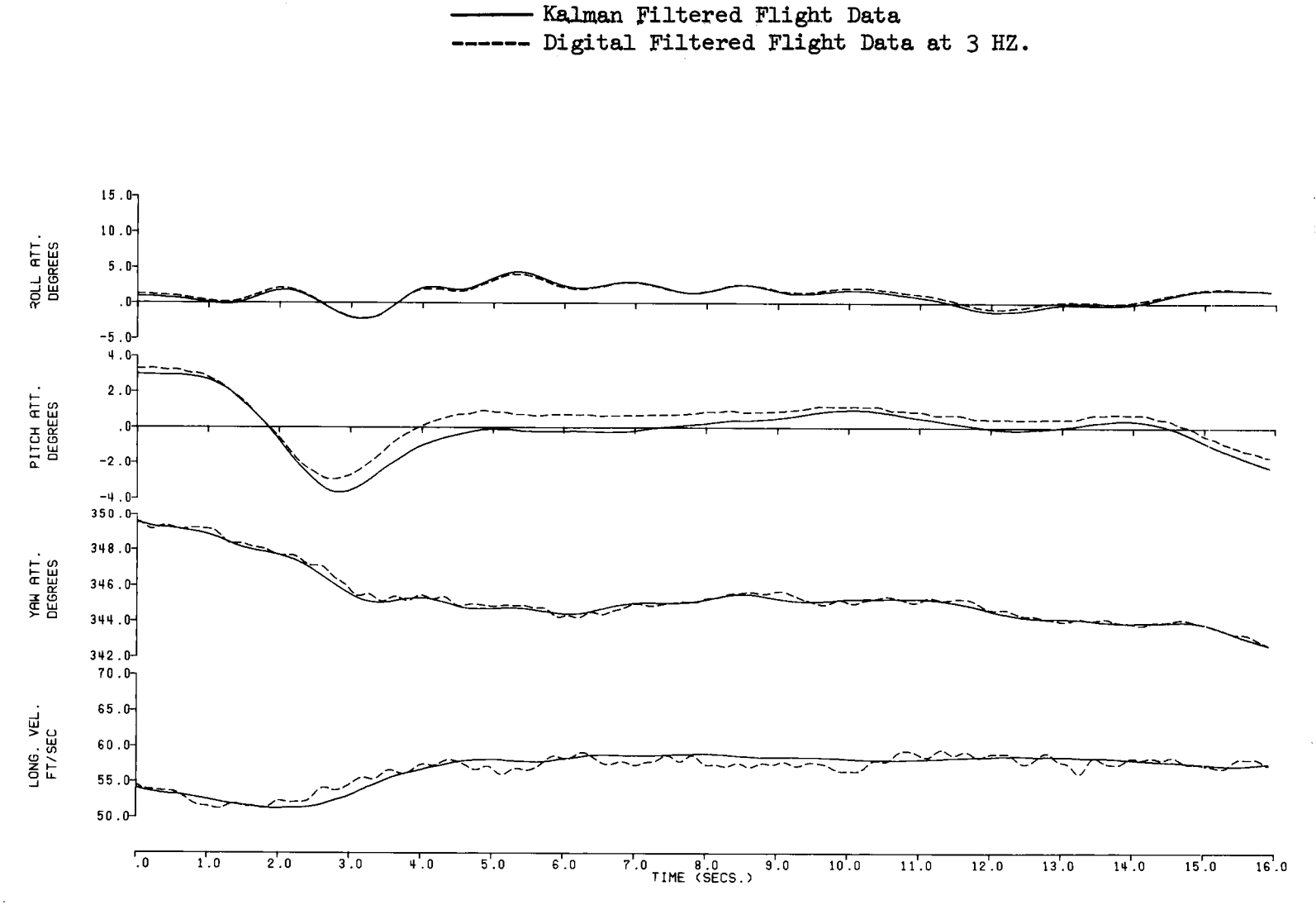

Figure 26. - Comparison of Flight Test Data From CH-54B using the Kalman and Digital Filtering Methods (45 knots, 16 sec. Maneuver).

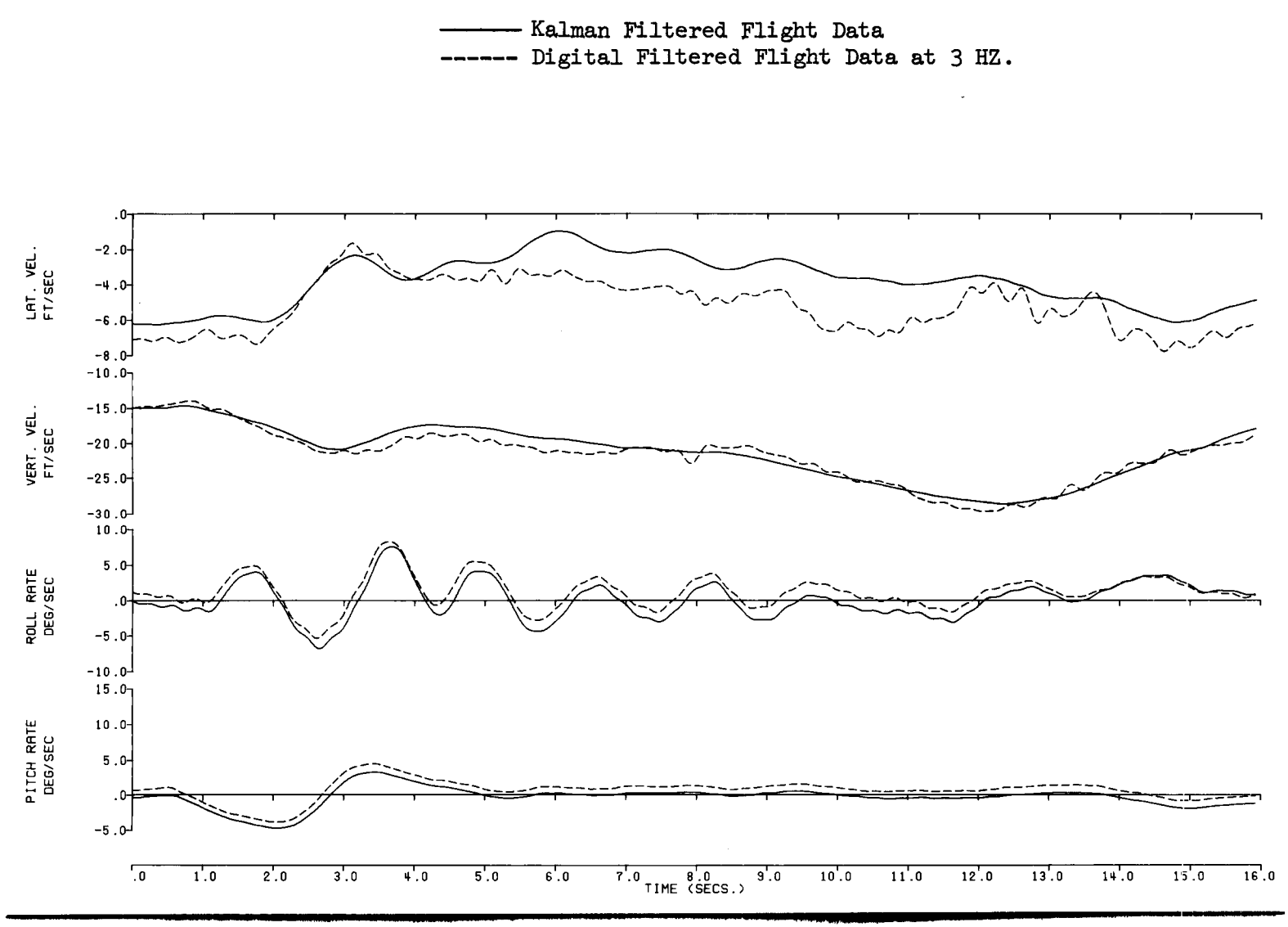

Figure 26. - Continued.

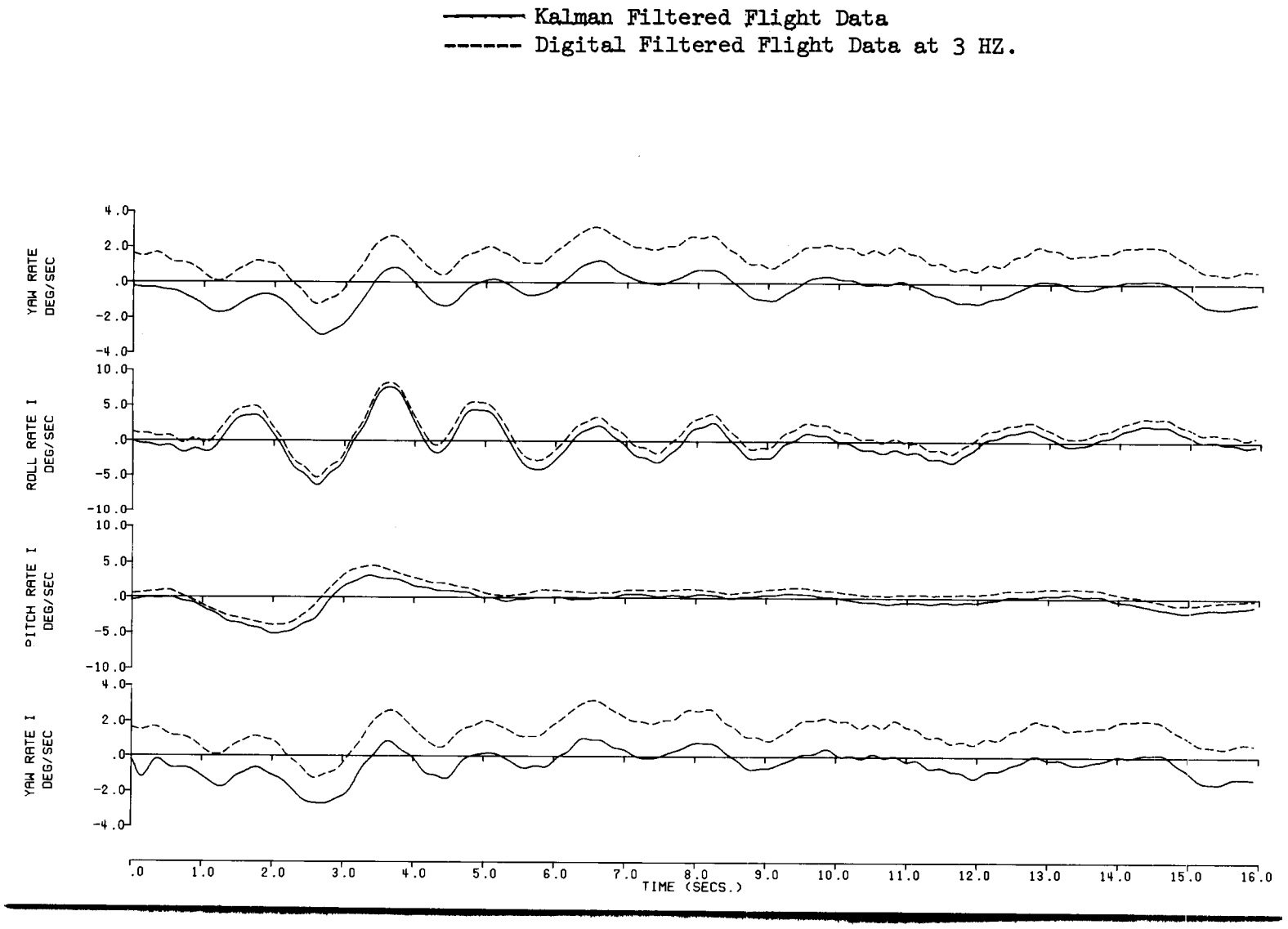

Figure 26. - Continued.

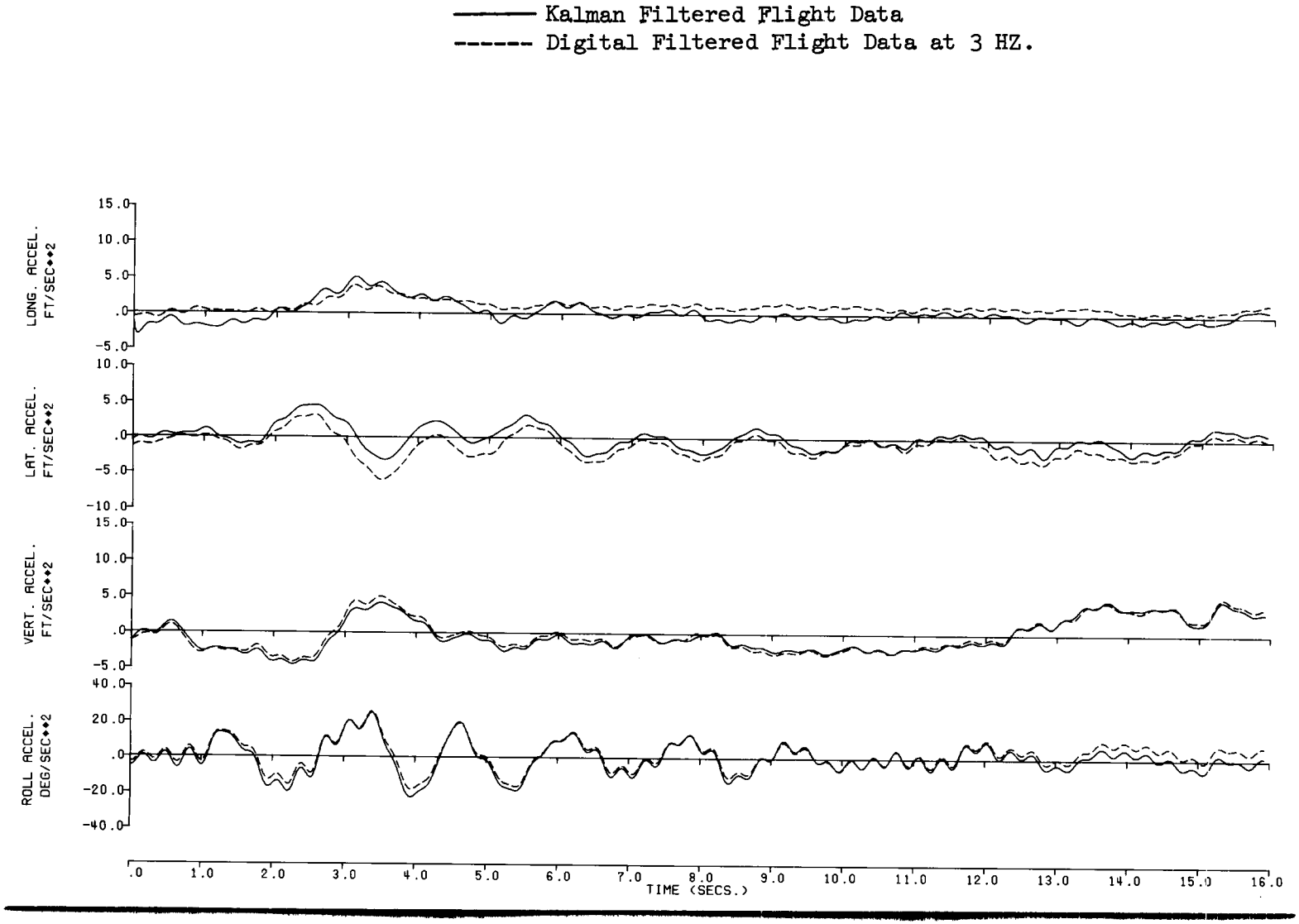

Figure 26. - Continued.

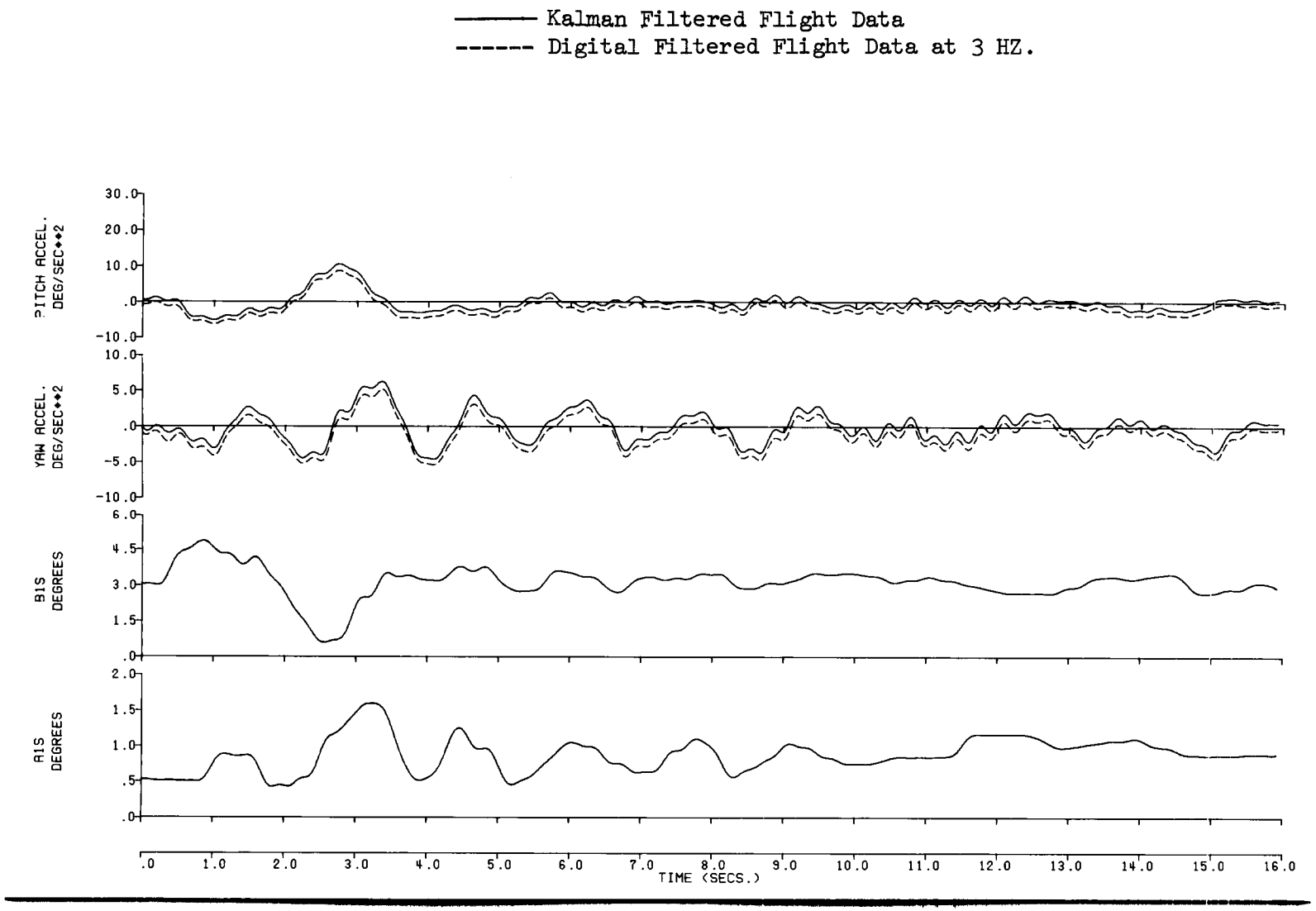

Figure 26. - Continued.

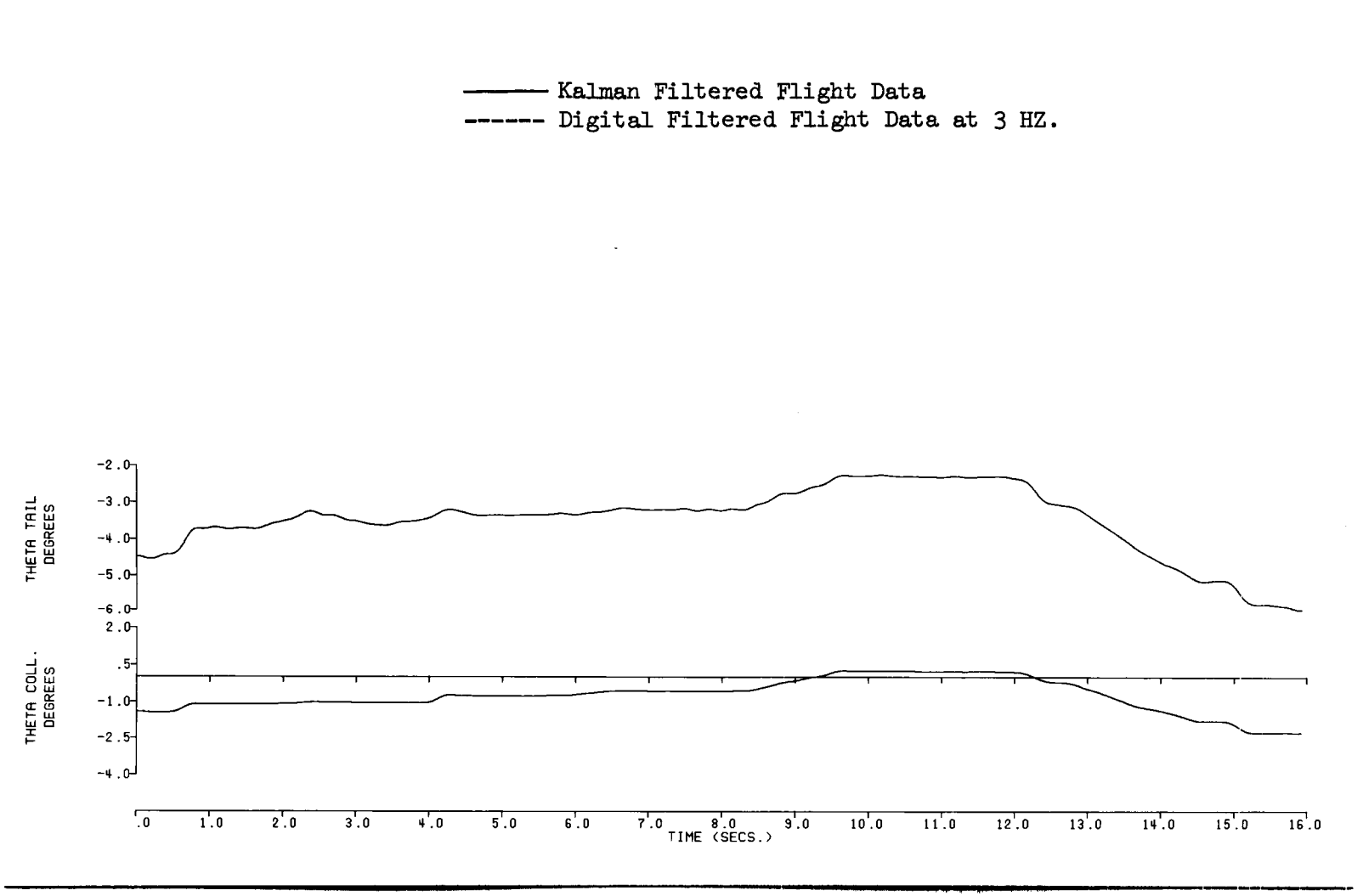

Figure 26. - Concluded.

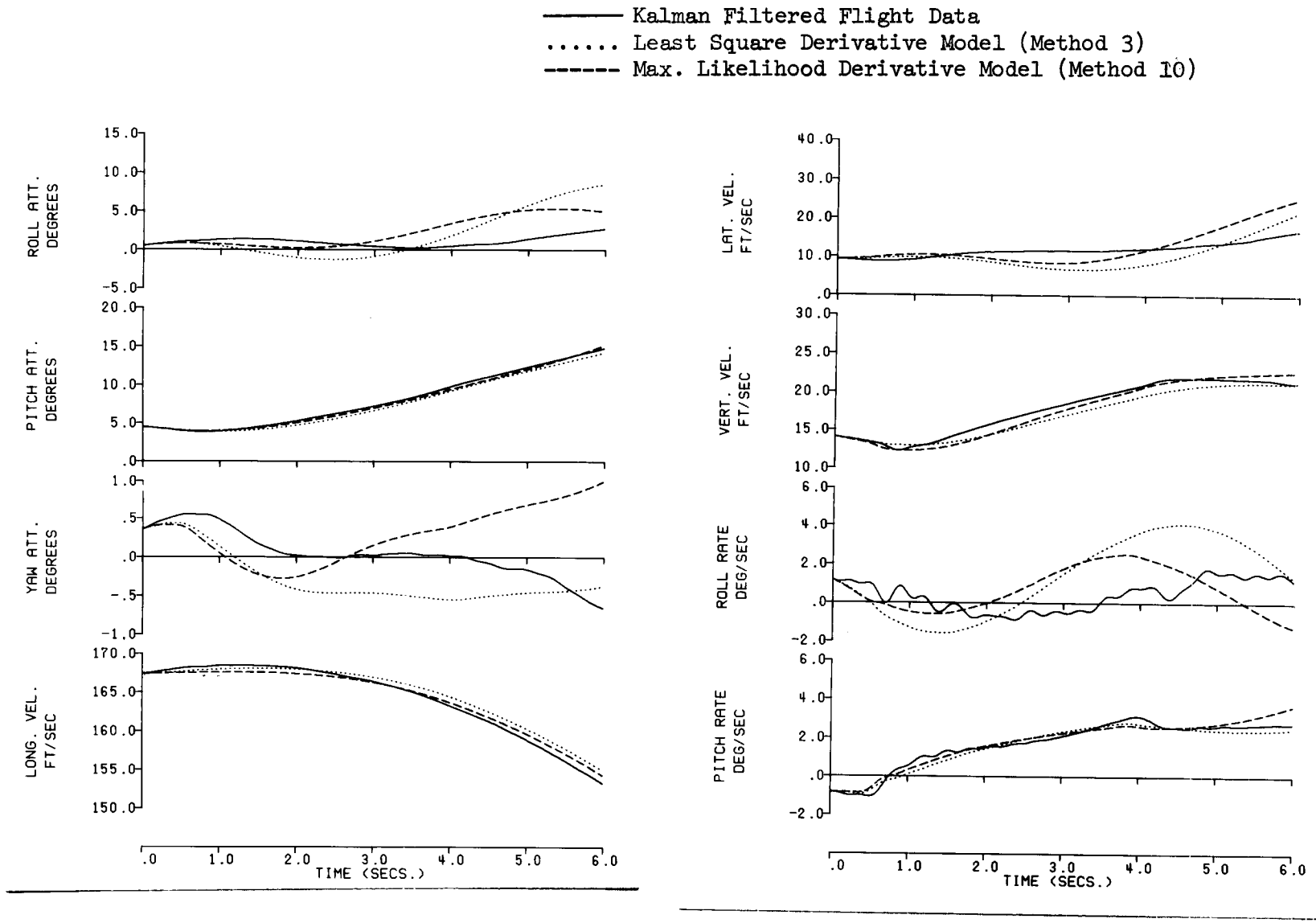

Figure 27 . - Time History Comparison of Identified Derivative Models Against CH-53A Flight Data (100 knots, Maneuver 1).

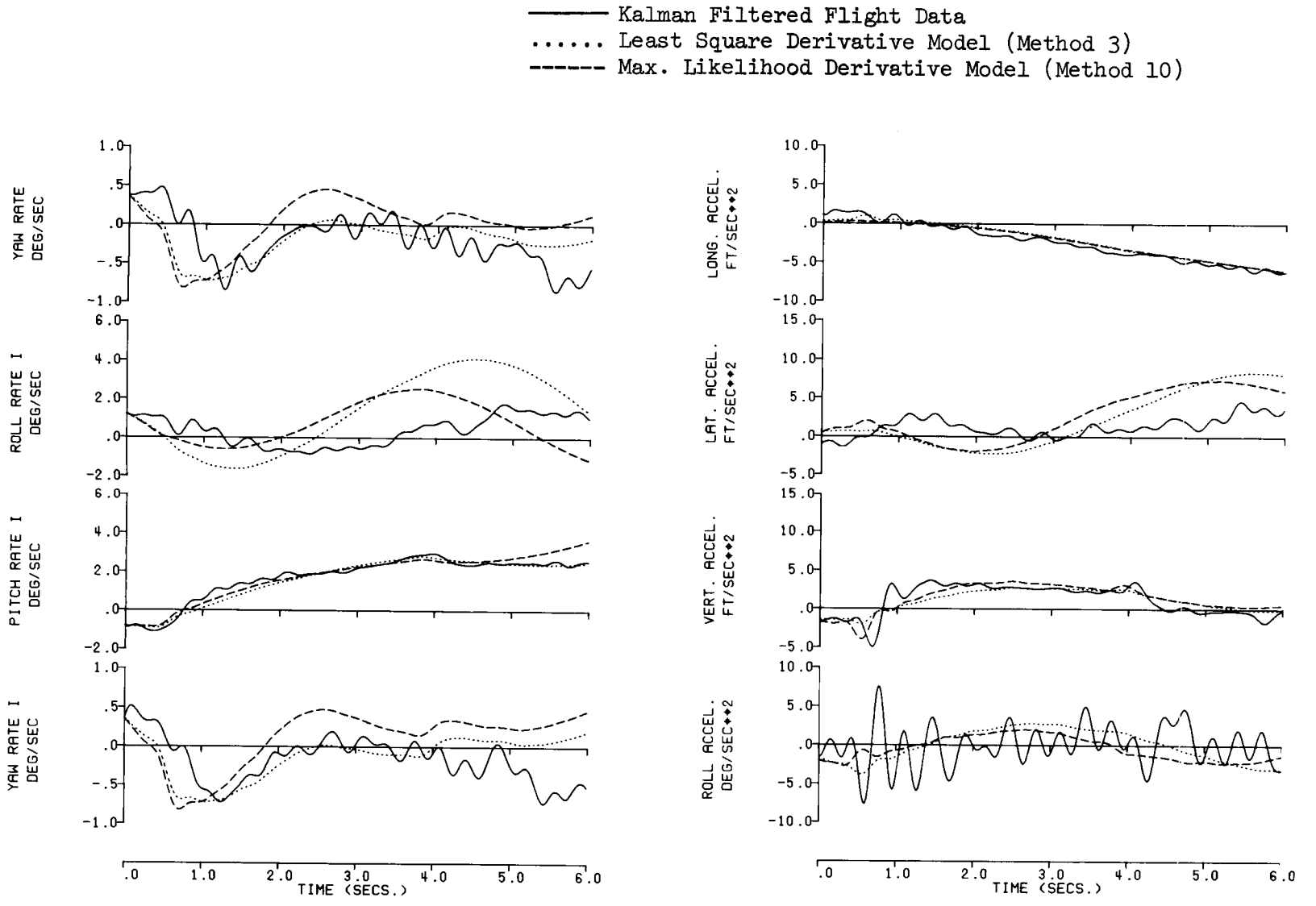

Figure 27. - Continued.

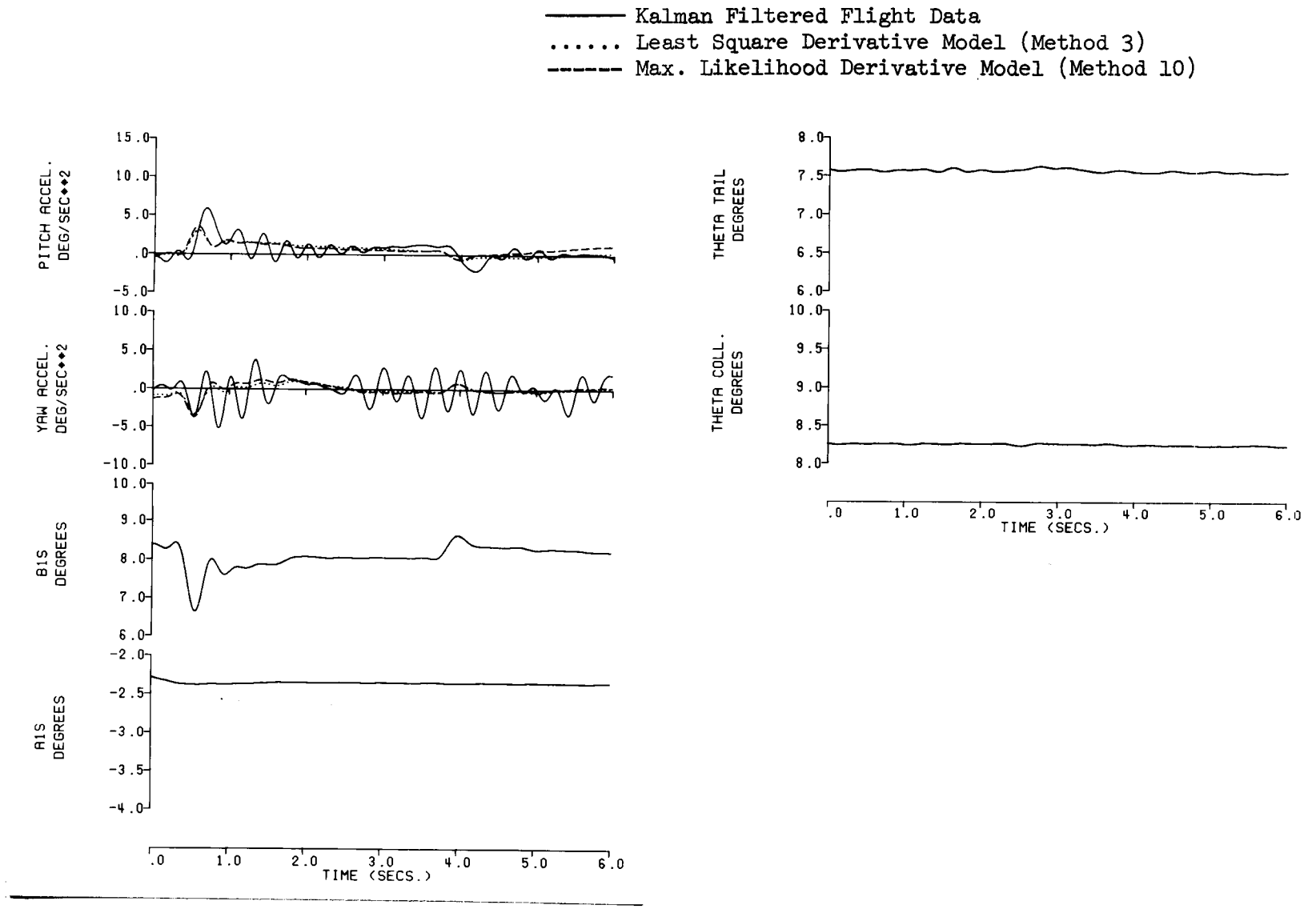

Figure 27. - Concluded.

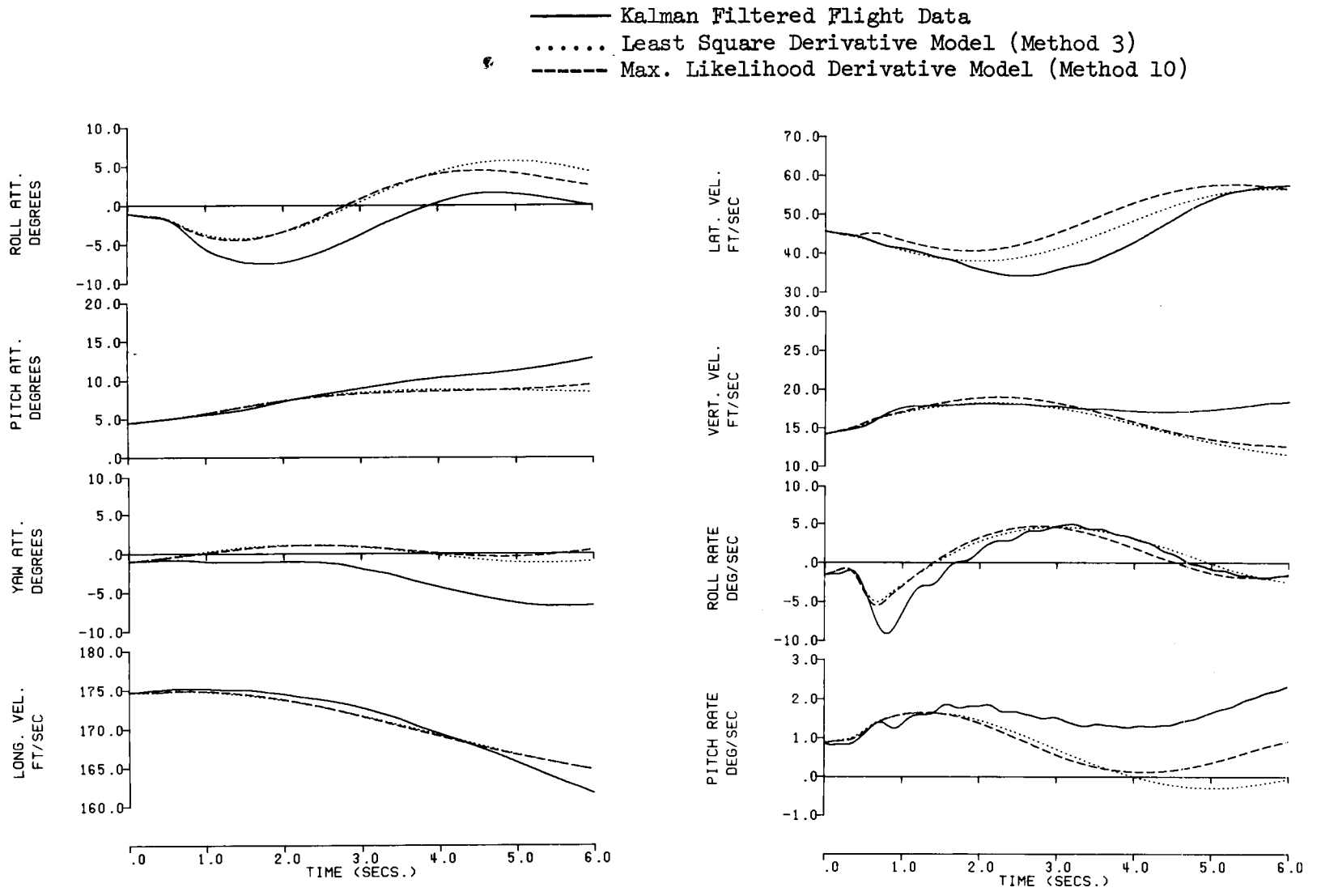

Figure 28. - Time History Comparison of Identified Derivative Models Against CH-53A Flight Data (100 knots, Maneuver 2).

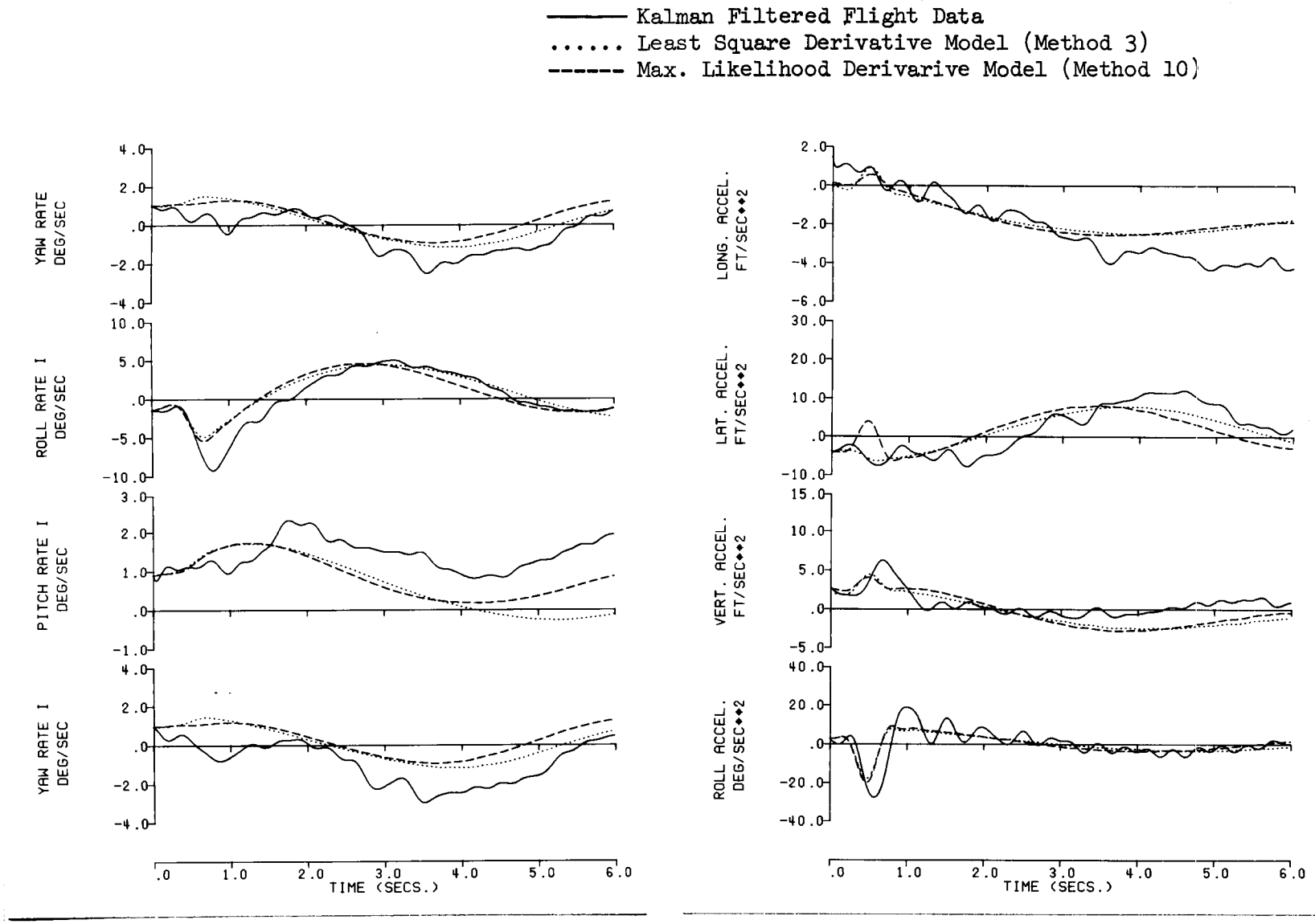

Figure 28. - Continued.

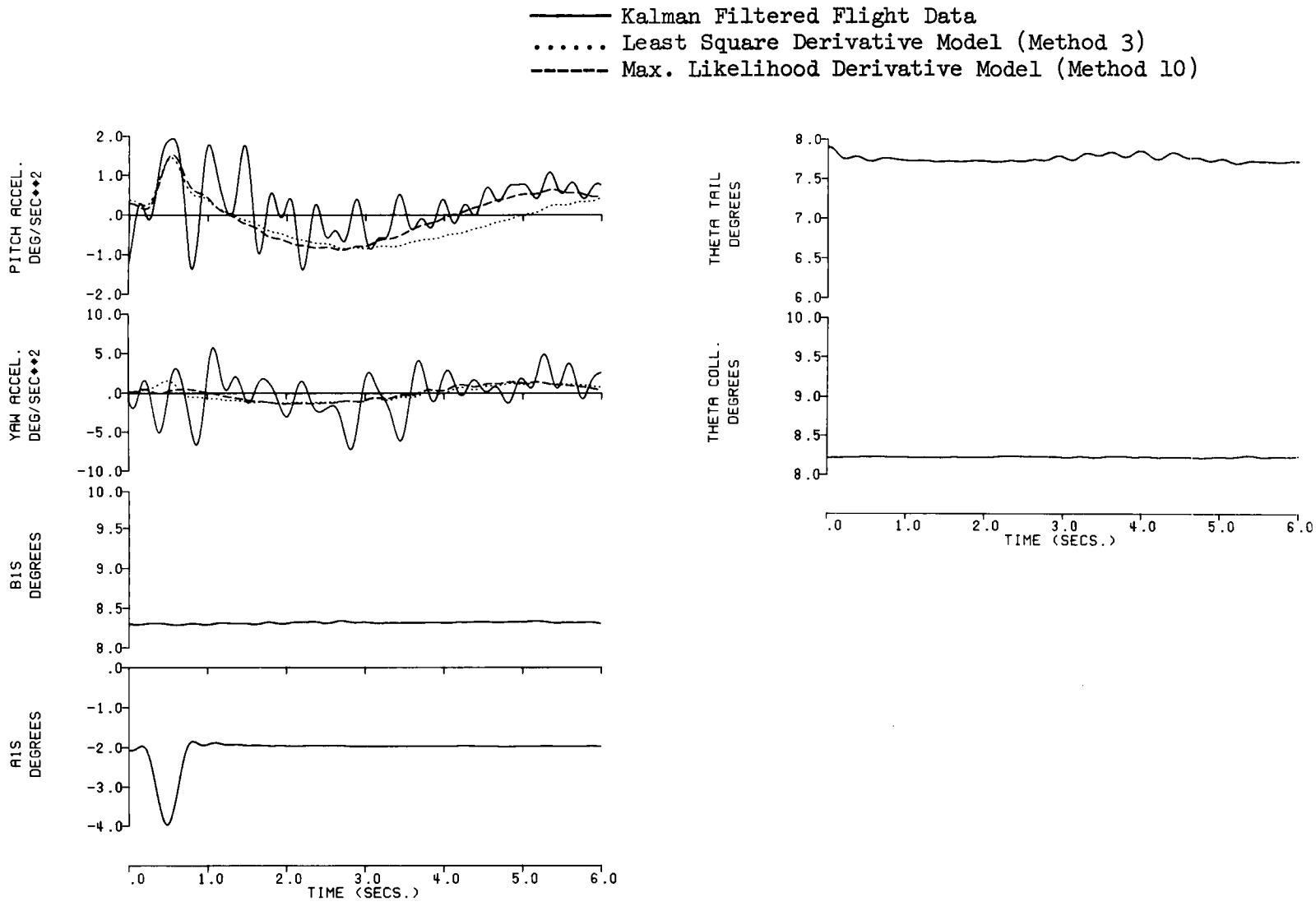

Figure 28 . - Concluded.

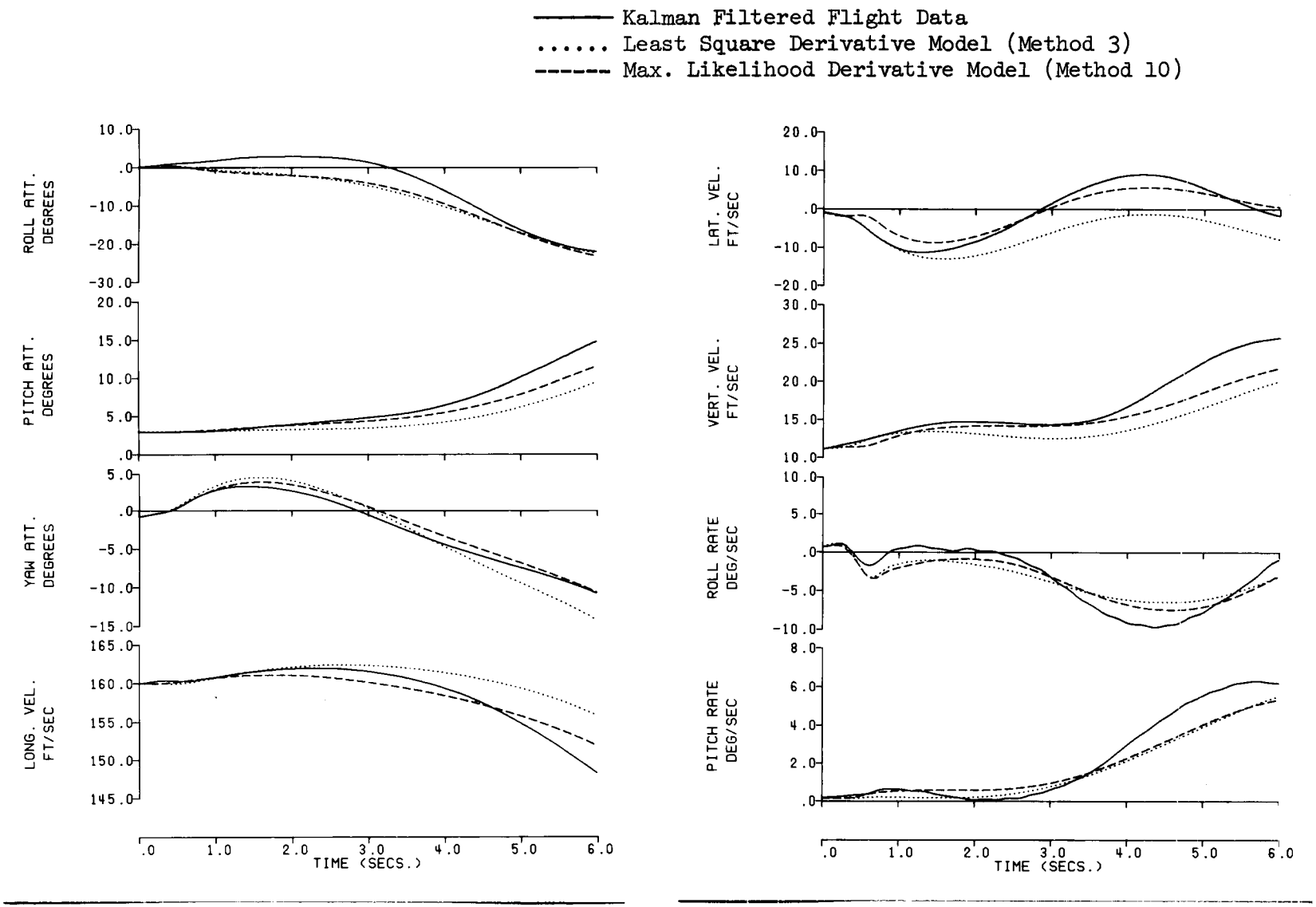

Figure 29. - Time History Comparison of Identified Derivative Models Against CH-53A Flight Data (100 knots, Maneuver 3).

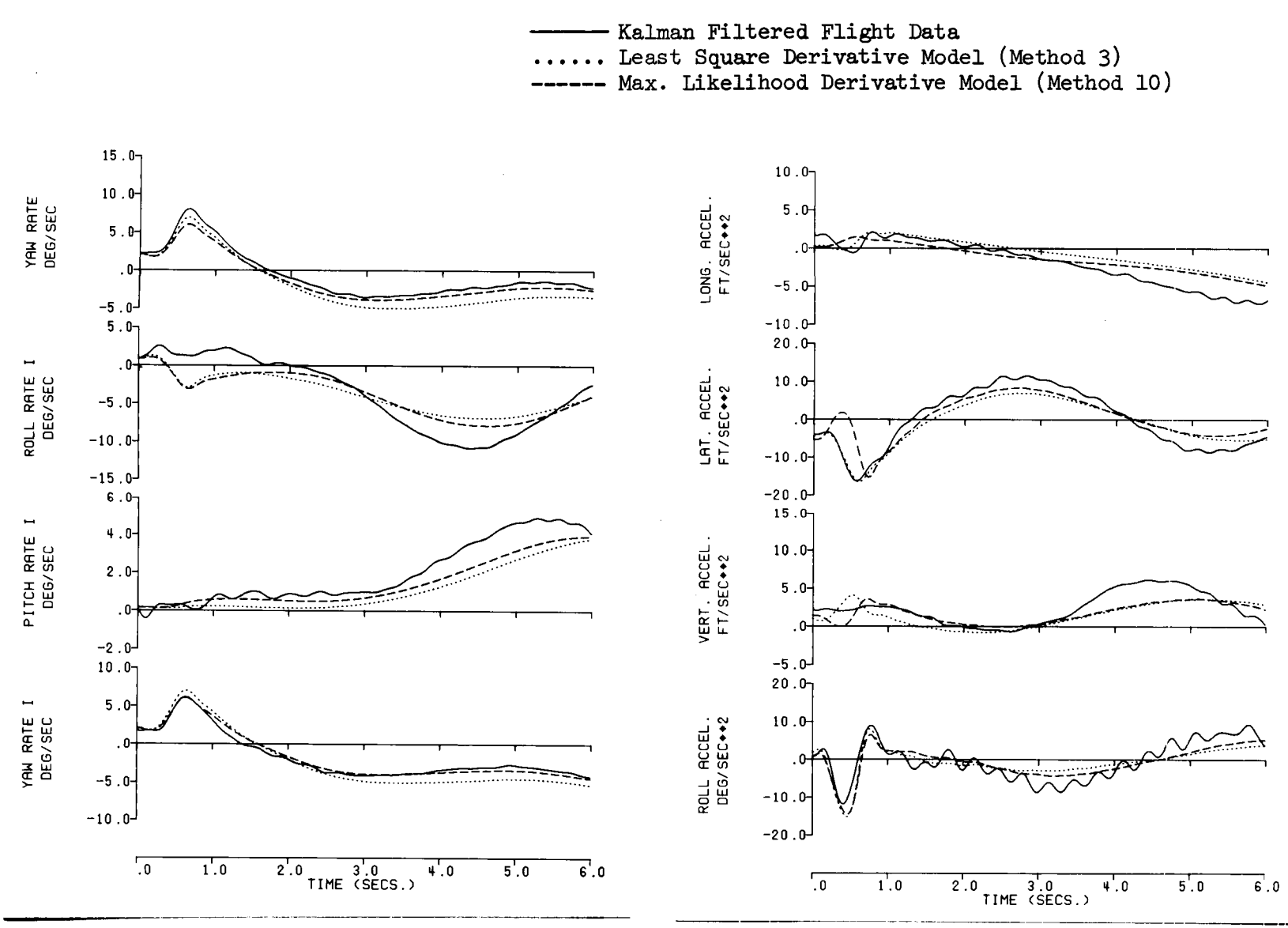

Figure 29. - Continued.

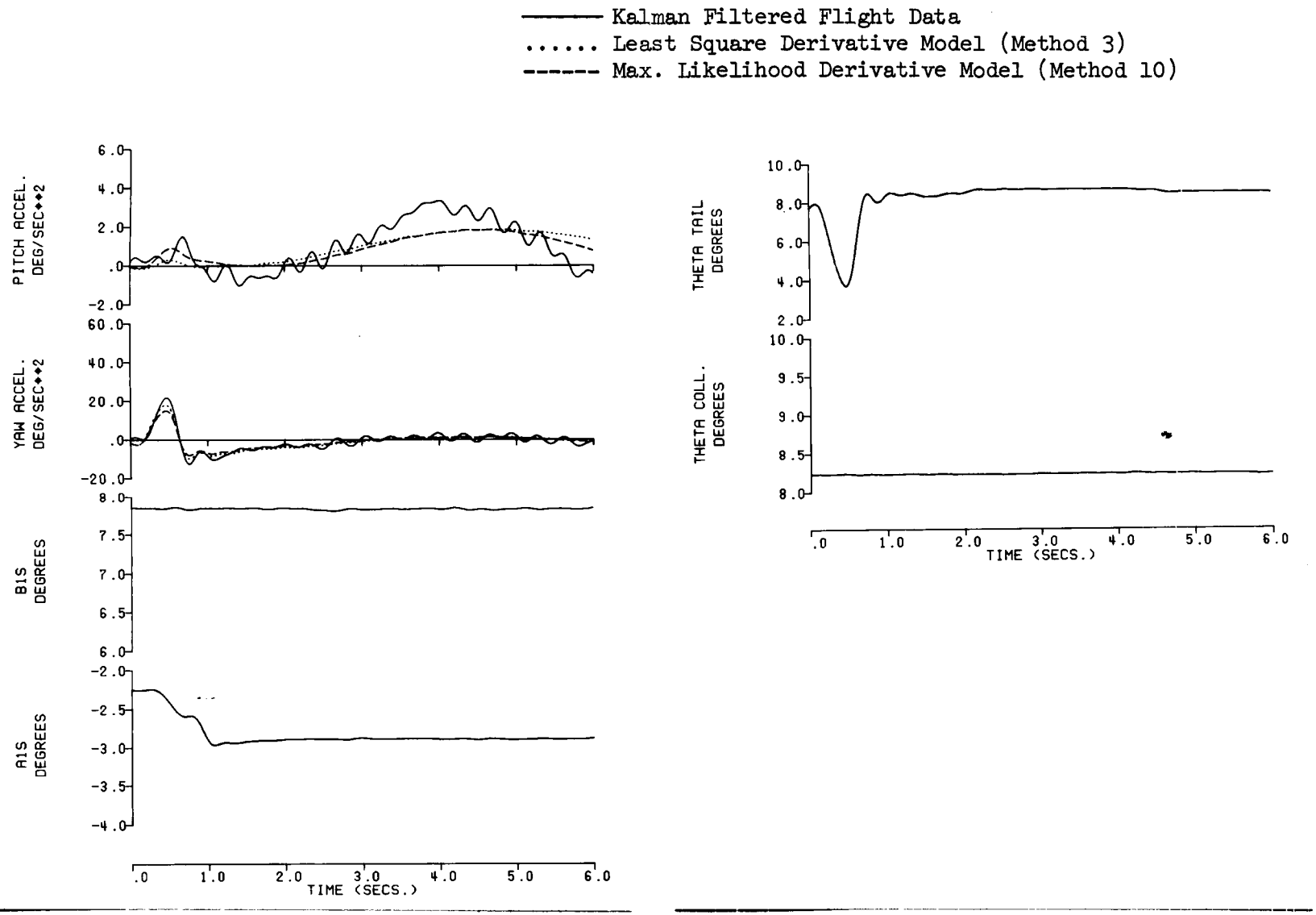

Figure 29. - Concluded.

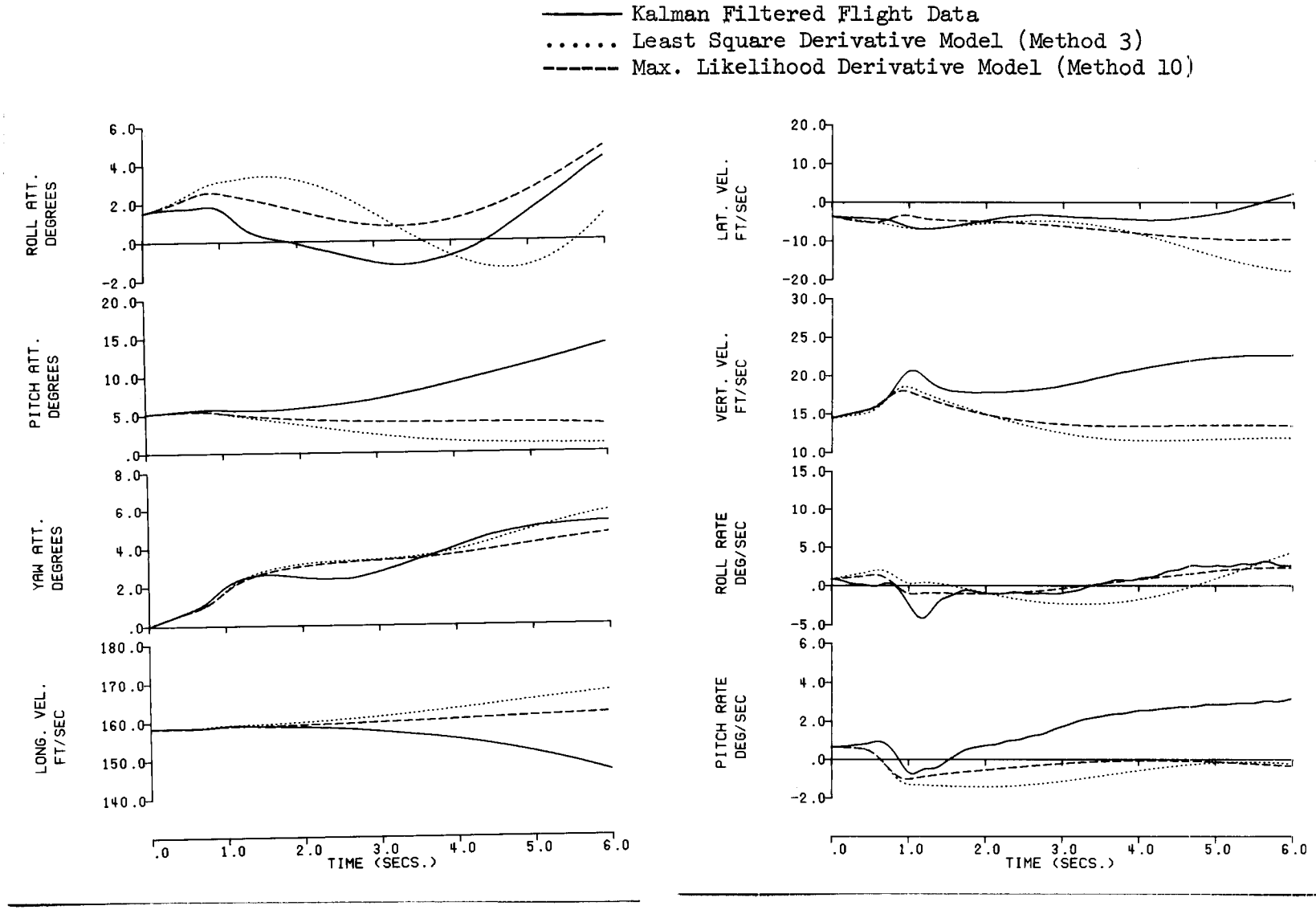

Figure 30 . - Time History Comparison of Identified Derivative Models Against CH-53A Flight Data (100 knots, Maneuver 4).

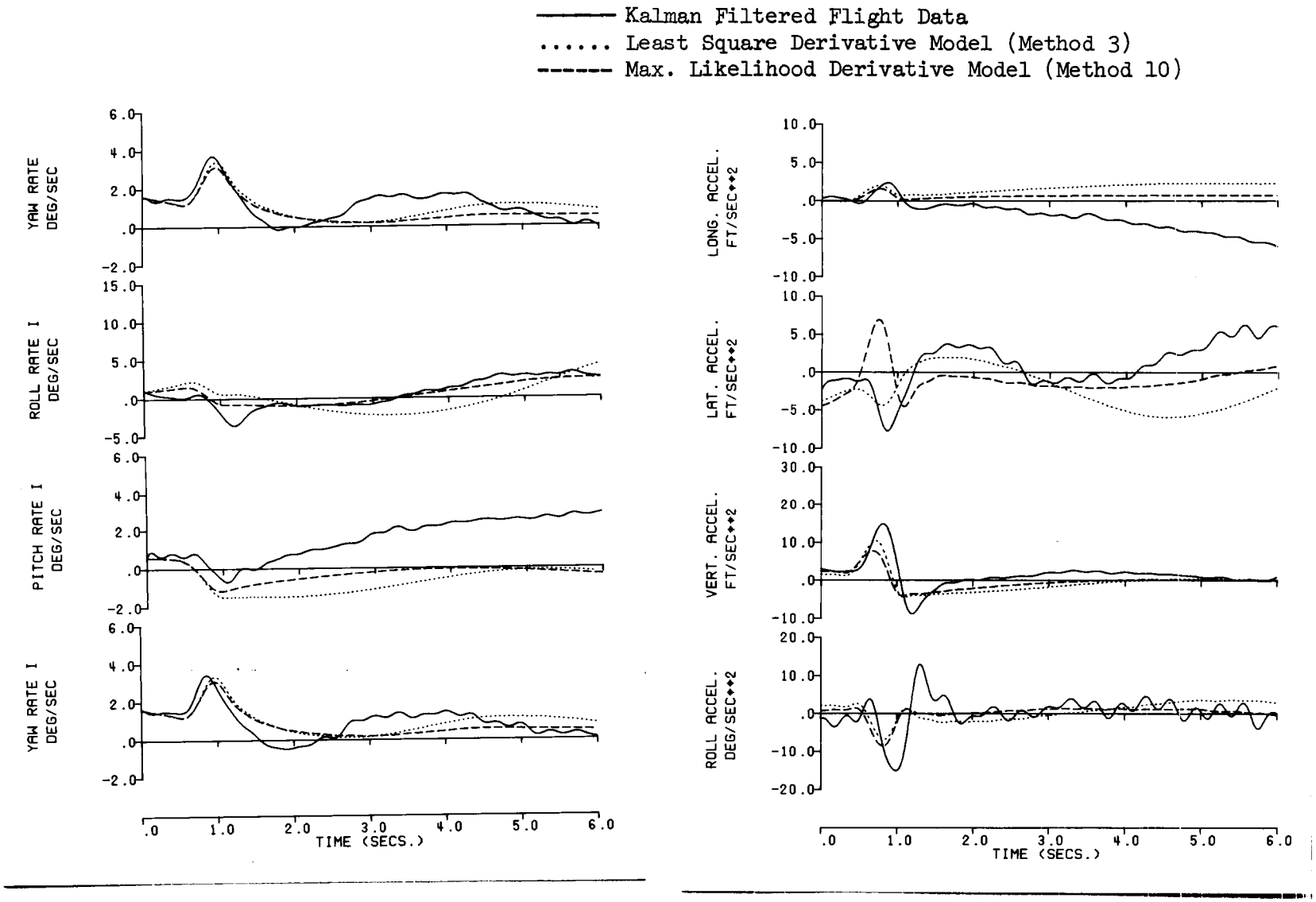

Figure 30. - Continued.

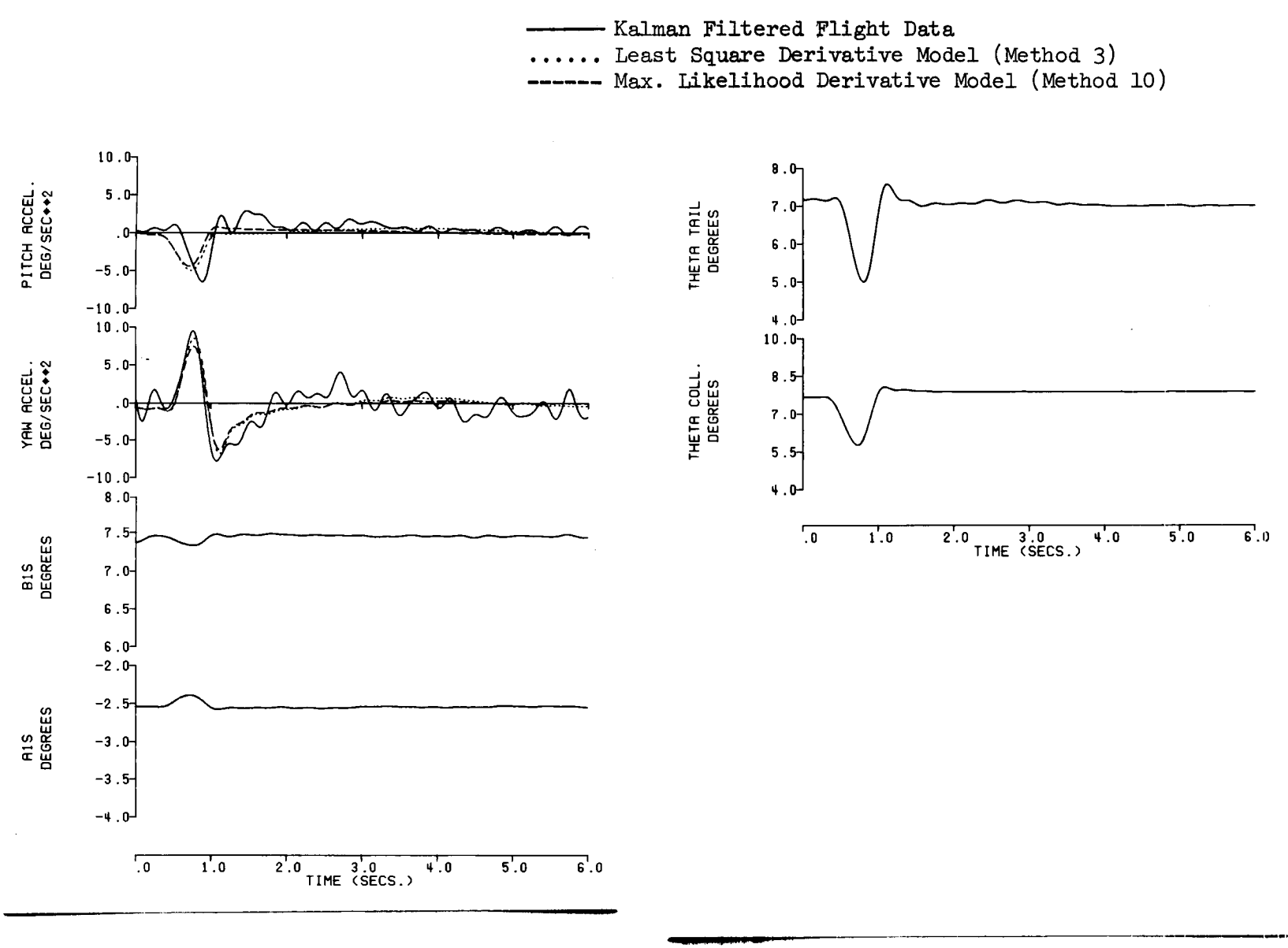

Figure 30. - Concluded.

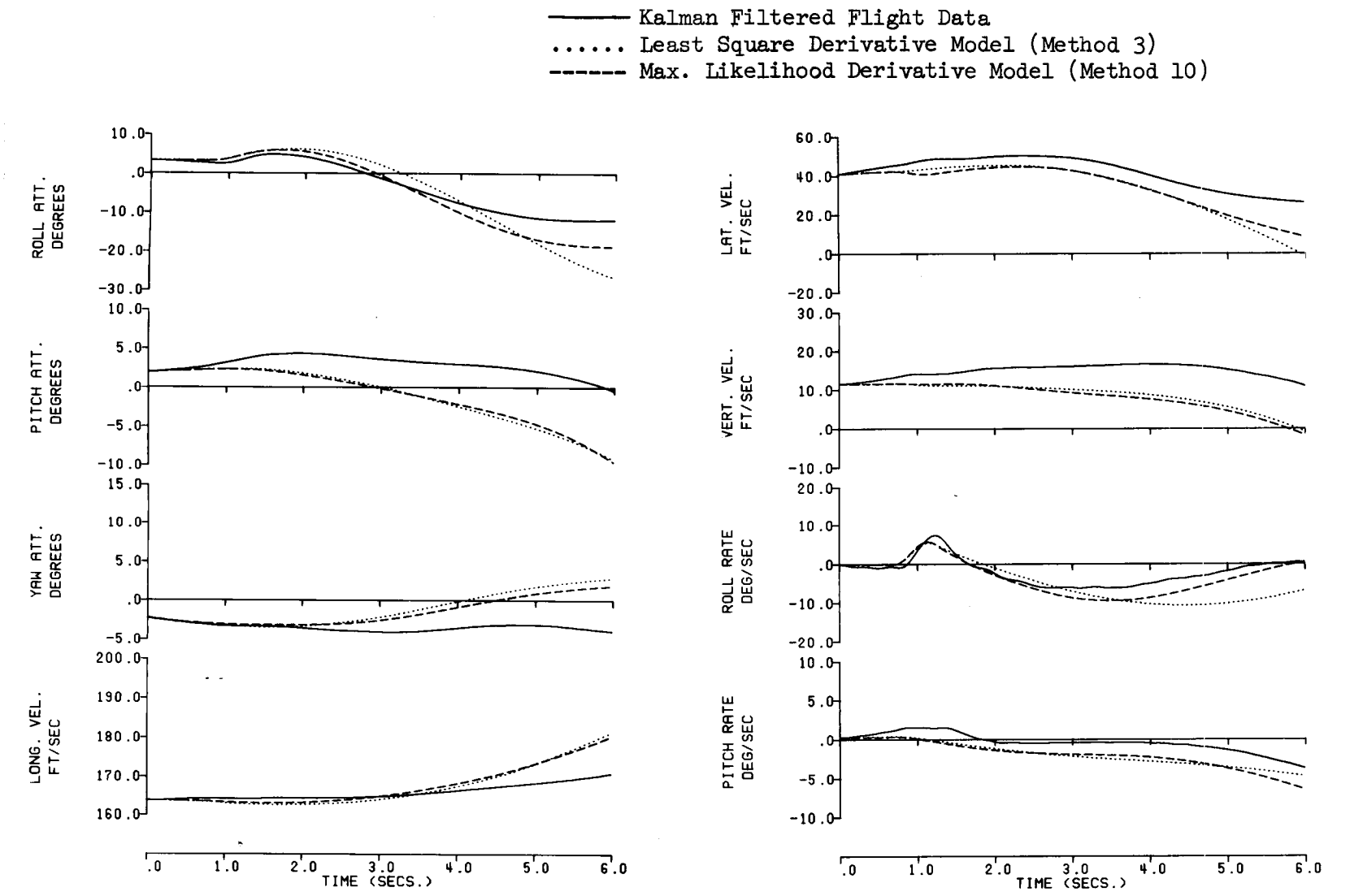

Figure 31. - Time History Comparison of Identified Derivative Models Against CH-53A Flight Data (100 knots, Maneuver 5). (Data not used in the Identification.)

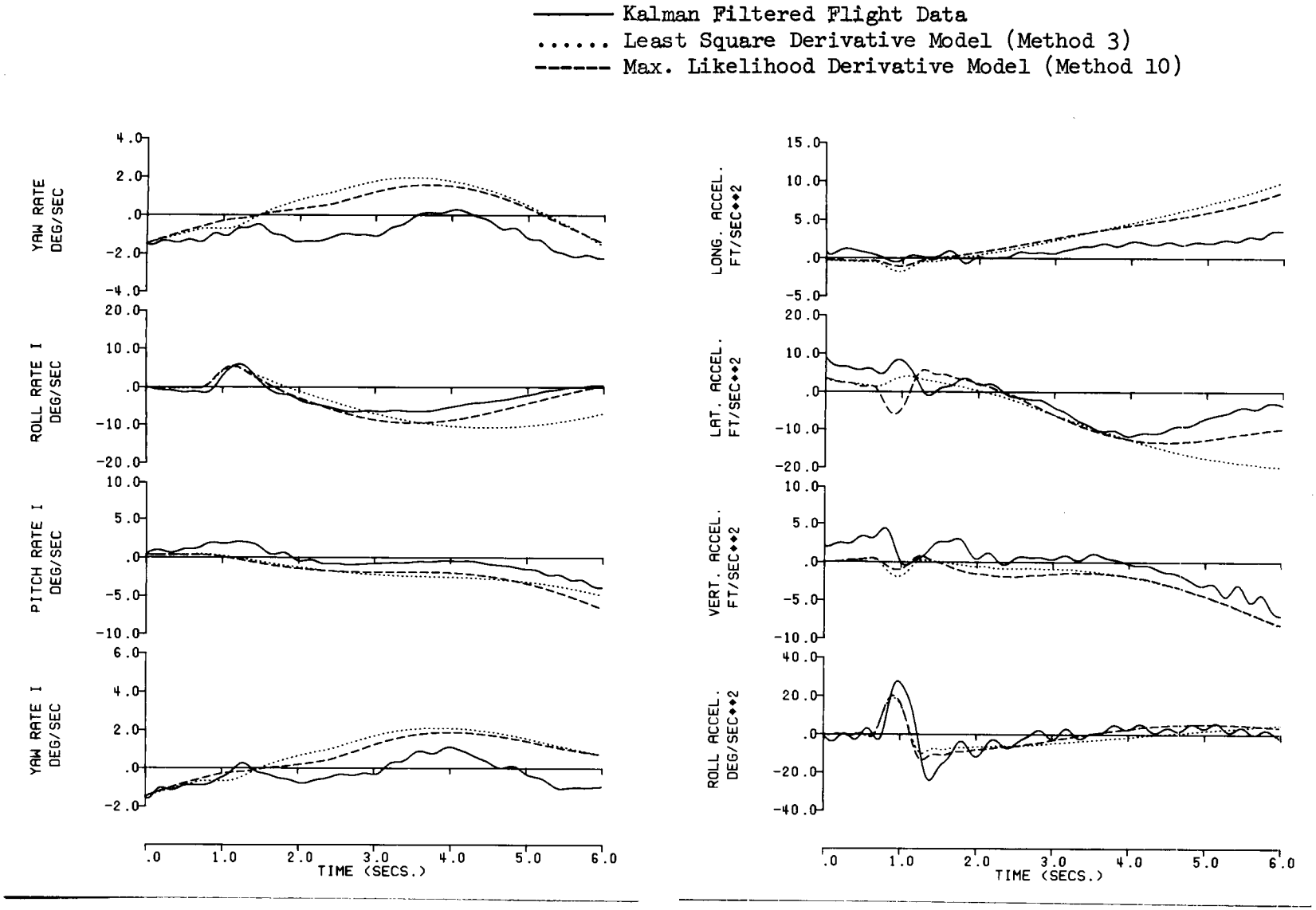

Figure 31. - Continued.

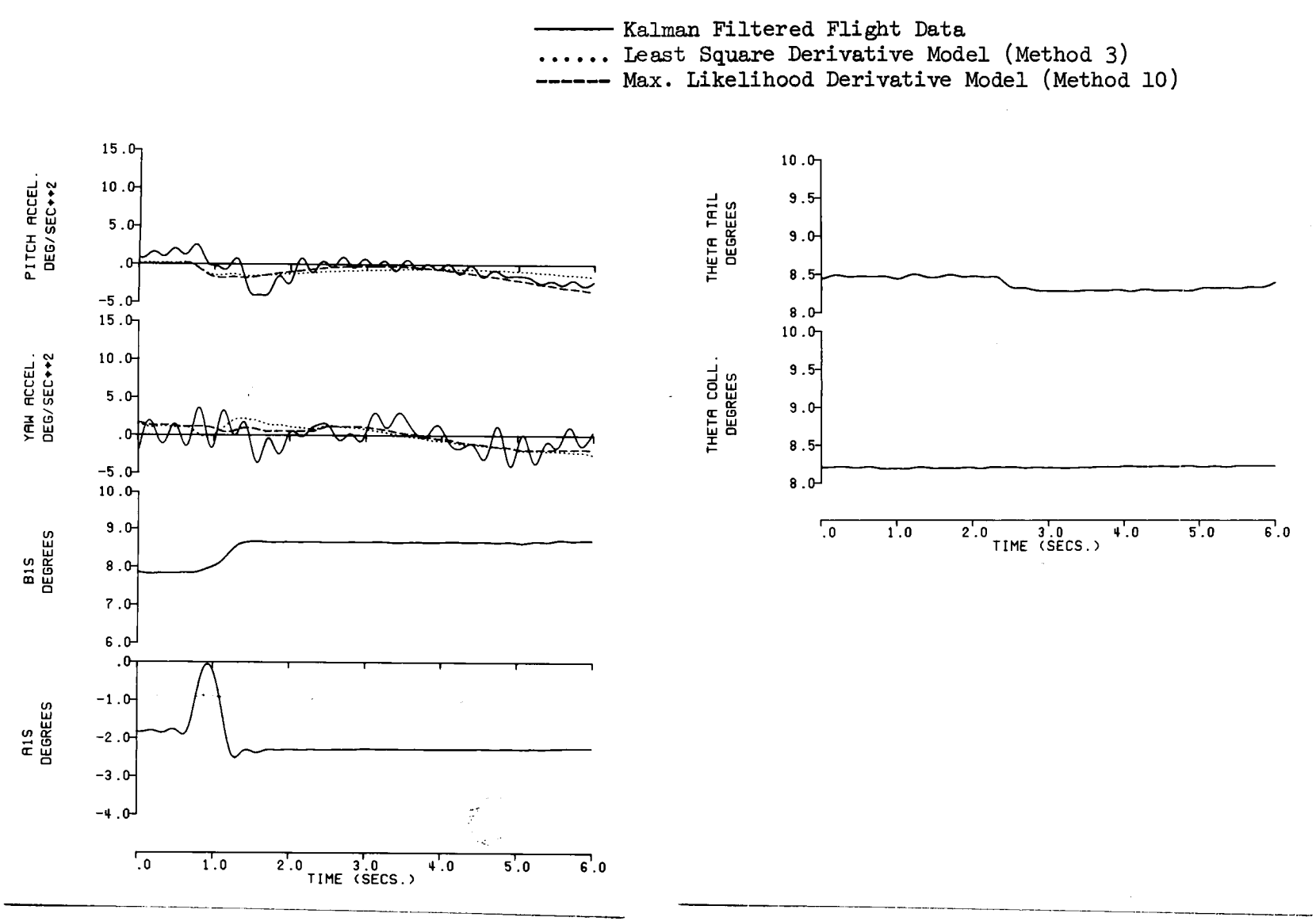

Figure 31. - Concluded.

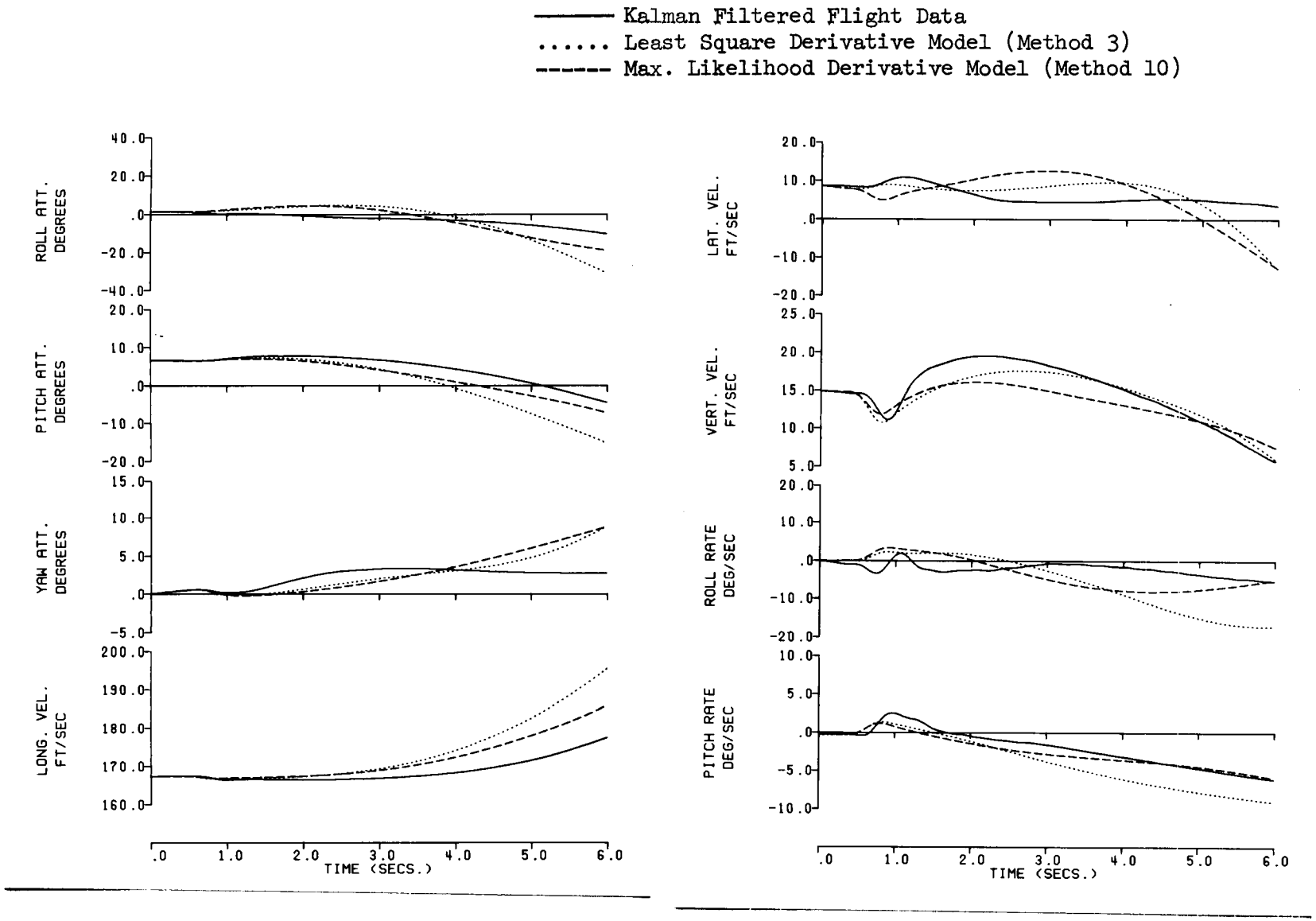

Figure 32. - Time History Comparison of Identified Derivative Models Against CH-53A Flight Data (100 knots, Maneuver 6). (Data not used in the Identification.)

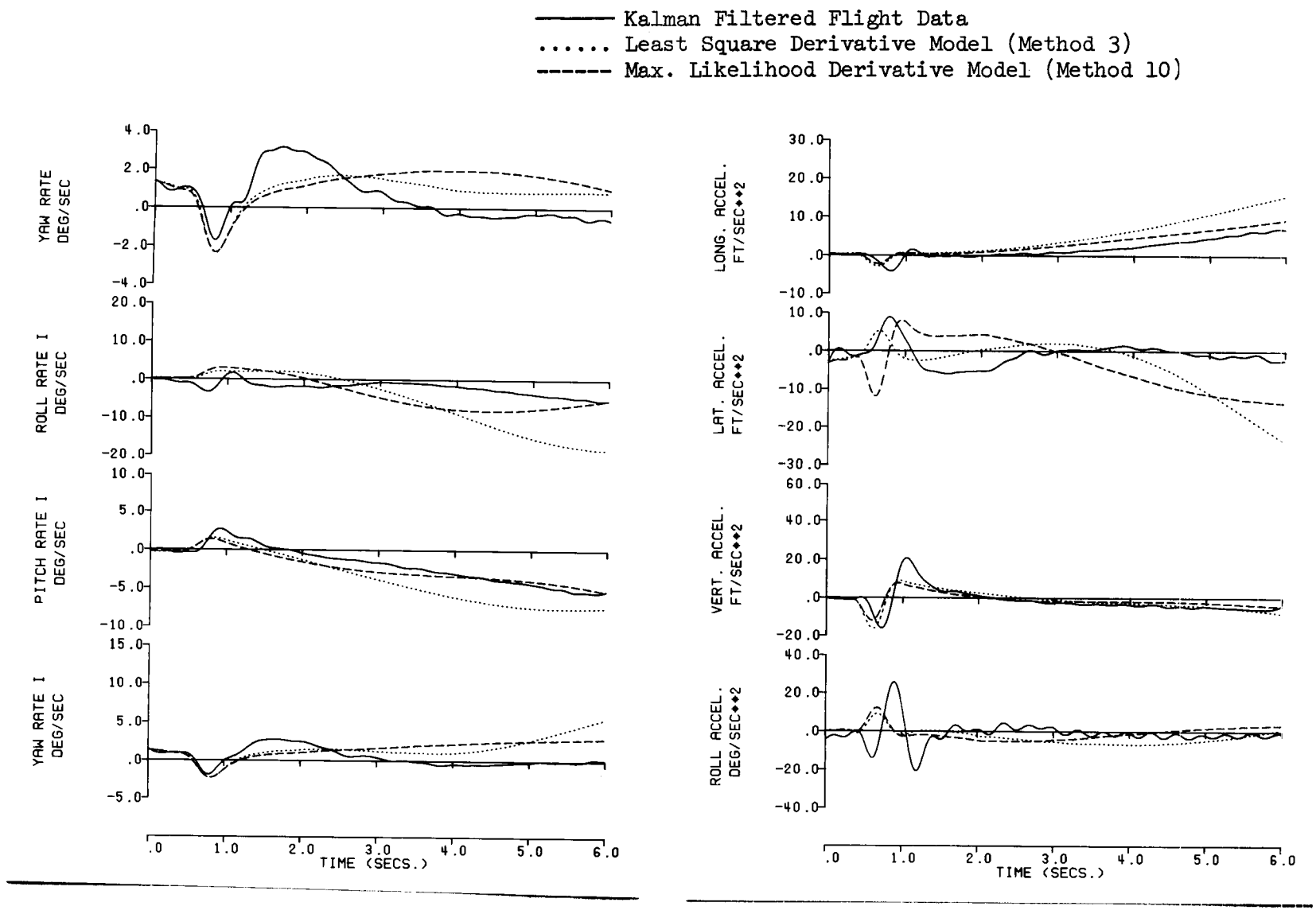

Figure 32. - Continued.

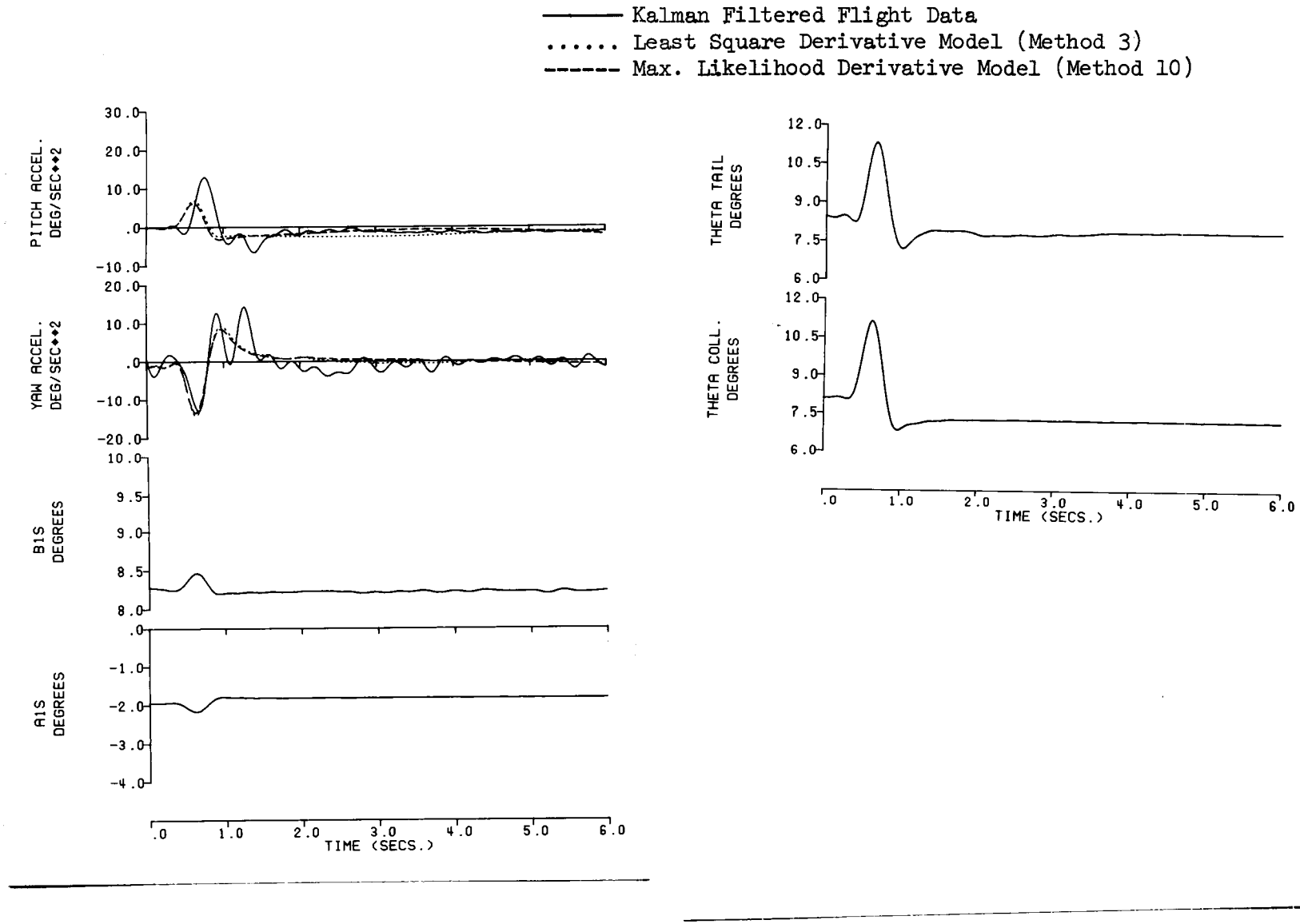

Figure 32. - Concluded.

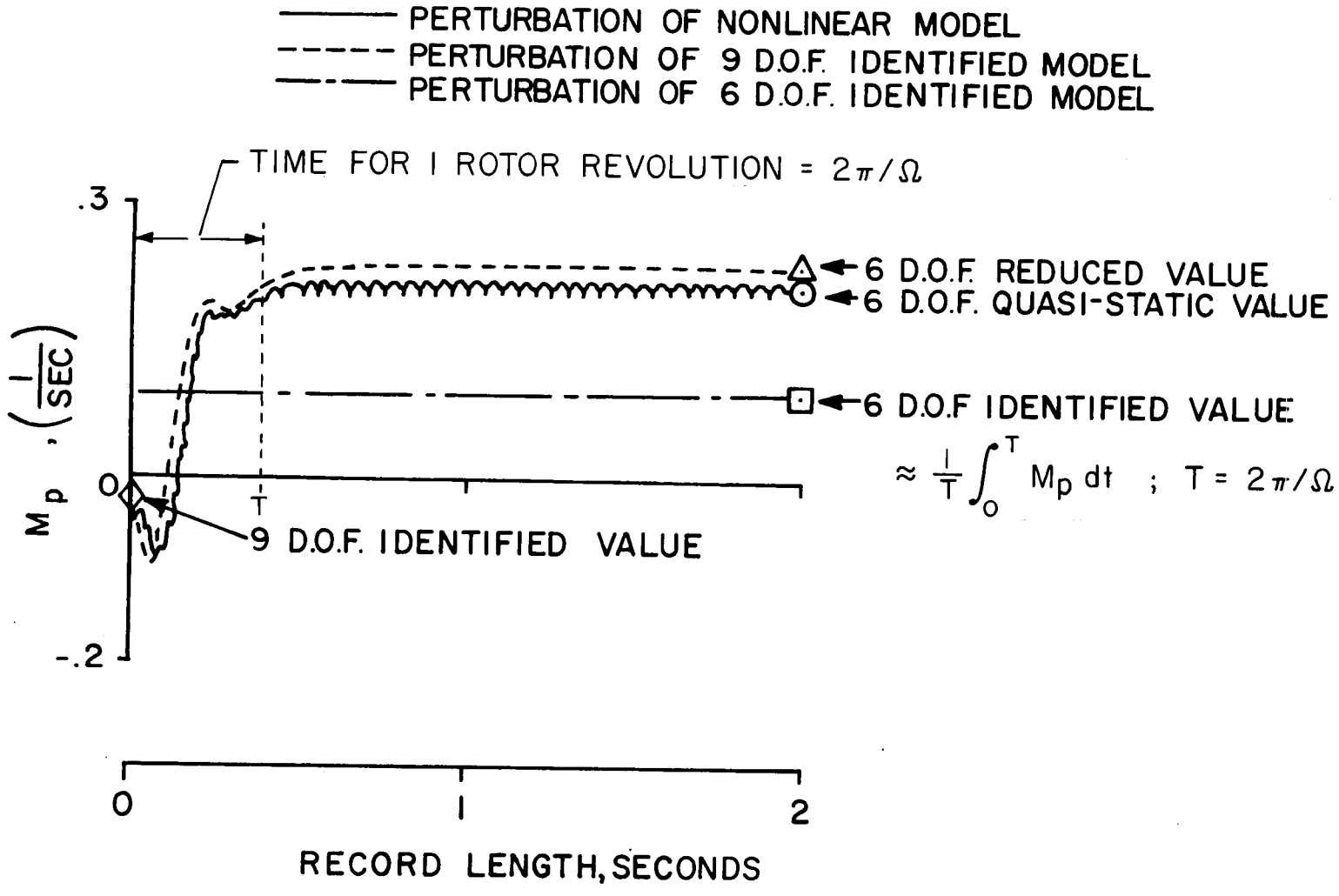

Figure 33. Stability Derivative Obtained From A Nonlinear Helicopter Computer Model Showing The Interpretation of Conventional Quasi-Static and System Identified Derivatives.

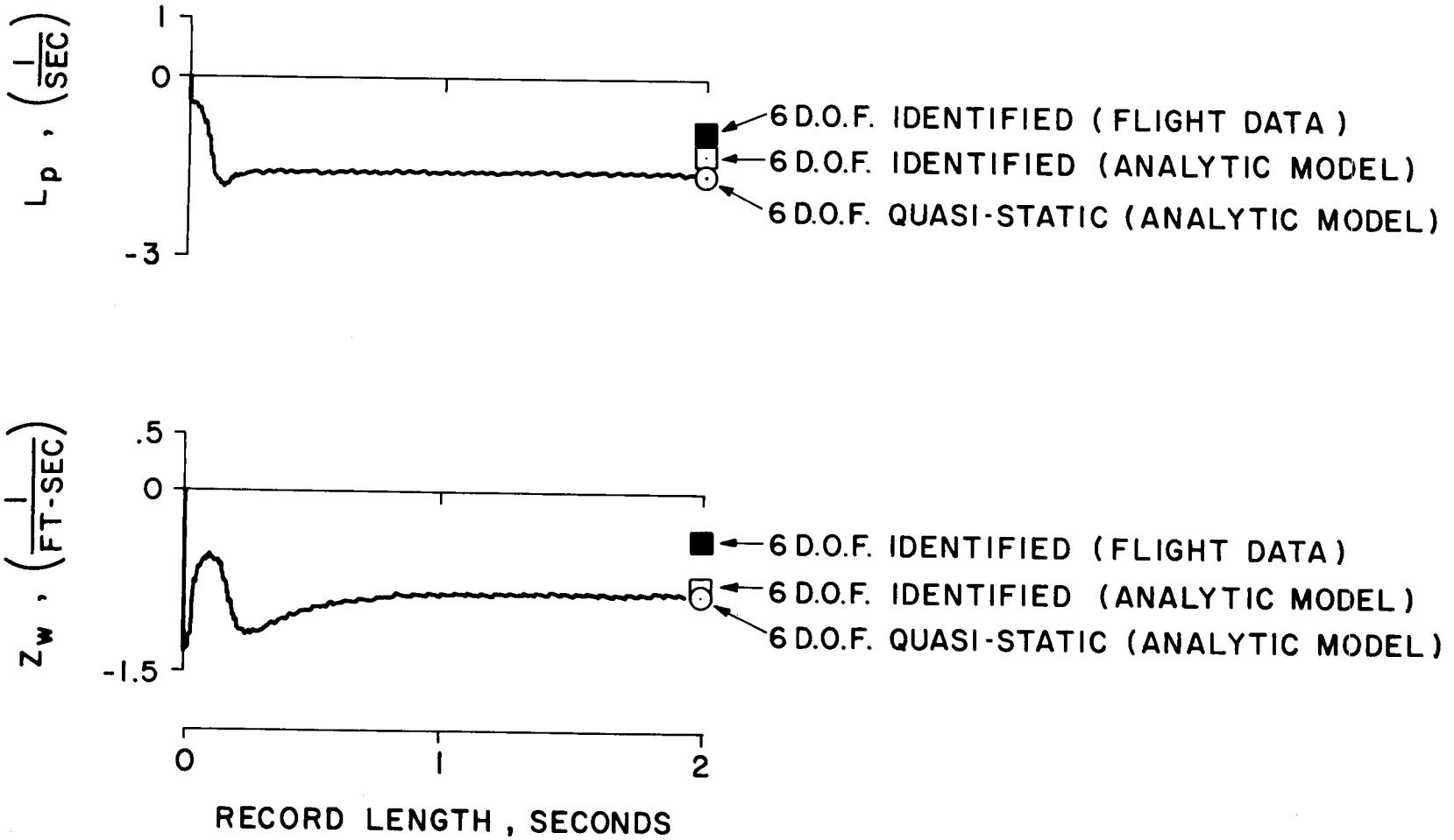

Figure 34. Comparison of Derivatives Identified From Flight Data Using the MLE vs. Analytically Predicted Values (CH-53A, 100 Knots).

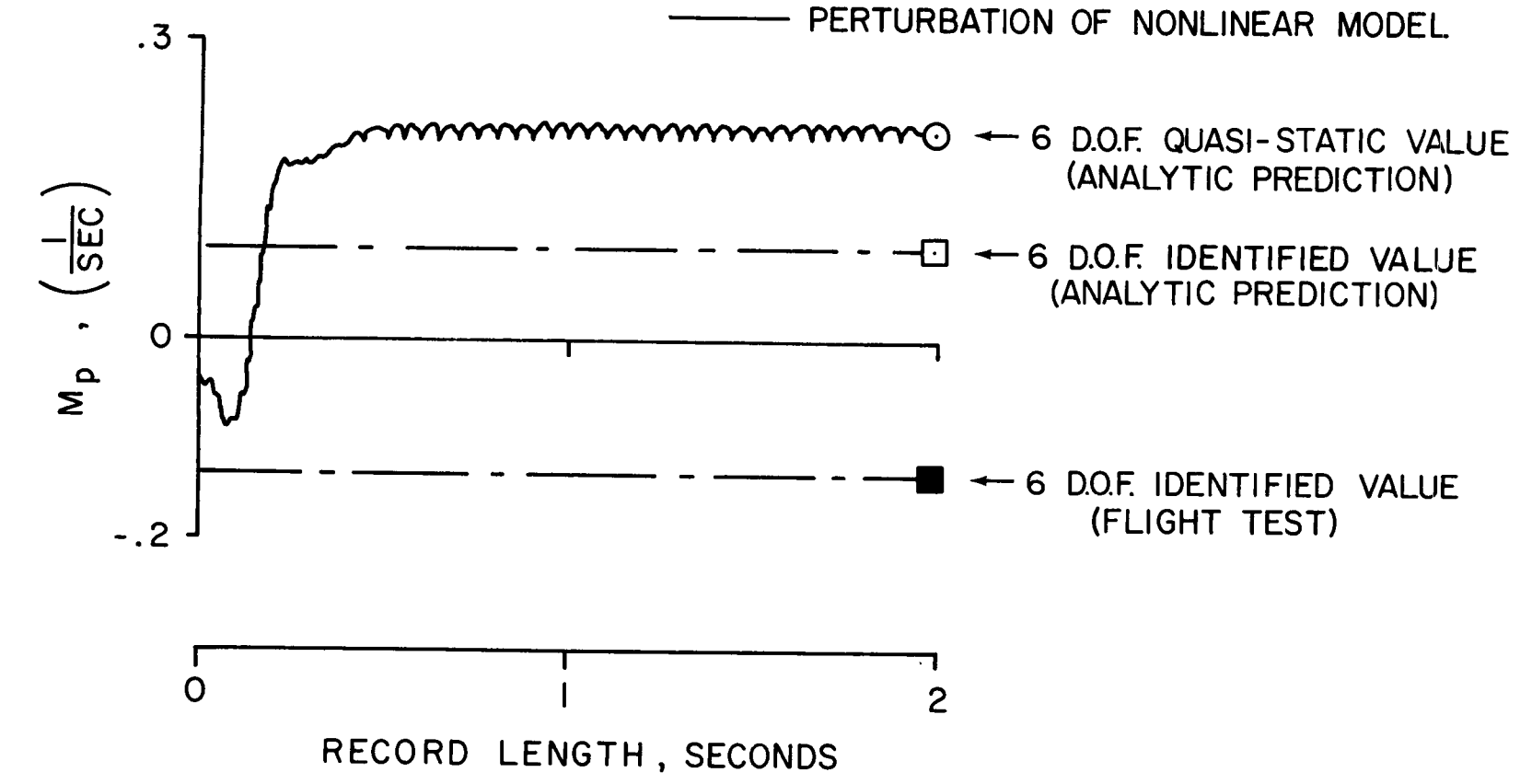

Figure 35. Comparison of the Derivative Mp Identified From Flight Data Using The MLE vs. Analytically Predicted Value (CH-53A, 100 Knots).

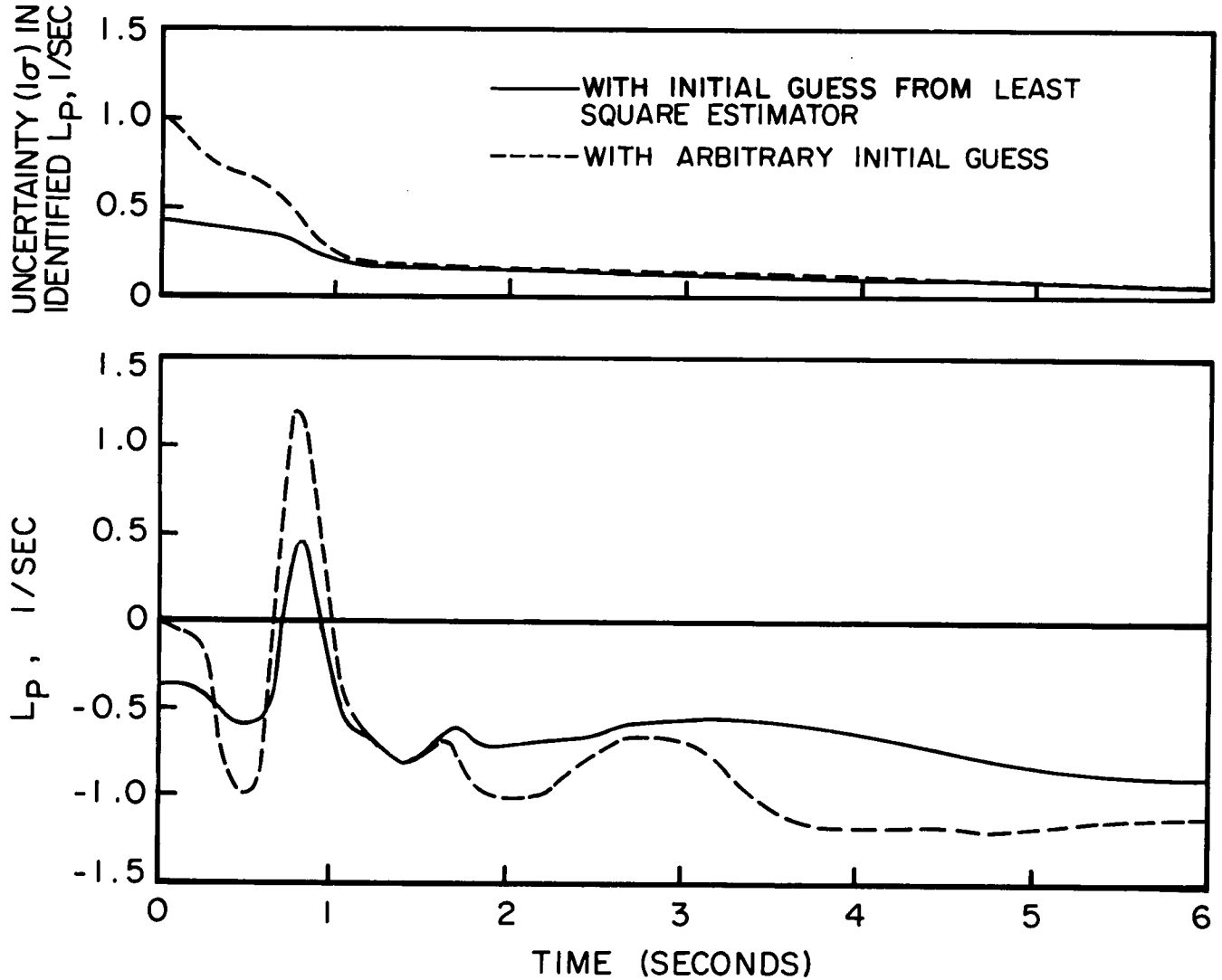

Figure 36. Roll Damping Derivative Convergence and Uncertainty From the MLE For The Two Different Initial Derivative Starting Values (From CH-53A Flight Data, 100 Knots).

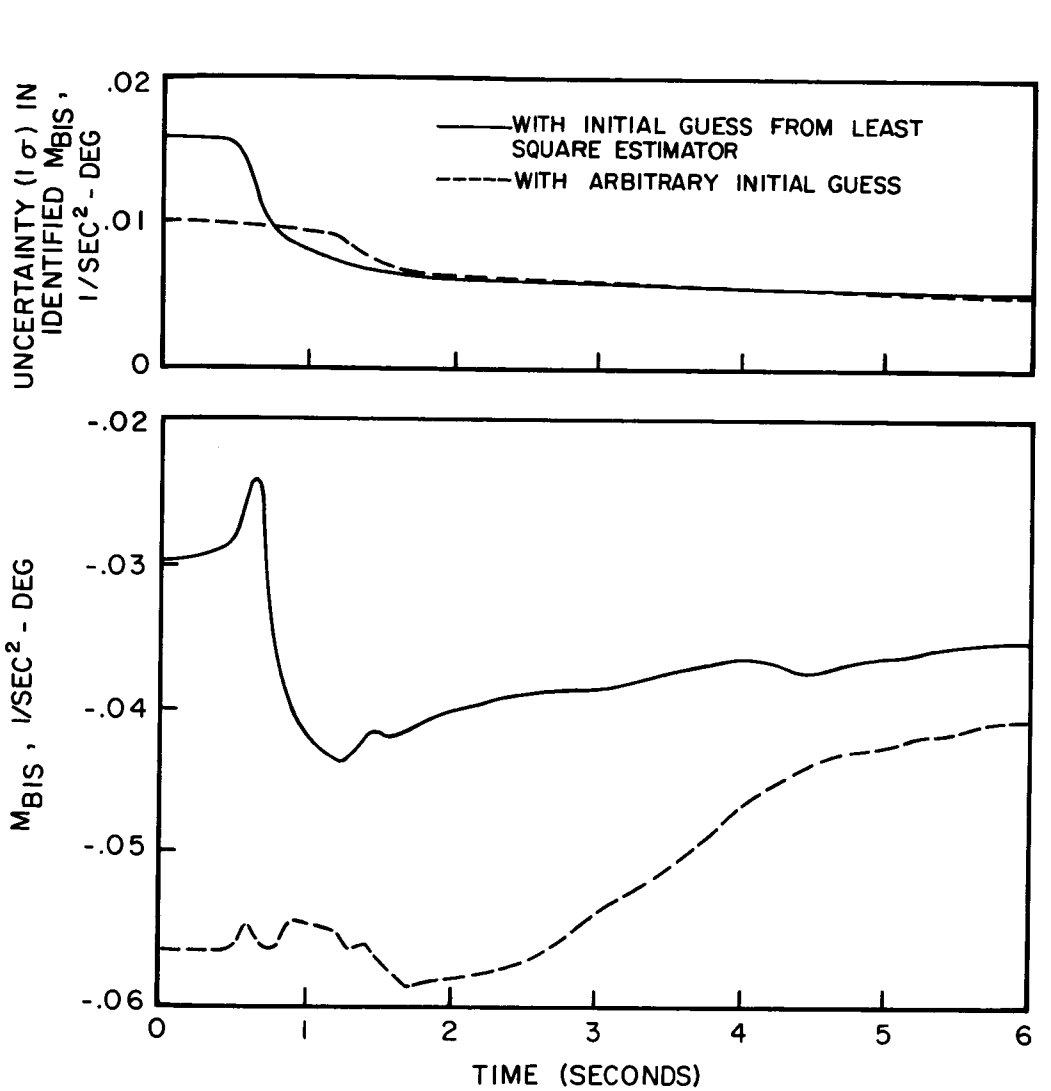

Figure 37. Pitch Control Derivative Convergence and Uncertainty From The MLE for Two Different Initial Derivative Starting Values (From CH-53A Flight Data, 100 Knots).

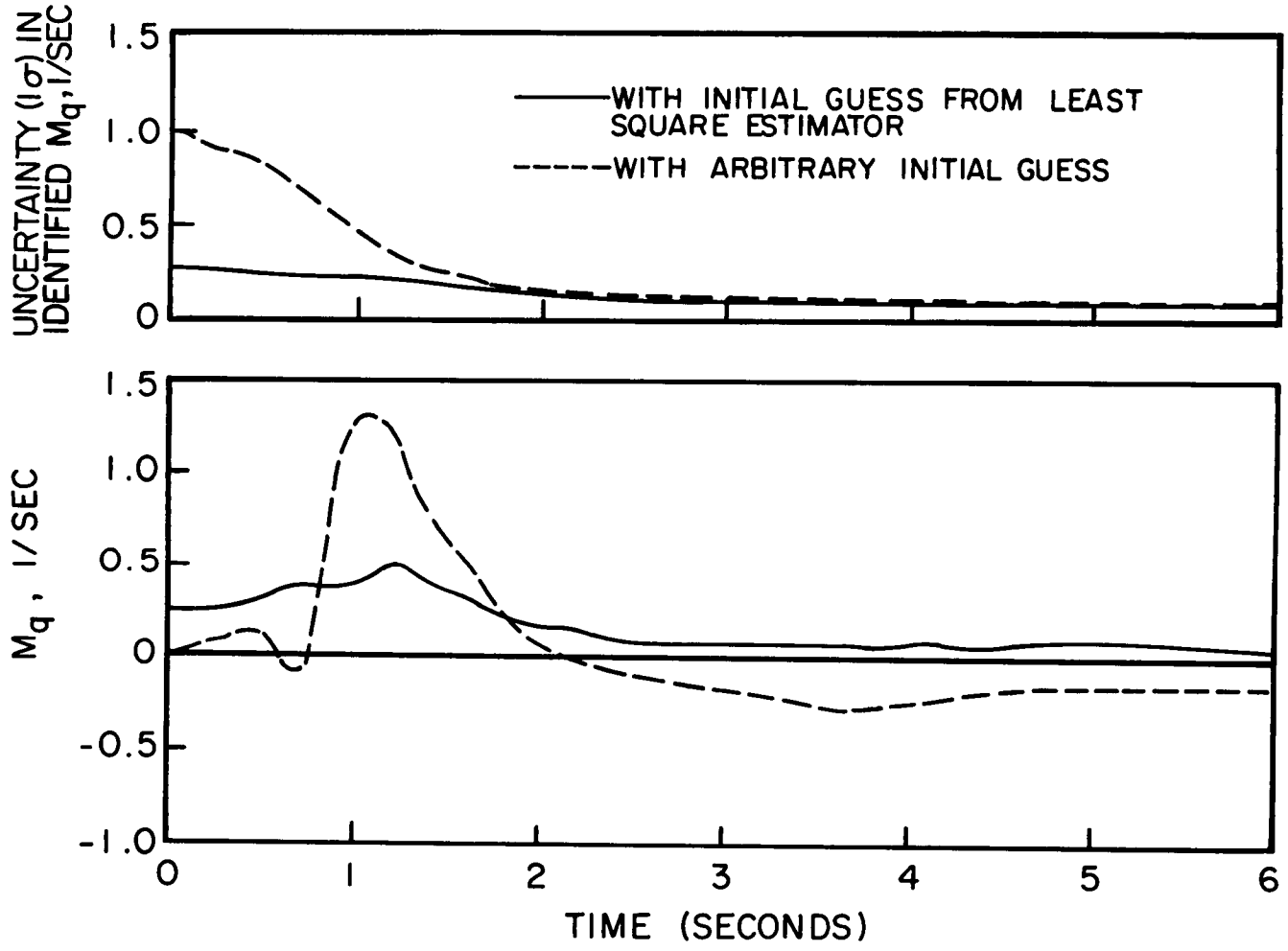

Figure 38. Pitch Damping Derivative Convergence and Uncertainty From The MLE For Two Different Initial Derivative Starting Values (From CH-53A Flight Data, 100 Knots).

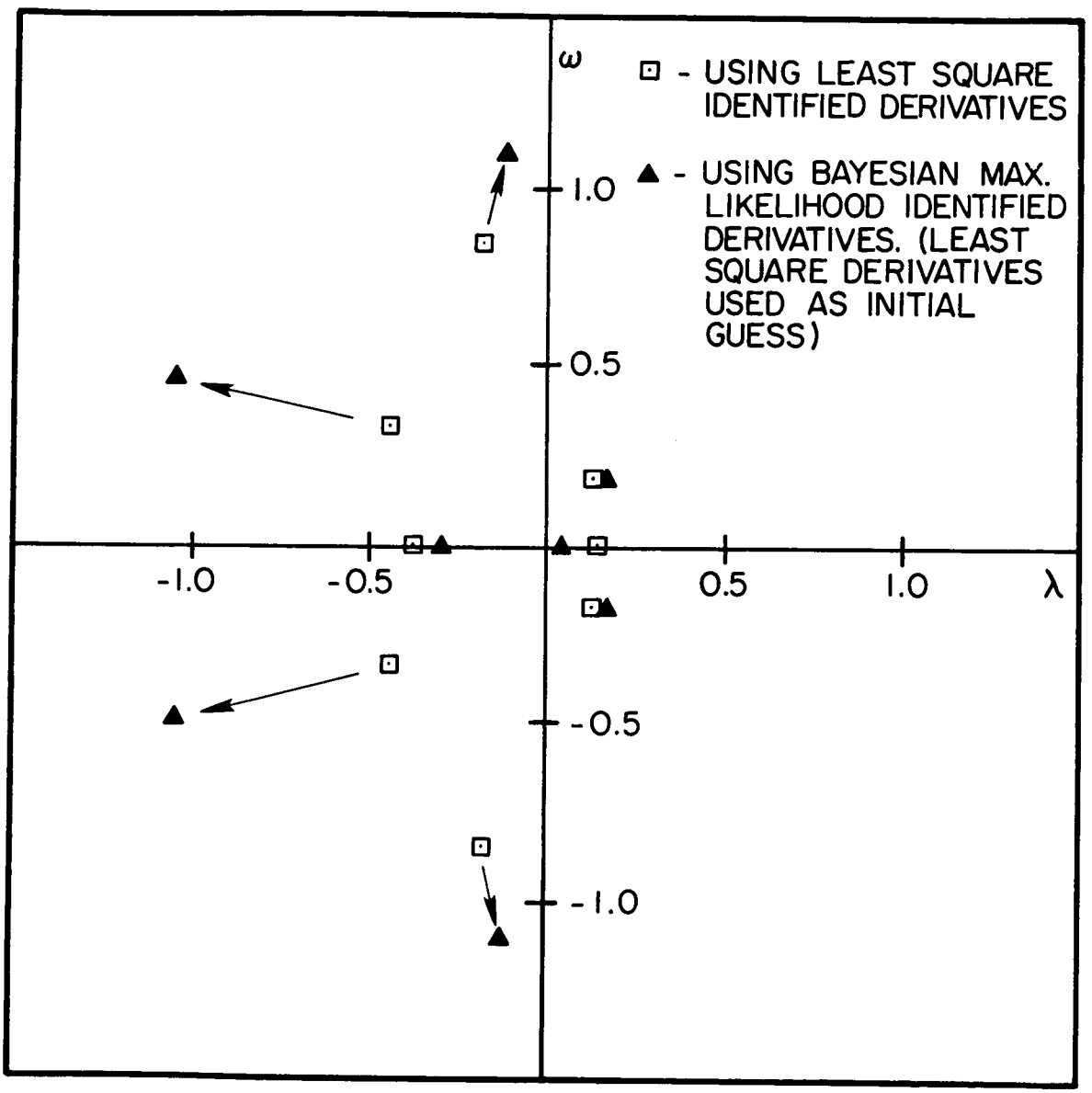

Figure 39. Characteristic Roots Obtained From The Identified Derivatives of The LSE(Method 3) and The MLE (Method 10) (From CH-53A Flight Data, 100 Knots, AFCS Off)

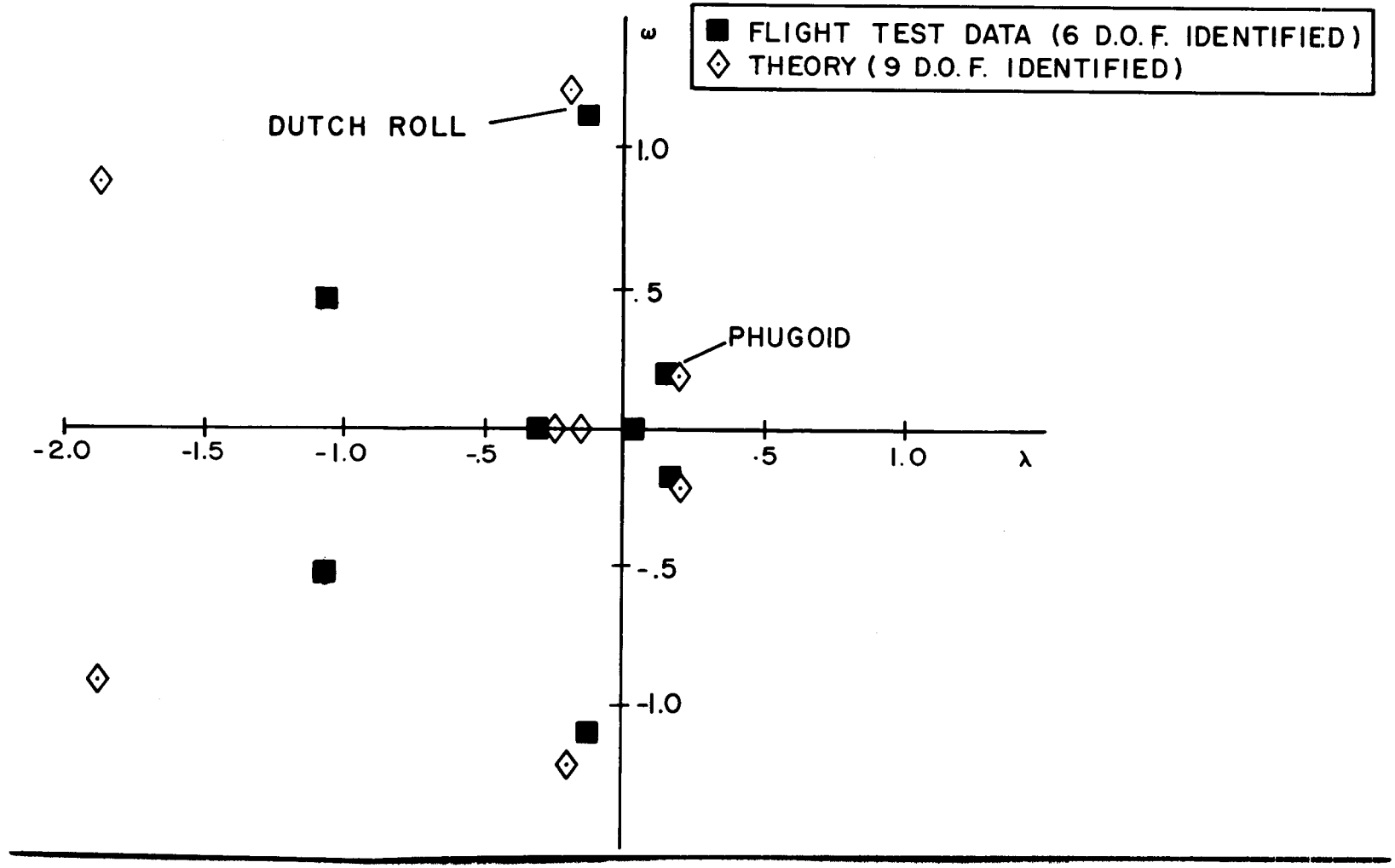

Figure 40. Comparison of Characteristic Roots Identified From Flight Data vs. Analytic Computer Model Roots. (CH-53A, 100 Knots, AFCS OFF).

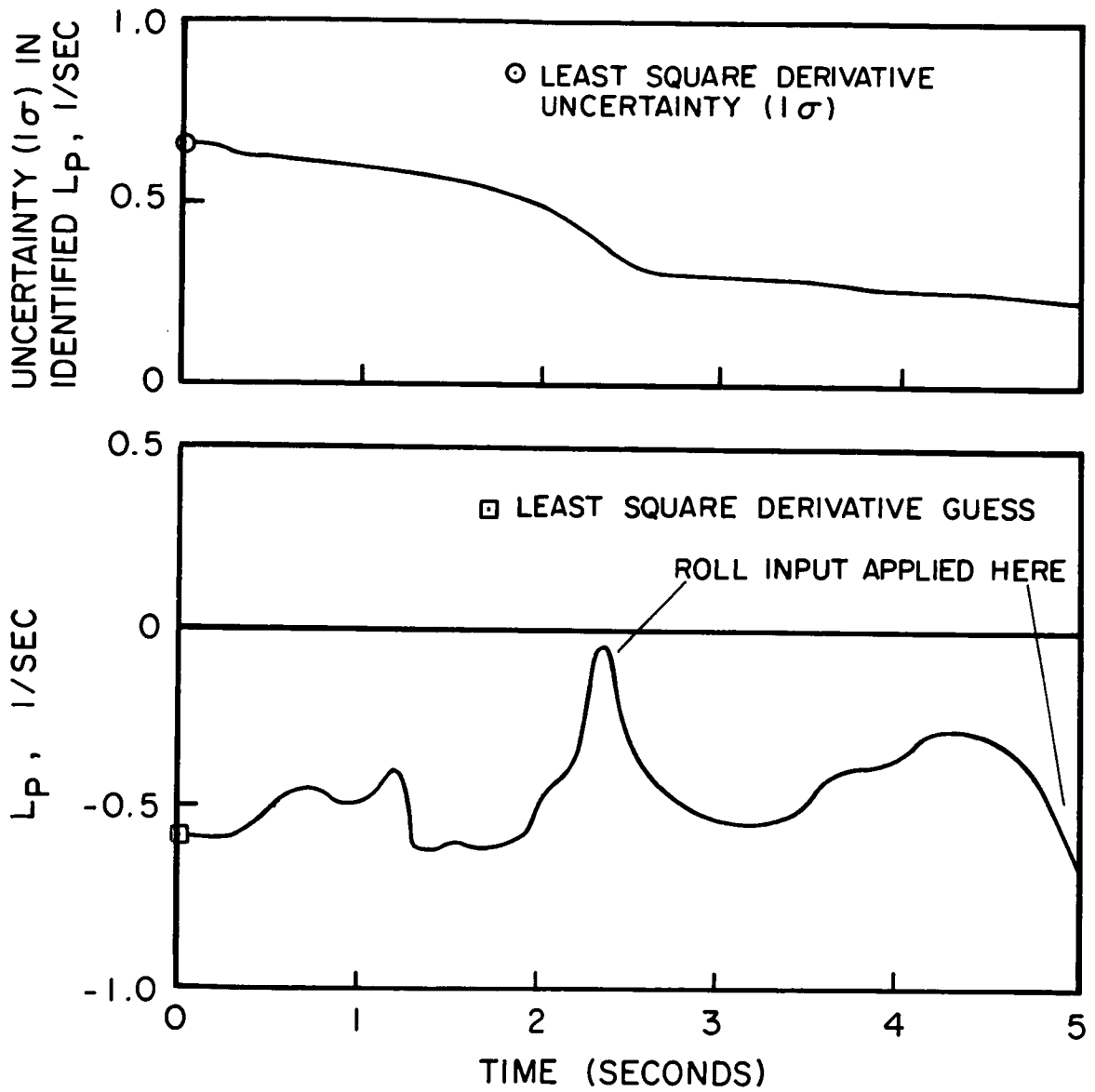

Figure 41. Roll Damping Derivative Convergence and Uncertainty From The MLE (Method 9) Showing Effect of Control Inputs On Convergence (From CH-53A, 150 Knots).

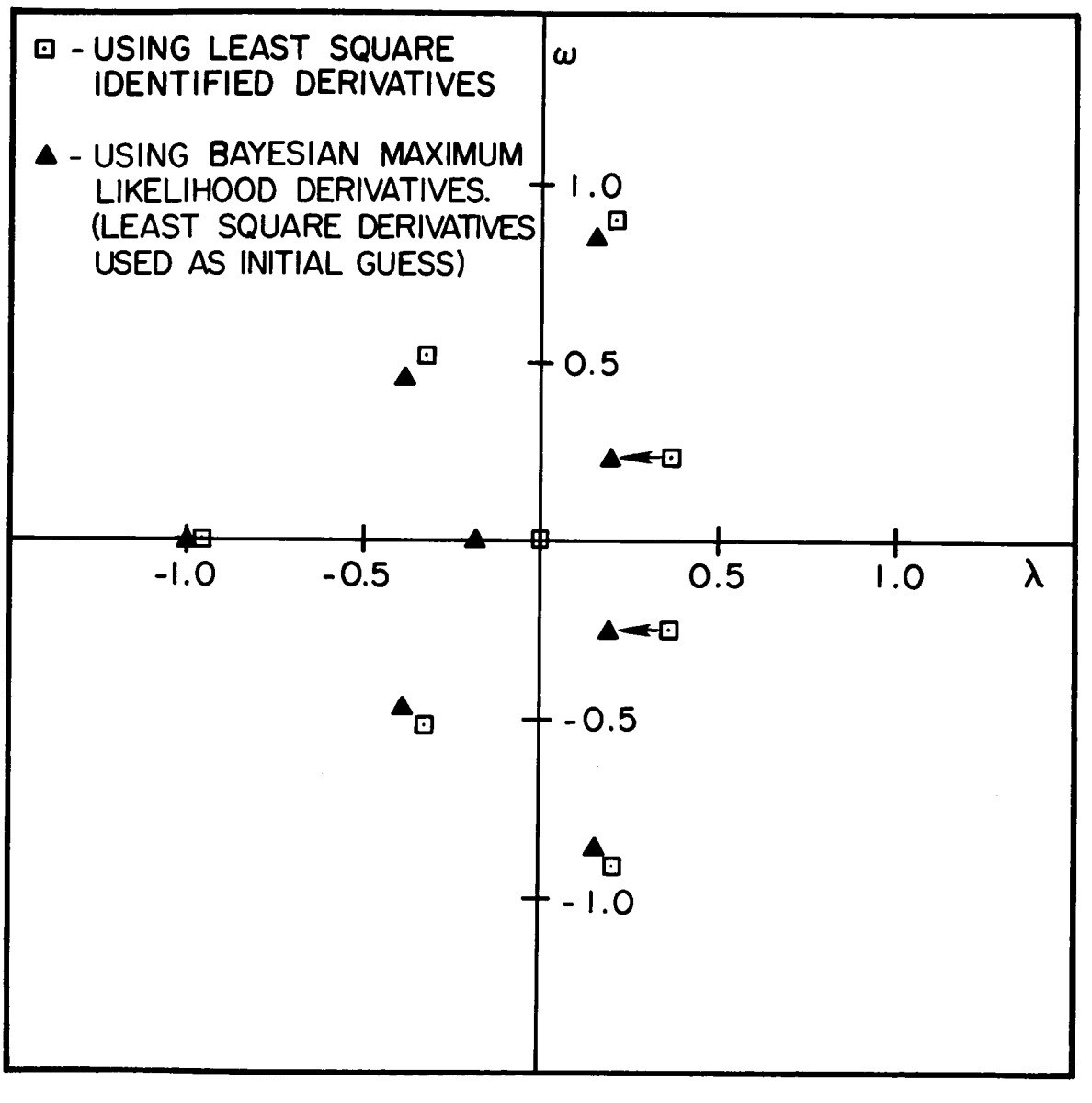

Figure 42. Characteristic Roots Obtained From The Identified Derivatives of The LSE (Method 3) and The MLE (Method 9) (From CH-53A Flight Data, 150 Knots, AFCS Off).

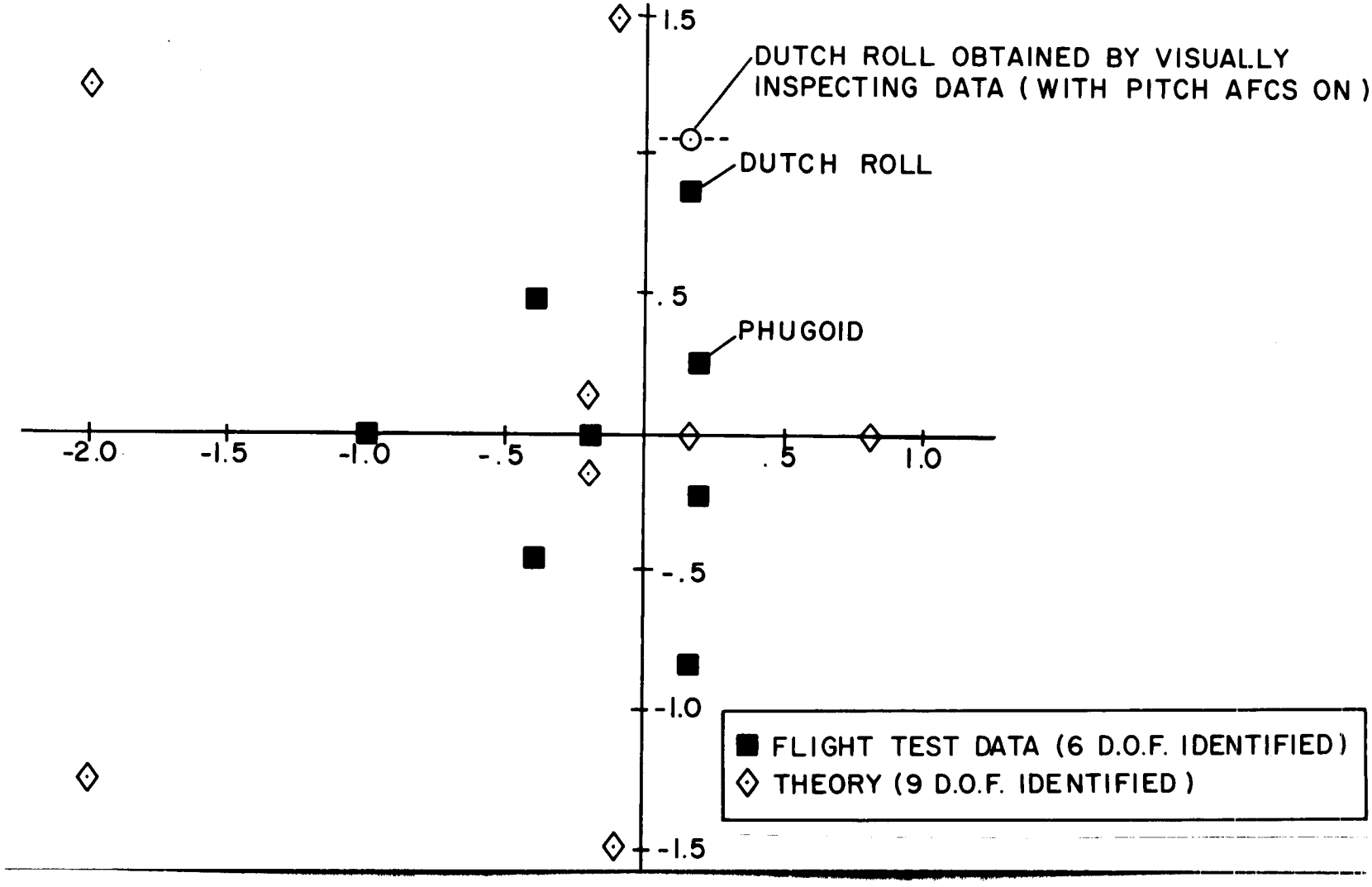

Figure 43. Comparison of Characteristic Roots Identified From Flight Data Vs. Analytic Computer Model Roots and Showing Unstable Dutch Roll Roots Obtained by Visually Inspecting Independent Test Data. (CH-53A, 150 Knots, AFCS Off).

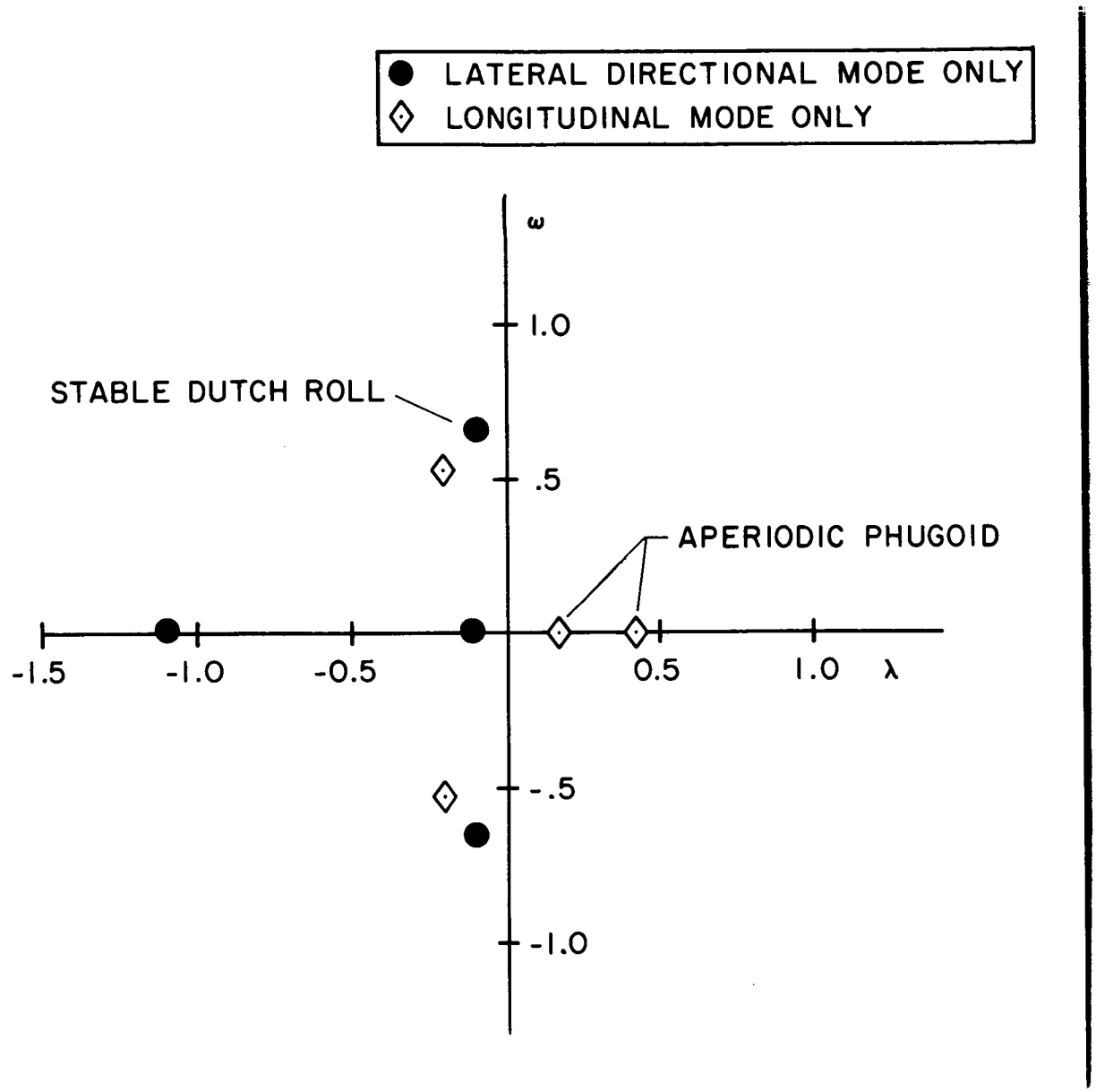

Figure 44. Characteristic Roots Obtained By Complete Decoupling of Longitudinal From the Lateral Identified Derivatives Showing That The Unstable Dutch Roll Roots are Caused By Longitudinal-to-Lateral Coupling. (From CH-53A Flight Data, 150 Knots, AFCS Off).

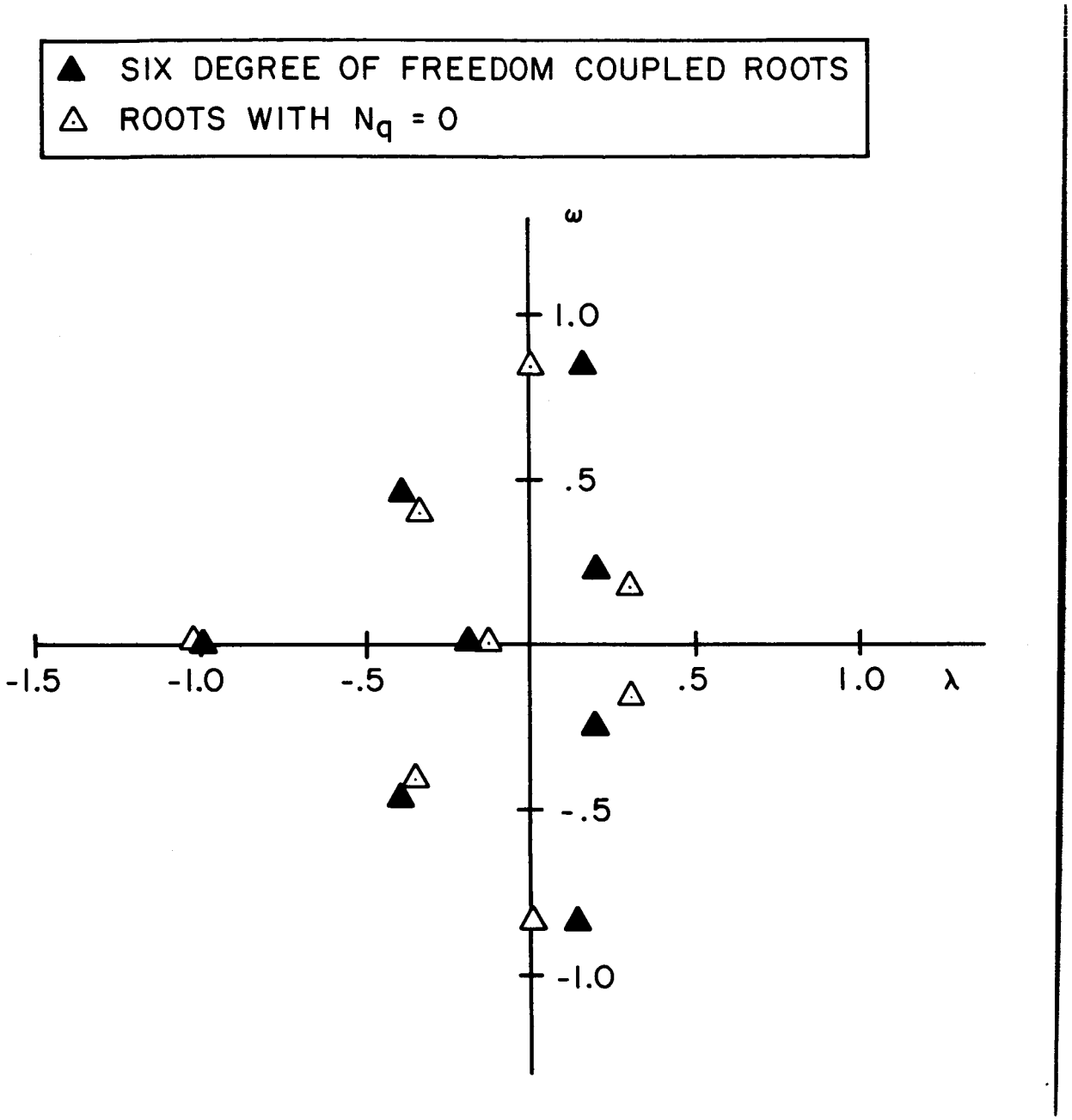

Figure 45. Characteristic Roots Obtained From The Full Identified Derivative Array Vs. Roots Obtained When the Derivative Nq is Set To Zero. Demonstrating the Destabilizing Effect of Nq. (From CH-53A Flight Data, 150 Knots, AFCS Off).

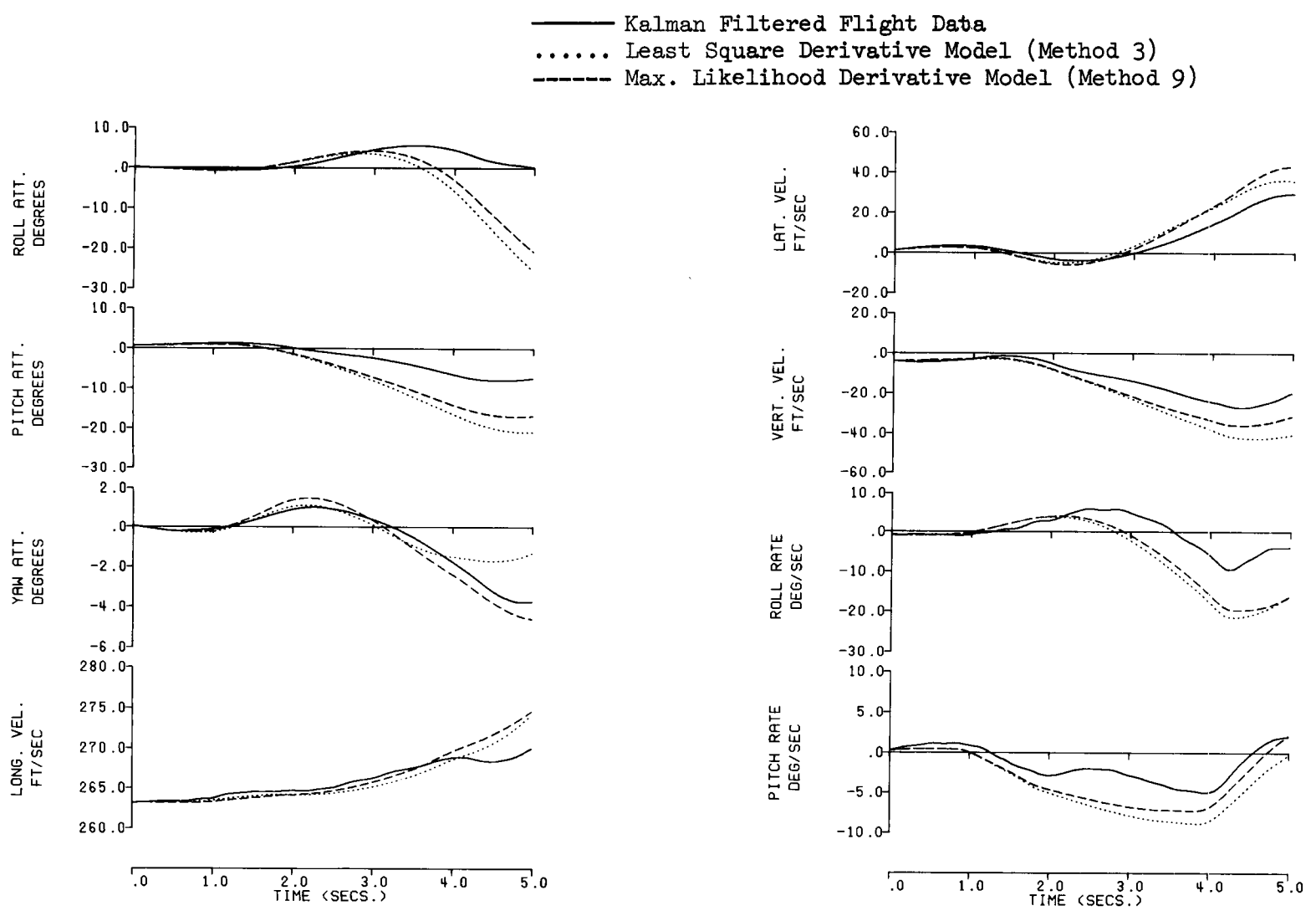

Figure 46. - Time History Comparison of Identified Derivative Models Against CH-53A Flight Data (150 knots, Maneuver 1).

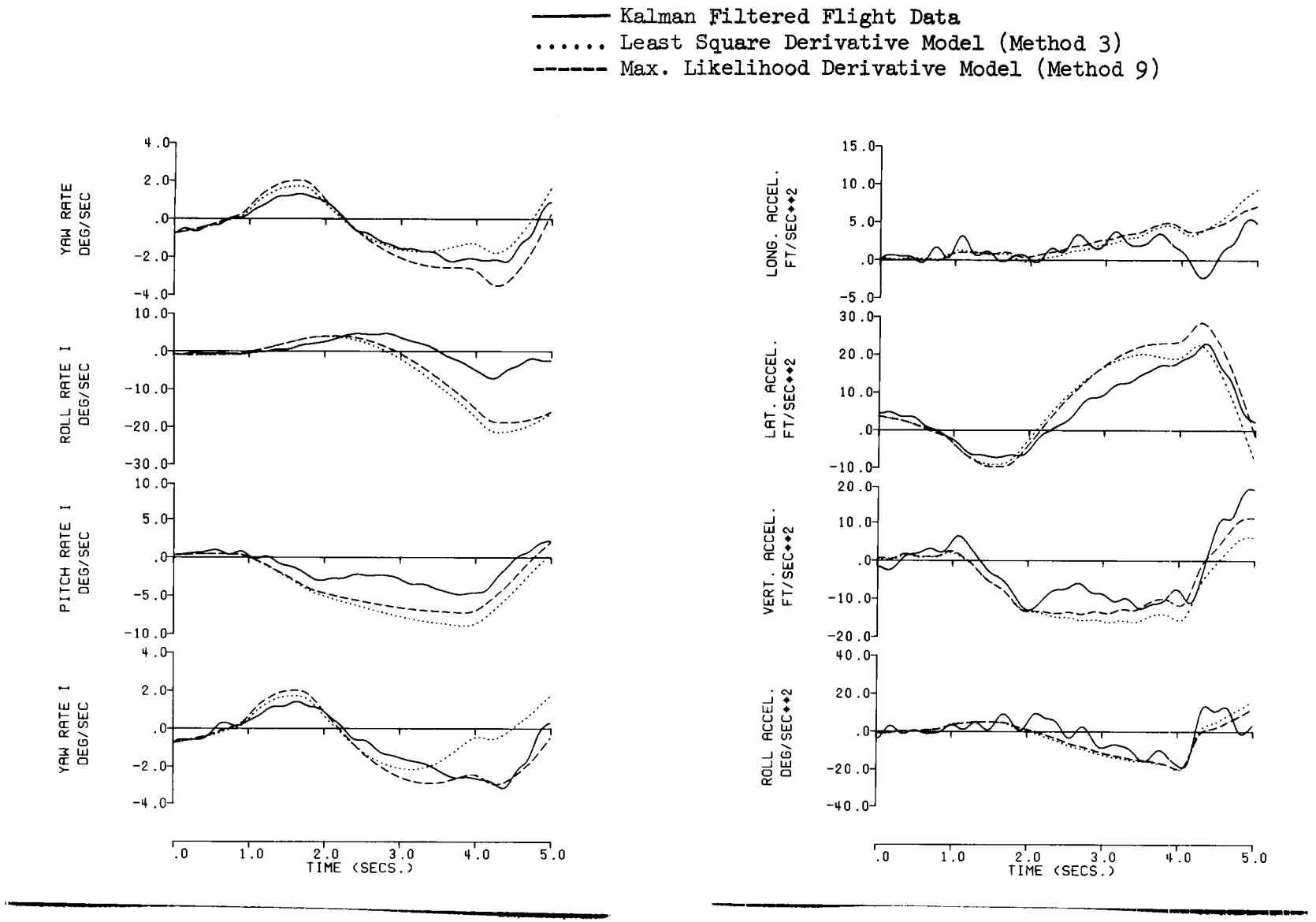

Figure 46. - Continued.

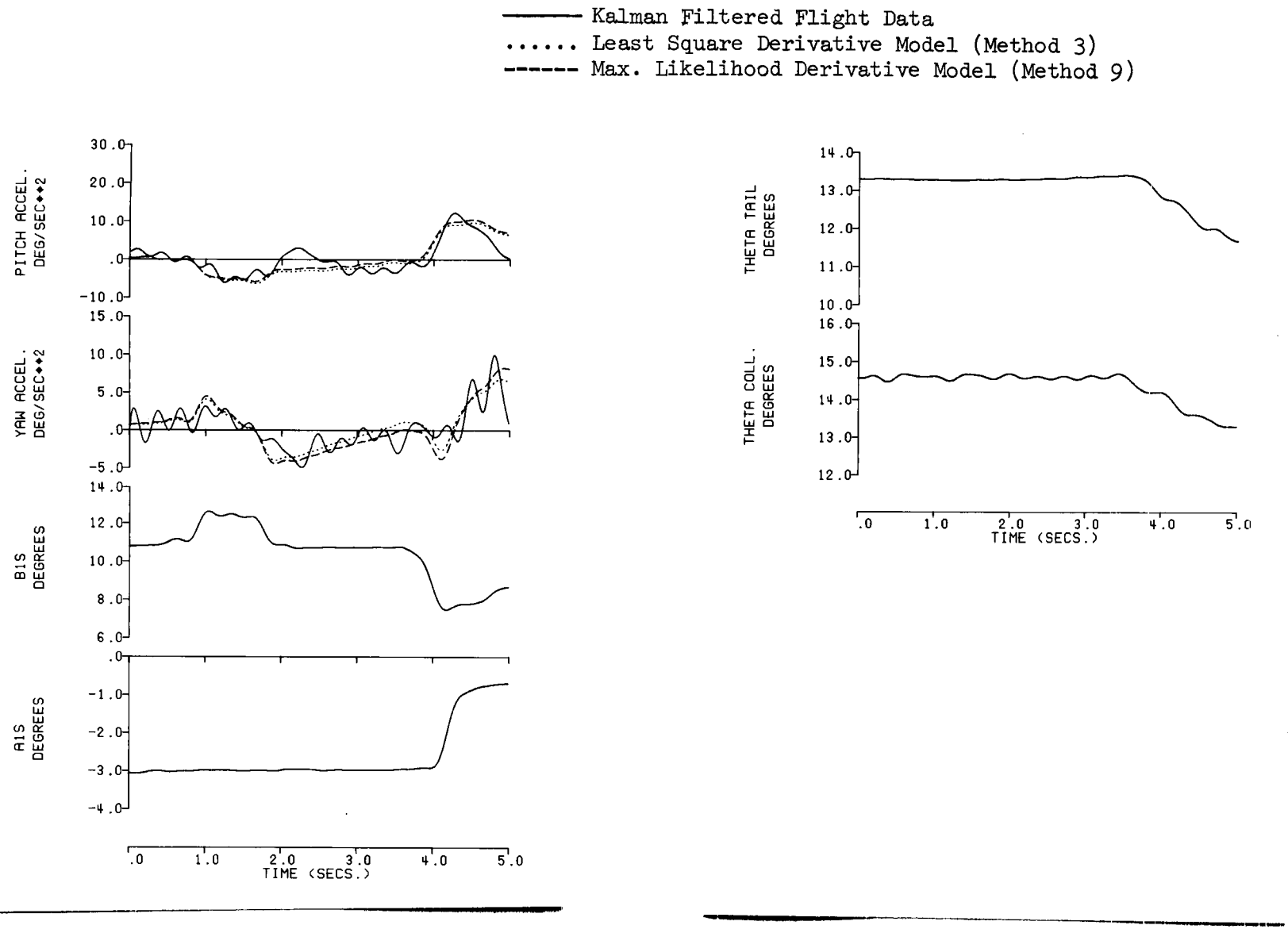

Figure 46. - Concluded.

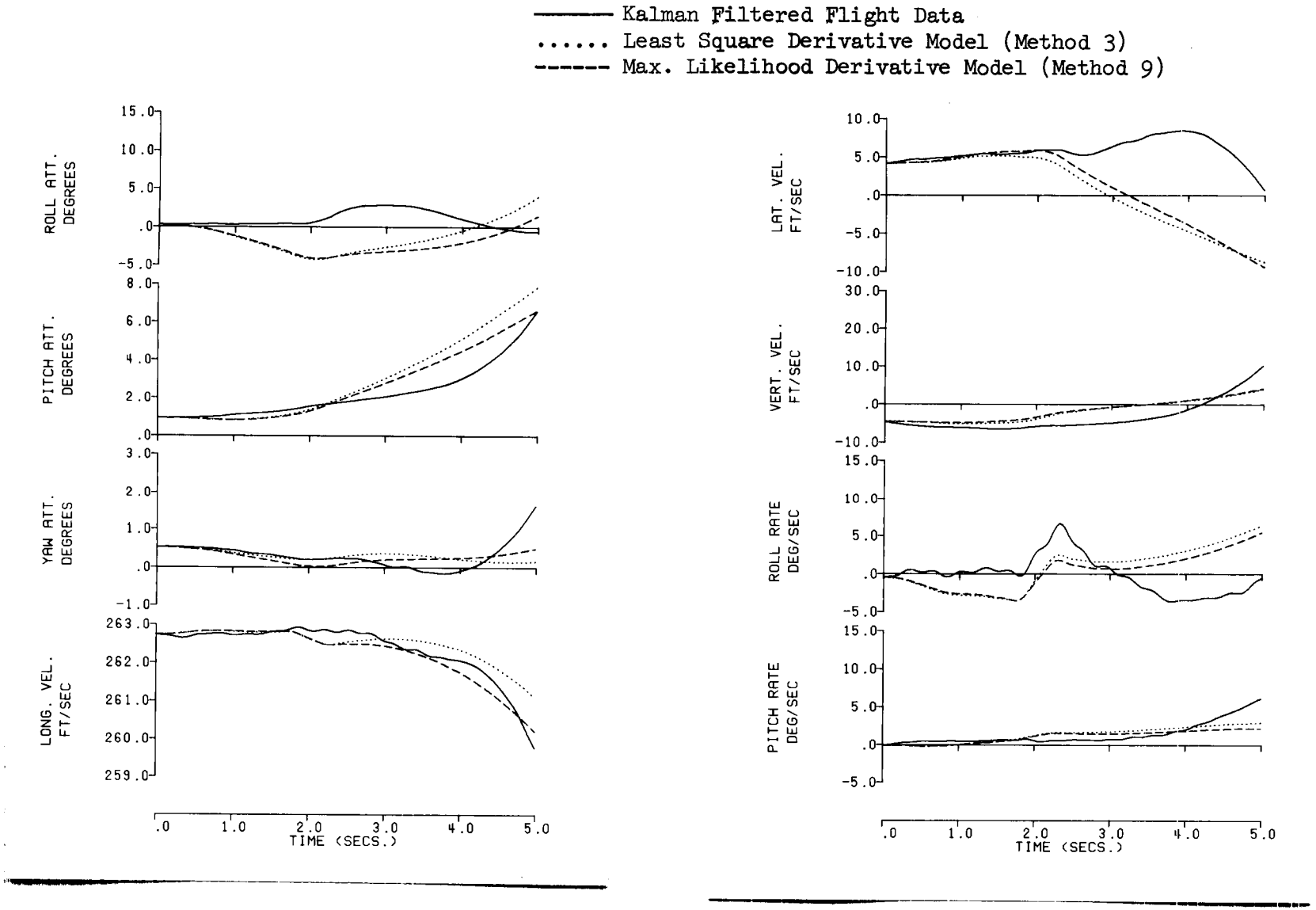

Figure 47. - Time History Comparison of Identified Derivative Models Against CH-53A Flight Data (150 knots, Maneuver 2).

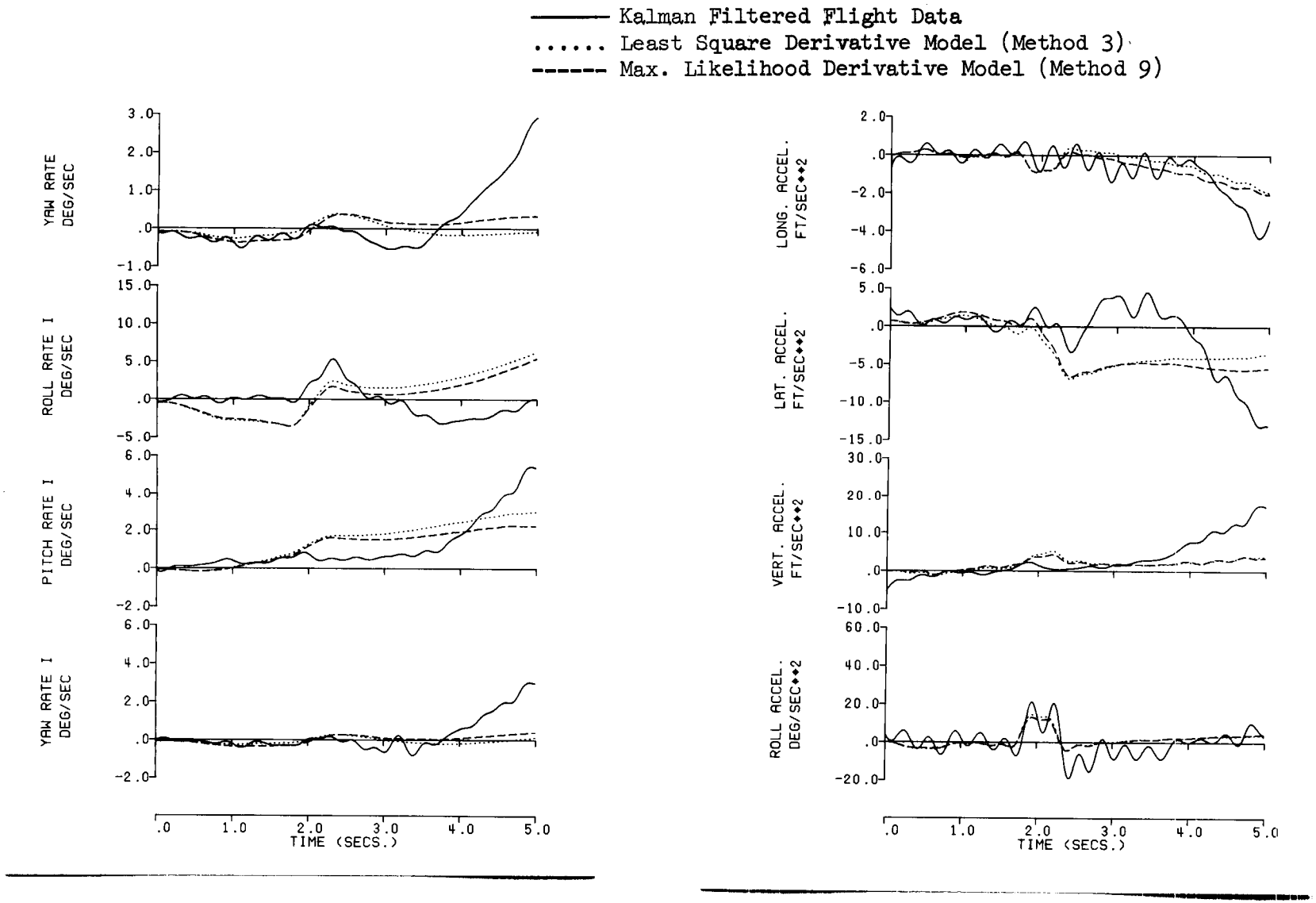

Figure 47. - Continued.

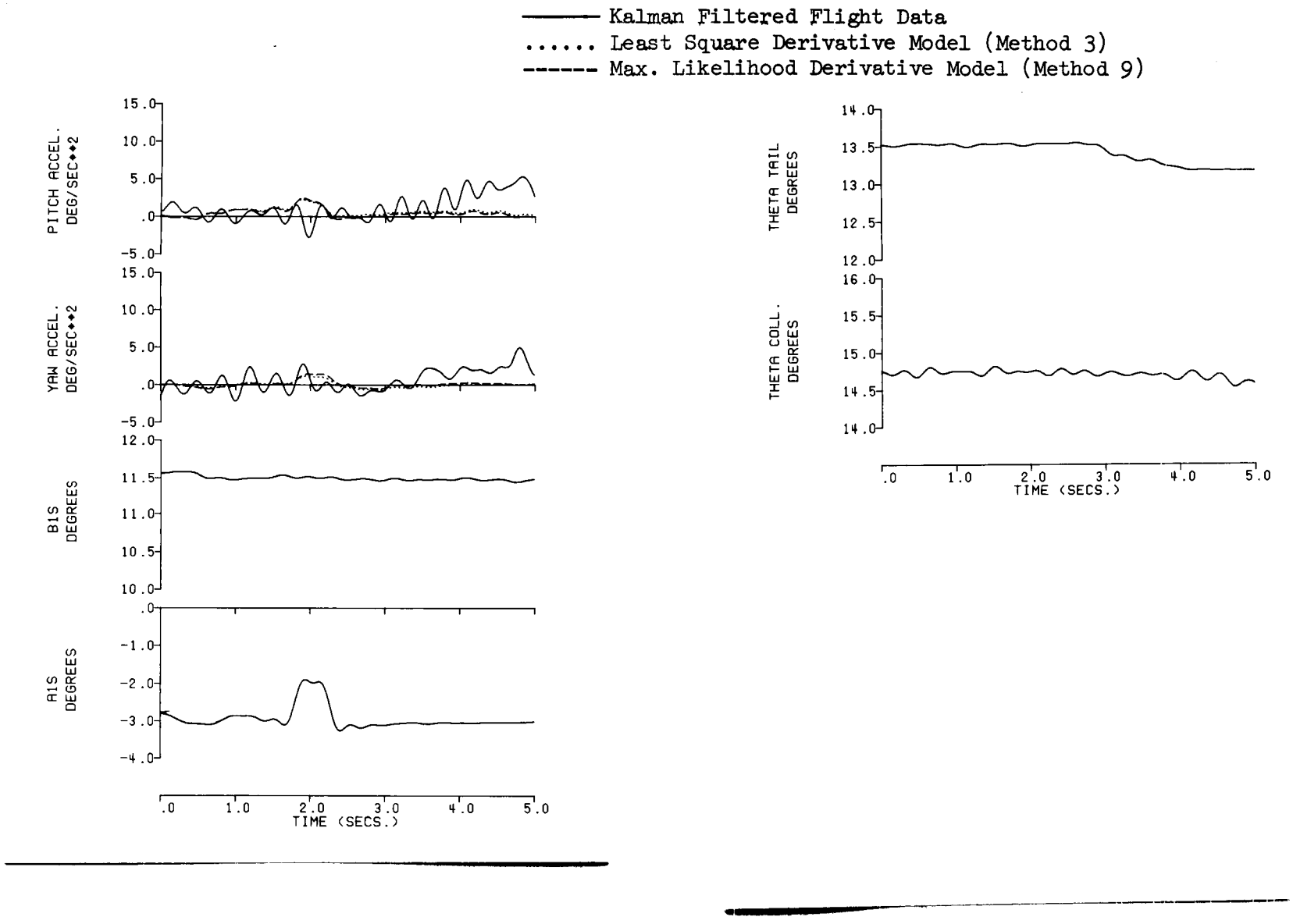

Figure 47. - Concluded.

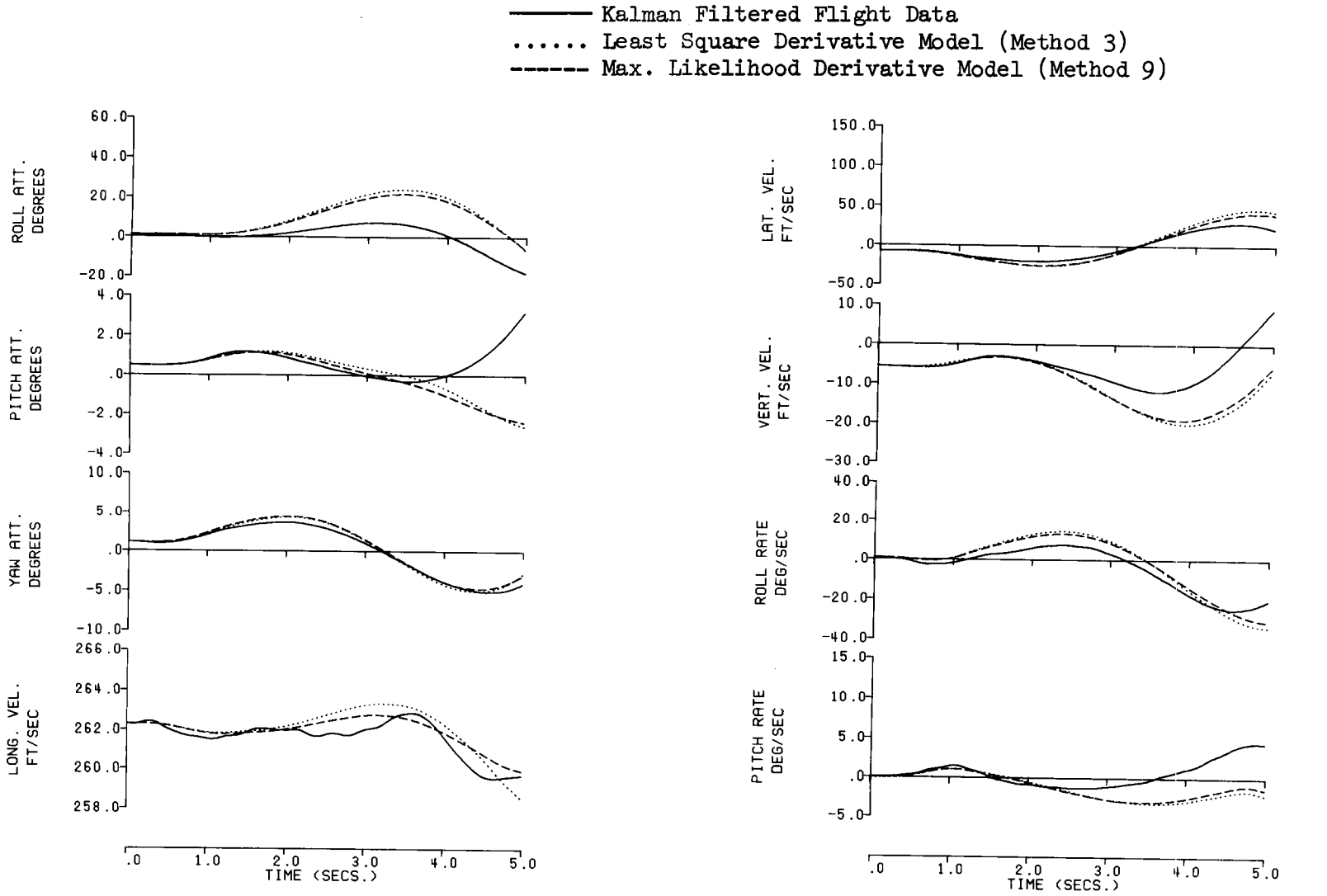

Figure 48. - Time History Comparison of Identified Derivative Models Against CH-53A Flight Data (150 knots, Maneuver 3).

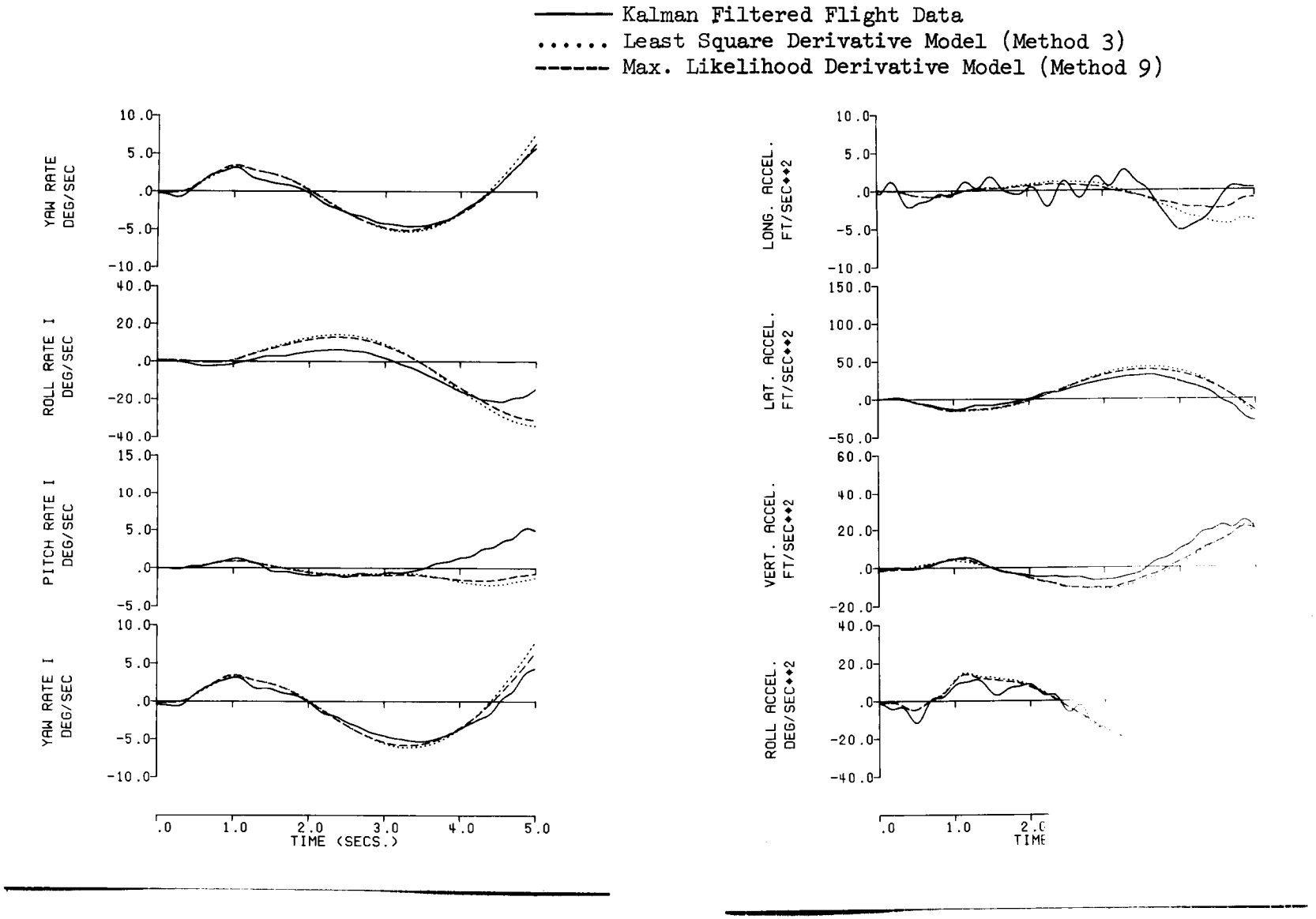

Figure 48. - Continued.

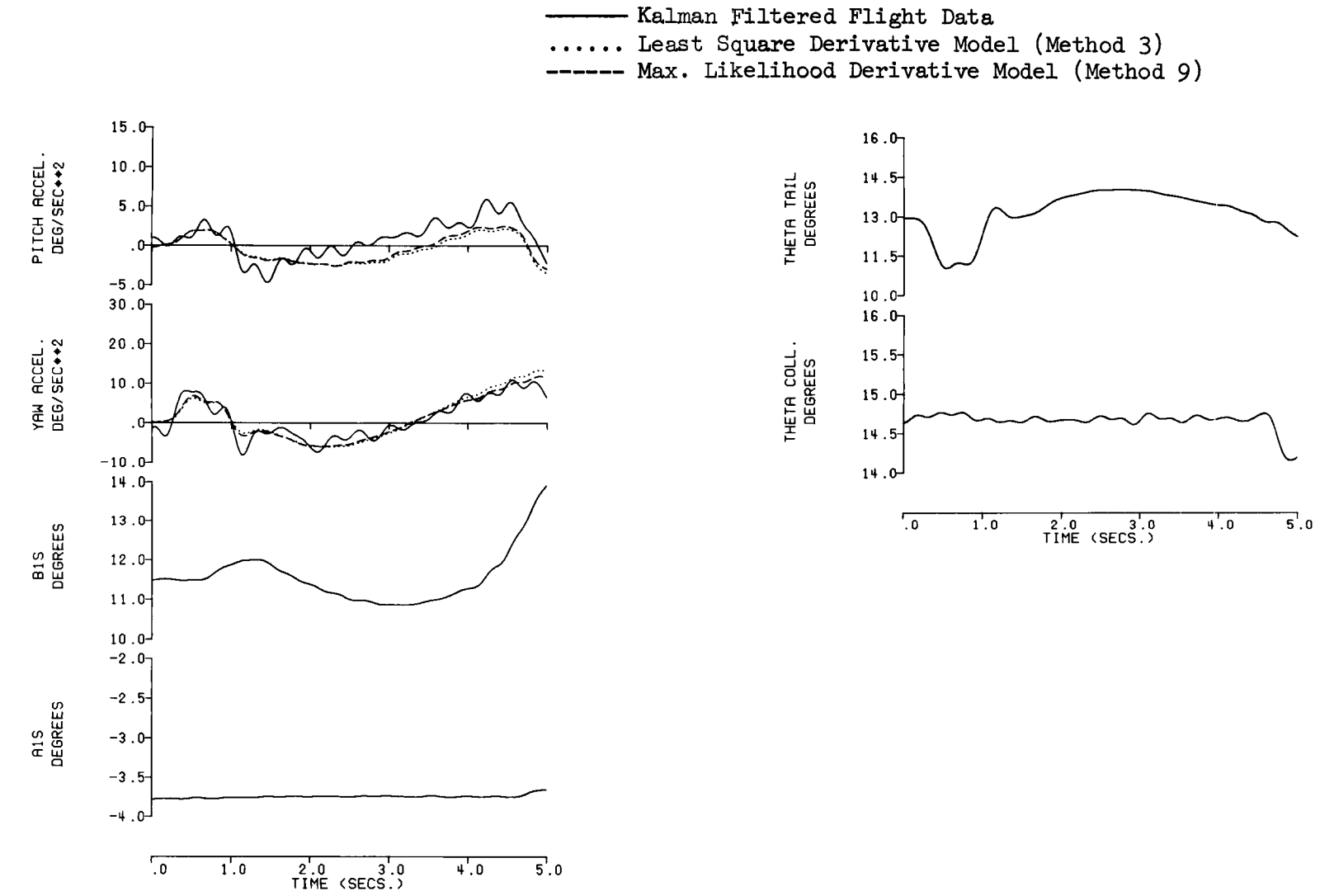

Figure 48. - Concluded.

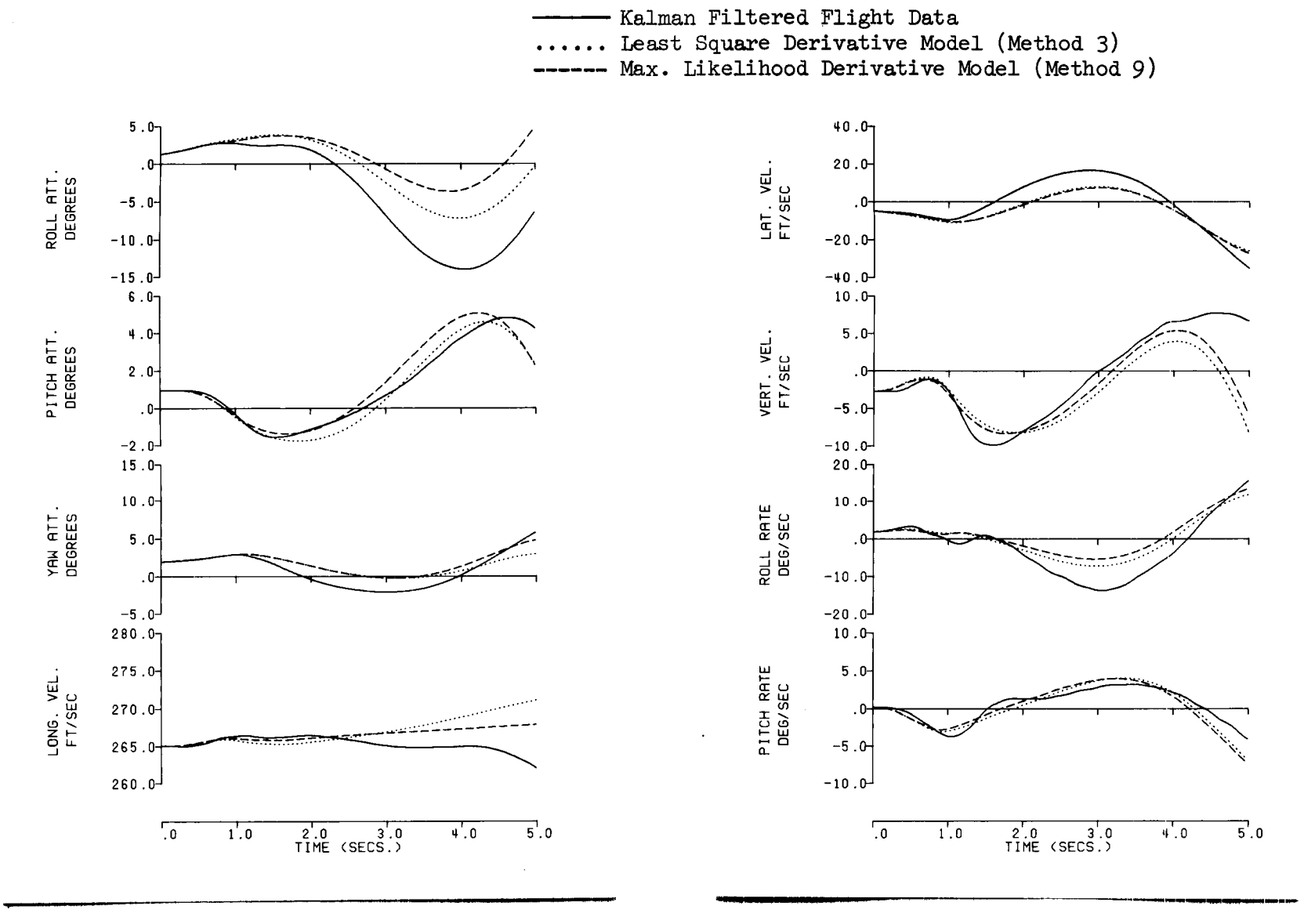

Figure 49. - Time History Comparison of Identified Derivative Models Against CH-53A Flight Data (150 knots, Maneuver 4).

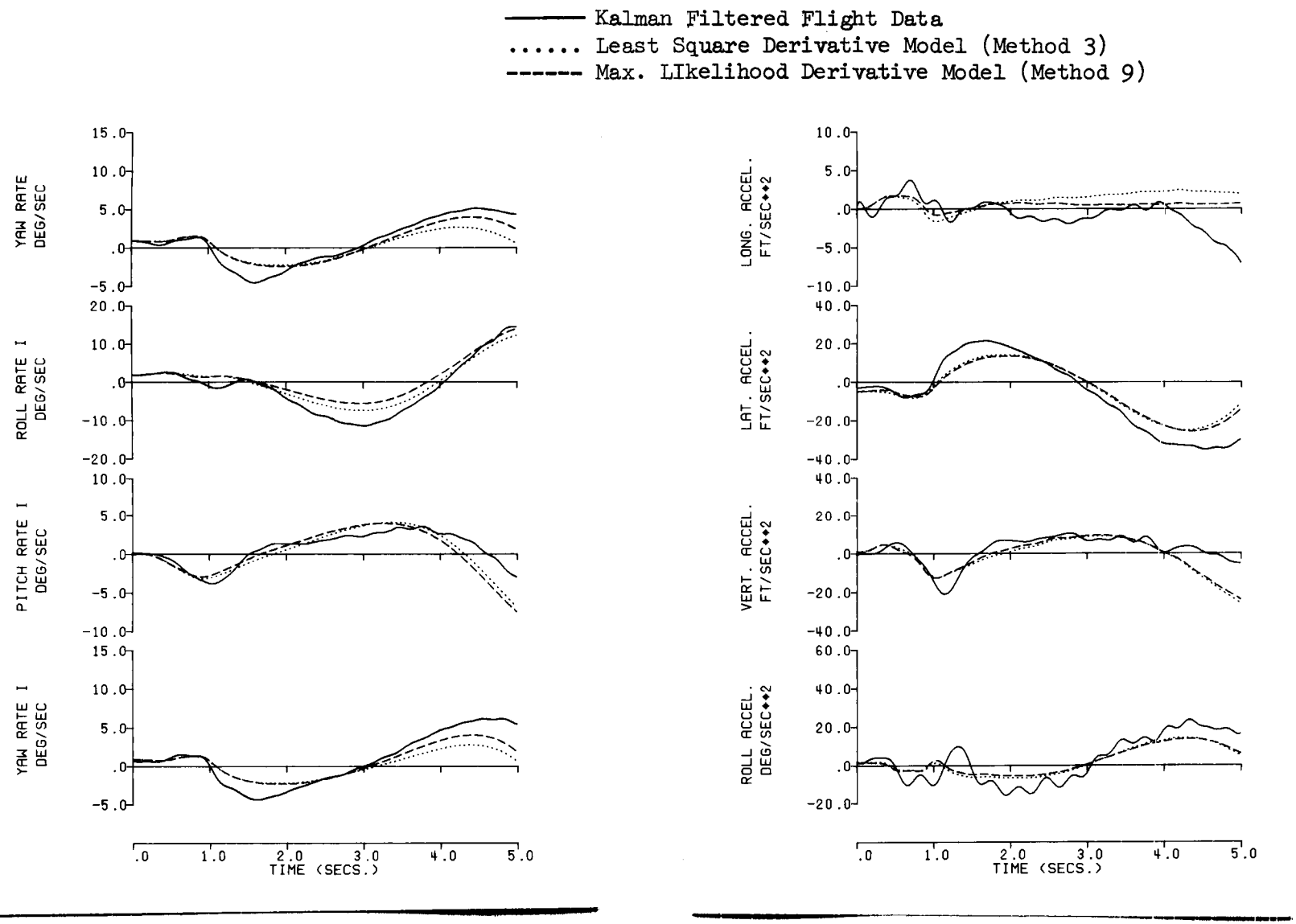

Figure 49. - Continued.

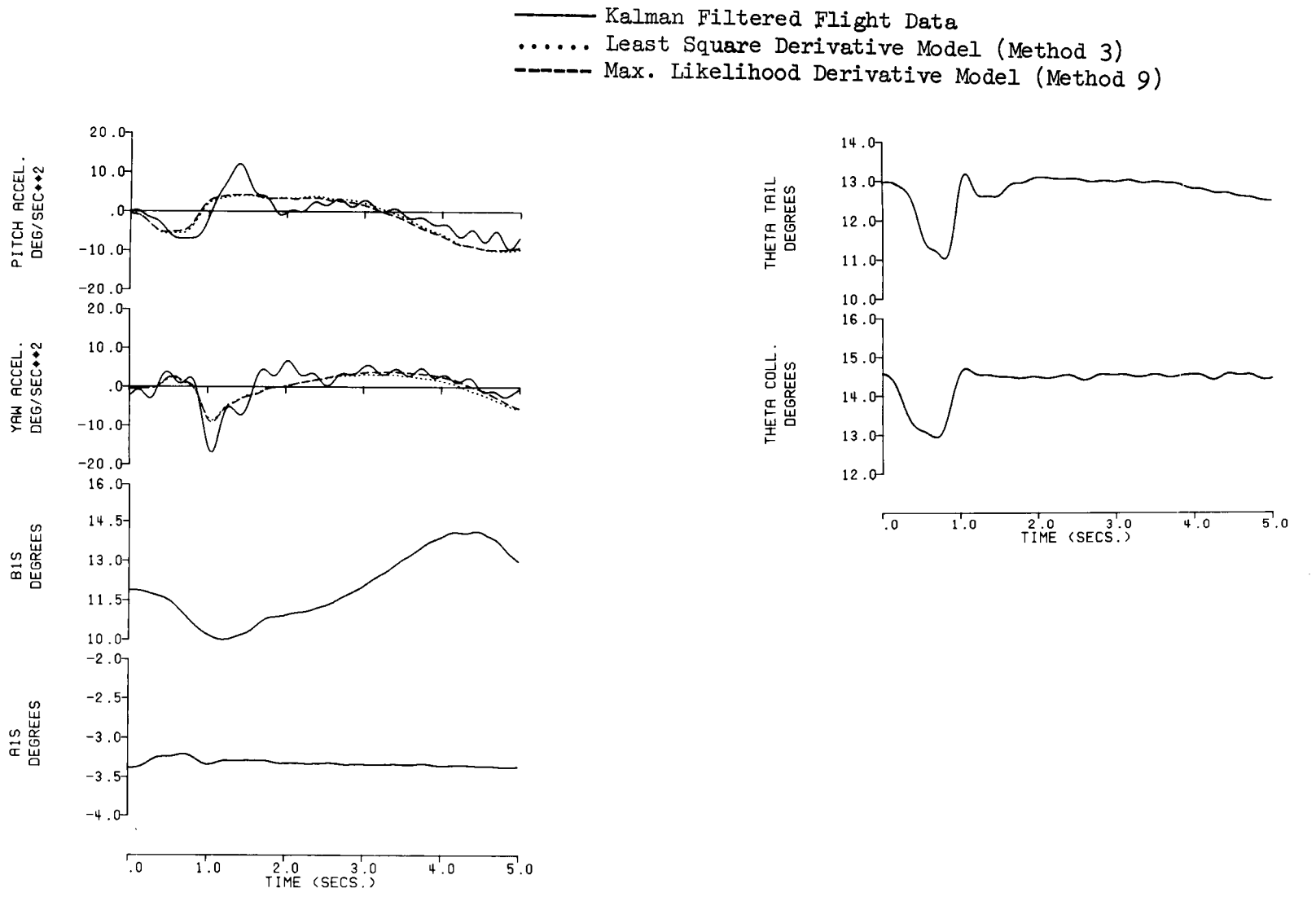

Figure 49. - Concluded.

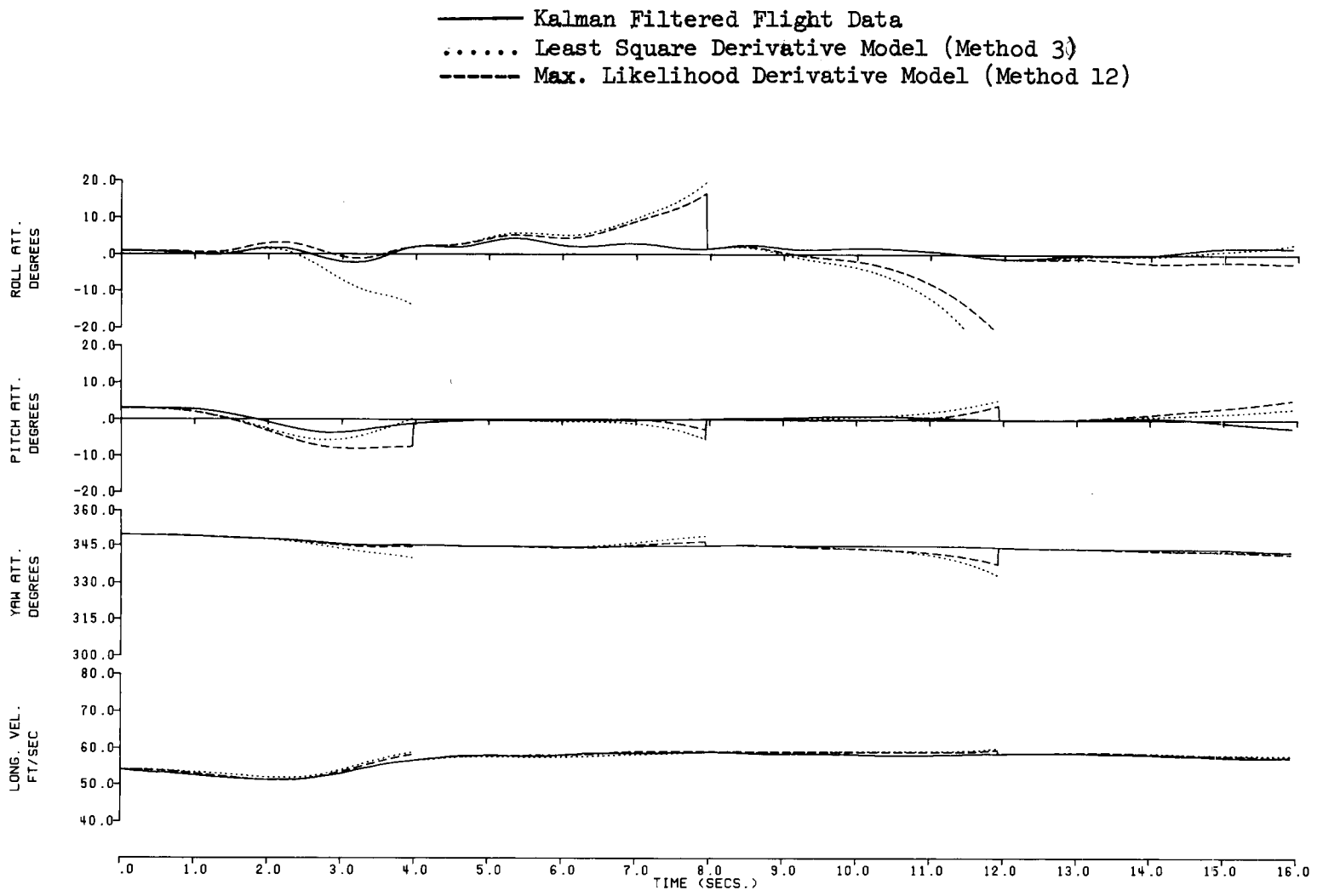

Figure 50. - Time History Comparison of Identified Derivative Models Against CH-54B Flight Data (45 knots, 16 sec. Maneuver).

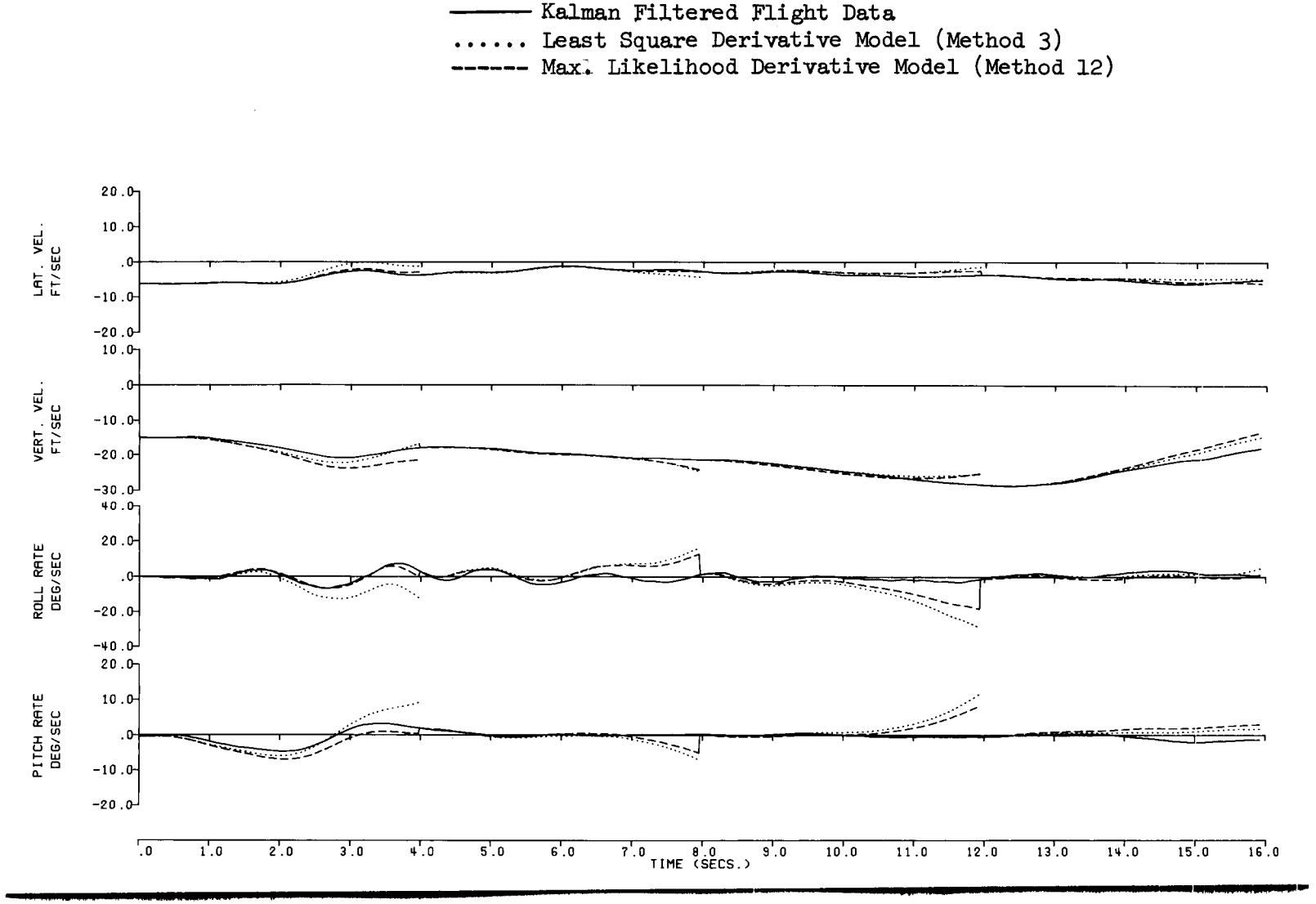

Figure 50. - Continued.

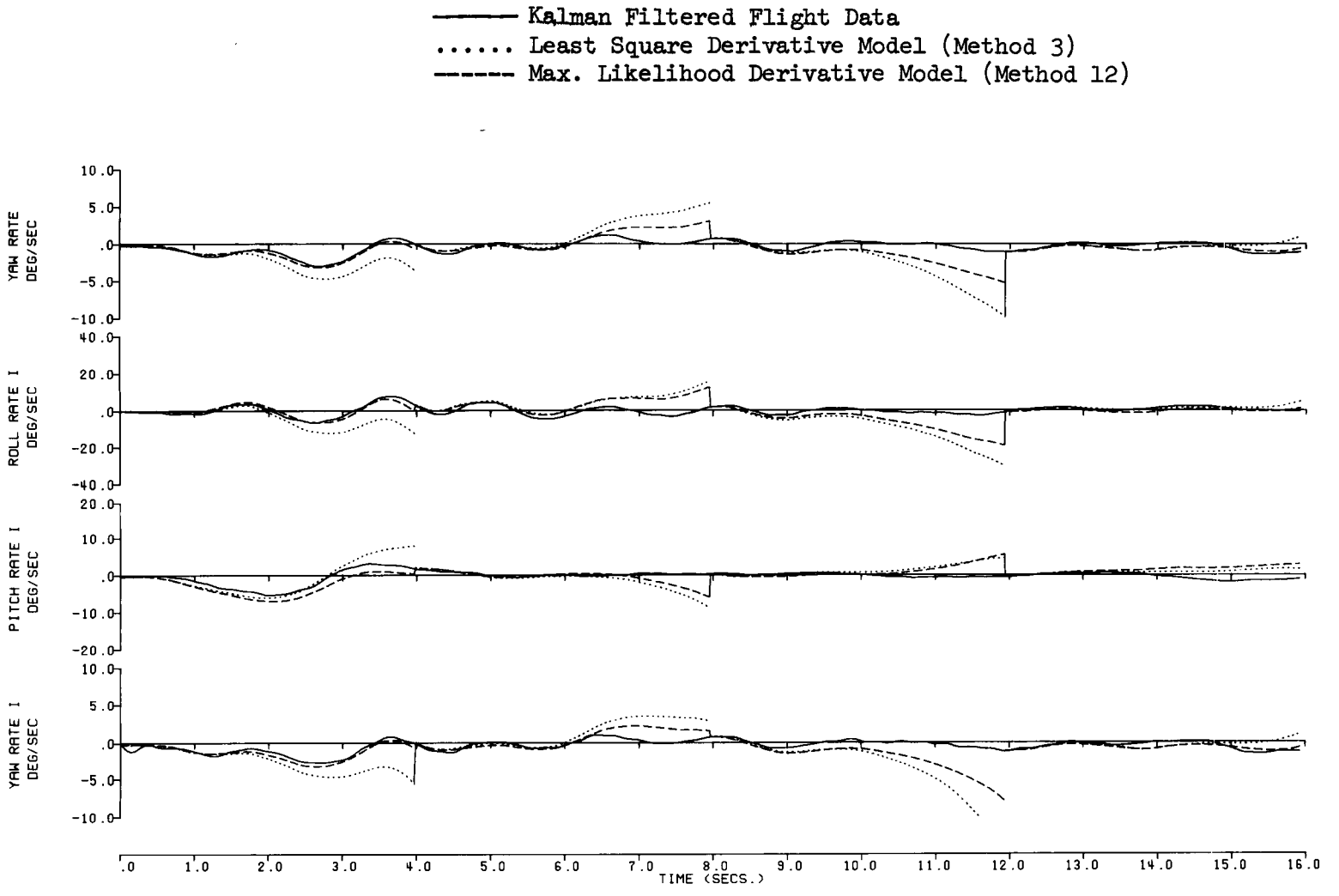

Figure 50. - Continued.

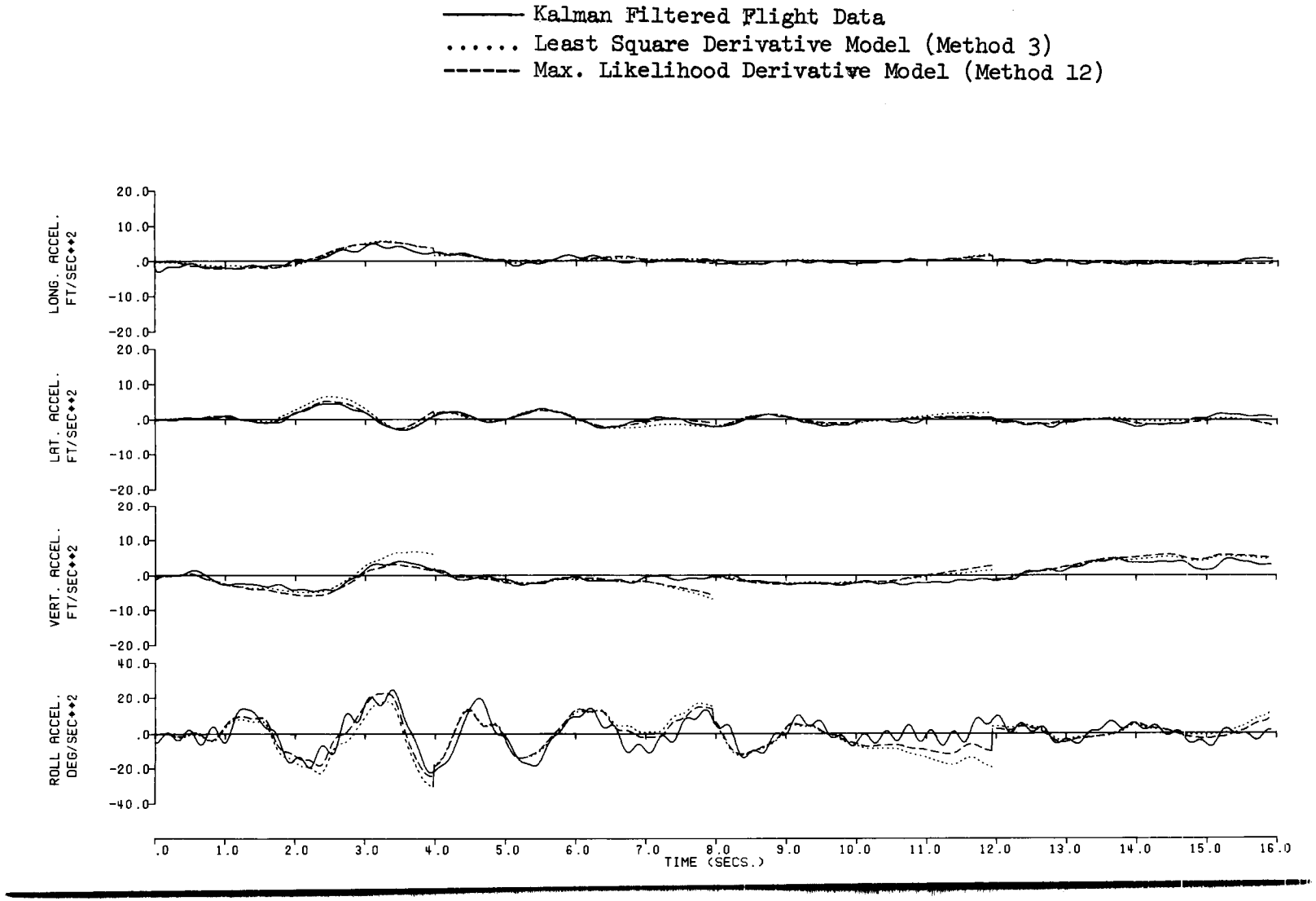

Figure 50. - Continued.

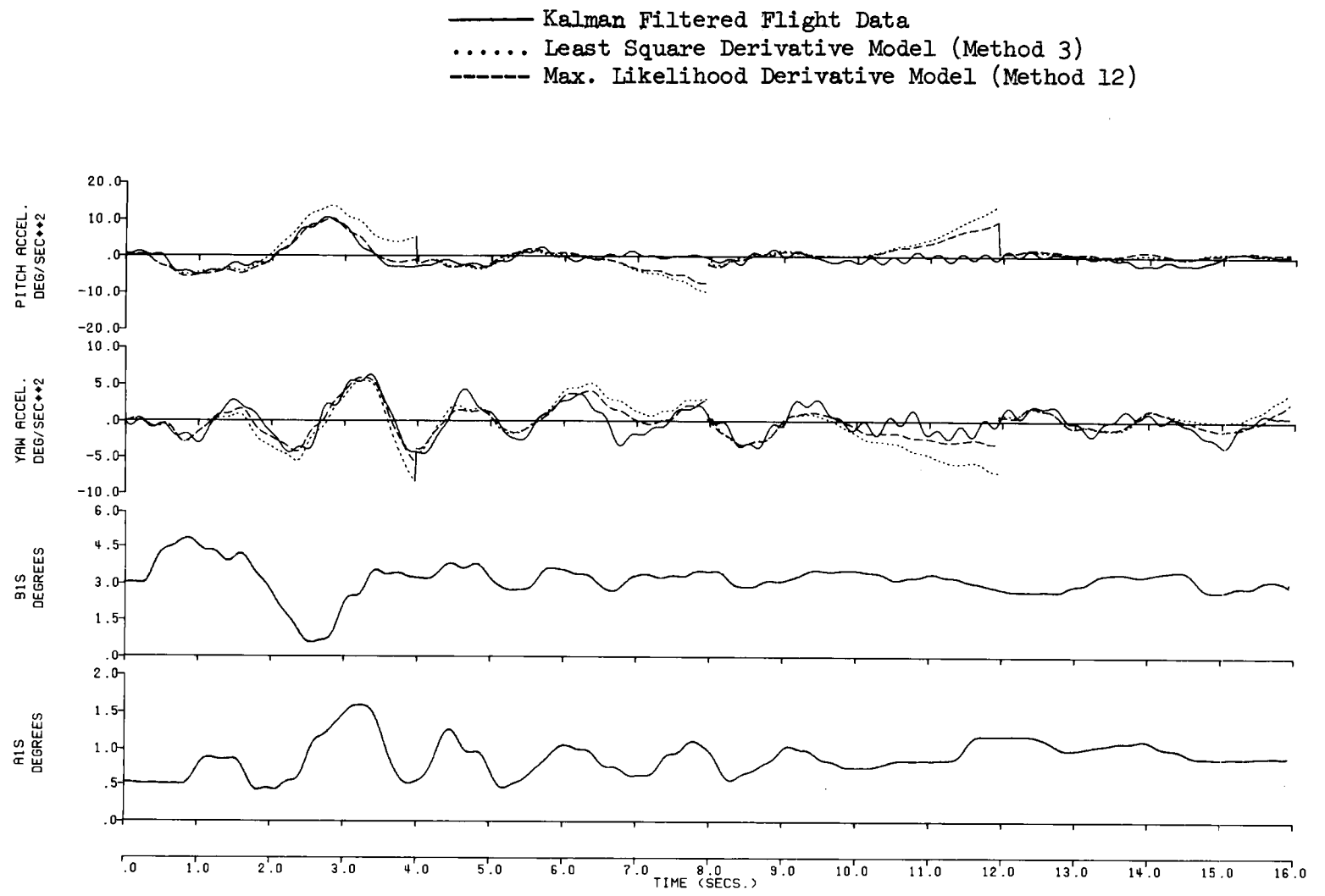

Figure 50. - Continued.

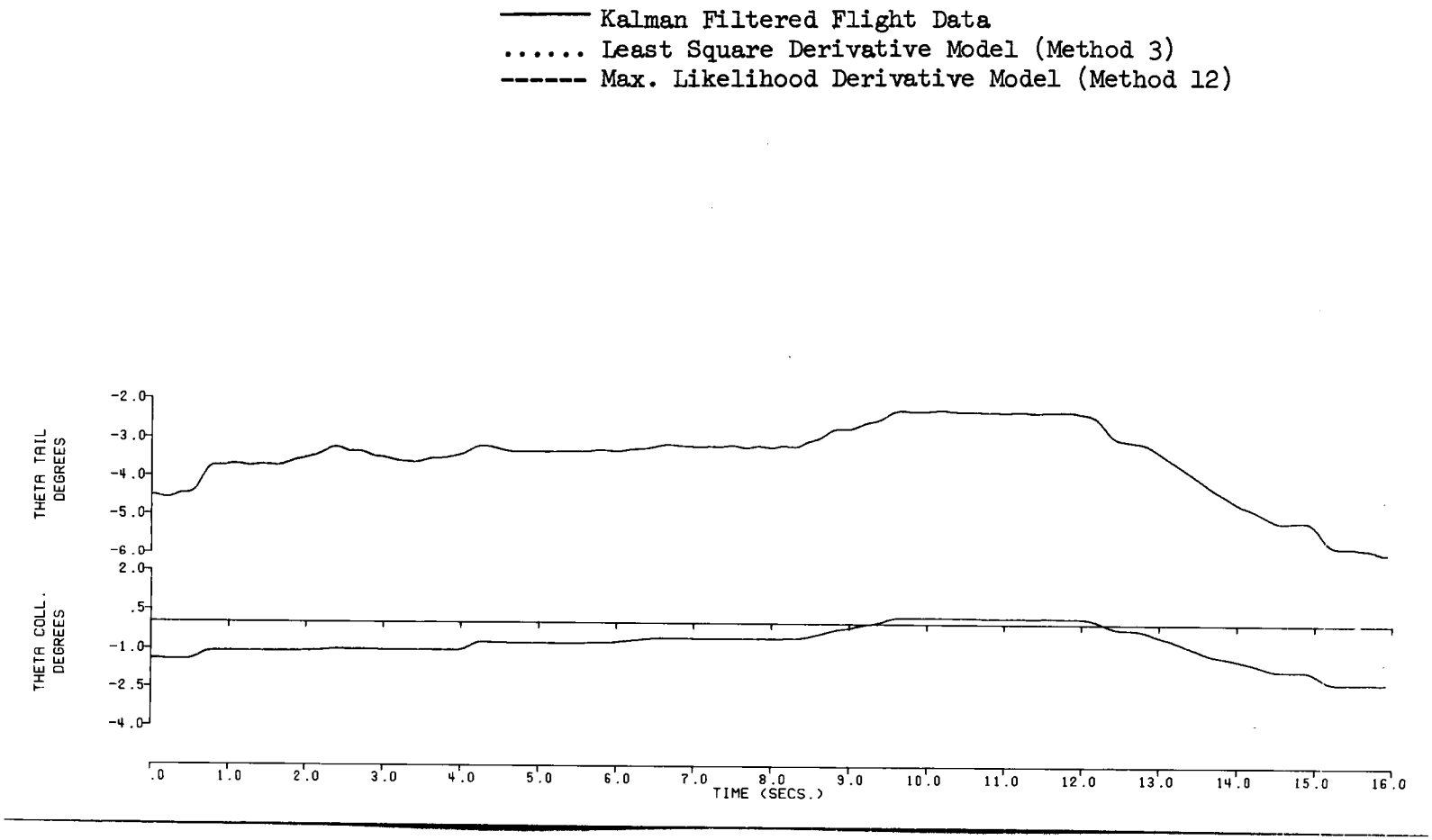

Figure 50. - Concluded.

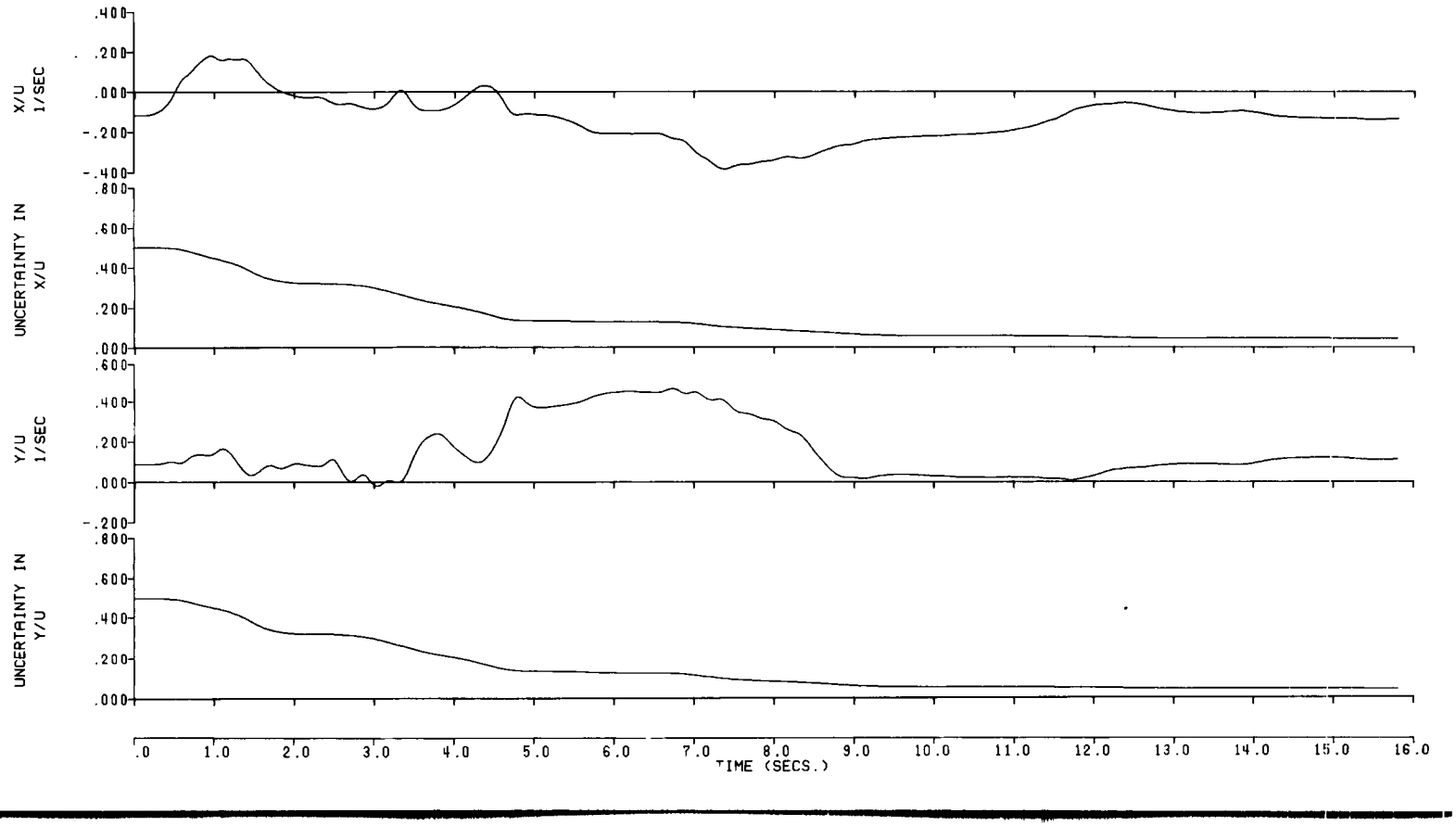

Figure 51. - Stability Derivative Convergence and 1 Sigma Uncertainty for CH-54B using Method 12. (16 sec. Maneuver)

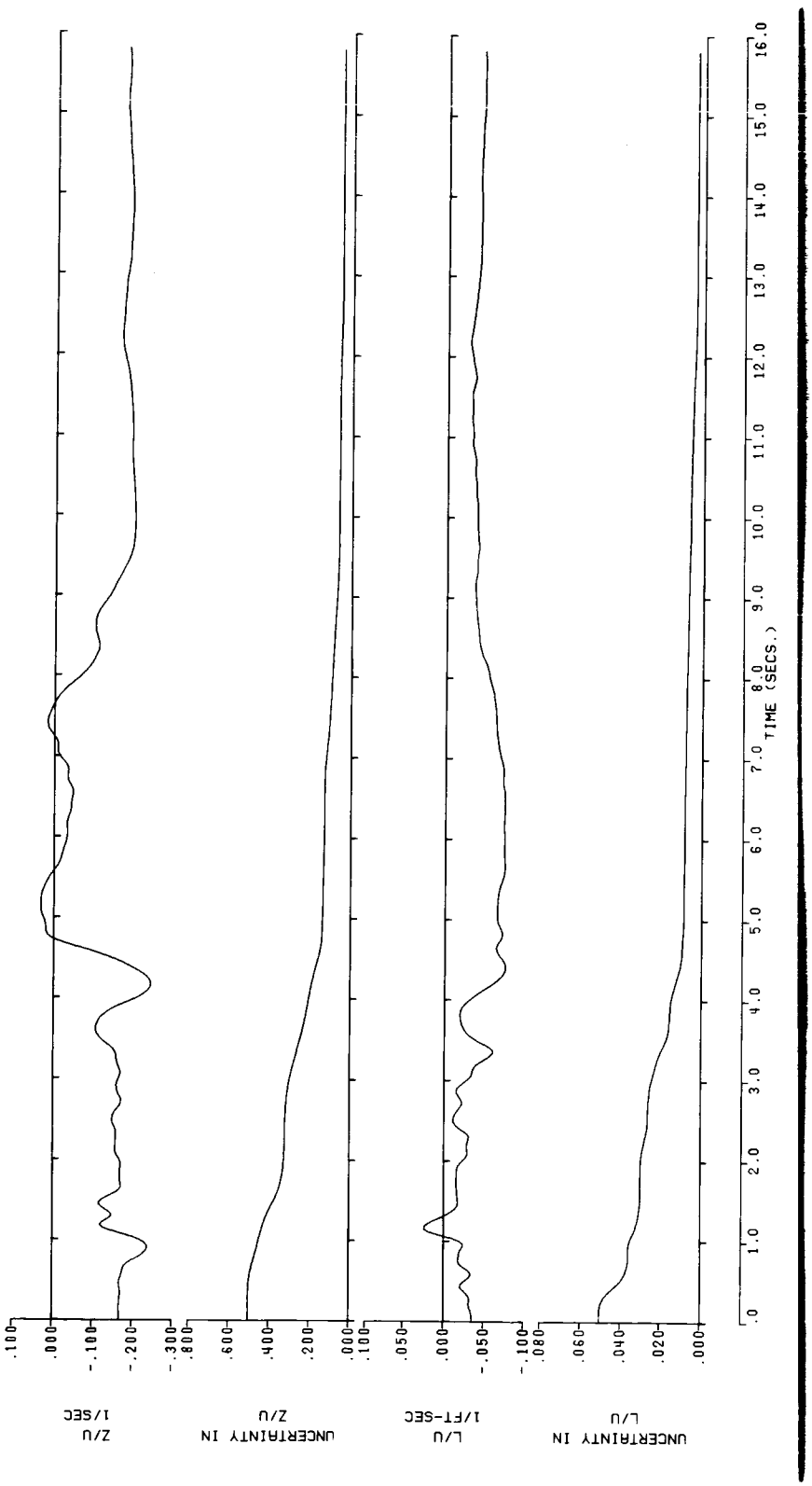

Figure 51. - Continued.

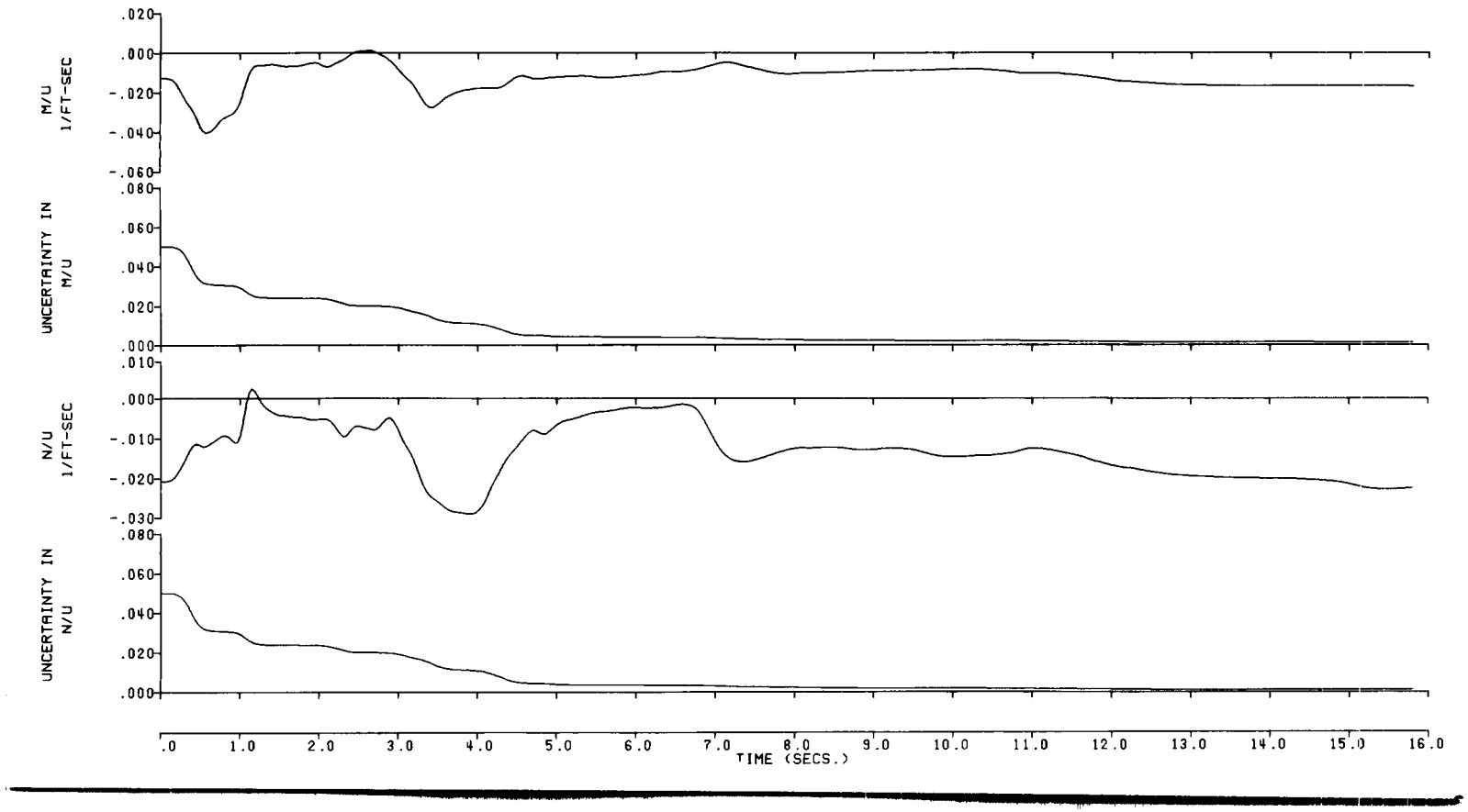

Figure 51. - Continued.

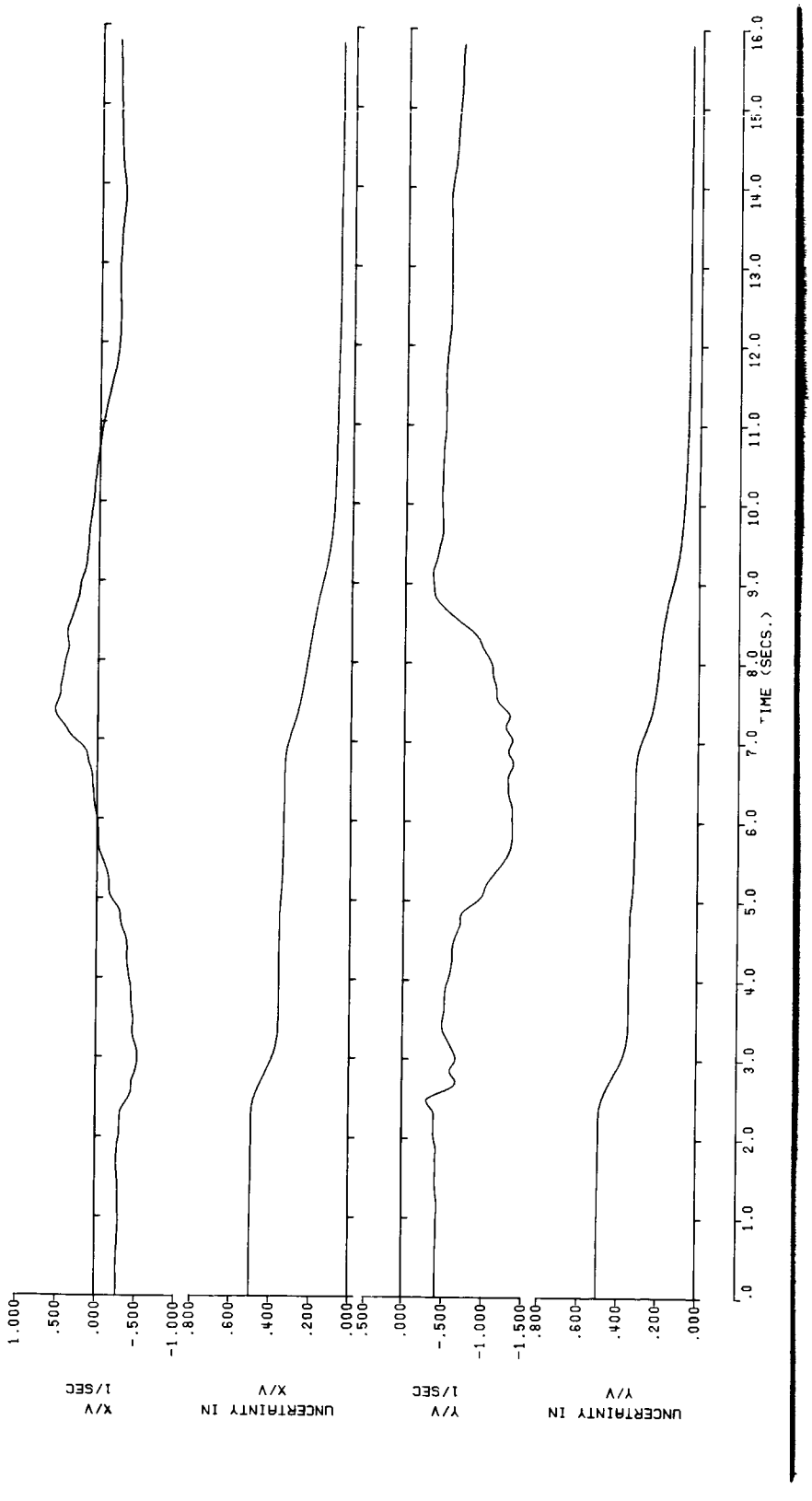

Figure 51. - Continued.

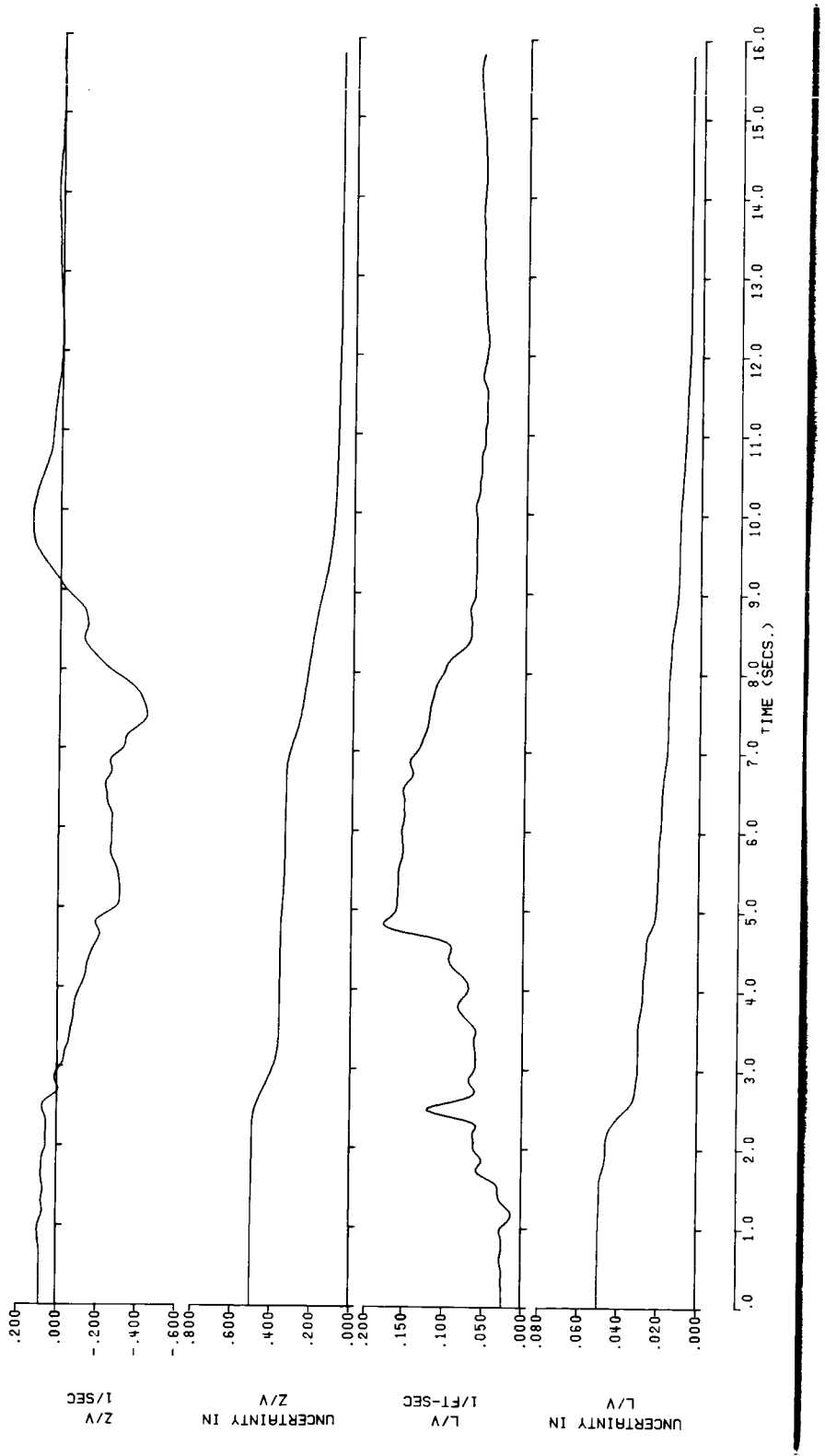

Figure 51. - Continued.

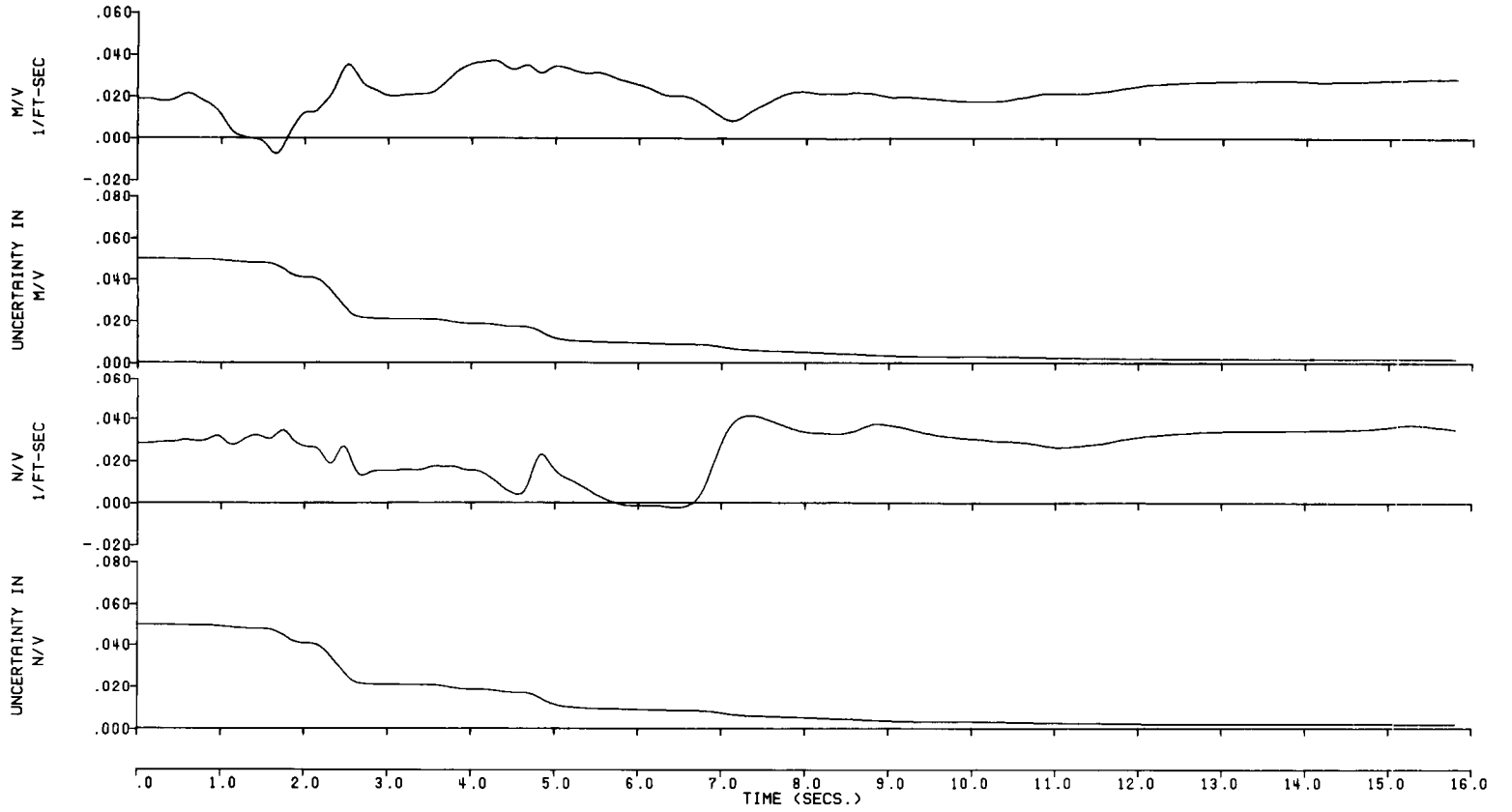

Figure 51. - Continued.

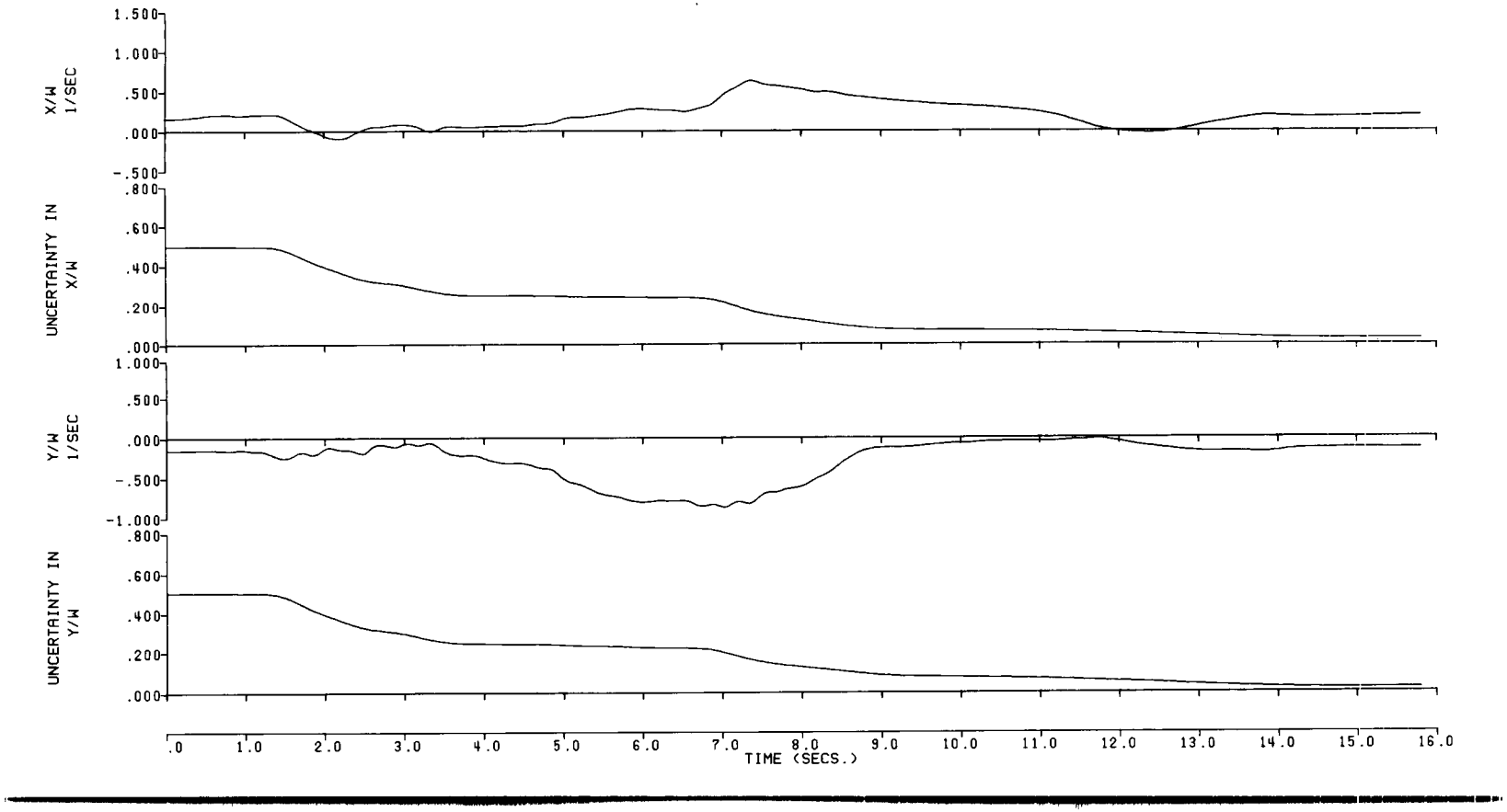

Figure 51. - Continued.

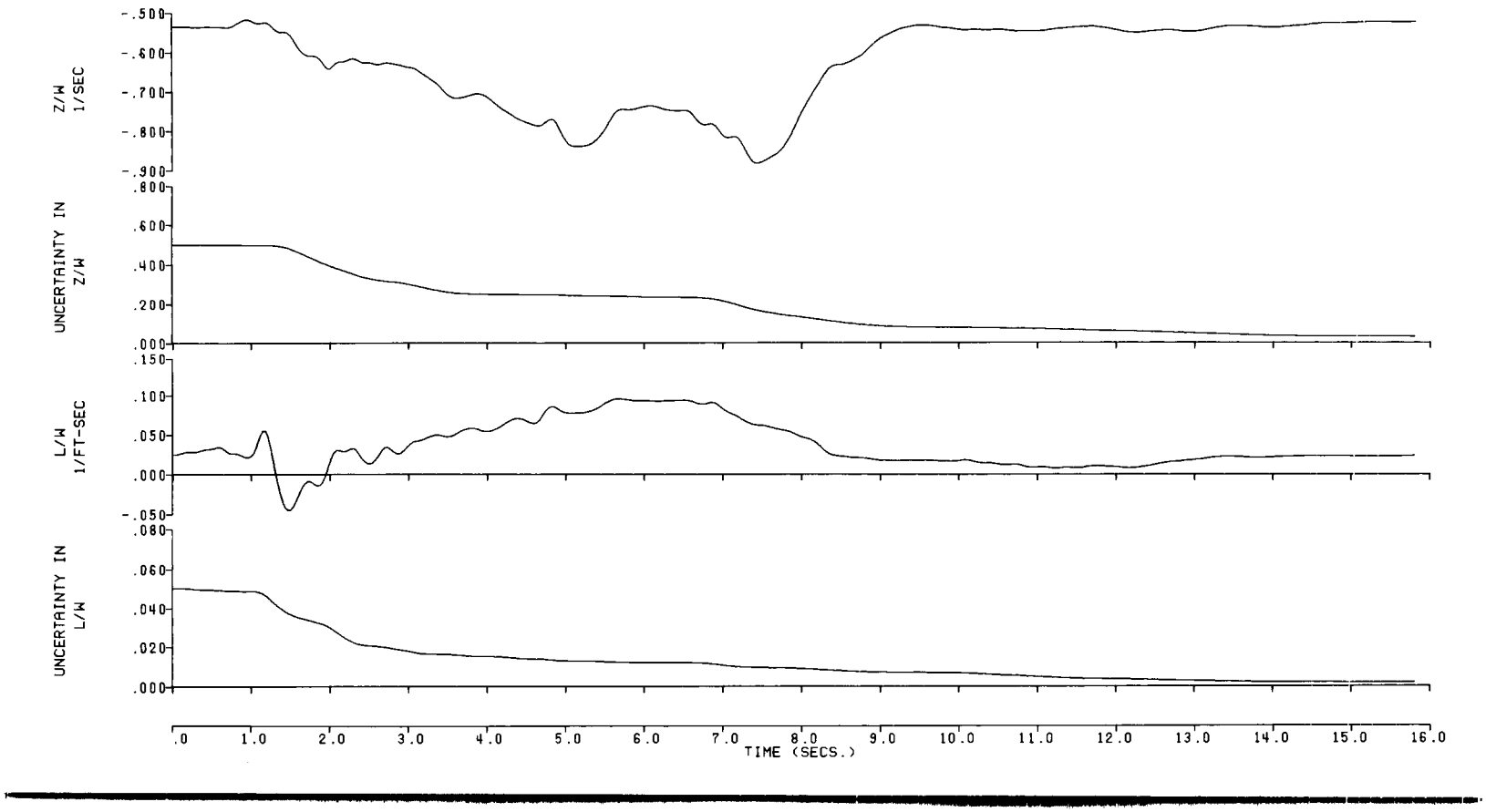

Figure 51 . - Continued.

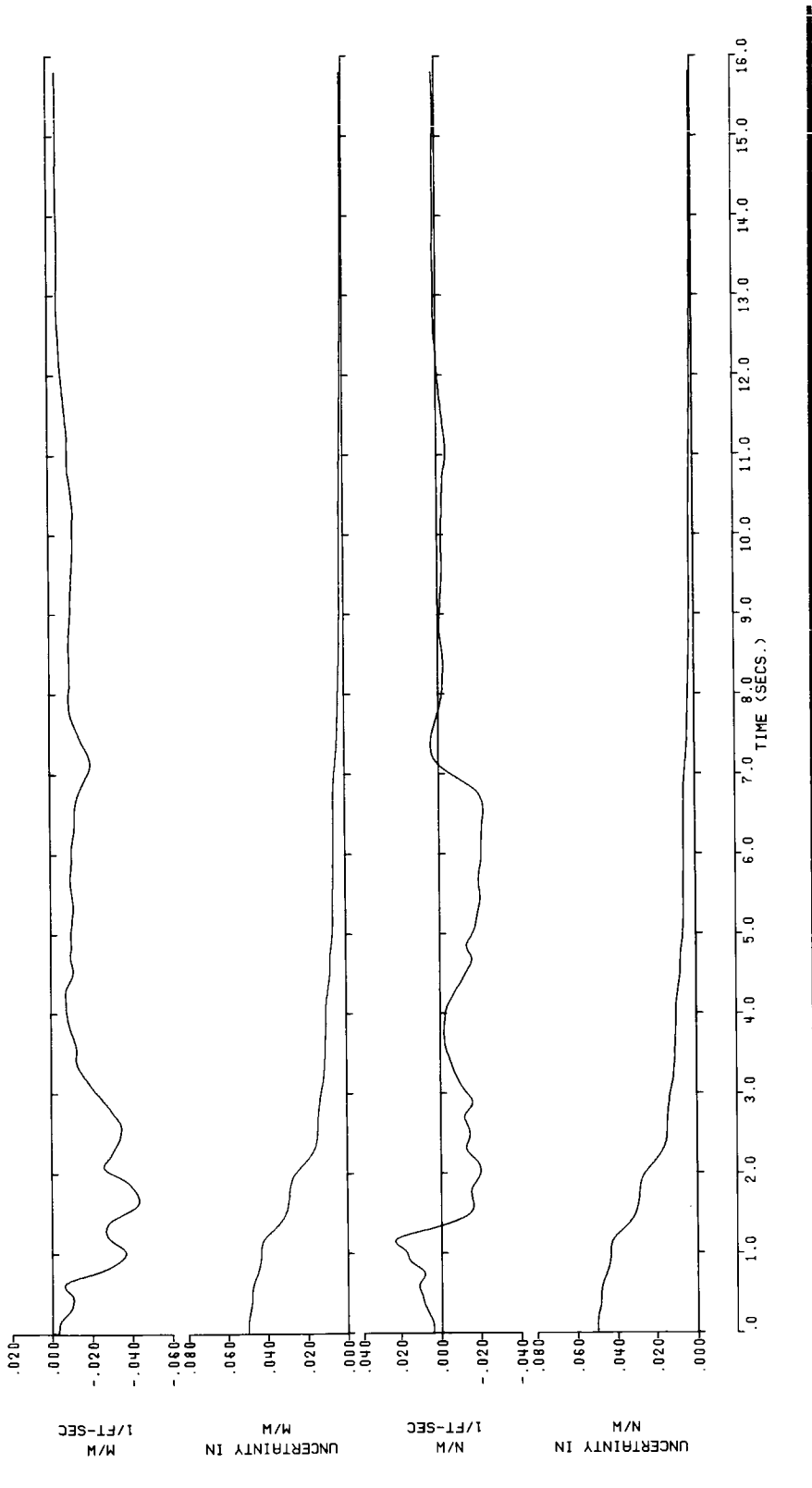

Figure 51. - Continued.

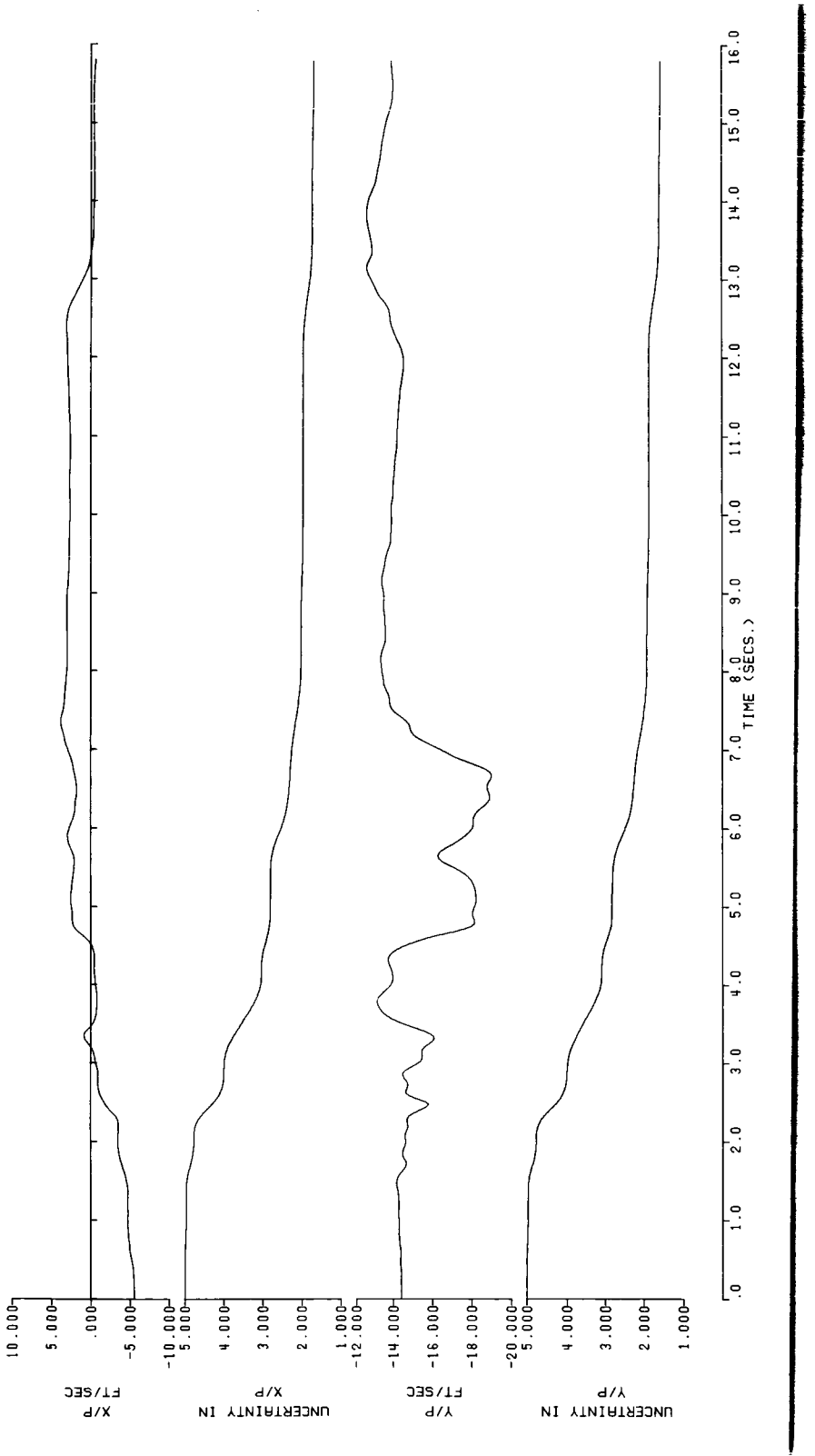

Figure 51. - Continued.

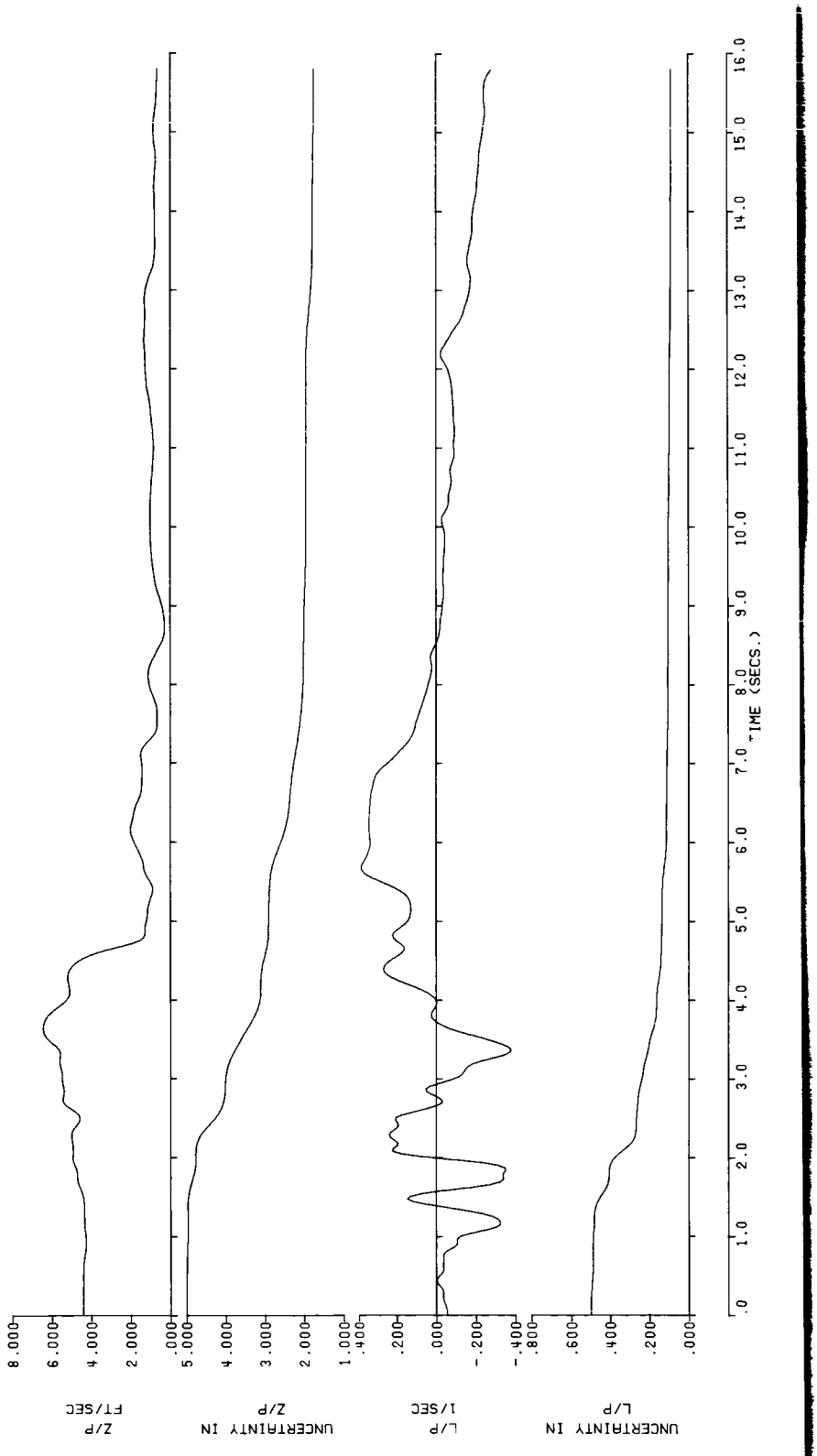

Figure 51. - Continued.

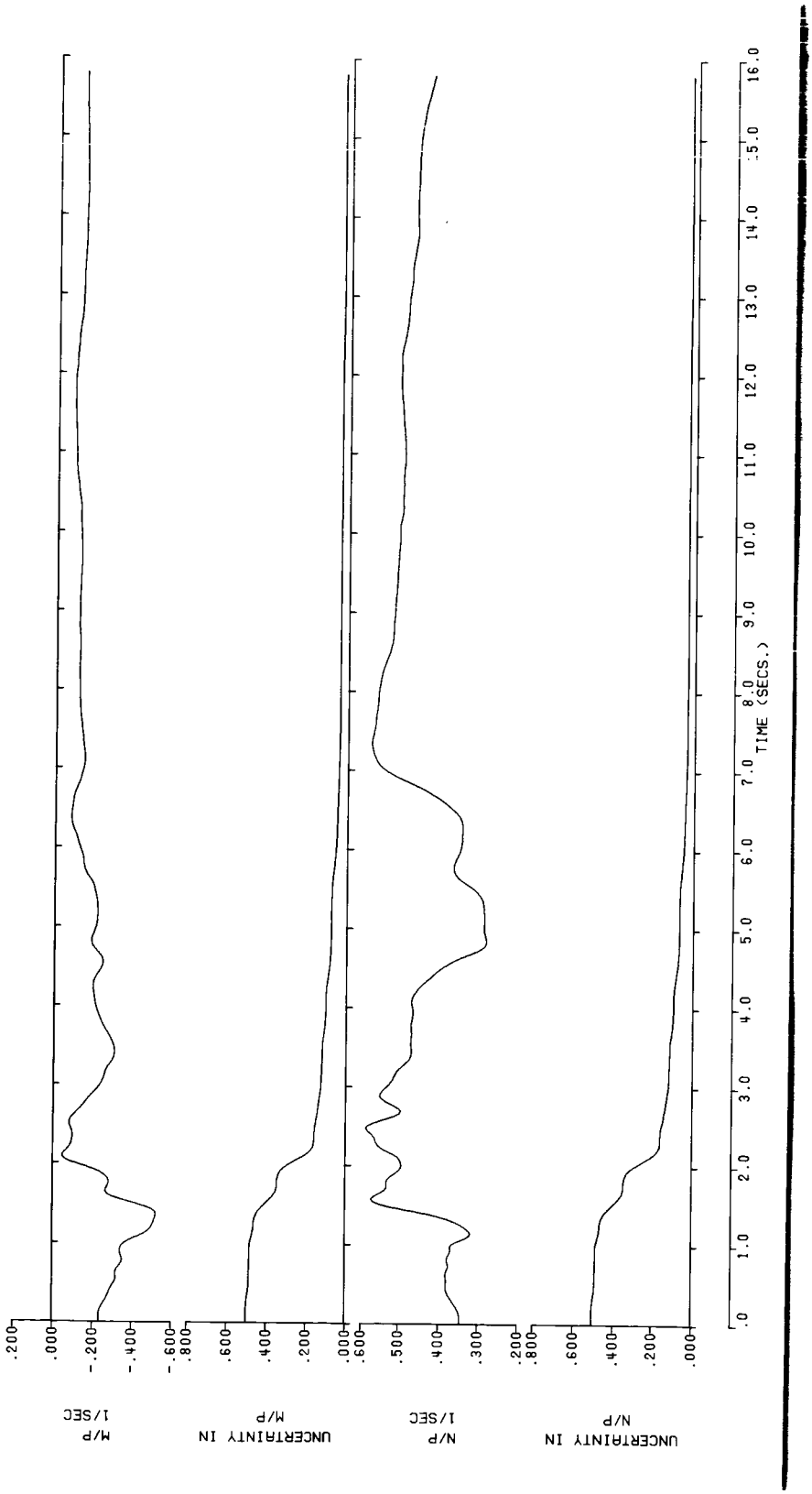

Figure 51. - Continued.

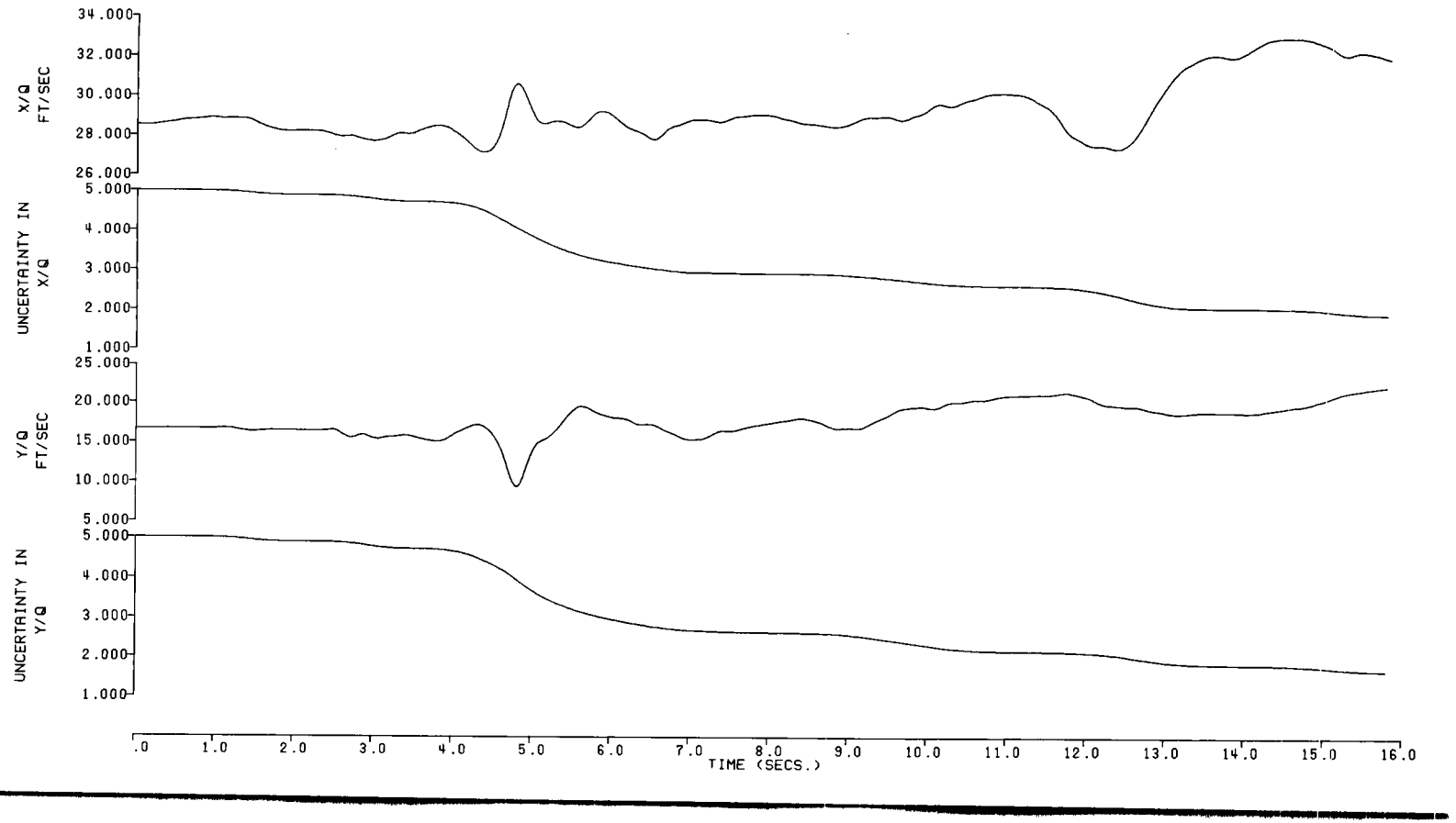

Figure 51. - Continued.

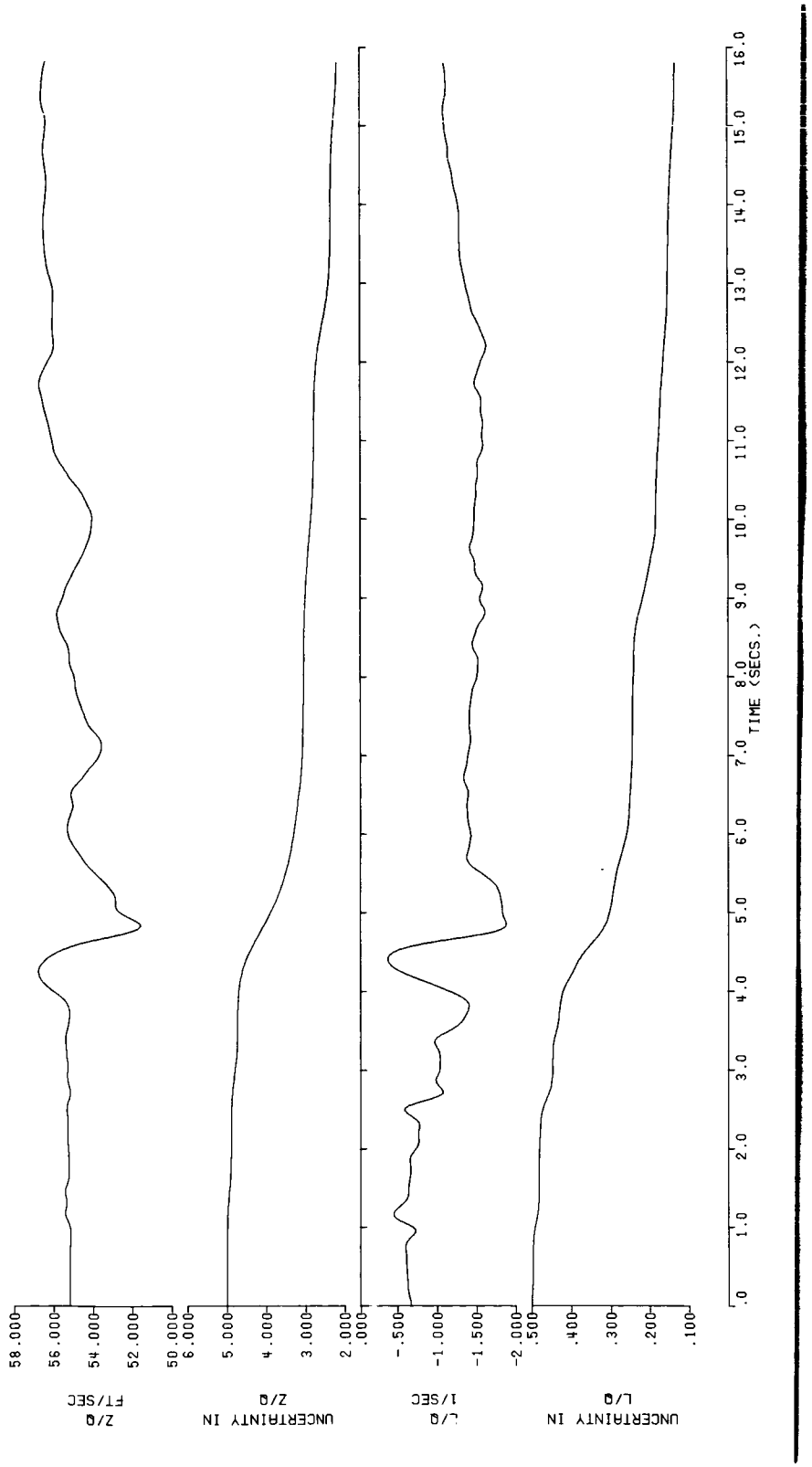

Figure 51. - Continued.

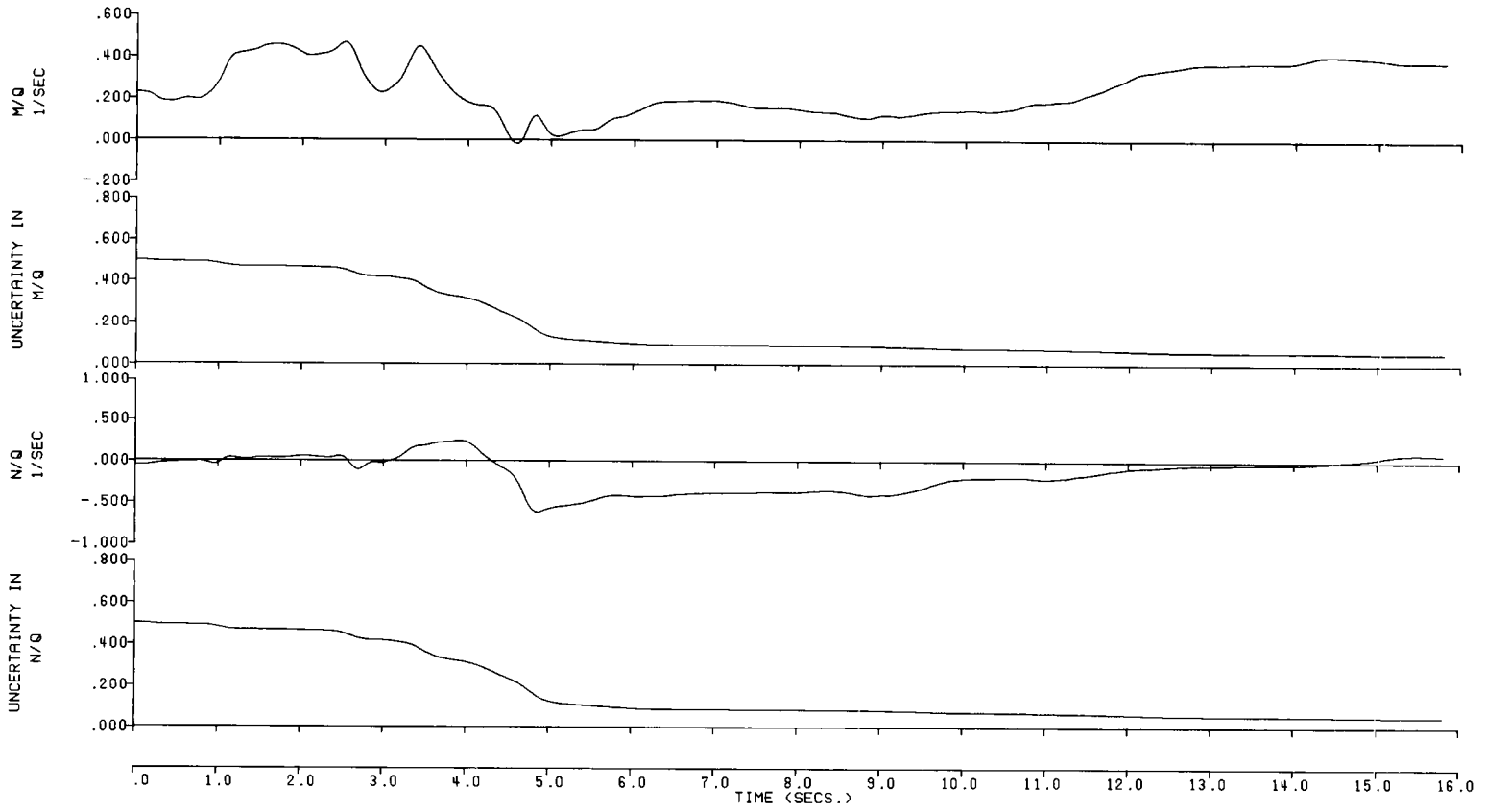

Figure 51. - Continued.

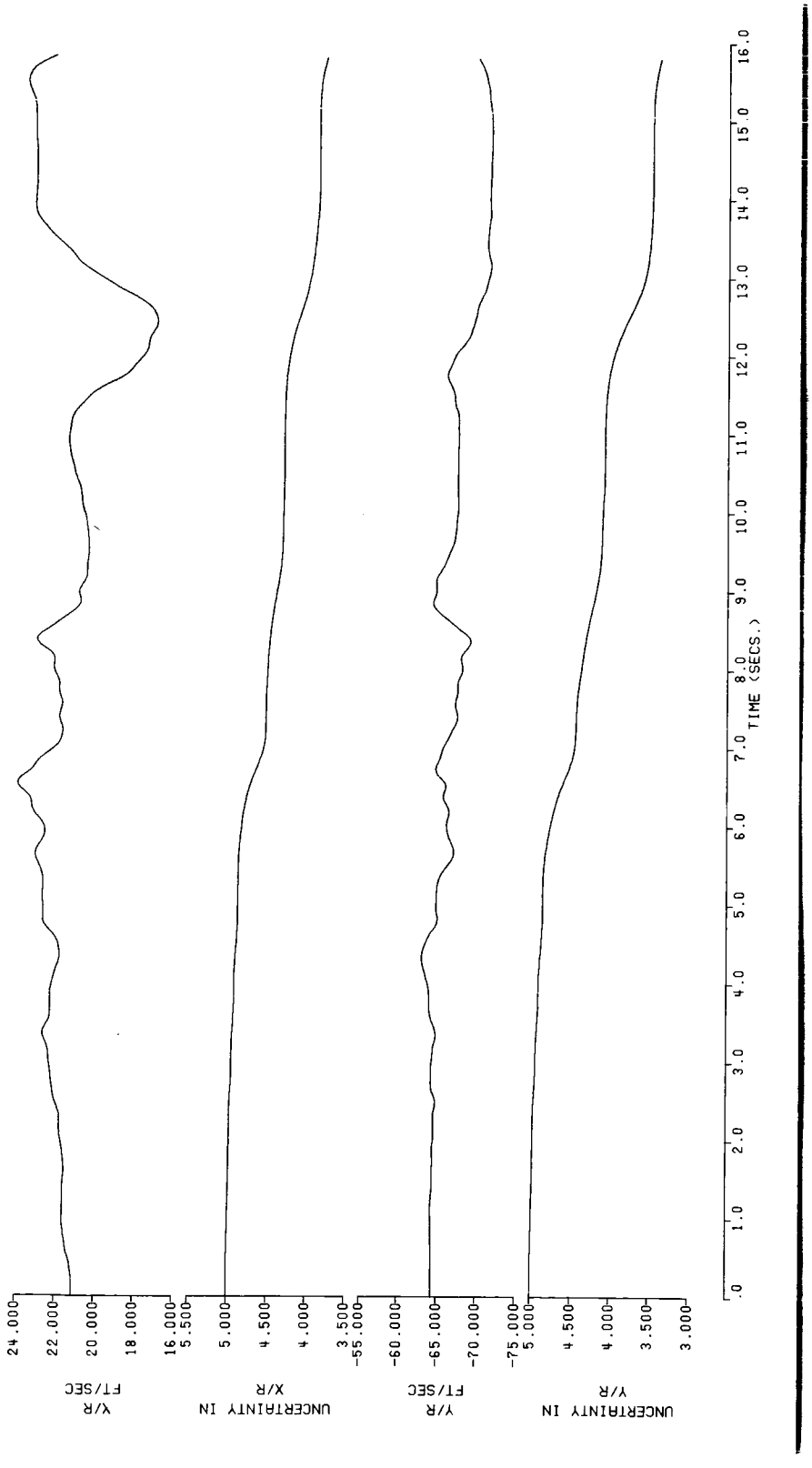

Figure 51. - Continued.

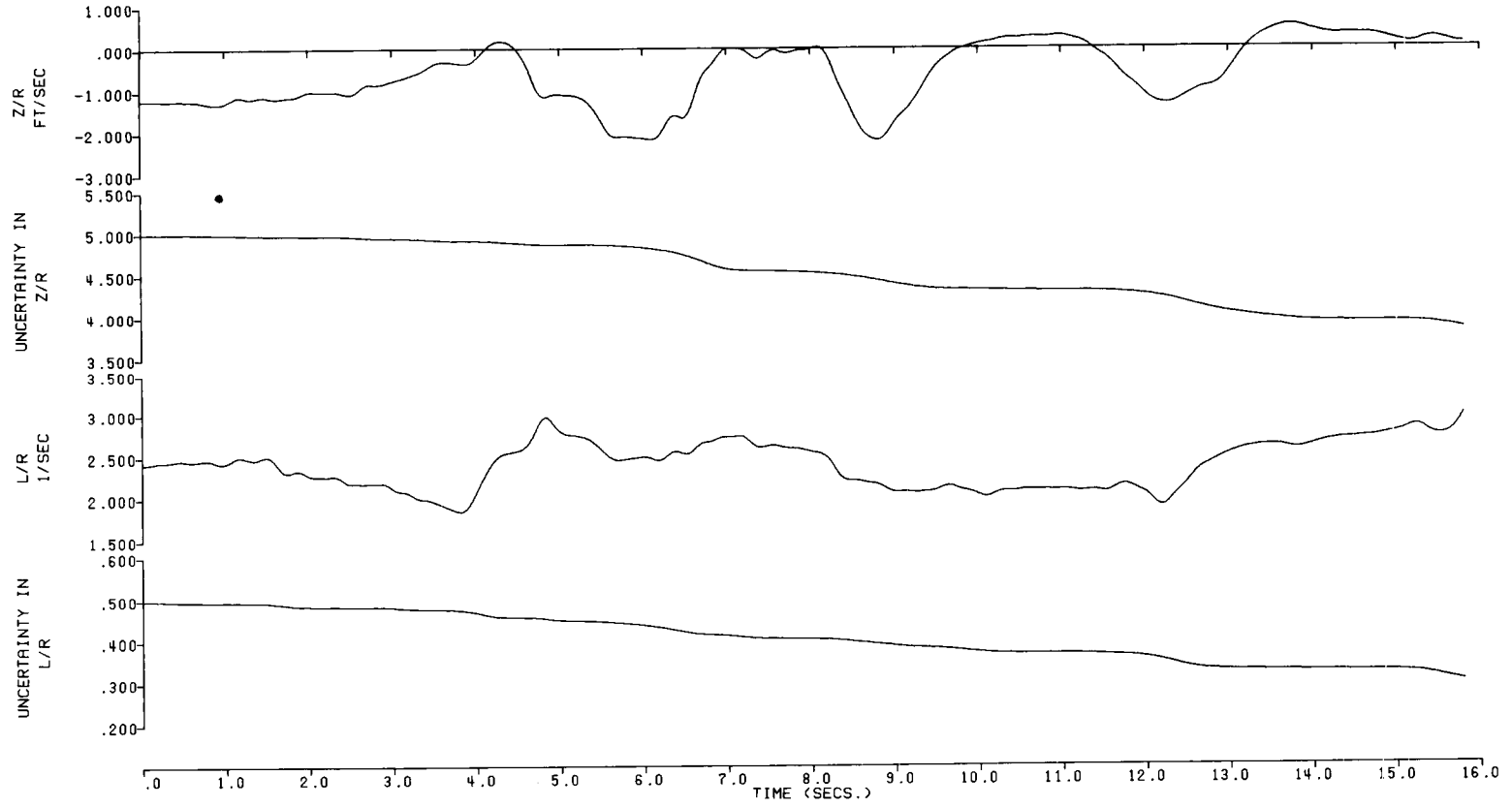

Figure 51. - Continued.

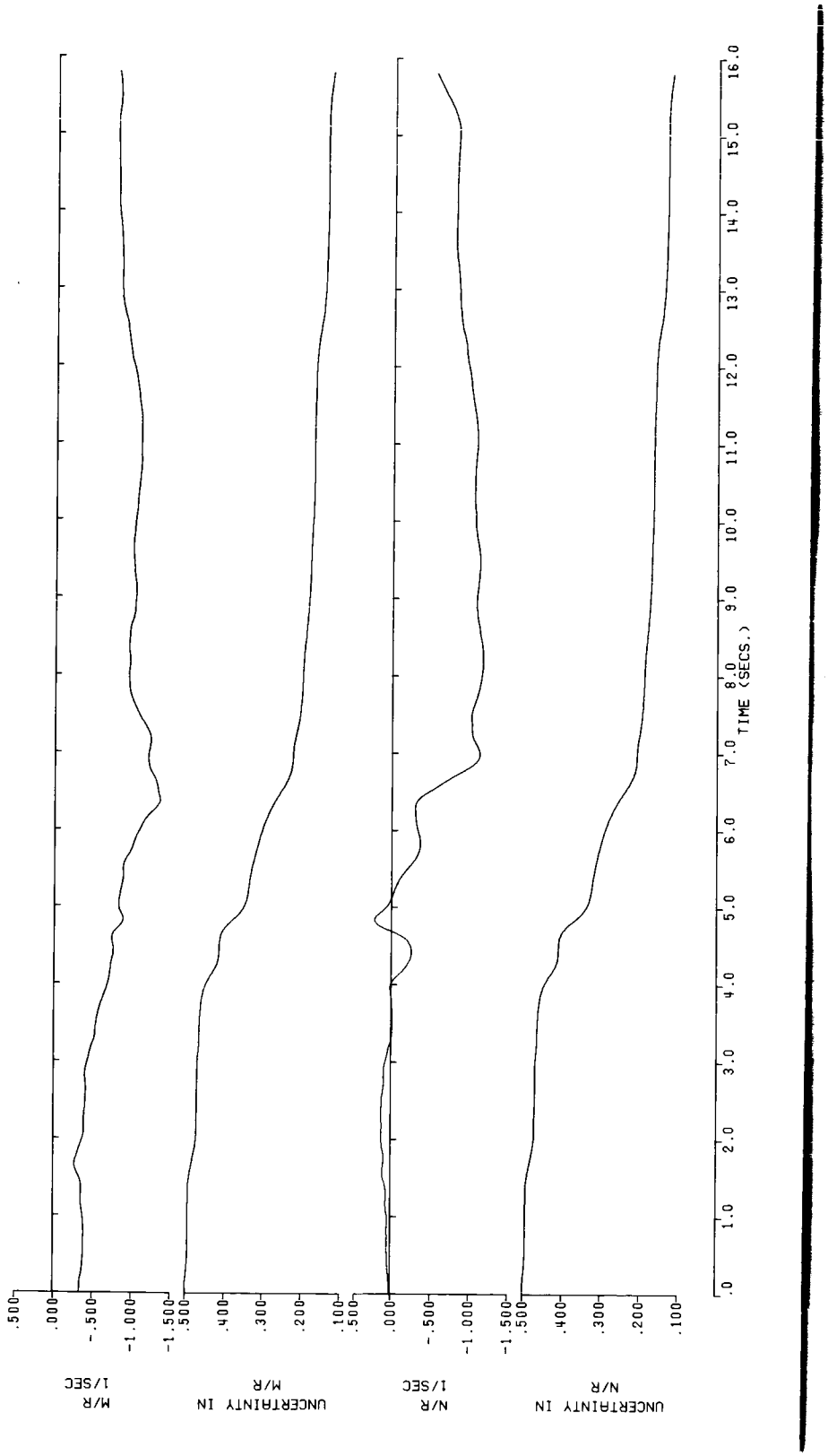

Figure 51. - Continued.

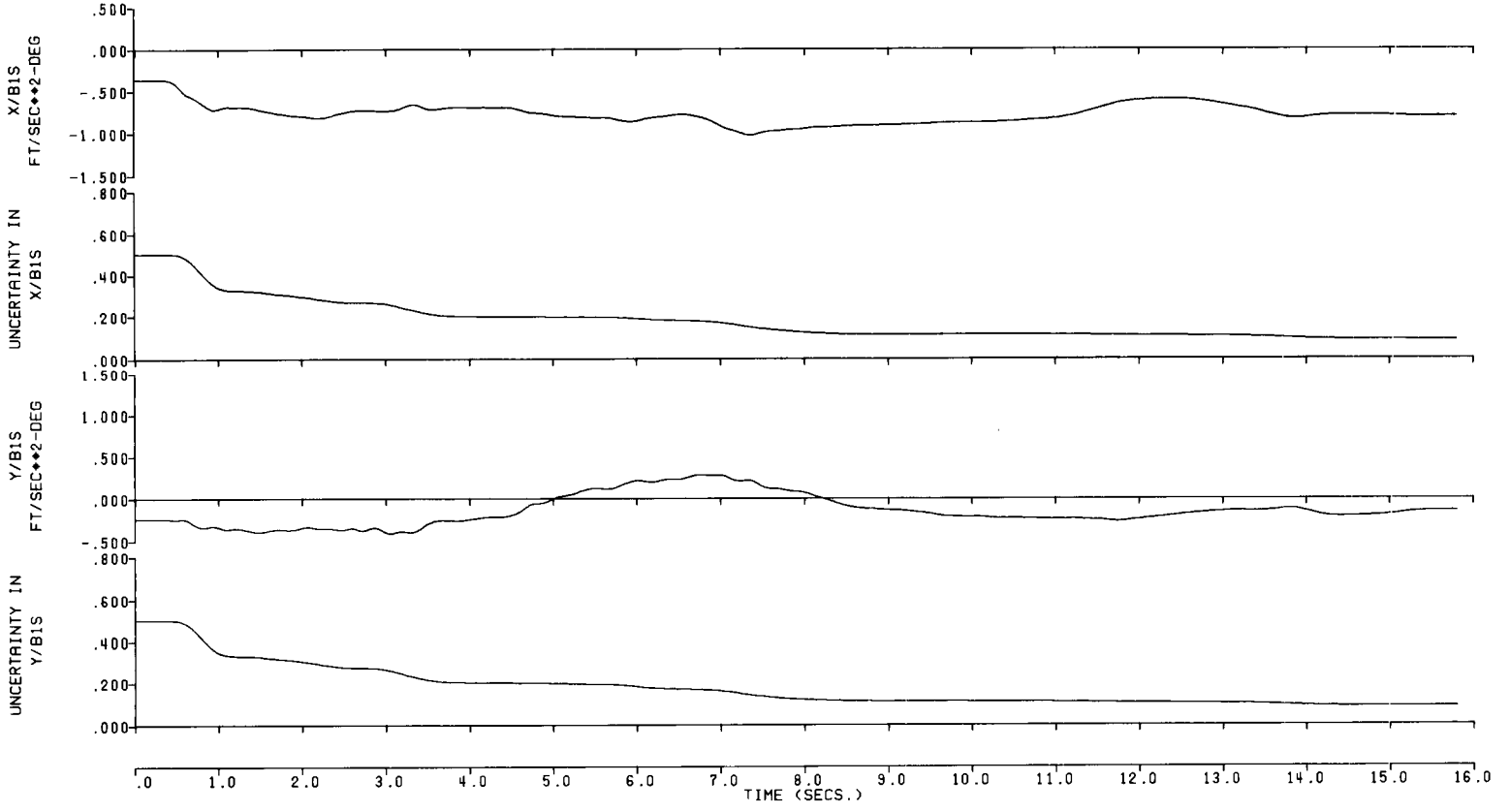

Figure 51. - Continued.

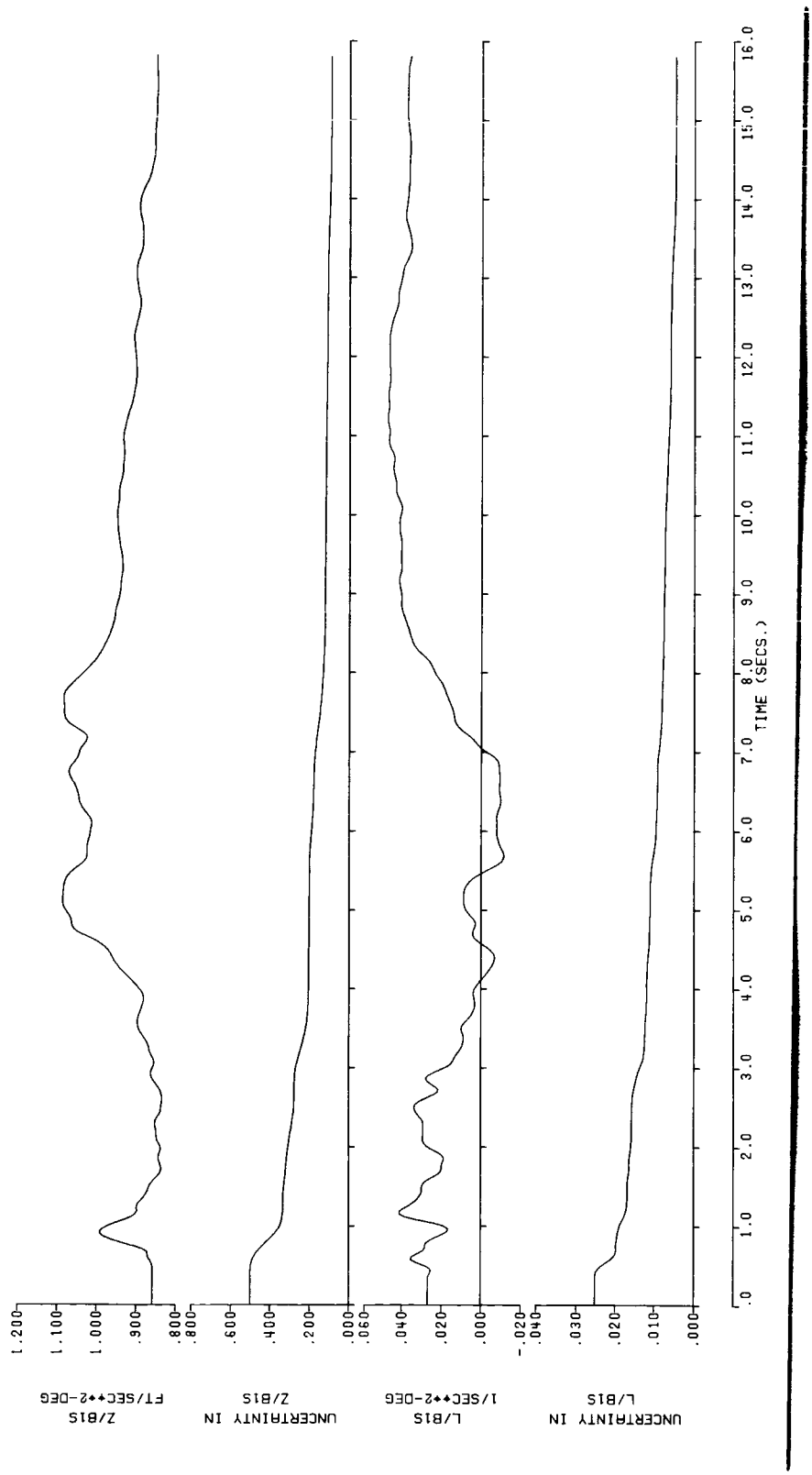

Figure 51. - Continued.

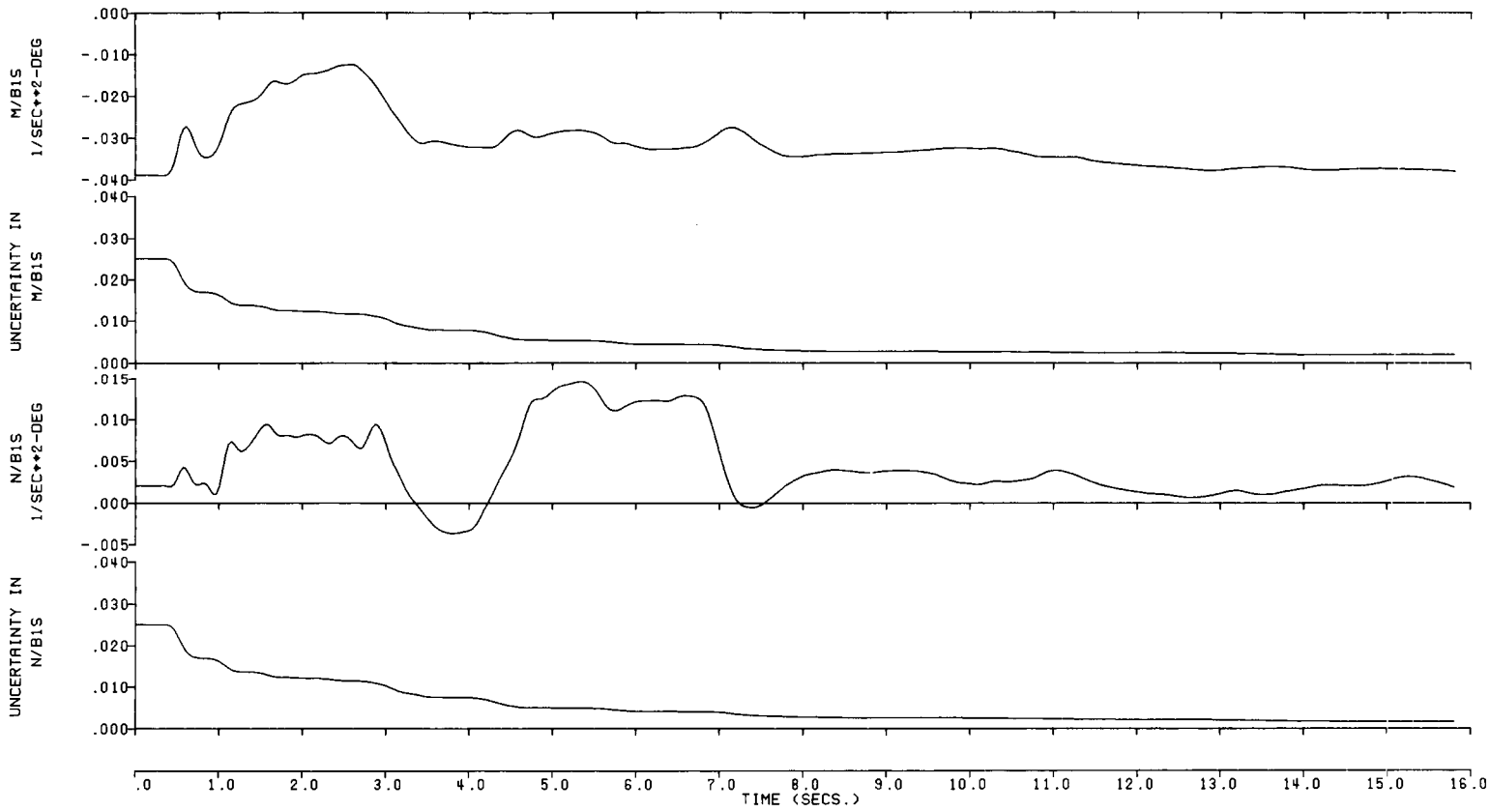

Figure 51. - Continued.

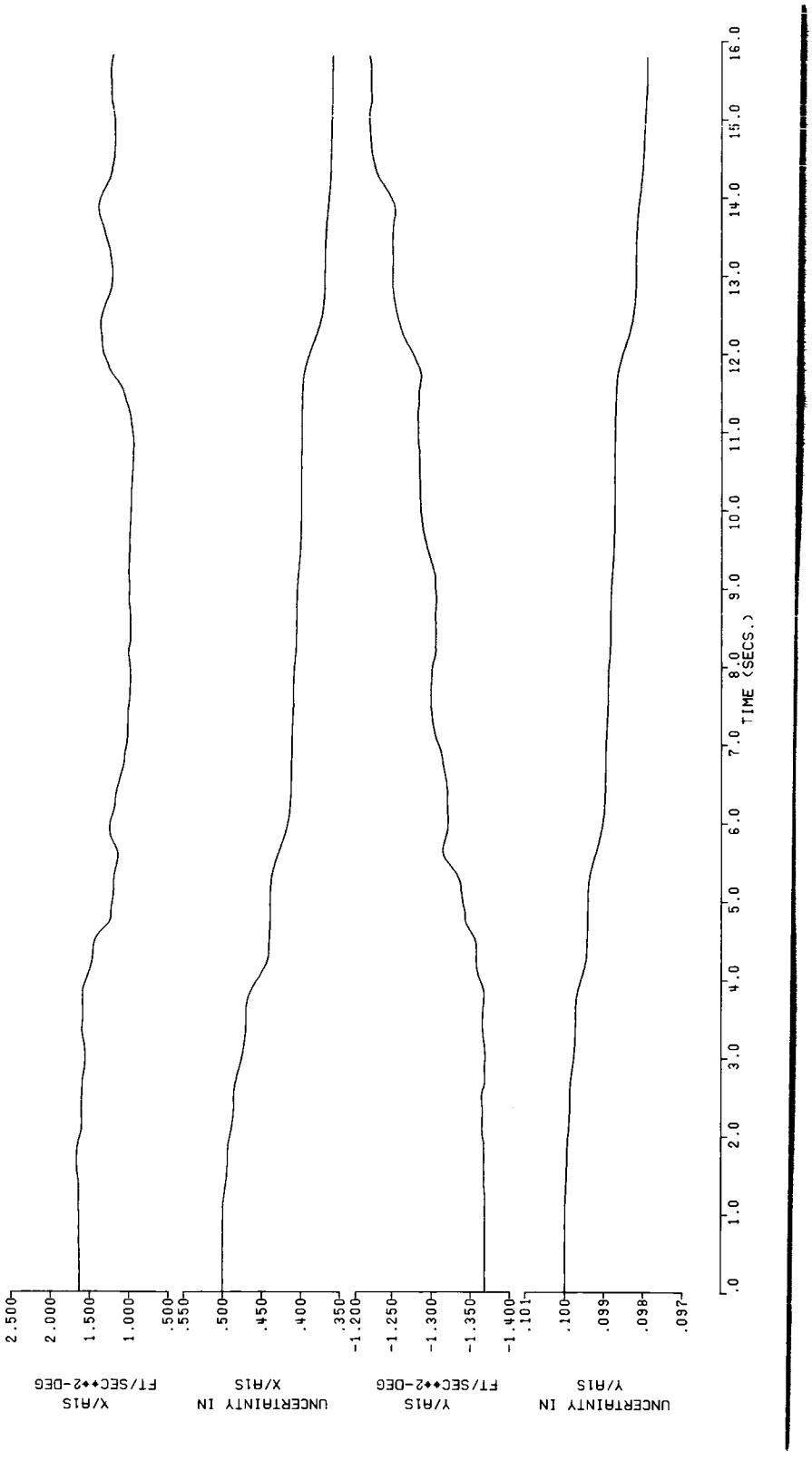

Figure 51. - Continued.

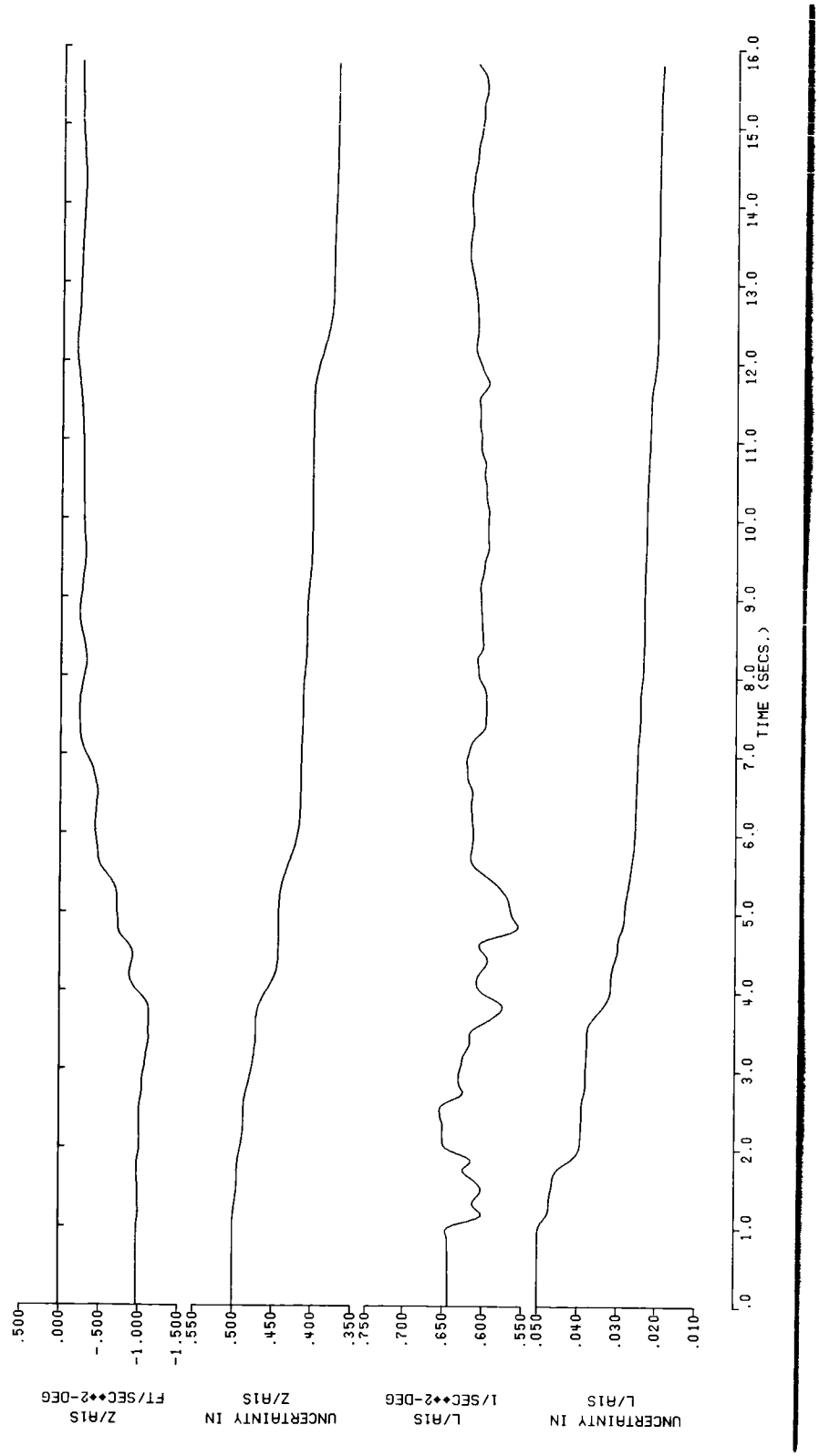

Figure 51. - Continued.

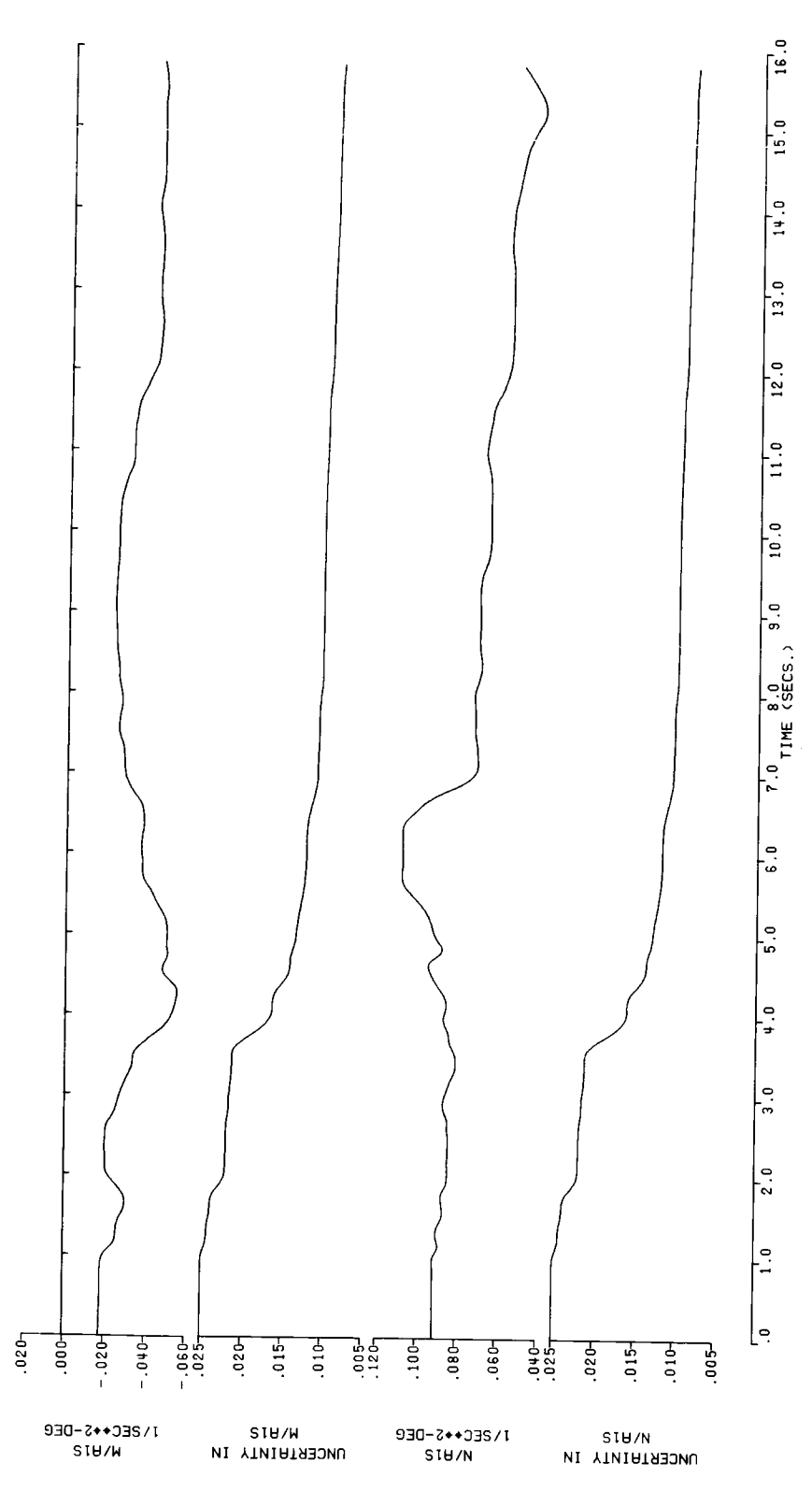

Figure 51. - Continued.

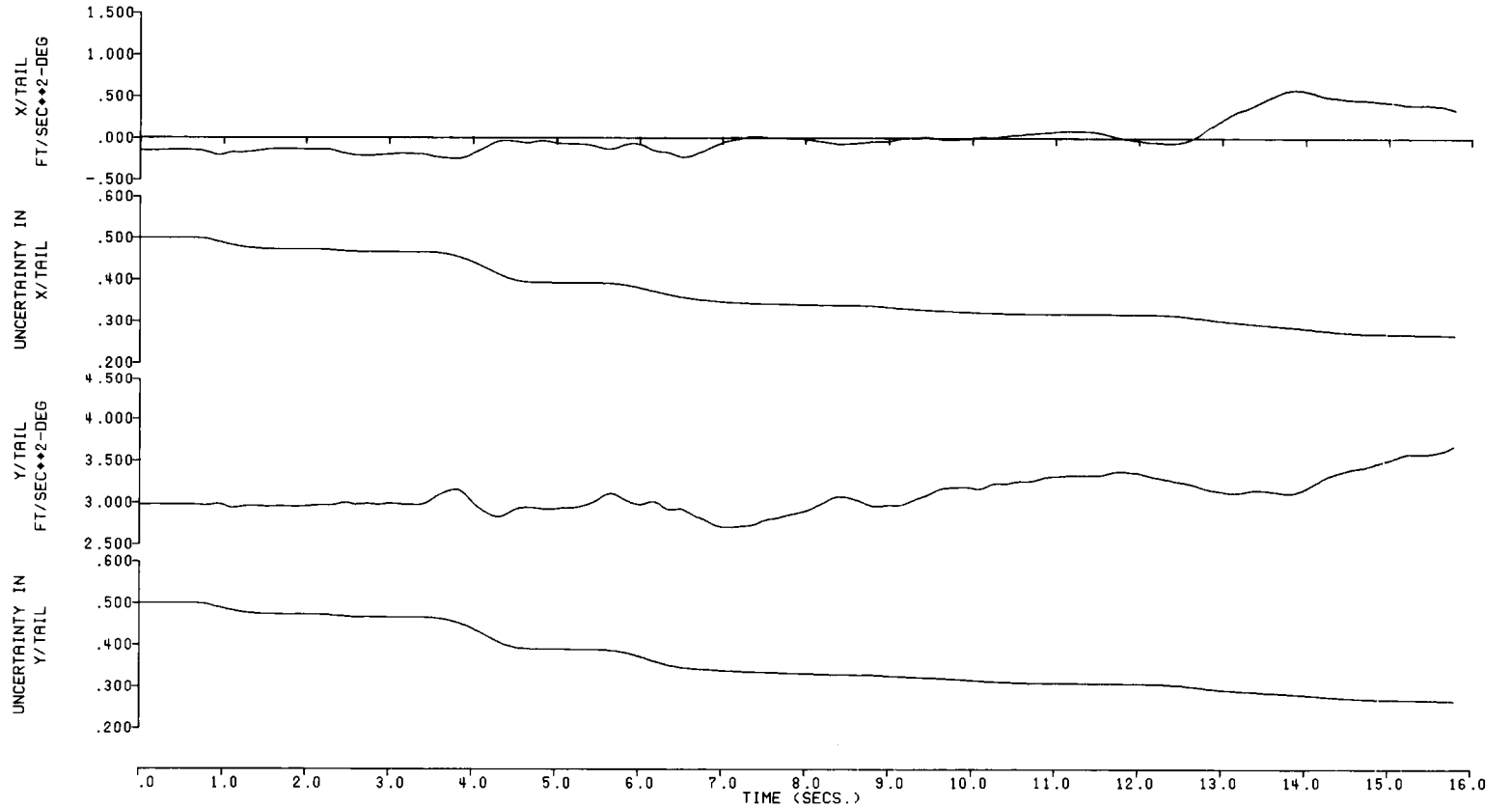

Figure 51. - Continued.

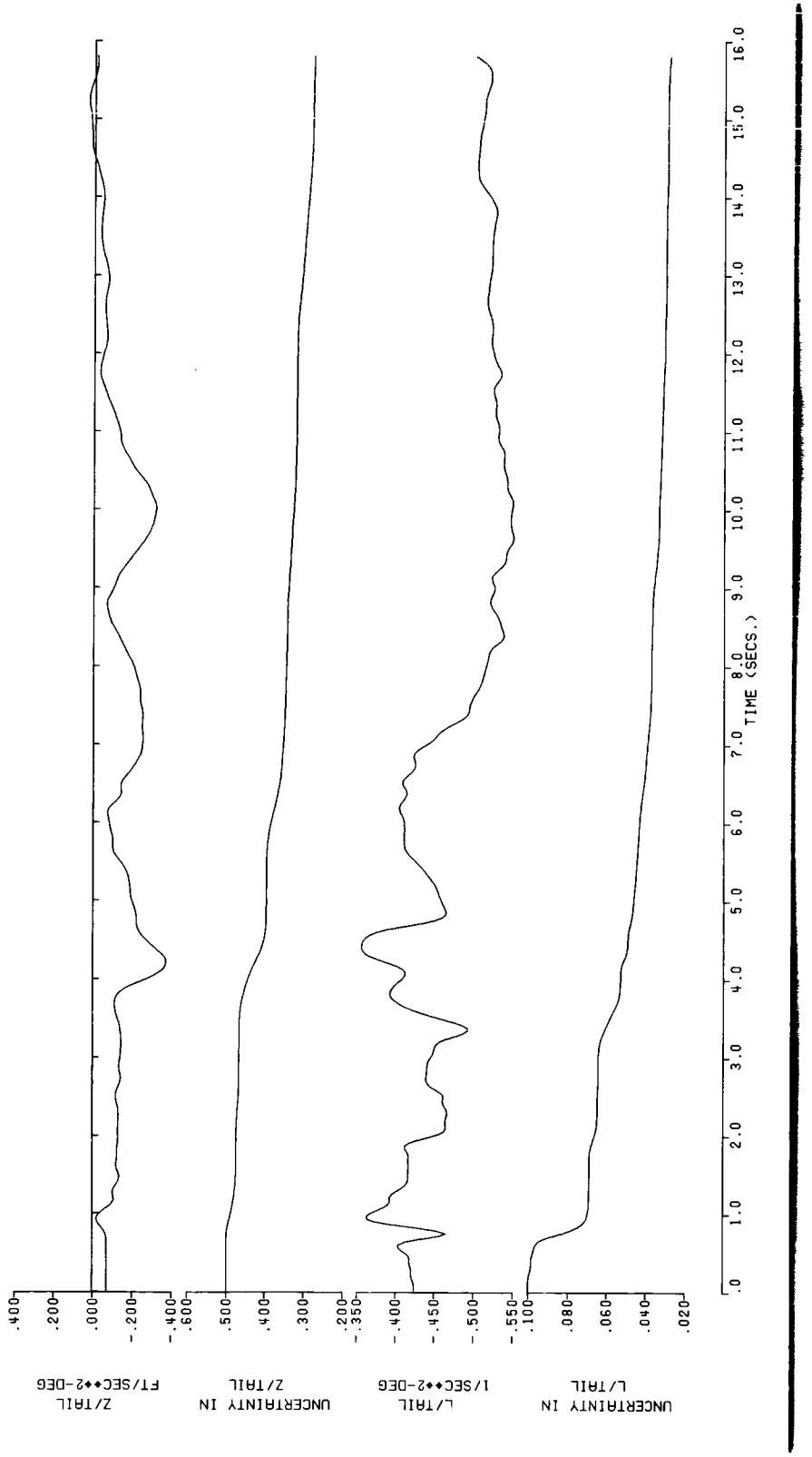

Figure 51. - Continued.

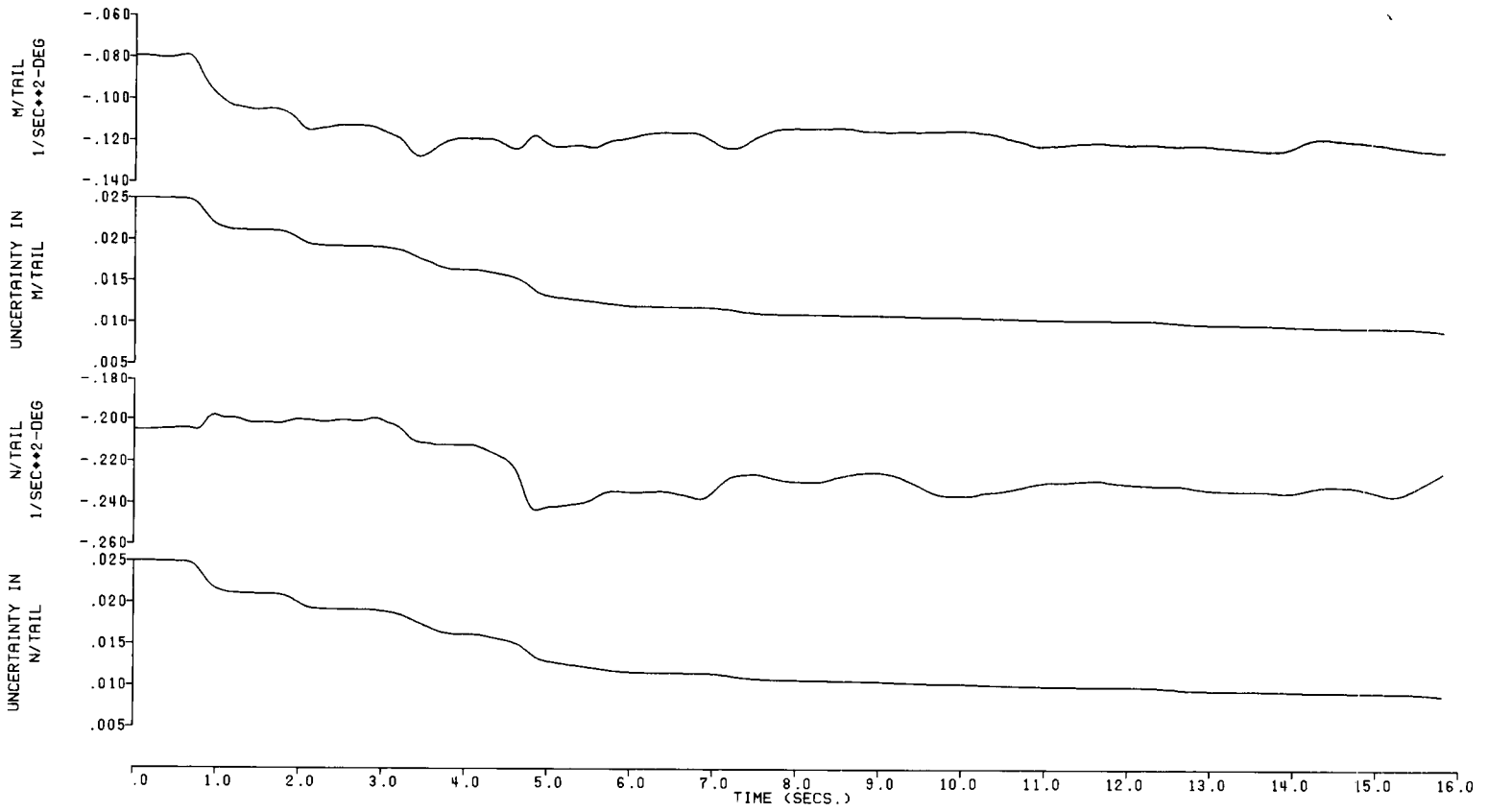

Figure 51. - Continued.

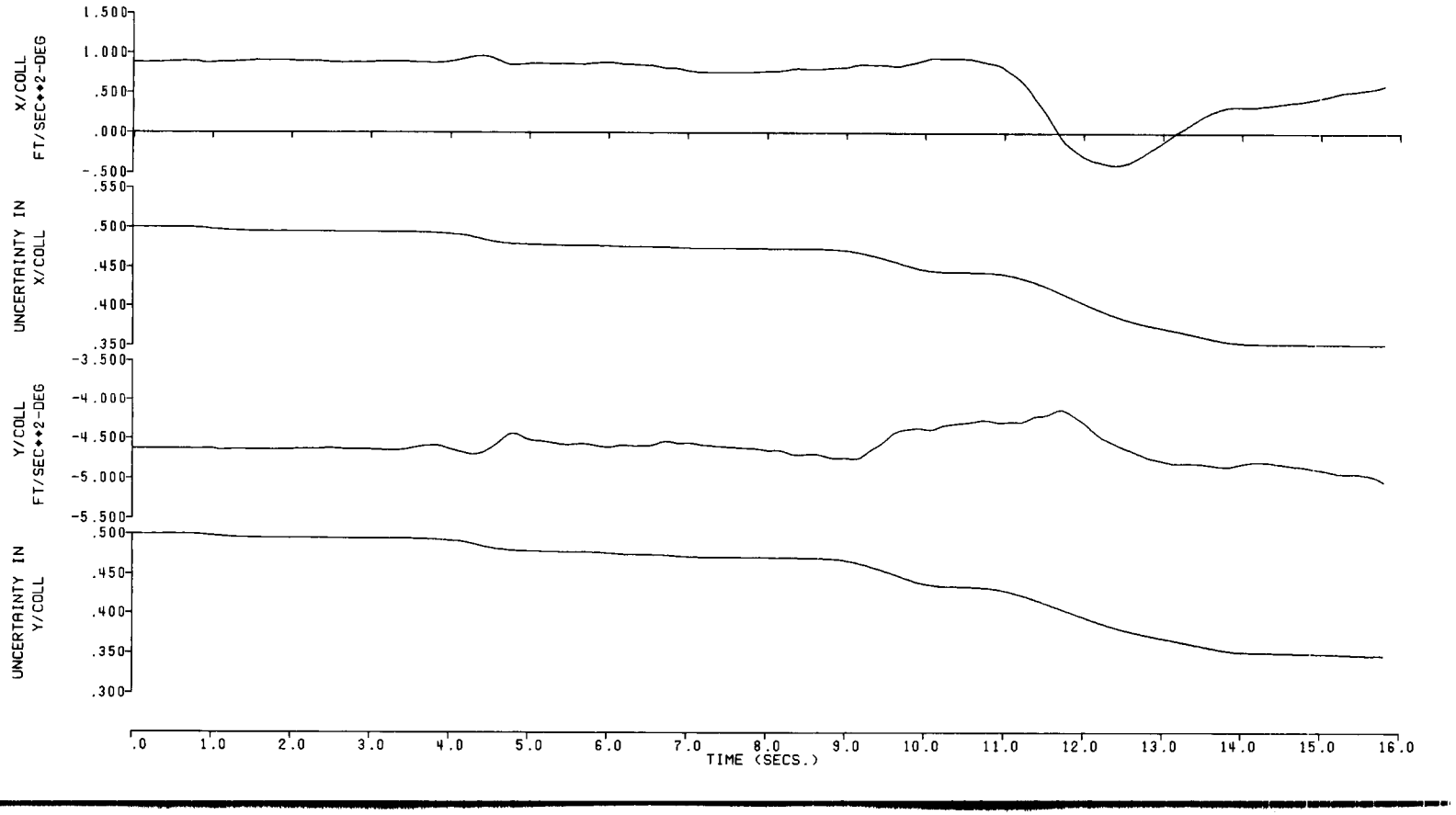

Figure 51. - Continued.

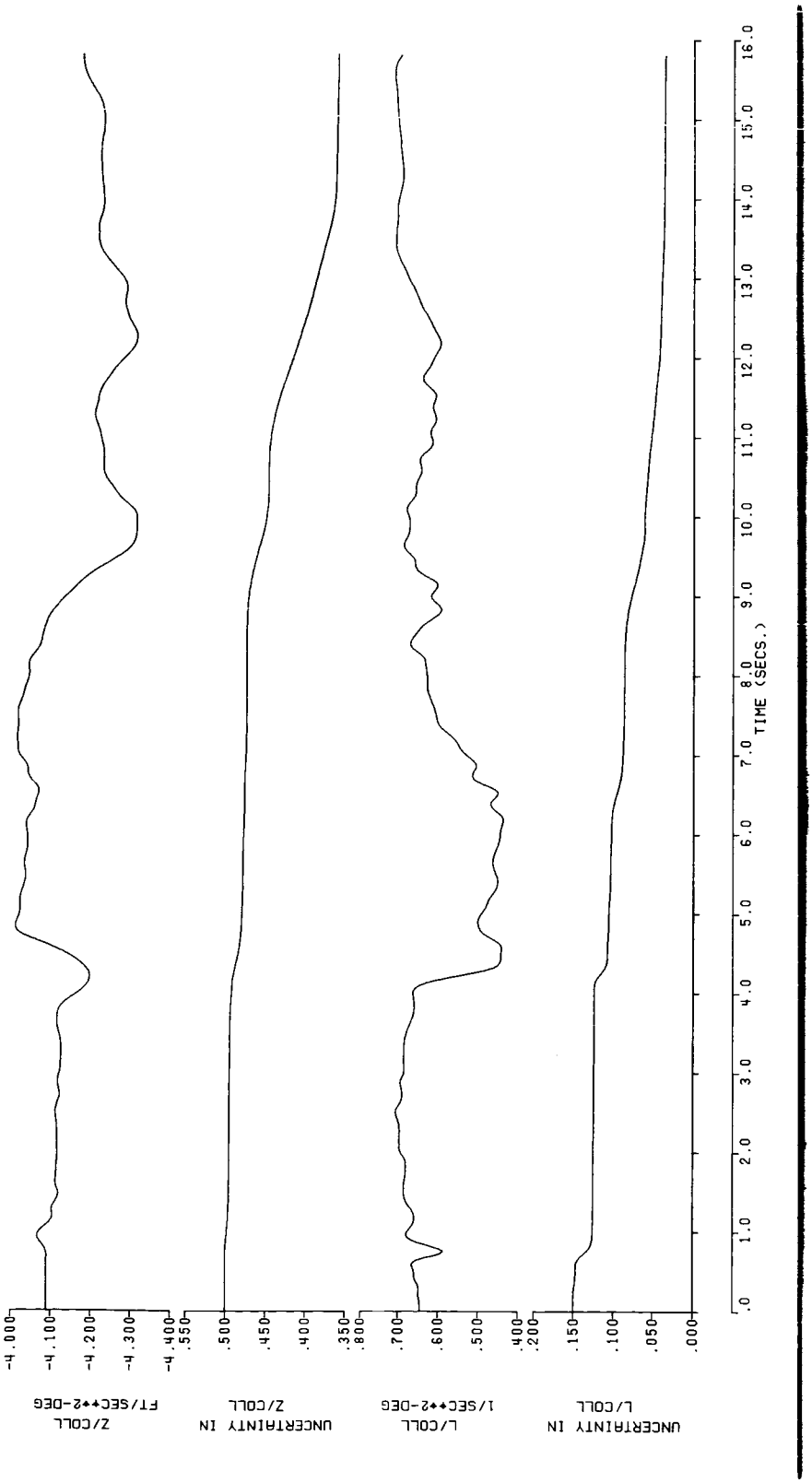

Figure 51. - Continued.

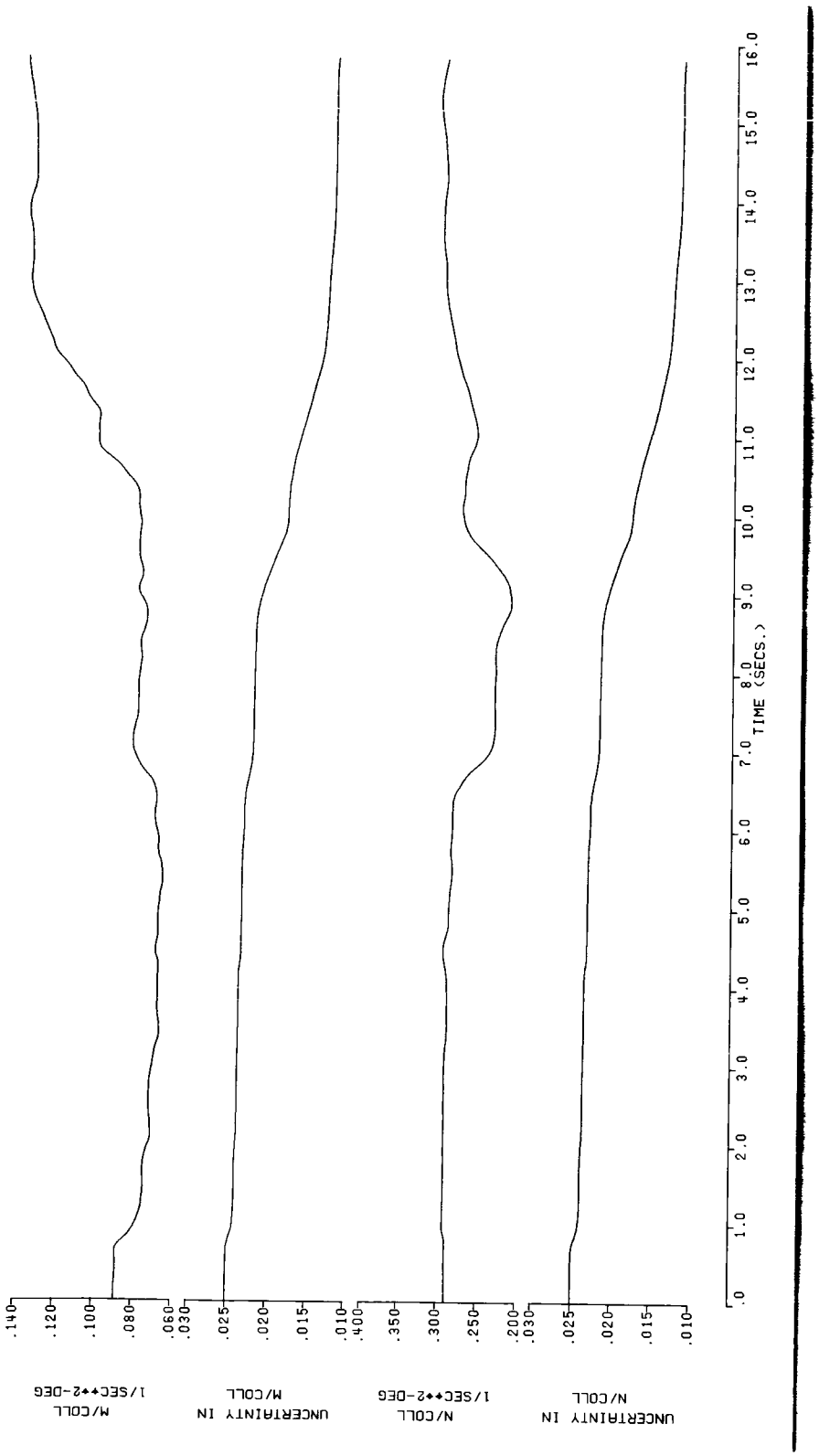

Figure 51. - Concluded.

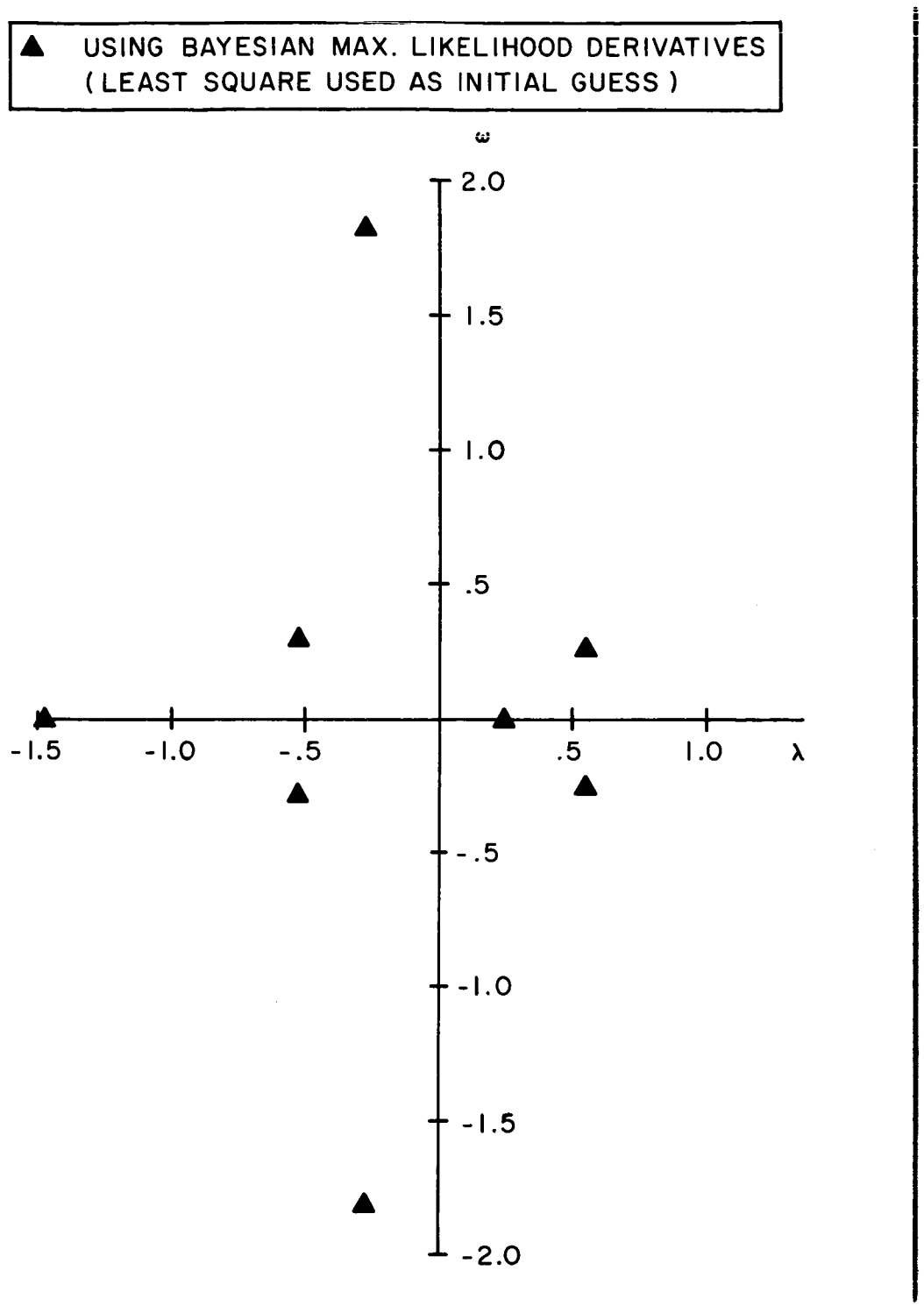

Figure 52. Characteristic Roots Obtained From The Identified Derivatives of The MLE (Method 12). (From CH-54B Flight Data, 45 Knots, AFCS Off).

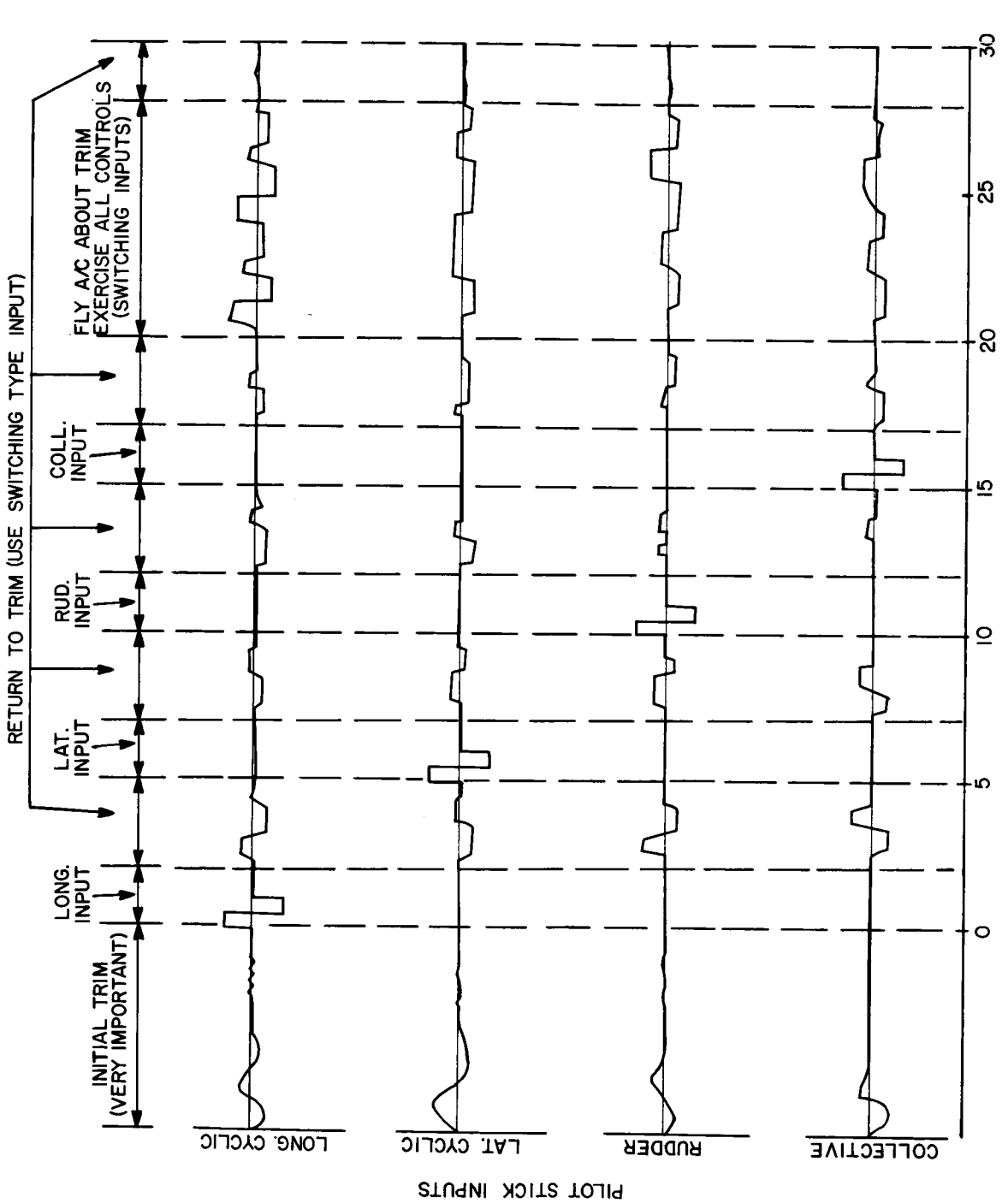

Figure 53. Pilot Input Sequence Recommended For Test Programs To Generate Data For Stability Derivative Identification.

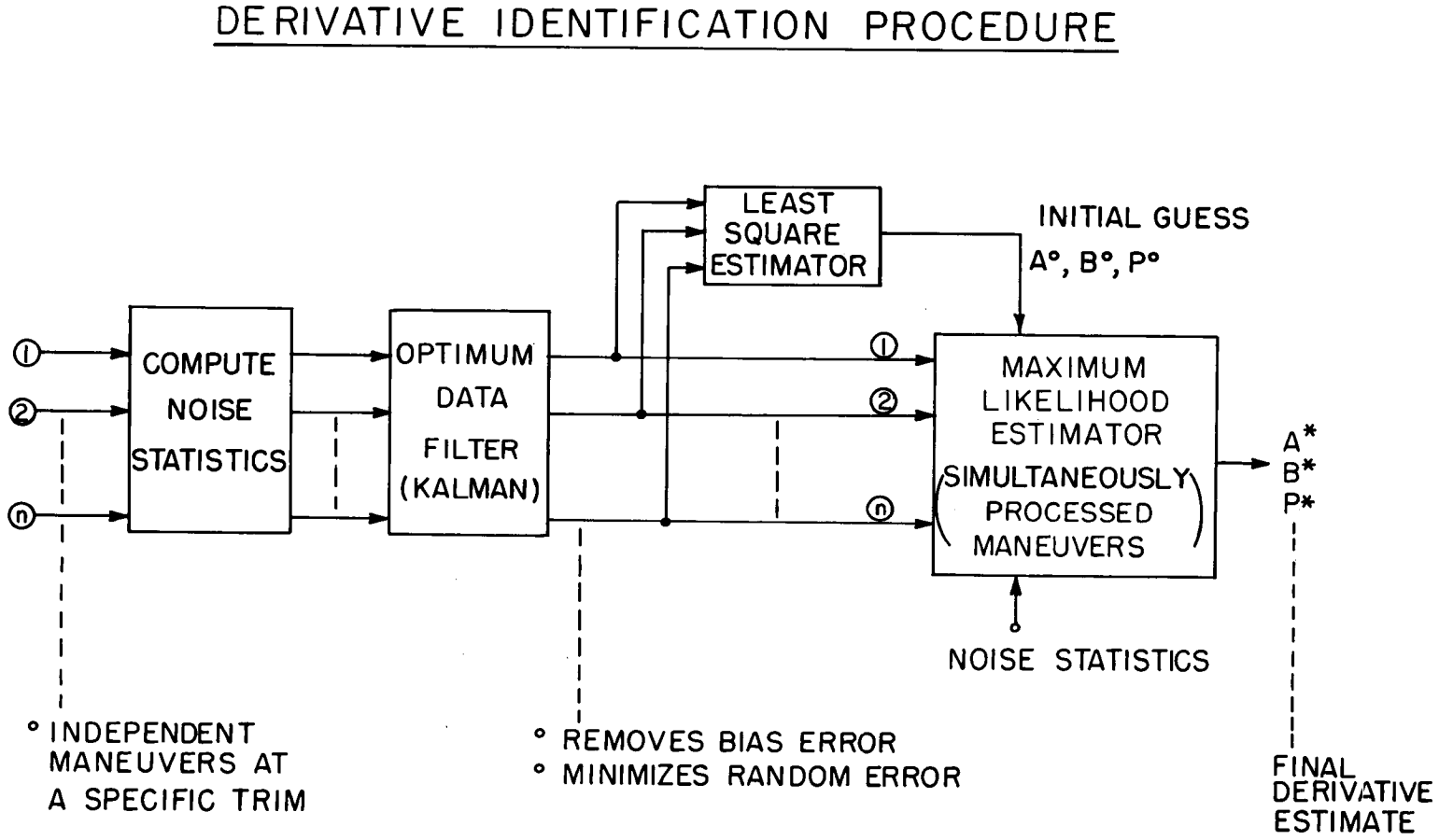

Figure 54. Stability Derivative Identification Procedure Found to Be Most Accurate For Extracting Derivatives from Helicopter Flight Data.